



University of
Salford
MANCHESTER

**SEMI-ACTIVE CONTROL FOR INDEPENDENTLY ROTATING
WHEELSET IN RAILWAY VEHICLES WITH MR DAMPERS**

ATOUSA ZAEIM

School of Computing, Science & Engineering

University of Salford

Salford, UK

**Submitted in Partial Fulfilment of the Requirements of
the Degree of Doctor of Philosophy**

2021



I DEDICATED THIS THESIS TO

MY HUSBAND TOM

AND

MY PARENTS

CONTENTS

1	CHAPTER 1:	21
1.1	BACKGROUND	21
1.2	RAILWAY VEHICLES	21
1.3	WHEELSETS	22
1.4	VEHICLE SUSPENSION SYSTEMS	24
1.4.1	Passive Primary Suspensions.....	25
1.4.2	Passive Secondary Suspension	26
1.5	ACTIVE SUSPENSIONS	26
1.5.1	Active Primary Suspension.....	28
1.5.2	Active Secondary Suspension.....	29
1.5.3	Semi-Active control.....	30
1.5.4	Actuators and Sensors for an Active Suspension	32
1.6	SEMI-ACTIVE DEVICES	34
1.7	RESEARCH TOPIC	38
1.8	AIM AND OBJECTIVE	39
1.9	CONTRIBUTIONS	40
1.10	RESEARCH METHODOLOGY	41
1.11	STRUCTURE OF THESIS	43
2	CHAPTER 2: LITERATURE REVIEW	44
2.1	INTRODUCTION	44
2.2	ACTIVE SECONDARY SUSPENSIONS	44
2.2.1	Active Secondary Configurations.....	44
2.2.2	Control Strategies.....	47
2.3	SEMI-ACTIVE SECONDARY SUSPENSIONS	47
2.3.1	Control Strategies.....	48
2.4	ACTIVE PRIMARY SUSPENSIONS	49
2.4.1	Wheelsets (Solid Axle and Independently Rotating Wheelsets)	49
2.4.2	Active Control Configurations (Stability and Curving).....	50
2.4.3	Control Strategies.....	53
2.5	SEMI-ACTIVE PRIMARY SUSPENSION	56

2.6	ACTUATORS IN RAILWAY VEHICLES	57
2.7	SENSING	60
2.8	SEMI-ACTIVE DEVICES	61
2.8.1	Magnetorheological Damper	62
2.8.2	Other Variable Dampers	68
2.9	SUMMARY	69
3	CHAPTER 3: MODELLING OF THE VEHICLE DYNAMIC SYSTEMS ...	70
3.1	INTRODUCTION	70
3.2	ANALYSIS OF THE MODEL	70
3.3	MODELLING OF INDEPENDENTLY ROTATING WHEELSET	70
3.4	MODELLING OF A TWO-AXLE RAILWAY VEHICLE WITH INDEPENDENTLY ROTATING WHEELSETS (IRW)	77
3.5	MODELLING OF A CONVENTIONAL BOGIE RAILWAY VEHICLE WITH INDEPENDENTLY ROTATING WHEELSETS (IRW)	84
3.6	MAGNETORHEOLOGICAL DAMPER	93
3.7	SUMMARY	99
4	CHAPTER 4: ACTIVE CONTROL	100
4.1	INTRODUCTION	100
4.2	ACTIVE CONTROL SCHEME	101
4.3	WHEELSET CONTROLLER	102
	Wheelset Stability Control Design	112
	Wheelset Guidance Control Design	112
	Control Gain G_s & G_g for Two axle Vehicle	112
	Wheelset Controller for Conventional Bogie Vehicle	123
4.4	SIMULATION AND RESULT	127
4.5	SUMMARY	141
5	CHAPTER 5: SEMI-ACTIVE CONTROL	142
5.1	INTRODUCTION	142
5.2	SEMI-ACTIVE CONTROLLER	143
5.3	MAGNETORHEOLOGICAL DAMPER CONTROLLERS	146
5.4	INVERSE DYNAMICS (FEEDFORWARD) DESIGN	148

5.5	FEEDBACK (PI) CONTROLLER	151
5.6	EVALUATION OF CONTROL PERFORMANCE.....	152
5.7	SUMMARY	158
6	CHAPTER 6: SIMULATION RESULTS AND ASSESSMENTS.....	159
6.1	INTRODUCTION	159
6.2	TRACK INPUT.....	159
	Low Speed Curve	159
	High Speed Curve	161
	Track Irregularities – Generic Track Data at The Speed of 83m/s, 300 Kmh – 1	162
	Track Irregularities – Measured Track Data at The Speed of 50m/S.....	163
6.3	TWO AXLE VEHICLE.....	165
	6.3.1 In curve track Curve track at the speeds of 83m/s, 300 Kmh – 1 and 20	
	m/s, 72 Kmh – 1	165
	6.3.2 Straight Track with Track Irregularities (Generic Track Data Irregularity at	
	The Speed of 83m/s, 300 Kmh – 1)	181
	6.3.3 Straight Track with Irregularity (Measured Track Data at The Speed of	
	50m/S, 180 Kmh – 1).....	190
6.4	BOGIE VEHICLE	198
	6.4.1 Curve track.....	198
	6.4.2 Straight Track with Track Irregularities (Generic Track Data Irregularity)	
	213	
	6.4.3 Straight Track with Irregularity (Measured Track Data).....	222
6.5	SUMMARY	233
7	CHAPTER 7: CONCLUSIONS AND FUTURE WORK.....	234
	7.1 CONCLUSIONS.....	234
	7.2 FURTHER WORK.....	236
8	REFERENCE	238
	APPENDIX A: PARAMETER VALUES.....	247

List of Figures

<i>Figure 1-1- Basic side and end view of wheelsets and bogie showing how suspension units are located</i>	22
<i>Figure 1-2- Wheelset kinematic oscillation [5]</i>	23
<i>Figure 1-3- Secondary and primary Passive suspension</i>	25
<i>Figure 1-4- Principles of an active suspension system [4]</i>	27
<i>Figure 1-5- Secondary and primary Active suspension</i>	28
<i>Figure 1-6- Secondary and primary Semi- Active suspension</i>	31
<i>Figure 1-7- Semi-active damper force-velocity characteristics</i>	31
<i>Figure 1-8- Actuator force controller [27]</i>	33
<i>Figure 1-9- Semi-active damper on- off class</i>	35
<i>Figure 1-10- Semi-active damper constantly variable class</i>	35
<i>Figure 1-11- Semi-active suspension [33]</i>	36
<i>Figure 1-12- – Flowchart of the research</i>	42
<i>Figure 2-1- Active Suspension System (a) Low-bandwidth (b) High-bandwidth</i>	46
<i>Figure 2-2- Active steering via yaw torque (yaw actuator)</i>	51
<i>Figure 2-3- Active steering via yaw torque (pair of longitudinal actuators)</i>	52
<i>Figure 2-4- Active steering via lateral force</i>	52
<i>Figure 3-1- Independently Rotating Wheels (IRW)</i>	71
<i>Figure 3-2- Side view of the left and right wheels</i>	71
<i>Figure 3-3- Forces action on wheelset in plan view</i>	73
<i>Figure 3-4- Forces action on wheelset in plan view</i>	74
<i>Figure 3-5- Forces combining in the lateral direction</i>	74
<i>Figure 3-6- Plan view of a two axles vehicle</i>	78
<i>Figure 3-7- Plan view diagram of conventional bogie vehicle</i>	85
<i>Figure3-8- No magnetic</i>	94
<i>Figure 3-9- Magnetic field</i>	94
<i>Figure 3-10- Chains have</i>	94
<i>Figure 3-11- Bingham model</i>	95
<i>Figure 3-12- Bouc-Wen model</i>	95
<i>Figure 3-13- Modified Bouc-Wen</i>	95
<i>Figure 3-14- Damping force vs. velocity of Modified Bouc-Wen model (1Hz,0.1mm/s)</i>	98
<i>Figure 3-15- Damping force vs. velocity of Modified Bouc-Wen model (5Hz,0.1mm/s)</i>	98
<i>Figure 4-1- Active control scheme of conventional bogie vehicle with IRWs</i>	102
<i>Figure 4-2- Modal control diagram</i>	104
<i>Figure 4-3- Lateral mode</i>	110
<i>Figure 4-4-Yaw mode</i>	111
<i>Figure 4-5- Root locus for the design of the stability controller for lateral mode</i>	116
<i>Figure 4-6- Zoom in version</i>	116

Figure 4-7- Root locus for the design of the stability controller for yaw mode.....	117
Figure 4-8- Zoom in version.....	117
Figure 4-9- Root locus of two axle vehicle with guidance controller for lateral mode	118
Figure 4-10- Zoom in version.....	119
Figure 4-11- Root locus of two axle vehicle with guidance controller for yaw mode	119
Figure 4-12- Zoom in version.....	120
Figure 4-13- Two axle vehicles lateral displacement between wheelset and track on curve, 83 m/s.....	128
Figure 4-14- Two axle vehicles lateral displacement between wheelset and track on curve, 20 m/s.....	128
Figure 4-15- Two axle vehicles lateral displacement between wheelset and straight track with irregularity, 83 m/s.....	129
Figure 4-16- Two axle vehicles angle of attack on curve, 83 m/s.....	130
Figure 4-17- Two axle vehicles angle of attack on curve, 20 m/s.....	130
Figure 4-18- Two axle vehicles angle of attack on straight track with irregularity, 83 m/s.....	131
Figure 4-19- Longitudinal creep force on curve track, 83 m/s.....	132
Figure 4-20- Longitudinal creep force on curve track, 20 m/s.....	132
Figure 4-21- Longitudinal creep force on straight track, 83 m/s	133
Figure 4-22- Lateral creep force on curve track, 83 m/s.....	134
Figure 4-23- Lateral creep force on curve track, 20 m/s.....	134
Figure 4-24- Lateral creep force on straight track, 83 m/s	135
Figure 4-25- Active control power on curved track, speed 83.3 m/s.....	136
Figure 4-26- Active control power on curved track, speed 20 m/s.....	136
Figure 4-27- Active control power on straight track with irregularities, speed 83.3 m/s	137
Figure 4-28- Active Control force on curved track, speed 83.3 m/s.....	138
Figure 4-29- Active Control force on curved track, speed 20 m/s.....	138
Figure 4-30-Active control force on straight track with irregularities, speed 83.3 m/s	139
Figure 5-1- Schematic of the semi-active control system with the MR damper.....	143
Figure 5-2- Semi-active minimum and maximum damping forces	144
Figure 5-3- Damping force vs. velocity of Modified Bouc-Wen model	145
Figure-5-4- Semi active controller include Lookup table and MR damper, robust with PI controller	148
Figure 5-5- Look up table.....	149
Figure 5-6-MR damper.....	149
Figure 5-7- Semi active system structure with Look up table and MR damper	151
Figure 5-8- The PI local controller for the MR damper.....	152
Figure 5-9- Validity of inverse MR damper (0.5 Hz, Amplitude=0.1mm)-sin input.....	153
Figure 5-10- Validity of inverse MR damper (0.5 Hz, Amplitude=0.1mm)-sin input.....	154
Figure 5-11- Validity of inverse MR damper (0.5 Hz, Amplitude=0.1mm)-step input.....	154
Figure 5-12- Validity of inverse MR damper, Amplitude=0.1mm, step input	155
Figure 5-13- Validity of inverse MR damper + PI controller (0.5 Hz, Amplitude=0.1mm)-sin input.....	156
Figure 5-14- Validity of inverse MR damper + PI controller (0.5 Hz, Amplitude=0.1mm)-sin input.....	156

Figure 5-15- Validity of inverse MR damper + PI controller (0.5 Hz, Amplitude=0.1mm)-step input.....	157
Figure 5-16- Validity of inverse MR damper+ PI controller, Amplitude=0.1mm, step input.....	157
Figure 6-1- Curve track input at 20 (m/s)	160
Figure 6-2- Cant Angle Input (theta = 6°)	160
Figure 6-3- Curvature track Input (R= 3470 m)for 83m/s, 300 Km/h – 1.....	161
Figure 6-4- Cant Angle Input (theta = 6°)	162
Figure 6-5- Generic track data at the speed of 83m/s, 300 Km/h – 1.....	163
Figure 6-6- Measured Track Data at The Speed of 50m/S.....	164
Figure 6-7- Two axle vehicle angle of attack on curve, 83 m/s- Front wheelset.....	165
Figure 6-8- Two axle vehicle angle of attack on curve, 83 m/s- Rear wheelset	166
Figure 6-9- Two axle vehicle angle of attack on curve, 20 m/s- Front wheelset.....	166
Figure 6-10- Two axle vehicle angle of attack on curve, 20 m/s- Rear wheelset	167
Figure 6-11- Two axle vehicle lateral displacement between wheelset and track on curve, 83 m/s- Front wheelset.....	168
Figure 6-12- Two axle vehicle lateral displacement between wheelset and track on curve, 83 m/s- Rear wheelset	169
Figure 6-13- Two axle vehicle lateral displacement between wheelset and track on curve, 20 m/s- Front wheelset.....	169
Figure 6-14- Two axle vehicle lateral displacement between wheelset and track on curve, 20 m/s- Rear wheelset	169
Figure 6-15- Two axle vehicle lateral creep force on curve track, 83 m/s- Front wheelset.....	170
Figure 6-16- Two axle vehicle lateral creep force on curve track, 83 m/s- Rear wheelset	171
Figure 6-17- Two axle vehicle lateral creep force on curve track, 20 m/s- Front wheelset.....	171
Figure 6-18- Two axle vehicle lateral creep force on curve track, 20 m/s- Rear wheelset	172
Figure 6-19- Comparison of lateral creep force and centrifugal force on curve track, 83 m/s- Front wheelset	173
Figure 6-20- Comparison of lateral creep force and centrifugal force on curve track, 20 m/s- Front wheelset	173
Figure 6-21- Two axle vehicle longitudinal creep force on curve track, 83 m/s- Front wheelset	175
Figure 6-22- Two axle vehicle longitudinal creep force on curve track, 83 m/s- Rear wheelset.....	175
Figure 6-23- Two axle vehicle longitudinal creep force on curve track, 20 m/s- Front wheelset	175
Figure 6-24- Two axle vehicle longitudinal creep force on curve track, 20 m/s- Rear wheelset.....	176
Figure 6-25- Two axle vehicle control force on curved track, speed 83.3 m/s- Front wheelset.....	177
Figure 6-26- Two axle vehicle control force on curved track, speed 83.3 m/s- Rear wheelset	177
Figure 6-27- Two axle vehicle control force on curved track, speed 20 m/s- Front wheelset.....	178
Figure 6-28- Two axle vehicle control force on curved track, speed 20 m/s- Rear wheelset	178
Figure 6-29- Two axle vehicle control power on curved track, speed 83.3 m/s- Front wheelset	179
Figure 6-30- Two axle vehicle control power on curved track, speed 83.3 m/s- Rear wheelset	180
Figure 6-31- Two axle vehicle control power on curved track, speed 20 m/s- Front wheelset.....	180
Figure 6-32- Two axle vehicle control power on curved track, speed 20 m/s- Rear wheelset	180
Figure 6-33- Two axle vehicle angle of attack on computer generic track, 83 m/s- Front wheelset.....	181

Figure 6-34- Two axle vehicle angle of attack on computer generic track, 83 m/s -Rear wheelset	182
Figure 6-35- Two axle vehicle lateral displacement between wheelset and track on computer generic track, 83 m/s- Front wheelset.....	183
Figure 6-36- Two axle vehicle lateral displacement between wheelset and track on computer generic track, 83 m/s- Rear wheelset	183
Figure 6-37- Two axle vehicle lateral creep force on computer generic track, 83 m/s- Front wheelset	184
Figure 6-38- Two axle vehicle lateral creep force on computer generic track, 83 m/s- Rear wheelset	185
Figure 6-39- Two axle vehicle longitudinal creep force on computer generic track, 83 m/s- Front wheelset ...	186
Figure 6-40- Two axle vehicle longitudinal creep force on computer generic track, 83 m/s- Rear wheelset	186
Figure 6-41- Two axle vehicle control force on computer generic track, 83 m/s- Front wheelset.....	187
Figure 6-42- Two axle vehicle control force on computer generic track, 83 m/s- Rear wheelset	188
Figure 6-43- Two axle vehicle control power on computer generic track, 83 m/s- Front wheelset	189
Figure 6-44- Two axle vehicle control power on computer generic track, 83 m/s- Rear wheelset	189
Figure 6-45- Two axle vehicles angle of attack on measured track, 50 m/s- Front wheelset.....	190
Figure 6-46- Two axle vehicles angle of attack on measured track, 50 m/s- Rear wheelset	191
Figure 6-47- Two axle vehicles lateral displacement between wheelset and track on measured track, 50 m/s- Front wheelset.....	192
Figure 6-48- Two axle vehicles lateral displacement between wheelset and track on measured track, 50 m/s- Rear wheelset.....	192
Figure 6-49- Two axle vehicle lateral creep force on measured track, 50 m/s- Front wheelset	193
Figure 6-50- Two axle vehicle lateral creep force on measured track, 50 m/s- Rear wheelset.....	194
Figure 6-51- Two axle vehicle longitudinal creep force on measured track, 50 m/s- Front wheelset.....	195
Figure 6-52- Two axle vehicle longitudinal creep force on measured track, 50 m/s- Rear wheelset.....	195
Figure 6-53- Two axle vehicle control force on measured track, 50 m/s- Front wheelset	196
Figure 6-54- Two axle vehicle control force on measured track, 50 m/s- Rear wheelset.....	197
Figure 6-55- Two axle vehicle control power on measured track, 50 m/s- Front wheelset.....	197
Figure 6-56- Two axle vehicle control power on measured track, 50 m/s- Rear wheelset.....	198
Figure 6-57- Bogie vehicles angle of attack on curve, 83 m/s- Front bogie.....	199
Figure 6-58- Bogie vehicles angle of attack on curve, 83 m/s- Rear bogie.....	199
Figure 6-59- Bogie vehicles angle of attack on curve, 20m/s- Front bogie.....	200
Figure 6-60- Bogie vehicles angle of attack on curve, 20m/s- Rear bogie.....	200
Figure 6-61- Bogie vehicles lateral displacement between wheelset and track on curve,.....	201
Figure 6-62- Bogie vehicles lateral displacement between wheelset and track on curve,.....	202
Figure 6-63- Bogie vehicles lateral displacement between wheelset and track on curve,.....	202
Figure 6-64- Bogie vehicles lateral displacement between wheelset and track on curve,.....	203
Figure 6-65- Bogie vehicle lateral creep force on curve track, 83 m/s- Front bogie.....	204
Figure 6-66- Bogie vehicle lateral creep force on curve track, 83 m/s- Rear bogie	204
Figure 6-67- Bogie vehicle lateral creep force on curve track, 20 m/s- Front bogie.....	205
Figure 6-68- Bogie vehicle lateral creep force on curve track, 20 m/s- Rear bogie	205

<i>Figure 6-69- Bogie vehicle longitudinal creep force on curve track, 83 m/s- Front bogie</i>	206
<i>Figure 6-70- Bogie vehicle longitudinal creep force on curve track, 83 m/s- Rear bogie</i>	207
<i>Figure 6-71- Bogie vehicle longitudinal creep force on curve track, 20 m/s- Front bogie</i>	207
<i>Figure 6-72- Bogie vehicle longitudinal creep force on curve track, 20 m/s- Rear bogie</i>	208
<i>Figure 6-73- Bogie vehicle control force on curved track, speed 83.3 m/s- Front bogie</i>	209
<i>Figure 6-74- Bogie vehicle control force on curved track, speed 83.3 m/s- Rear bogie</i>	209
<i>Figure 6-75- Bogie vehicle control force on curved track, speed 20 m/s- Front bogie</i>	210
<i>Figure 6-76- Bogie vehicle control force on curved track, speed 20 m/s- Rear bogie</i>	210
<i>Figure 6-77- Bogie vehicle control power on curved track, speed 83.3 m/s- Front bogie</i>	211
<i>Figure 6-78- Bogie vehicle control power on curved track, speed 83.3 m/s- Rear bogie</i>	212
<i>Figure 6-79- Bogie vehicle control power on curved track, speed 20 m/s- Front bogie</i>	212
<i>Figure 6-80- Bogie vehicle control power on curved track, speed 20 m/s- Rear bogie</i>	212
<i>Figure 6-81- Bogie vehicles angle of attack on computer generic track, 83 m/s- Front bogie</i>	213
<i>Figure 6-82- Bogie vehicles angle of attack on computer generic track, 83 m/s- Rear bogie</i>	214
<i>Figure 6-83- Bogie vehicles lateral displacement between wheelset and track on computer generic track, 83 m/s- Front bogie</i>	215
<i>Figure 6-84- Bogie vehicles lateral displacement between wheelset and track on computer generic track, 83 m/s- Rear bogie</i>	215
<i>Figure 6-85- Bogie vehicles lateral creep force on computer generic track, 83 m/s- Front bogie</i>	216
<i>Figure 6-86- Bogie vehicles lateral creep force on computer generic track, 83 m/s- Rear bogie</i>	217
<i>Figure 6-87- Bogie vehicles longitudinal creep force on computer generic track, 83 m/s- Front bogie</i>	218
<i>Figure 6-88- Bogie vehicles longitudinal creep force on computer generic track, 83 m/s- Rear bogie</i>	218
<i>Figure 6-89- Bogie vehicles control force on computer generic track, 83 m/s- Front bogie</i>	219
<i>Figure 6-90- Bogie vehicles control force on computer generic track, 83 m/s- Rear bogie</i>	220
<i>Figure 6-91- Bogie vehicles control power on computer generic track, 83 m/s- Front bogie</i>	221
<i>Figure 6-92- Bogie vehicles control power on computer generic track, 83 m/s- Rear bogie</i>	221
<i>Figure 6-93- Bogie vehicles angle of attack on measured track, 50 m/s- Front bogie</i>	222
<i>Figure 6-94- Bogie vehicles angle of attack on measured track, 50 m/s- Rear bogie</i>	223
<i>Figure 6-95- Bogie vehicles lateral displacement between wheelset and track on measured track, 50 m/s- Front bogie</i>	224
<i>Figure 6-96- Bogie vehicles lateral displacement between wheelset and track on measured track, 50 m/s- Rear bogie</i>	224
<i>Figure 6-97- Bogie vehicles lateral creep force on measured track, 50 m/s- Front bogie</i>	225
<i>Figure 6-98- Bogie vehicles lateral creep force on measured track, 50 m/s- Rear bogie</i>	226
<i>Figure 6-99- Bogie vehicles longitudinal creep force on measured track, 50 m/s- Front bogie</i>	227
<i>Figure 6-100- Bogie vehicles longitudinal creep force on measured track, 50 m/s- Rear bogie</i>	227
<i>Figure 6-101- Bogie vehicles control force on measured track, 50 m/s- Front bogie</i>	228
<i>Figure 6-102- Bogie vehicles control force on measured track, 50 m/s- Rear bogie</i>	229
<i>Figure 6-103- Bogie vehicles control power on measured track, 50 m/s- Front bogie</i>	229

Figure 6-104- Bogie vehicles control power on measured track, 50 m/s- Rear bogie 230

List of Tables

<i>Table 1-1- Categories of suspension</i>	37
<i>Table 3-1- Eigenvalues of single independently rotating wheelset</i>	76
<i>Table 3-2- Eigenvalues of Two- Axle railway vehicle without controller</i>	83
<i>Table 3-3- The eigenvalue of the conventional bogie railway vehicle without controller model</i>	92
<i>Table 3-4- Parameter values of the Modified Bouc-Wen model [123]</i>	97
<i>Table 4-1- The eigenvalue of the two-axle railway vehicle for controlled model</i>	122
<i>Table 4-2- The eigenvalue of the conventional bogie railway vehicle with controller model</i>	125
<i>Table 4-3 Active control quantitative performance in different track with different speeds</i>	140
<i>Table 5-1- Force generated by MR damper</i>	150
<i>Table 5-2- Look up table</i>	150
<i>Table 6-1- Quantitative performance evaluations for Two axle vehicles</i>	231
<i>Table 6-2- Quantitative performance evaluations for Bogie vehicles</i>	232

Abbreviations

<i>Symbols</i>	<i>Parameters</i>
V_s	Vehicle forward speed
ω	Rotational speed of wheel
r_0	Wheel radius
g	Gravity
f_{1L}, f_{1R}	left and right wheelset longitudinal contact forces
f_{2L}, f_{2R}	left and right wheelset lateral contact forces
γ_1	Longitudinal Creepage
γ_2	Lateral Creepage
F_x	longitudinal creep force
F_y	lateral creep force
λ	Wheel conicity

f_{11}, f_{22}	Longitudinal and lateral coefficients
F_m	force due to gravity
θ_c	Cant angle of the curve track
F_c	centrifugal force
F_m	force due to gravity
m_w	Wheelset mass
m_v	Vehicle mass
m_b	Bogie mass
L_g	Half gauge of wheelset
L_v	half wheelset spacing of vehicle
J_w	Wheelset yaw inertia
J_v	vehicle yaw inertia
J_ϕ	wheel inertia

J_b	Bogie inertia
J_c	Vehicle body inertia
R	Radius of the curved track at front and rear wheelsets
y_t	Random track (irregularities) lateral displacement, front and rear wheelset
y_w	Lateral displacement of wheelsets
y_v	Lateral displacement of vehicle body (Tow-axle vehicle)
y_b	Lateral displacement of bogie
y_c	Lateral displacement of vehicle body (Bogie vehicle)
θ_c	Cant angle of the curve track
ψ_w	wheelset Yaw motion
ψ_v	yaw angle of vehicle body (Tow-axle vehicle)
ψ_b	yaw angle of bogie
ψ_c	yaw angle of vehicle body (Bogie vehicle)

ϕ_w	Relative rotation angle of two wheels
τ_w	wheelsets Control torque
K_{py}	Primary lateral stiffness
K_{sy}	Secondary lateral stiffness
K_{sx}	Secondary longitudinal stiffness
C_{py}	Primary lateral damping
C_{sy}	Secondary lateral damping
C_{sx}	Secondary longitudinal damping
F_{pyw}	Forces of the primary suspension system in lateral direction
F_{syb}	Forces of the secondary suspension system in lateral direction
F_{sxb}	Forces of the secondary suspension system in longitudinal direction

List of Publications

1. T X Mei, A Zaeim, Hong Li, *Control of Railway Wheelsets – A Semi-Active Approach*.
The IAVSD International Symposium on Dynamics of Vehicles on Roads and Tracks
2019: Advances in Dynamics of Vehicles on Roads and Tracks pp 16-23
2. A Zaeim, T X Mei, Semi-active control for independent rotating wheelset in
a railway vehicle, Sparc 2018, Salford university

Acknowledgements

I would like to thank my supervisor, Professor TX Mei, for providing me the opportunity to do this work, for guiding me through the research and for lots of great inspiration, ideas, and comments.

I would like to acknowledge Mrs Marry Landon Goodman for the support and funding which has made this study possible.

I also would like to thank Davina Whitnall for her help and support during all the difficult days that I had with University of Salford.

I cannot begin to express my sincere gratitude and love to my husband Tom who endlessly supported me throughout this process, has constantly encouraged me when the tasks seemed arduous and insurmountable and also for his faith in me while I didn't have faith in myself.

Also, I would like to thank our beloved Chewie and Louie (our little cutie dogs) who always cheers me up when I was in desperate need of it.

Last but not least, I would like to thank my parents for their love and support throughout my life and specially during last few years from the other side of the world. Thanks to them for giving me strength to reach for the stars and chase my dreams. Without their support it was impossible for me to finish this my thesis.

Abstract

This thesis presents details of an investigation of a controller for MR damper in the implementation of semi-active control, for primary suspensions of the independently rotating railway vehicles.

This research focuses on using MR damper and it addresses on three main aspects when designing semi-active control systems for this application.

One aspect is magnetorheological dampers categorised as a controllable fluid damper which can reversibly change from a flowing viscose fluid to semi-solid viscose fluid. The second aspect is the controllable yield strength can change in a millisecond by inducing an electric or magnetic field. Third aspect is MR damper is cheaper than actuators which are usually use in full active controller

This research is a combination of a lookup table based on the inverse MR damper model to control the current input (to the MR damper) from required force and relative velocity of the device. The MR damper produces the desired force as precisely as possible. However, it is not possible to have precise knowledge of MR parameters and it is also difficult to account for the hysteresis present in MR dampers in the lookup table. Therefore, an additional local PI feedback controller is also used to improve the robustness for the MR control.

As the main result, this study provides a comparison between semi-active controller with the use of MR damper and a full active controller system. The results show semi-active controller with the use of MR damper performed as good as full active controller.

However semi-active control systems with MR dampers offer an overall efficiency and robustness when compared to the full active control system. Also, this system delivers comparable performance with the benefit of increased reliability and lower cost.

In order to assess the developed system comprehensively, a two-axle vehicle model and a full bogie vehicle model are both evaluated individually in the study.

The performance and robustness assessments of the developed semi-active controller with the full active control system are evaluated with the use of both two-axle vehicle model and the full bogie vehicle model with different operational track features such as curved track and straight track with lateral irregularities with various travel speeds.

This study designed and developed a semi-active control systems with use of MR damper in primary suspension for independent rotation wheelsets in railway vehicles. Computer simulation results verified the suggested semi-active control is able to provide required stability and guidance control for independently- rotating wheelsets. Also, the result performed as well as full active control with the advantage of utilizing a lower cost device for semi-active control rather than an expensive actuator for full active control.

Chapter 1:

1.1 Background

In today's world, railway is a particularly popular form of transportation. In comparison with other forms of transportation, trains are safe, high speed, cheaper and environmentally friendly [1, 2]. By the expansion of high-speed trains, there is increasing demanded for improved ride quality, reduced noise and enhanced stability of railway vehicle [3]. On the other hand, suspension systems have a significant impact on ride quality and stability, which are mechanisms which physically connect the railway vehicle body from bogies, or bogies from the wheelsets. In other words, the suspension system supports the railway vehicle weight and isolates the railway vehicle body from disturbances due to the surface on which it is travelling. It is notable that, in general, suspension is one of the most necessary parts of a railway vehicle to improve stability and running behaviour.

1.2 Railway Vehicles

A conventional railway vehicle consists of a railway vehicle body, two bogies and four wheelsets. Bogies are classified as front and rear bogies. Each bogie is connected to two wheelsets through primary suspensions and connected to the vehicle body through secondary suspensions as it shown in Figure1-1. Bogies are used in railway vehicles to support the railway vehicle body as well as improve stability and curving performance. All primary and secondary suspensions are designed in lateral and longitudinal directions. Active and semi- active controller designs are intended to improve ride quality by controlling the secondary suspension or improve stability and guidance by controlling the primary suspensions [4].

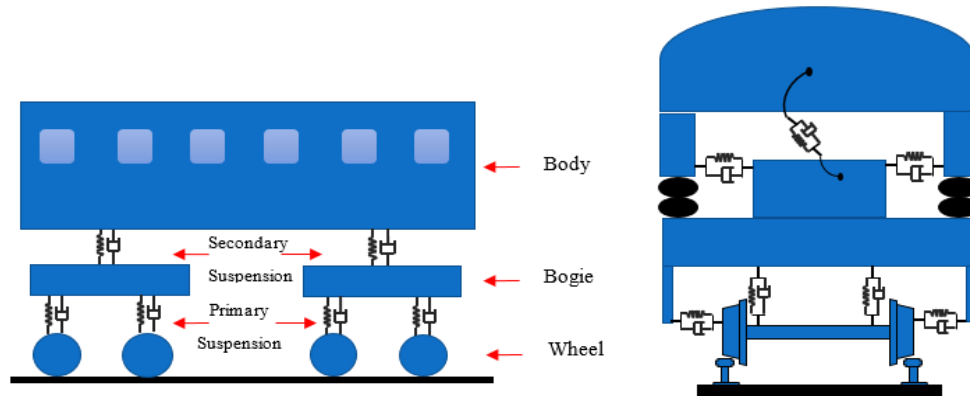


Figure 1-1- Basic side and end view of wheelsets and bogie showing how suspension units are located

1.3 Wheelsets

The most common railway wheelsets are solid axle wheelsets, which have been used effectively for more than 170 years for the reason that they are naturally self-curving and centring;

A solid axle wheelset consists of two coned/profiled wheels that rigidly fixed to an axle hence they rotate at the same angular displacement. The radius of the wheel on the contact point between the wheel and the rail is the rolling radius.

When an unconstrained wheelset travels through a curved track it is displaced laterally such that the outer wheel runs on the larger radius and inner wheel run on a smaller radius. Hence, it makes the wheelset move toward the curve and provide a natural centring/curving action.

However, solid axle wheelset is inherently unstable, which is best explained when it runs on a straight track. While the wheelsets are moving forward on the track and are displaced laterally, the wheelset moves toward the track centre line, cross it and overshoot to the other side, which can cause an oscillating motion along the track. The basic mechanism of the wheelset therefore results in an effect known as the kinematic oscillation of the wheelset as shown in Figure 1-2.

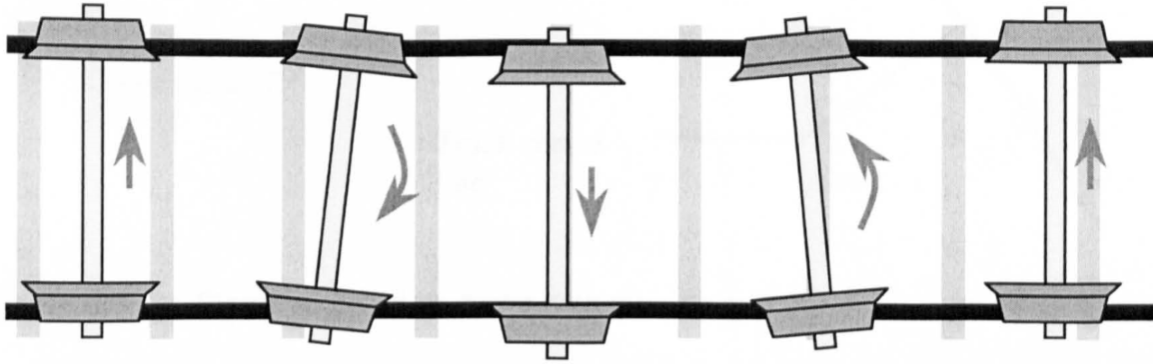


Figure 1-2- Wheelset kinematic oscillation [5]

To combat this instability, the conventional solution is to connect each wheelset to bogie through a longitudinal spring. These springs produce non conservative creep forces at the wheel-rail contact point and provide stability for hunting motion. The stiffness of the spring is selected at the critical speed when the wheelset becomes unstable. However, the force which is generated by the stabilising longitudinal springs interferes with the natural curving behaviour of the wheelset while wheelset moving along a curve because two wheels of the wheelset are forced away from the pure rolling lines resulting in large creepages between rail surfaces and wheels [6].

It is always a challenge to trade-off between stability and curving for passive suspension. A stiff spring will give better high-speed running stability but does not perform well with curving. Conversely, a softer spring cannot provide good high-speed running stability while the performance on curves is better [5-7].

An alternative way of confronting this problem is the use of independently rotating wheelsets (IRW). In independently rotating wheelset the two wheels on the same axle rotate independently of each other [6, 8, 9]. In this system, by taking out the limitation of the rotational motion of the two wheels, the longitudinal creep force through the wheels is notably reduced, and thus there is no need for the pure rolling action of the wheelset.

Independently rotating wheelsets have some disadvantages, such as the lack of natural self-curving as in the case of solid axle systems. This is because the two wheels are able to rotate freely with respect to each other. Therefore, for independently rotating wheelsets some sort of guidance control to deliver stability on curves is essential.

Controlling the wheel-rail deflection directly is one method by which to restore the guidance action of the wheelset. However, this method would be very expensive to achieve in practice because feedback is not available. [10]. On the other hand, instability still exist in independently rotating wheelsets systems, and additional affect is necessary to avoid vibrations in practice [11, 12].

1.4 Vehicle Suspension Systems

Suspensions in railway technology can be categorized in two different ways:

1. Primary suspensions, which provide the stability and guidance.
2. Secondary suspensions, which control the ride quality.

To date, passive suspensions are most commonly used in railway vehicles. A passive suspension typically consists of a spring and damper with constant stiffness and damping coefficients, which are calculated by the designer considering railway vehicle speed, acceleration and characteristics of the railway track. Passive dampers cannot supply energy to the suspension system and, depending on relative velocity, will just only dissipate the input energy. It is notable that passive suspension is not flexible, as the suspension properties are fixed meaning damping rate is constant. Therefore, such suspension performance depends on the wide range of bandwidth excitation might be bounded [13-16]. Passive suspension has a number of advantages. For instance, it is cost-effective and has simplicity of design. In addition, the efficiency associated with a large frequency range of excitations induced by any track irregularities can be limited [14-19]. Figure 1-3 shows a primary and secondary passive suspension unit.

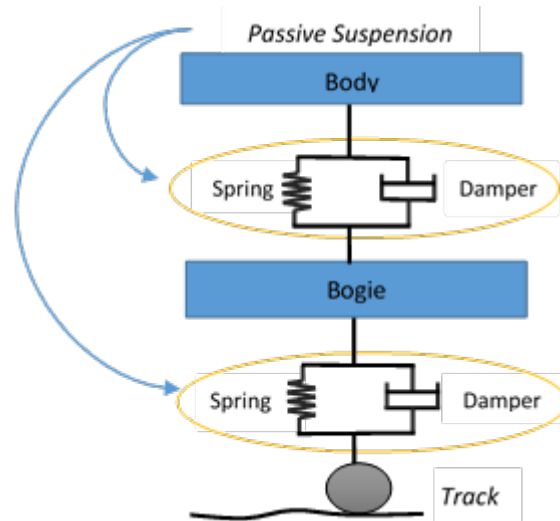


Figure 1-3- Secondary and primary Passive suspension

1.4.1 Passive Primary Suspensions

Primary suspension links the wheelsets and bogies. Primary suspension units are designed to improve stability and provide guidance. However, it has always represented one of the biggest challenges in the field of railway vehicles with use of passive suspension. A railway vehicle at critical speed on a straight track is entirely dependent on stiff wheelset guidance, particularly in the longitudinal direction, which is frequently used together with stiff yaw damping between vehicle body and bogie. However, this can badly affect curving performance, because high stiffness of primary suspension decreases radial steering ability. Larger track shift forces and a larger amount of wheel and rail wear is a consequence [20].

Over the years, designing a bogie suspension system has been developed and improved. It was identified that use of a cushion is essential to decrease vibration felt inside the carriages in the space between the body of the railway vehicle and the wheel. This usually consists of a leaf steel spring mounted on the axles. Over time, this has been developed to a bogie system which act as a primary filter for isolating vibration with a more complex suspension.

Most railway vehicles utilise bogies to carry and guide the railway vehicle along the tracks. Bogies are designed to carry the weight of vehicle it supports. In addition to guiding railway vehicle along the track using the wheels and improve curving by reduced wheel-spacing. Also, deliver some degree of cushioning facing to the turbulence which is transmitted from the track

irregularity during travel. A conventional bogie frame is turned into the curve through the leading wheelset as it is guided by the rails. However, there is a degree of lateral motion and a lot of force is required to allow the change of direction.

1.4.2 Passive Secondary Suspension

The suspension that connects the vehicle body to the bogie is called the secondary suspension, which provides improved ride quality by offering better isolation of the railway vehicle body from excitations transmitted from track irregularities. The secondary suspension is usually controlled in the lateral direction, including the yaw mode, and in the vertical direction, including the pitch mode.

High-speed railway technology has developed noticeably in recent years, not just as an efficient means of transportation but also an economical one. However, increasing the speed and the expansion of high-speed railway vehicles can decrease the ride stability, ride comfort, and also increase costs of train maintenance due to affect vibration of the railway vehicle body and bogies. In view of controlling such vibrations, different types of suspension have been designed. Suspensions units usually include passive springs and dampers in either parallel or/and series, where the static weight of the railway vehicle is supported through spring and damper control where the input from the track is passed on to the vehicle and dissipates vibrational energy [14, 21]. Also, in railway vehicle air-spring suspension used in secondary suspension to improve ride quality [22].

In other words, improved suspension designs can make it possible to achieve a better ride quality by isolating the vehicle body from track irregularities, therefore reduce the body displacement and acceleration as well as improve stability and guidance [13].

1.5 Active Suspensions

Active suspension systems can overcome passive suspension limitations by controlling particular variables that are not possible with passive suspension as shown in Figure 1-4.

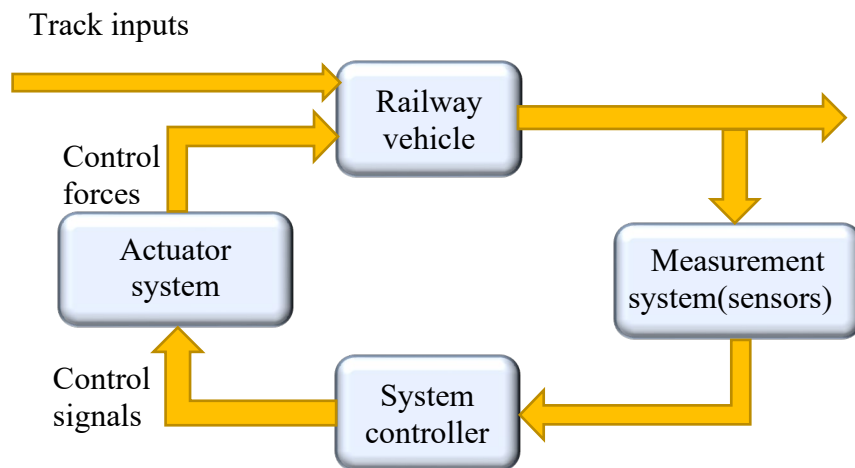


Figure 1-4- Principles of an active suspension system [4]

Active suspensions, with the use of actuators and sensors, can be used to control the system by dissipating energy or applying a force to the system from the suspension itself [23]. However, it is obvious that such a system needs an external source to generate power to activate different components. An active controller can show better control performance over a large frequency range [13, 15]. But, active suspension system have a few disadvantages, such as high cost, complicated design and also the requirement for high power [24]. Figure 1-5 shows a primary and secondary active suspension unit.

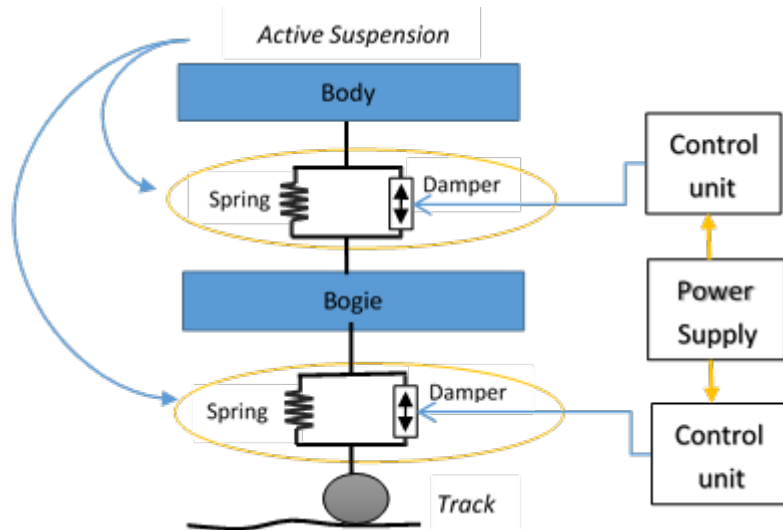


Figure 1-5- Secondary and primary Active suspension

Active suspension systems can be divided into different classes such as primary full active suspension and secondary full active suspension, primary semi-active suspension and secondary semi-active suspension depending on the location and control method that it used.

1.5.1 Active Primary Suspension

An active controller can be used in the primary suspensions [25]. Active primary suspension is designed to increase running stability quality on a straight track as well as improve curving performance, which is very difficult trade-off for passive suspensions. An active controller can be used for either independently rotating wheelsets (IRW) or a solid axle [26-28].

Control strategies are different in independently rotating wheels and solid axle. In independently rotating wheels the approach of active control is to increase stability and improving guidance control on curving and straight track. The main aim of active control for solid axle is to provide effective stabilization for hunting problem as the conventional solid axle wheels is kinematically unstable. In addition, it is essential to provide steering for solid axle wheelset on the curve if the yaw stiffness in vehicle (passive) suspensions severely interferes with curving.

There is a diversity of methods to improve stability and guidance through active technology. In between can be mentioned methods like actuated solid wheelset, actuated independently rotating wheel, driven independently rotating wheel, directly steered wheels and secondary yaw control, which is explained in literature review [28, 29]. However, issues mentioned earlier are the reasons for developing better technology to overcome the mentioned challenges.

1.5.2 Active Secondary Suspension

The active control for secondary suspension improves passenger comfort by producing better isolation of the body of the vehicle from excitations transmitted from track irregularities. The secondary suspension is usually controlled in the lateral direction, including the yaw mode, and in the vertical direction, including the pitch mode.

In an active controller, actuator can be utilized to replace the passive suspension, thus the active controller will control suspension behaviour. However, in practical application it would be more effective to use a combination of actuator and passive components. They can be used either in parallel or series [16].

In parallel case, the size of an actuator can be noticeably reduced because in this instance, the passive component is mainly responsible for providing a constant force to support the body mass of a vehicle in the vertical direction or quasi-static curving forces in the lateral direction. In series case, where a spring fitted in series with the actuator can be useful to help with the high frequency problem due to lack of response in the actuator movement and control output at high frequencies. Therefore, in real applications a combination of a parallel spring (for load-carrying) and a series spring (for help with the high frequency response) can be the best configuration to optimise design and performance.

In the series spring, the stiffness can be of comparatively high value or a softer, low value depending on the technology. Comparatively high value of stiffness can be used for technologies such as hydraulics which have good high frequency performance. In addition, softer, low value stiffness can be used for other methods where achieving a high bandwidth is more problematic [30].

Essentially, active secondary suspension methods are utilized to obtain a couple of following options. Providing and improving ride comfort can be one of the primary aims. In addition, the feasibility of increasing speed of railway vehicle and utilizing the improved performance to maintain desirable ride quality, reduced journey time and increased utilisation of the railway vehicle bringing benefits that offer a clear rationale for the use of an active suspension technology in secondary suspension [28].

One of the control methods which has been extensively studied is sky-hook damping. Sky-hook damping is a high bandwidth system that is utilized to provide better performance for suspension, by the provision of damping to an absolute datum [31].

However, the control approach can have a significant effect on deterministic features such as curves and gradients. Although this can be modified in the control design, for example, by filtering out the low frequency components from the measurements that is largely caused by track deterministic features. It should be considered that reducing the deterministic deflections to an acceptable level will compromise the performance achievable with pure sky-hook damping [28].

1.5.3 Semi-Active control

A semi-active suspension system has the same basic configuration as the passive suspension, but with a controllable damping rate for the damper. Semi-active suspension, however, can be considered as a system which is a combination of active and passive suspension. The damping force in semi-active suspension is able to change in response to different inputs; furthermore, one of the principal advantages of semi-active suspension is that, for different variations to the damping force, the system does not need high power. One of the other advantages of semi-active suspension is that if for any reason the control system fails, the system still can behave as passive suspension [15, 32]. Figure 1-6 shows a primary and secondary semi-active suspension unit.

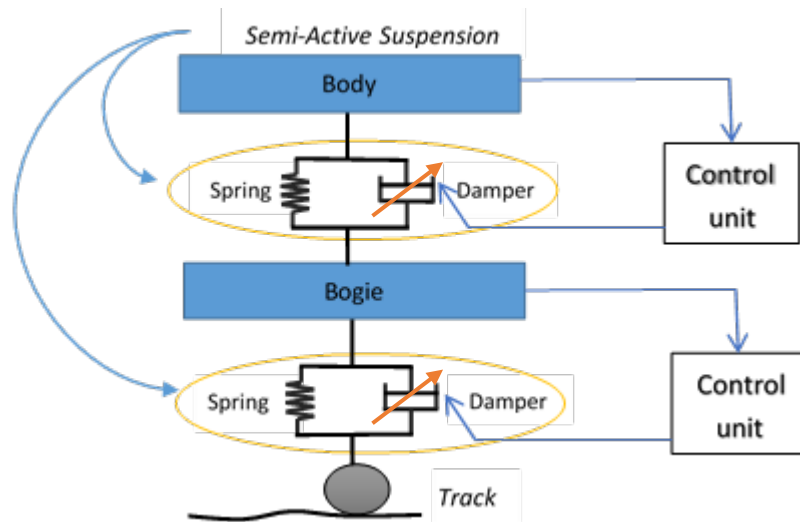


Figure 1-6- Secondary and primary Semi- Active suspension

One disadvantage of a semi-active damper is that the force remains dependent on the suspension velocity of the damper movement, which means that a large force cannot be generated at low speed. A second is that the tracking of any required force is an issue; a semi-active damper is not able to develop a positive force when the speed reverses, and because of this such a system can only dissipate energy, as the injection of energy is not possible [27]. This issue shown clearly in Figure 1-7. This limitation upon controllability restricts the performance of a semi-active suspension to a significant degree.

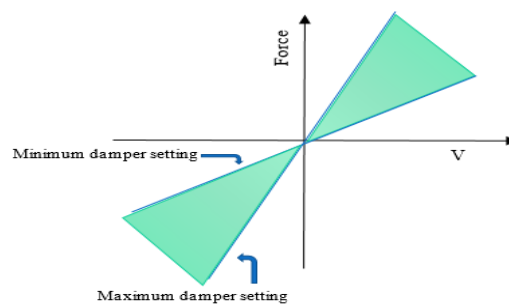


Figure 1-7- Semi-active damper force-velocity characteristics

1.5.4 Actuators and Sensors for an Active Suspension

In conventional suspension, passive damper can be used to substitute with actuator, either between wheelsets and bogies or between bogies and body. The active suspension actuators included sensors add particular control law that can be able to produce the control force demanded for the actuator. An actuator actively produces the demanded damping force according to control system desire force for wide range of bandwidth and without time delay. However, how this achieves depend on actuators performance [20]. Though, it is not realistic and in real applications the balance of the parameters such as cost, bandwidth actuator performance can be a challenge. There are few different types of actuators that have being used in railway vehicle that will be mentioned below.

1. **Servo-Hydraulic Actuator:** The positive points of this style of system is high forces can be generated from a relatively small size device, however they have high power consumption. High frequency movements can be problematic for this system, it can be challenging to pump the oil in and out of the actuators at high frequencies resulting in reduced effectiveness in the actuator, maintaining lower forces in the presence of high frequency movements is a regular occurrence for train wheelsets, as such this is a fundamental issue. Initial purchase cost and on-going maintenance cost maybe high.
2. **Servo-pneumatic Actuators:** Similar to servo hydraulic systems except air is used instead of oil as the operating fluid, maintaining air pressure is inherently inefficient due to ongoing power consumption. Reasonably high forces can be generated however not as high as hydraulic. Pneumatic systems performance in high frequency applications is limited due to the compressibility of air. Pneumatic systems are widely used in rail vehicle applications.
3. **Electro-Mechanical Actuators:** Torque from an electric motor is converted it into a linear force by rotating a leadscrew, this in turn exerts a linear force on the nut (as this is restrained and unable to rotate but slide in a transverse direction).

Accuracy and repeatability levels are always much higher when compared to hydraulic and pneumatic systems, there is also the advantage of no fluids to leak from the system. High frequency movements require rapid acceleration of the motor, large motors maybe required to generate required acceleration. Gearboxes can be added to the system to generate higher forces however this may have a detrimental impact on response to high frequency movements. Implementing Pulse Width Modulated" (PWM) control of the motor will avoid the power losses observed with a servo–valve.

4. **Electro–magnetic Actuators:** Range of motion can be limited however for active control applications in rail vehicles this will not be a limiting factor. Implementing Pulse Width Modulated" (PWM) control allows for efficient control. The main disadvantage is the physical size as the system can be large

The track input has a significant effect on the dynamic system, which will induce actuator movement. Thus, to keep the actuator force as much as possible close to the desired force, the control signal will be adjusted by actuator force controller. Subsequently, the desired force is determined depending on the railway vehicle output signals measured by sensors. The feedback signals in turn depend on force that are produced by actuator managing the mechanical system. Hence, the control loop is closed.

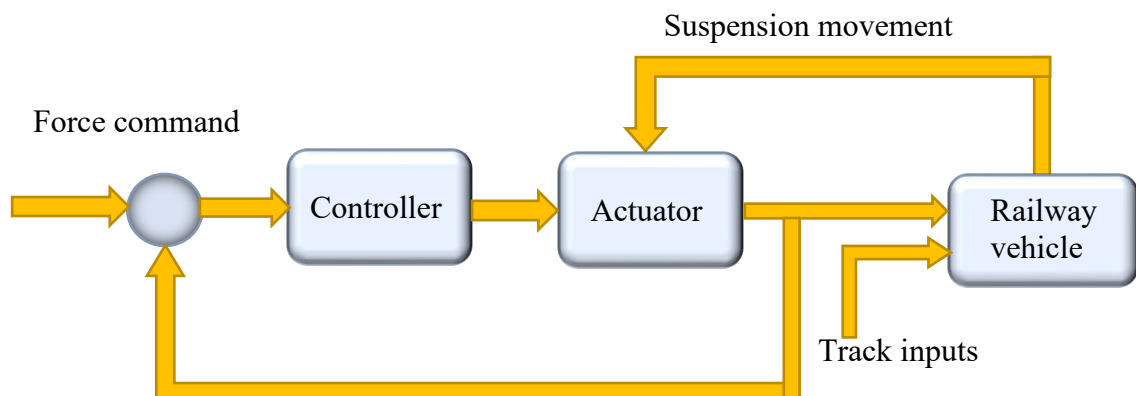


Figure 1-8- Actuator force controller [27]

Figure 1-8 shows the actuator force control, which is a generalised scheme of a force-controlled actuator [27].

1.6 Semi-Active Devices

Controllable devices are mainly suitable for semi-active suspension systems. Different varieties of energy dissipating devices, such as variable orifice, variable stiffness, electromagnetic devices and controllable fluid dampers include electrorheological dampers (ER) and magnetorheological dampers (MR) have been utilized to obtain the desired damping force for the intention of a semi-active damping controller.

However, variable orifice damper combined with oil cylinders and mechanical valves. Variable orifice damper changes the size of an orifice in the hydraulic flow valve, adjusting the damping force. Therefore, the system reliability could be reduced, and the maintenance could be costly. Also, performance of this type of dampers can significantly reduce due to the time delay of the valves with mechanical elements [14].

The controllable fluid damper can reversibly change from a flowing viscous fluid to semi-solid viscous fluid. The yield strength is controllable and can change in milliseconds by inducing an electric or magnetic field [14].

Control of semi-active damper can be clustered into two types: on-off class and constantly variable class. On-off class semi-active damper depends on an appropriate control algorithm that can be switched to on (maximum damping) or off (minimum damping) mode as shown in Figure 1-9.

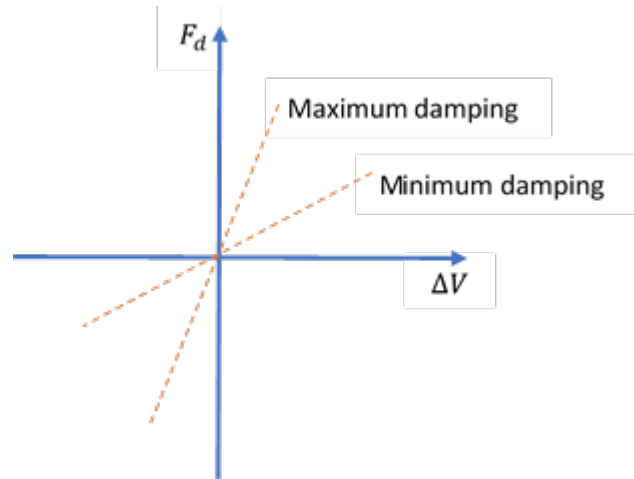


Figure 1-9- Semi-active damper on- off class

The different between on-off switched semi-active damper and constantly variable semi-active damper is when constantly variable semi-active damper is in the on-mode, damping coefficient and corresponding damper force can be varied by different range of magnitude. Figure 1-10 shown the constantly variable damper class.

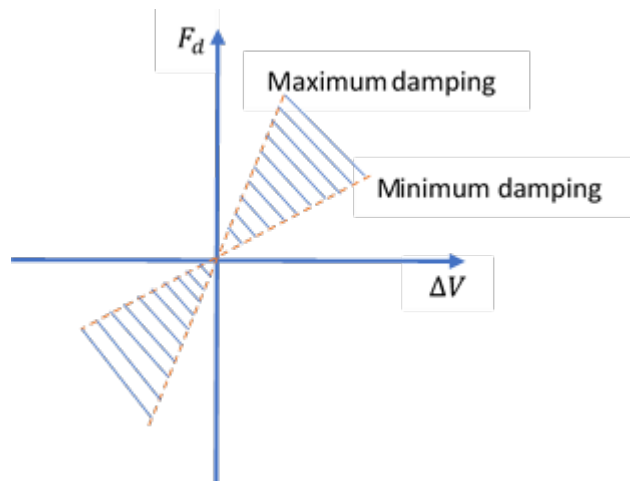


Figure 1-10- Semi-active damper constantly variable class

The performance of a semi-active control system is mostly governed by the control strategy employed. Semi-active controller systems include typically a system controller as well as a damper controller as it shown in figure 1-11. The system controller produces the desire force regarding to the feedback signal that measured by sensors. In addition, the damper controller sets the control signal in terms of tracking the desire damping force. The common design of semi-active controller is more focussed on control strategy.

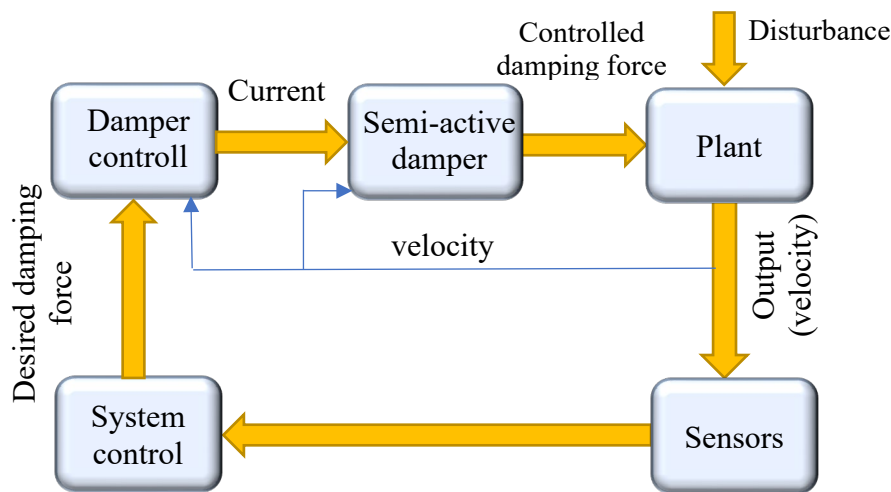


Figure 1-11- Semi-active suspension [33]

A smart fluid is a fluid that the properties such as viscosity is changeable by inducing an electric field or a magnetic field .An MR damper is a device with the advantage of a simple mechanism, quick response (almost milliseconds) and has only low power requirements, all of which are suitable for a railway vehicle [17]. An MR fluid can change its rheology from fluid to semi solid when so induced by a magnetic field. It is of particular interest here that an MR damper can change the damping force over a variable range with only a very low current (1-2 Amps) or a very low voltage (12-24 Volts) [34]. Therefore, such a device can be considered suitable for use on a railway vehicle.

The reason for using MR damper in this research is because of the fast time response, low power demand, simple mechanical structure and, if for any reason if the device fails, it is safe and will work as a passive damper. In addition, the nature of the MR damper changes when the

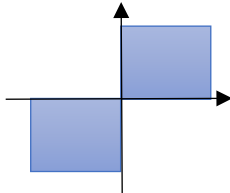
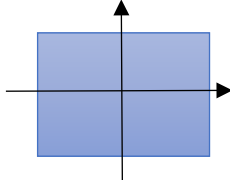
rheological fluid is exposed to a magnetic field, changing its stiffness and damping coefficient. Therefore, MR dampers are able to change their effective damping force upon the application of the control current/voltage to the damper. A semi-active control that uses an MR damper requires a systems controller and a damper controller. The system controller generates the desired damping force concerning the dynamic responses of the suspension, and the damper controller adjusts the input current to track the desired damping force.

Controllable suspension can be accomplished relevant to the energy input and the bandwidth of the actuator. It is possible to categorize controllable suspension in three ways:

1. The controllability range, or in other words the range of force that the actuator delivers.
2. Control bandwidth, or how fast the actuator can respond.
3. The power required for maximum controllability range and control of the bandwidth.

Briefly, the categories of dampers are as shown in table 1-1 and Figure 1-12 [35].

Table 1-1- Categories of suspension

System	Damper control range
Semi-Active	
Active	

Invariably, in terms of controllability range, active and semi-active suspension units are capable of controlling vehicle dynamics. However, it should be noted that the active controller performs better due to the relatively large range of forces it can deliver but, large energy

requirement. On the other hand, semi-active suspension is always play safer due to passive constrain. Also, the requested power will always be very low. [35].

1.7 Research Topic

Active suspension technologies used for railway vehicles have been studied by various researchers to negate the drawbacks of using passive suspension technologies to obtain high control performance over the wide bandwidth of the frequency excitations due to the irregularities of the rail tracks. Nevertheless, high cost, external power supplies, high power demand, and sophisticated control implementations are some of the constraints for active suspension technologies. [14, 36]. However, a semi-active suspension can be another decent option to avoid disadvantages of active controlled.

One of the few great benefits of using semi-active suspension is that, separate power supply for the actuator or high power is not needed. In addition, semi-active controllers compared to active controller is more cost-effective that it makes it possible to use reduplicated for safety. Additionally, in the case of any failure, the control system will perform safely as it will revert to a passive system.

The disadvantage of a semi-active dampers is that the force depends on the damper movement velocity. In other words, the damper is not able to produce a large force once the velocity is low. In addition, a semi-active system is not able to develop a positive force while the speed is not positive (reverses). The lowest and highest levels of force which are limited in two quadrants shown is figure 1-10, While the coverage for an actuator in a full-active system is all four quadrants, (table 1-1). That can explain why performance in semi-active suspension can be limited to a notable degree.

This study is focussed on the development of a semi active control strategy for the primary suspensions for independently rotating wheelset in terms of improving guidance and stability.

primary semi-active stabilization for independently rotating wheelset can be very interesting due to the fact that it offers lower power. Moreover, it is low cost because the semi-active controller does not need sensors and the actuator uses dampers (such as MR damper), which are much cheaper than actuators. In addition, they do not need a large power source as they only generate low power. However, it can be very challenging as the limitation of semi

active device due to they cannot produce force then the system must always dissipate energy meanwhile control is safety critical and always needed. Therefore, the semi-active control can be applying just for systems which, need to absorb energy rather than produce it.

1.8 Aim and Objective

This study is aimed to develop an effective semi-active control scheme for improved ride stability and guidance for primary suspension in an independently rotating wheelset railway vehicle.

In order to achieve this aim, the following research objectives have been identified:

A literature review was first carried out to study the previous work and to establish a fundamental understanding of railway wheelset dynamics, railway vehicle suspensions, the concepts of active control and semi active control studies. Hence, the literature review led to the identification of knowledge gaps and potential research topics for this study. therefore, study carry out with an extensive literature review on MR dampers and its control.

This was followed by the development of the mathematical models representing the single independently rotating wheelsets, the Two-Axle Vehicle with Independently Rotating Wheelsets and conventional bogie railway vehicle and the implementation of the models in the MATLAB Simulink platform. Also, a mathematical model of the modified Bouc-Wen model (prototype of magnetorheological dampers) was developed to represent the dynamic behaviour of a magnetorheological dampers.

The models were then used to design and fine-tune the active controllers. An analysis of the power/force requirements of such active control approaches was also completed leading to the development of the semi-active control strategy for independently rotating wheelsets in the next step. MR damper is used as the actuator device for the proposed semi-active control. However, a controller is essential to control current in order for MR dampers to generate the desired force. Due to complexity of mathematical models and highly nonlinear magnetorheological damper inverse model method has been used as a local magnetorheological damper controller. The technique used in this study for inverse model is Lookup table. The lookup table has been used to attain controlled current regarding to demanded damping force, the controlled current is fed to the magnetorheological damper.

The research followed up by model the full active steering control systems for independently rotating wheelset in MATLAB Simulink platform, based on measured relative rotation speed of the two wheels on the same axle, and the relative yaw velocity between the wheelset and vehicle body as the required feedback.

Next step shows the design details of a novel semi-active scheme for the control of independently rotating wheelsets (IRW) in railway vehicles, using magnetorheological (MR) dampers to provide the necessary stabilization and guidance control. Magnetorheological (MR) dampers are used to replace the actuators in the full active control, leading to a solution that would be safer, cheaper in costs and smaller in size than the full active control systems. Because the semi-active control devices such as MR dampers can only dissipate energy, one of the keys focuses of the study is to develop and verify the control strategy that does not require the injection of power into the system in the provision of the stability control and guidance/steering. To ensure that the MR dampers will produce the control force as demanded by the wheelset control, a lookup table for the inverse MR damper model is used in this study to obtain the control current according to the desired damping force, whereas a local PI control is also used to improve the robustness of the MR damper control. Computer simulations are used to demonstrate that the MR dampers with the combination of the local feedforward and feedback controls can produce the output forces in semi-active control conditions.

Eventually, a comprehensive evaluation of the proposed semi-active controller was carried out by comparing the results of the semi active controller with the full active controller for both the two-axle vehicle and the conventional bogie vehicle. The performance of the semi-active control was assessed using a number of different track conditions including the irregularities and curved tracks at different operating speeds

1.9 Contributions

Objectives associated with this research are leading to the eventual study of MR damper and its effect on the overall performance of semi-active in primary suspension wheelset (as an alternative to passive suspension with springs/dampers or an active controller) to improve stability and provide guidance.

Essentially the research contribution of this study is a novel control strategy with the use of semi-active approach for primary suspension to improved ride stability and guidance in an IRW wheelset railway vehicle. Additionally, the result of semi-active controller is comparable and

performs as well as the active control approach. However, the study demonstrates advantages and benefits of semi-active control, such as a lower cost device, lower power which is not injected into the system and increased reliability.

1.10 Research Methodology

This study is accomplished using the computer simulation based on the dynamic models of a two-axle vehicle and a conventional bogie vehicle with independently rotating wheelsets since it enables to avert the practical difficulties and investigate dynamics of the vehicle thoroughly. Also, the design and analysis of the active control and semi-active control strategies for guidance and stability of wheelsets for the two axle and the conventional bogie vehicle have been carried out. To evaluate the vehicle dynamics and control configurations, three different types of track data, curved, Generic track data irregularity and Measured track data have been used in the research.

As it is shown in Figure 1.12, the research started by establishing a fundamental understanding of railway wheelset dynamic, railway vehicle suspensions and also the concepts of active control and semi active control studies. Literature reviews are then carried out to study the previous work and identify the areas of further study in order to focus and improve any potential areas.

This is followed by the development of the mathematical models representing the plan view dynamics for the two-axle vehicle and the conventional full bogie vehicle and the implementation of the models in the MATLAB Simulink platform. The models are also used to design and fine-tune the active controllers and also to analyse the power requirements of such active control approaches leading to the development of the semi-active control strategy for the independently rotating wheelsets in the next step. MR dampers are used as the control device for the proposed semi-active control and a local control for the MR dampers is also developed to ensure that the control device can provide the control effort as demanded by the wheelset controller.

Lastly, a comprehensive evaluation of the proposed semi- active controller has been carried out by comparing the results of the semi active controller with the full active controller for both the two-axle vehicle and the conventional bogie vehicle.

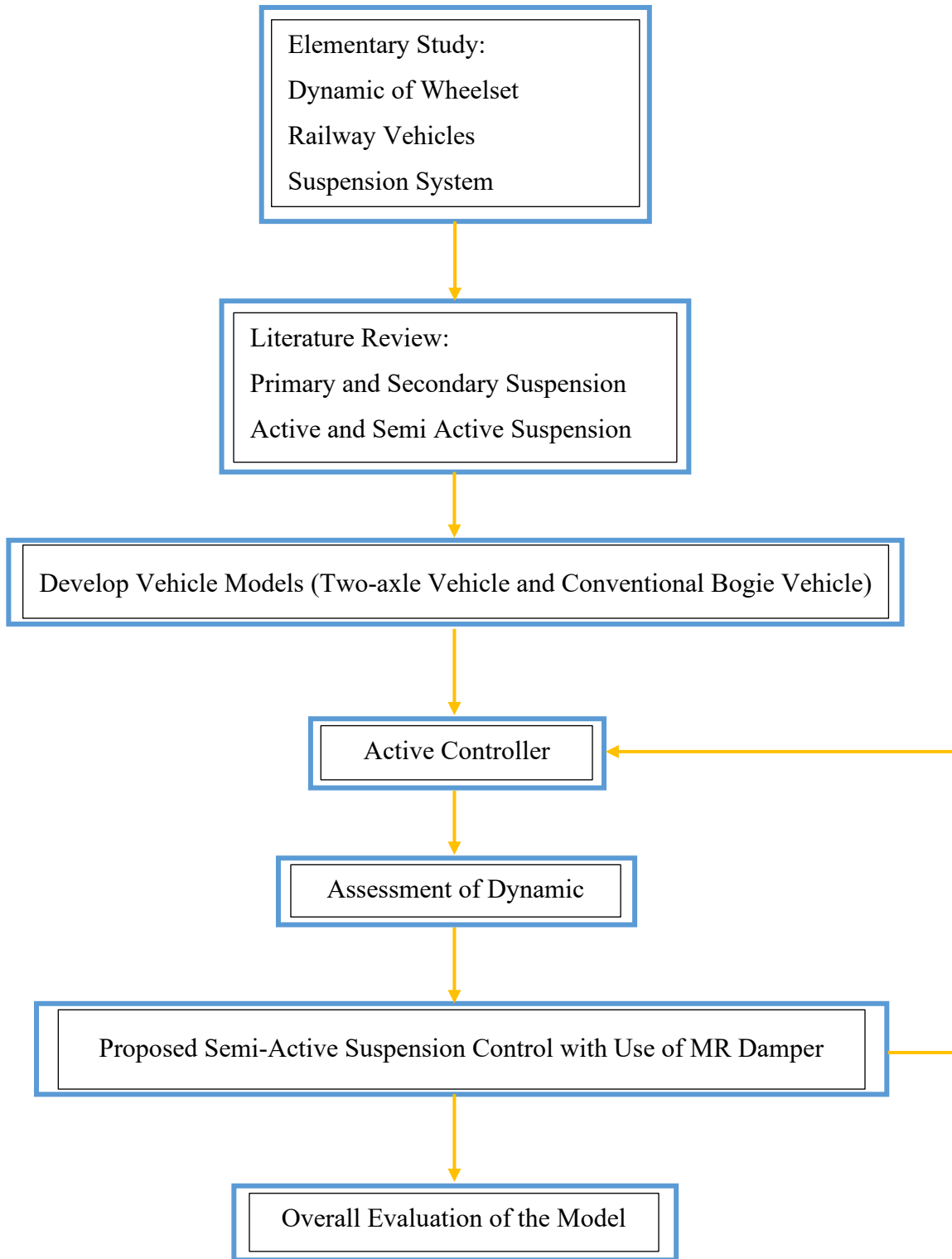


Figure 1-12- – Flowchart of the research

1.11 Structure of Thesis

The structure of this thesis as follows:

Chapter one is the introduction, which includes a brief background of railway vehicles, wheelsets, vehicle suspensions systems full active and semi active suspension as well as presenting the research topic, aim and objectives and research methodology.

Chapter two presents a literature review on existing suspension systems, primary and secondary suspensions, and their categorisation as either passive, full-active or semi-active; the literature review also gives a comprehensive study into these systems with use of MR dampers, and ultimately compares active and semi-active systems.

Chapter three is concerned with the modelling of the vehicle dynamics, including the modelling of the independent rotation wheelset, two axle vehicle, conventional bogie vehicle and magnetorheological damper

Chapter four presents the design and tuning of the full active controller. This chapter presents the wheelset active controller for stability and guidance controller for two axle vehicle and develop the active controller for conventional bogie vehicle. In addition, it presents the simulation results under different track conditions.

In Chapter five, the proposed semi-active suspension control with use of MR damper has been presented. The design process, tuning, and applications for the primary suspension system of the railway vehicle are also presented.

Chapter six presents the evaluation of the full active and semi-active MR dampers for both two-axle and the conventional bogie vehicle using computer simulations. Both curved track and straight track with irregularities are used in the assessment at different vehicle speeds

Chapter seven provides the main conclusions of this study and recommendations for future work.

CHAPTER 2: LITERATURE REVIEW

2.1 Introduction

The operation of railway vehicles is closely related to the quality and geometries of railway track and increase in vehicle speed clearly produces higher forces and accelerations on the vehicle that has a negative effect on ride comfort performance. One of the possible ways to solve the problem is to build very high-quality tracks for high-speed railway vehicles. However, this solution is not economic and maintaining such tracks will be very costly. Another way is to design rail vehicles with better suspensions to obtain acceptable cost and improved performance. There have been many comprehensive studies about in both passive and active solutions for improvements in running stability and curving performance in the primary suspensions and improving ride quality in the secondary suspensions [25, 28, 37, 38].

It is well accepted that active control systems can overcome the limitation of the passive suspensions. Active suspensions, with the use of actuators and sensors, can be used to control the system by dissipating energy or applying a force to the system from the suspension itself. However, active suspension systems have a few disadvantages, such as high cost, complicated design and also the requirement for high power.

This chapter presents an overview of active and semi-active suspension technologies, their control algorithms and also details the devices which have been used in these applications.

2.2 Active Secondary Suspensions

The study of active suspensions started in the 1950s and 1960s due to the obvious limitations of passive suspensions. The principle underlying active suspension is the use of a controllable actuator instead of purely passive suspension device [13].

2.2.1 Active Secondary Configurations

The main aim of the secondary suspension is to isolate the vehicle body from track irregularities. However, the performances due to the wide frequency range of excitations induced by rail track irregularities may be limited. Therefore, the most remarkable advantages

are expected by the implementation of active control. In active control, actuators replace passive traditional springs and dampers, this actively produces a desired control force requested by the controller. Active control technology presents an improved ride quality, as active suspension units can not only generate energy for a system, they can also store or dissipate energy, important properties that distinguish such units from conventional passive suspension [16].

Active suspension types can be categorized as being either low bandwidth or high bandwidth. The difference between these two categories is illustrated using Figure 2-1. In an active controller, an actuator is typically placed in parallel with the passive spring that can decrease actuator static force requirements (high-bandwidth or stiff active suspension). To reduce the transmission of both high- and low-frequency loads to the vehicle, it is necessary for the actuator to have a large bandwidth. However, in practice this translates into an expensive actuator. Therefore, an alternative way is to utilise a low-bandwidth actuator in series with passive springs (low-bandwidth or slow active system). In this system, the passive spring produces the required isolation at high frequencies while the actuator handles vibration control at low frequencies (usually below 3 Hz) [25]

low bandwidth systems consist of passive elements which dictate the fundamental dynamic response, the purpose of the active element is related to low frequency activity such as levelling or centring. This restriction enables some reduction in force and/or velocity requirement for the actuators. Limiting lateral body motion resulting in improved ride quality

In comparison, high bandwidth active systems have a greater capability, the overall dynamic response will mainly be determined by the active control strategy, which will probably act throughout the frequency range which is relevant to the suspension function being controlled. The advantage of a high-bandwidth system is increased body motion control in turn offering a ride quality when compared to low bandwidth systems [25].

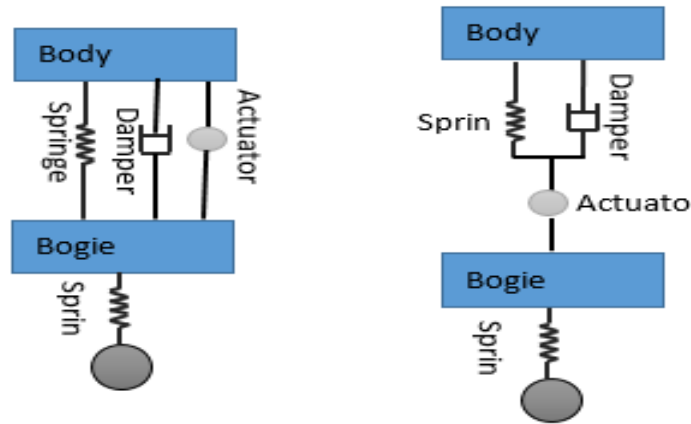


Figure 2-1- Active Suspension System (a) Low-bandwidth (b) High-bandwidth

The possible performance benefits of active secondary systems on ride comfort were investigated in [13, 39]. Different control methods such as the skyhook and LQG were used to study the improvement on ride quality, and the simulation results show that the controller using the skyhook approach performed better than others. However, it was noted that the main lack of success of active controllers when it comes to real application is the high cost, and that the challenge is to find solutions that improve ride quality while considering a trade-off between high performance, reliability as well as cost. This study was further extended in reference [40] by running the same test for a high-speed railway vehicle.

References [14, 36] clarified the structure and also advantages and disadvantages of an active controller. Active suspension systems allow for high control performance over a wide range of frequencies due to the excitations induced by rail track irregularities, but it should be noted that such a system demands a large power source and complicated control mechanisms. Therefore, mechanical power is added to the railway vehicles from the active suspension systems, and that may cause instability and could lead to derailment. Hence, the stability of the suspension systems needs to be taken into consideration.

In addition, increasing the cost and weight of such units, because of their demand for numerous sensors is just one more disadvantage of active controllers [13, 19].

2.2.2 Control Strategies

The best known control strategy for active suspensions is the principle of the skyhook damping which has been studied comprehensively with a number of implementation approaches. [41] investigated the how to optimise the balance between maximum deflection of the damper and acceptable levels of ride quality, especially the trade-off between the random and deterministic track input requirements. Results presented improvements of around 50% with implementation of the nonlinear Kalman filter method and around a 20% improvement in ride comfort was achieved with linear complementary filtering.

[42] examined traditional decentralised control compared to H_∞ decentralised control when applied to the integrated tilt control including active lateral secondary suspension when implemented in high-speed railway vehicles. H_∞ decentralised control was utilised to address the control loop interaction in the classical decentralised control, the performance of the local integrated suspension control was improved.

In [43], the design of an active suspension control was presented for a two-axle railway vehicle, by utilising an optimised linear quadratic regulator (LQR). The control objective was to decrease the yaw angle and lateral displacement of the wheelsets while the vehicle travels on curved and straight tracks with lateral irregularities, by replacing the longitudinal springs with active yaw dampers to provide the required yaw torque.

2.3 Semi-Active Secondary Suspensions

A semi-active suspension system uses a damper characterized by controlling the damping setting electronically, and the actual damping setting is relevant to the feedback in semi-active control strategies.

In comparison with full active systems, a semi-active system is considerably more cost effective, it requires far less power and can deliver improved ride quality [14]. In fact, amongst the different varieties of controlled suspensions, semi-active suspensions have been given the most consideration because they represent the best compromise between cost and performance. The damping forces produced in a semi-active suspension can be categorised as minimum and maximum damping force levels [17, 44, 45]. In addition, reference [46] described how an ideal

semi-active damper has a nonlinear relationship between force and velocity that can change to a maximum defined value.

2.3.1 Control Strategies

Various control strategies have been studied for secondary semi active suspension systems in terms of achieving high performance. In the last few decades, control strategies such as fuzzy logic control [47], skyhook, ground-hook and hybrid control [48], neural network predictive control algorithm [49], semi-active fuzzy control [50], and adaptive vibration control [51] have been studied.

Karnopp proposed the concept of semi-active suspension in the first place and used skyhook control method to improve ride quality [52]. The implementation of semi-active damping based on the hydraulic dampers for railway vehicles has demonstrated up to 15% improve the ride quality via the application of skyhook control method[44].

In early semi-active suspension designs, the damping force was adjustable by exerting control over the dampers via a closed-loop controller. Two kinds of dampers, two state dampers and a continuous variable damper, are utilized in semi-active suspension. However, the weakness of the two-stage damper is that it produces high-frequency harmonics that can create undesirable noise. Furthermore, the disadvantage of the continuous variable damper is that it is hard to find an appropriate device to be able to produce large forces at low velocity, and vice versa [16].

Four different semi-active control algorithms, Skyhook Control (SH), Acceleration Drive Damping (ADD), Mix SH-ADD control and Mix-1-Sensor that used electro-hydraulic dampers for the lateral secondary suspension have been investigated in [53, 54]. It was shown that semi-active control performance improved ride quality by reducing lateral-acceleration 34% compared to passive suspension only.

Semi-active suspension, as implemented on a quarter-sized model of a railway vehicle via the use of a PID controller based on a neural network, was studied in [55] with the objective of improving lateral ride comfort. The simulation results illustrated that the above increased ride quality and stability however it does not mention any quantified increase.

A semi-active control-based air spring suspension that could be used for both low and high frequencies was studied in [56], and it was demonstrated that the vibration and noise was reduced across a wide range of frequencies.

Reference [57] presented a study to control the damping force of the axle dampers installed vertically between the wheelset and bogie by limiting vibrations (and thus improving ride quality). An attempt to evaluate the optimal damping force for a semi-active controller was made through the use of the skyhook method controller. The result of the associated simulation and experimental test demonstrated that this method reduced the vertical vibration of the bogie about 60% at 5 to 15 Hz, and that the damping force of the axle dampers could be controlled.

2.4 Active Primary Suspensions

For many years, the trade-off between the stability and the performance on curved track has been one of the biggest challenges in the railway vehicles design using passive primary suspensions. Active control technology for primary suspensions to overcome the problem has recently begun to draw attention of researchers and engineers in railway industry.

2.4.1 Wheelsets (Solid Axle and Independently Rotating Wheelsets)

A conventional railway wheelset includes an axle and two wheels coned in profile, that are rigidly fixed to an axle. Therefore, both wheels rotate at the same rate of angular displacement. The radius of the wheel on the contact point between the wheel and the rail is the rolling radius.

While the wheels moving forward on the rail/track in a central position the angular displacement is the same. However, if the wheelset moves laterally or the wheelset moves to a curve, wheels move away from the central position. Due to the cone shape of wheels the outer wheel runs on the larger radius and inner wheel runs on a smaller radius. Then rolling radius will be different between two wheels. Basically, rotation speed between two wheels must be the same as the two wheels are rigidly fixed on the axle. Thus, forward speed toward the track is different between each wheel (the outer wheel moves faster than outer wheel). Which is the reason for centring and curving in solid axle wheelsets.

Traditionally to stabilise the wheelsets longitudinal springs are used between wheels and bogie. The stiffness of the spring is selected at the critical speed at when the wheelset becomes

unstable. However, the force generated by stabilising longitudinal springs can interfere with the natural curving behaviour of the wheelset while wheelset moving along a curve, leading to larger creep forces at the wheel-rail contact and high levels of wear especially on low speed sharp curves.

It is always a challenging trade-off between stability and curving because a stiff spring will give better high-speed running stability however it cannot perform a well in curving. vice versa softer springs cannot provide good high-speed running stability while the performance in curving is better.

An alternative solution of addressing this problem is the use of Independently Rotating Wheelsets (IRW). In an independently rotating wheelsets two wheelsets can rotate independently, hence longitudinal creep forces are substantially reduced. The dynamics of independently rotating wheelsets are similar to conventional solid axle, with the difference that two wheels are rotating independently at different speeds. However, the independently rotating wheelsets cannot provide the natural curving and track following of a solid-axle wheelset [5].

There is an asymmetry with independently rotating wheelsets because, on a steady curve, the wheelset can move with relative rotation of the wheels but with no lateral offset, or without relative rotation; the same lateral offset is found with a conventional solid-axle wheelset or any relative combination of the two thereof. In experiment, on a curve IRW will continue to move in a straight line and will simply be forced around the curve by the flange contact [58].

2.4.2 Active Control Configurations (Stability and Curving)

Goodall, R. [25] in a comprehensive survey of primary active suspensions, showed a key objective of primary active suspensions, is to control the wheelset kinematics by the longitudinal or lateral primary suspensions.

Active control can be applied to wheelsets directly or indirectly. The indirect method sees control effort applied through the bogie/secondary suspensions while the direct method applies control exertion directly to the wheelsets/ primary suspension. It should be noted that the direct methods can provide a much more effective control of wheelset dynamics than the indirect approaches, however that in real application it might not be efficient due to complicated electronic structure, high cost and also safety and reliability requirements [28, 29].

Active control technologies that are applied directly to wheelsets, depending on the wheelset configuration (i.e. Solid axle wheelsets (SW) or independently rotating wheelsets (IRW)), have differing control requirements.

Actuated Solid Axle (ASW)) or Independently Rotating Wheelsets (AIRW): In this configuration, the control scheme is able to exert force directly on the wheelset in the yaw, lateral or longitudinal directions [59].

Mei in [38] carried out a comprehensive review on the developments within active wheelset control. The study showed it is possible to apply a controlled torque to the wheelset in the yaw direction, mounting a yaw actuator as shown in figure 2-2 or pairs of longitudinal actuators as shown in figure 2-3 between wheelsets and bogie (body for vehicles without bogie) is a common design. Alternatively, actuators can be installed onto a solid axle wheelset in the lateral direction to improve curving performance as it shows in figure 2-4.

Mei and Goodall in [6] presented actuated independently rotating wheelsets (AIRW) and compared them with actuated solid axle (ASW) in terms of stability and curving performance, based on a two axle vehicle. It is shown that the required control torque for the independently rotating wheelset through a curve is less than the control torque needed for the solid axle wheelset, due to the longitudinal creep forces of an independently rotating wheelset being significantly lower.

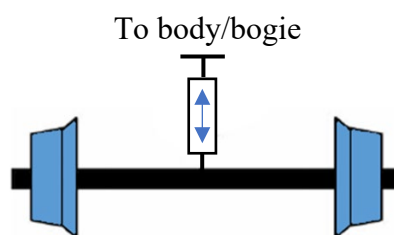


Figure 2-2- Active steering via yaw torque (yaw actuator)

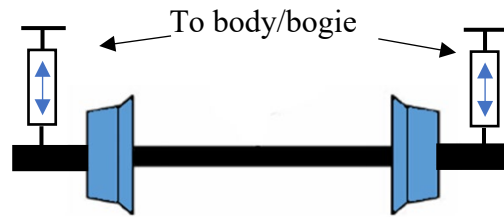


Figure 2-3- Active steering via yaw torque (pair of longitudinal actuators)

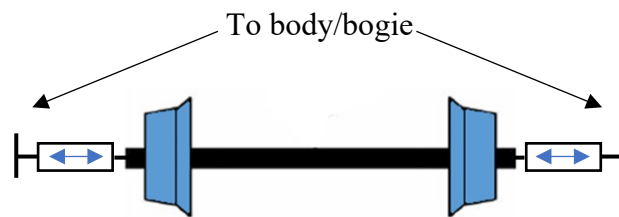


Figure 2-4- Active steering via lateral force

[60] utilised H_{∞} technique for active steering of the AIRWs to achieve stability and better curving performance against the uncertainties in the creep coefficients, wheelset conicity and other wheel-rail interface parameters.

Driven Independently Rotating Wheelsets (DIRW): It is another form of the actuation which is possible for independently rotating wheelsets through driving/breaking torques. In [8, 61], the driving torque is provided to IRW by using servomotors connected directly to the IRW through differential gearbox. The computer simulation in the study illustrated that the vehicle stability and curving performance were significantly improved. [62] presented the use of combination methods of DIRW and AIRW to improve curving performance. In this case, to improve both stability and curving performance for conventional vehicles, one active steering actuator for each wheelset and one traction motor for each wheel was proposed. [63] utilized the DIRW technique for tramcar trains in order to deliver guidance for curved track with the

objective of improved curving. In this study DIRW was used to deliver traction torques to the wheels to emulate a solid axle connecting the wheels such that a steering moment is introduced for the wheelsets.

Directly Steered Wheels (DSW): This method was used for guidance control on curves by actively steering the independent wheels in a manner similar to road vehicles [28]. [64] presented a DSW scheme for steerable wheels of a two-axle vehicle to improve curving. In this study a passive electromagnetic damper was used to overcome the yaw damping oscillations in a curved track. Numerical simulation results demonstrated potential improvement in curving.

2.4.3 Control Strategies

The control objectives for the solid axle wheelset and independently rotating wheelsets are different. An active controller needs to control stability of the wheelset while not interfering with the natural curving action for the solid axle wheelset. On the other hand, the expectation of an active controller is to provide guidance and steering for an independently rotating wheelset.

It is noticeable that active controllers can cover low bandwidth applications, for example to improve wheelset performance on curves by using actuators in series with the longitudinal stiffness [59]. On the other hand, by replacing or supplementing passive applications, high bandwidth active steering control is possible. Different methods of control are proposed to provide stability and guidance.

Control Approaches for Stability Control:

Stabilisation of independently rotating wheelsets can be achieved more easily than solid axle wheelsets. Mei and Goodall in [7] presented an active controller for independently rotating wheelsets through a different form of yaw damping. In this method control yaw torque is proportional to the axle yaw speed relative to the car body. In this study an active yaw damper was connected between wheelsets and body to imitate the passive yaw dampers

[12] presented the possibility to stabilise independently rotating wheelsets through passive yaw damping however, active steering is necessary to provide guidance on the curve. In this

method, a control scheme applied in the yaw direction considered the relative yaw velocities between vehicle body or body and the wheelset. This method can meet the stability required for independently rotating wheelsets and the control effort was notably reduced as longitudinal creep forces were significantly reduced in comparison to the control for the solid-axle wheelset.

Reference [65] investigated the use of variable longitudinal stiffness in the primary suspensions, utilizing the wheelset yaw displacement to determine the sensitivity of the critical hunting velocity to primary stiffness. To achieve this, a mathematical model of a single railway wheelset was developed to investigate the dynamics of the wheelset. Lateral stability results confirmed that the critical hunting velocity of the wheelset is most sensitive to the primary longitudinal and lateral stiffness.

In references [39, 59], it was noted that most primary vertical suspension designs have a longitudinal stiffness that can constrain the yaw of the solid-axle wheelset but can also provide kinematic stability. Whilst it is essential to increase stiffness for high-speed trains, this can reduce curving performance. To solve this problem and improve stability, an active primary yaw damper can be used instead of traction rod. This method was used in an attempt to decrease the steady-state wheelset yaw moment to zero, which can increase performance on curves. Two control strategies were used in this study; in the first strategy the angle that is essential for the radial alignment of the wheelsets produced, where actuators were used (replaced) to provide this alignment. In the second method, the yaw torque on the wheelset decreased to zero in curves this resulted in good performance on curves. However, it may be noted that the longitudinal primary stiffness remains. It is possible to design a suspension unit with low stiffness, but such designs give rise to consequent problems with transmitting braking forces from the wheel to the bogie.

Control Approaches for Guidance Control:

For independently rotating wheelsets, guidance control is essential to ensure track following. In high bandwidth systems it is critical to guarantee that wheels or wheelsets follow the track at an appropriate frequency to avert flange contact because of track irregularities. If the lateral deflection between the rail and wheelset can be measured, the guidance control can be relatively easy [66]. This paper also proposed a control method for DSW by utilizing a computed tracking error from wheel position relative to the centreline of the track. By using

this method, they attempt to reduce and minimise the tracking error therefore the wheel flange will not contact the rail.

Different methods such as AIRW, DIRW and DSW can be used for actuated independently rotating wheelset to provide essential guidance. However, choosing the right sensing and coping with uncertainties of the parameters is always challenging and, these considerations have to be addressed separately.

[67] presented a control approach for steering and stability for IRW, where practical sensors are used to measure the relative rotational speed of the wheels on an axle and the relative yaw velocity between the wheelset and the body. The study illustrated the feasibility to improve curving and passenger ride comfort both by actively controlled AIRW rather than conventional passive suspensions.

The use of relative speed measurements for the guidance control has been applied with a number of control designs. [68] presented a steering method that acquires a controlled difference of angular speed between the inner and outer wheel, the reference value being defined to keep the wheelset running centrally on the track by applying a yaw torque.

[69] saw the application of the feedback in the DIRW that modified the traction torques needed to achieve control and keep the rotational speed difference of the motors at zero like solid axle wheels.

In [70], the lateral displacement and the yaw velocity of the front wheelsets for DIRW are used to provide steering control.

Model based design methods have also been proposed to provide guidance and stability for IRW, with an integrated approach to take into account the non-linearities and uncertainties at the wheel-rail interface independently rotating wheelsets need controller strategies for curving which aim to reduce undesirable creep forces. Reasonable curving performance can be achieved if there is no longitudinal creep force, as longitudinal creep force causes undesirable yaw motion, then it is required to be eliminated. Also, equal lateral creep force is essential, because some force in the lateral direction is required to compensate for the cant deficiency. However, a distributed lateral force between all wheelsets is preferred [71].

presented an active steering control for IRW by utilizing H_∞ method. Also, a linearized model has been utilized in terms of developing a robust control strategy. It can show that an

active steering model improved performance on curves due to the reduction in the effects of nonlinearities. It is noticeable that nonlinearities of railway vehicles are highly related with nonlinear wheel–rail profiles as well as contact forces. Therefore, it can be very problematic while the wheel-rail contact point reaching the wheel flanges. Though, this problem had been solved by robust active steering control which is proposed in this study. This method of robust active steering control operates by steering the wheelset at the linear region of the wheel tread and rail surface [60].

Nevertheless, to design a controller for a wheelset a few issues must be considered. Firstly, some required feedback signal such as the relative movement between the wheelset and the track which is very difficult and costly to measure. However, to solve these problems cheap and practical sensors need to be found. Secondly, uncertainties and variations, so many parameters in railway vehicles vary such as conicity or creepage deviating from their face values while in operation as well as dynamic uncertainties like actuator dynamics. Therefore, the controller must be robust given all these uncertainties. Thirdly, the dynamic model of railway vehicles is high order and complex. Therefore, some form of simplification is needed [38].

Few references mentioned measurement taken on the wheel, but in real application it is highly recommended that mounted sensors are not implemented on the unsuspended masses as they can cause severe vibrations.

References [39, 72] investigated an active primary suspension in a two-axle rail vehicle. They removed the secondary suspension to decrease the vehicle weight, so the active primary suspension also had to compensate for any associated effects in this regard. The researchers concentrated purely on bounce and pitch motions. Two control methods, skyhook and LQG, were used to improve ride quality. The simulation results showed the controller using the skyhook model performed better.

2.5 Semi-Active primary Suspension

The literature review examined a diverse range of methods to improve stability and guidance through active technology [28, 29]. However, issues mentioned earlier, are the reasons for developing better technology to overcome the mentioned challenges.

To date, studies of semi-active approaches for the control of solid axle wheelset have been limited. Variable longitudinal stiffness in the primary suspensions has been proposed to

improve the hunting instability of railway carriages[73]. It would clearly be beneficial to be able to increase the stiffness for high speed operations and reduce it when a vehicle negotiates tight curves at low speeds, but mechanisms to achieve this could be problematic in practice. The use of variable dampers either in the primary suspensions to supplement the passive means [74] or in the secondary suspensions to replace the yaw dampers of fixed coefficient [75] can help to improve the vehicle performance, but they do not solve the fundamental trade-off between the stability and curving of the solid axle wheelsets. So far, no studies on the semi-active control of independently rotating wheelsets are found.

2.6 Actuators in Railway Vehicles

As briefly discussed in the previous chapter, there are a number of actuator technologies currently operated in railway vehicles. Actuator selection is dependent on the balance between actuator performance such as power, efficiency and bandwidth, against size, expense and maintenance cost considerations. When the application of active wheelset control is being considered it is necessary to evaluate the performance of each actuator type [76, 77].

Some active secondary suspensions in railway vehicles use servo–pneumatic actuators. In an active servo–pneumatic system air pressure is controlled; this has positive benefits to the suspension system.

[78] showed that air pressure (in the vertical direction) of an existing air spring system with fixed reservoir volume can be actively controlled via a variable volume reservoir. Controllable frequency bandwidth is restricted to 2–3 Hz and this is due to air being highly compressible, resulting in the operational range of the actuator being restricted. The bandwidth that wheelsets require for stability is between 6–8 Hz in dynamic mode. Therefore, servo–pneumatic actuators are not appropriate for the primary suspension.

[79] tested servo–pneumatic actuators on a roller rig with the objective of reducing vibration in the vertical, lateral and roll modes. Results showed up to a to 50% decrease in vertical, lateral and roll vibration may well be achieved by the application of active control.

[80, 81] investigated the improvement of ride quality. By replacing passive hydraulic dampers in the lateral direction with pneumatic actuators in the secondary suspension, vibrations were reduced therefore ride comfort increased

Hydraulic actuators operate on the principle of a control signal activating valves or pumps that control the flow of a hydraulic (non-compressible) fluid into and out of chambers in the actuator. A pressure difference is created between the chambers in the actuator cylinder, resulting in a force being applied to the actuator. Generally, hydraulic actuators have a fast response and they are capable of operating under demanding load for prolonged periods without excessive heat generation. However, hydraulic systems are highly non-linear, and they have issue with parameter uncertainty [82].

The use of hydraulic actuators is common in railway applications and frequently used in secondary suspensions due to the compact dimensions allowing them to easily fit in the restricted spaces between bogie and body. The behaviour of hydraulic actuators is well understood and has been the subject of numerous studies [69] undertook experimental analysis, where authors chose to use hydraulic actuators in place of pneumatic actuators. This gave the ability to control up to a 12 Hz frequency range, compared with the 2–3 Hz as noted earlier, to deliver a better control of vibrations. However, the weakness of hydraulic actuators are the risk of oil leakage, which has clear implications on maintainability, maintenance costs and safety [83].

An electro–mechanical actuator is powered by an electrical motor (preferably BLDC). This actuator type has been effectively implemented in numerous ASW control strategies [66].

EM actuators have several advantages, these include having a compact design, an operational bandwidth that is over the wheelset bandwidth, low maintenance cost and also demonstrate linear behaviour for the functioning torque/force range (0 – 5 kNm) necessary for wheelset control for ASW [72, 84]. [55] studied a DIRW arrangement with EM actuators incorporated through a gearbox. A recent study [74]] assessed the application of EM actuators with skyhook damping for secondary suspension, which concluded that the EM actuators operate to a satisfactory level with a frequency of 10 Hz [85].

Electromagnetic actuator design involves of two pairs of electromagnets mounted back to back, these operate in attraction mode. A force in both directions is produced by the magnets, these are in turn connected through the actuator, e.g., car body and bogie [86, 87].

. Electromagnetic actuators are often favoured as they can operate over a of large frequency bandwidth, this can be up to 50 Hz. Another advantage of the EM actuator is reliability as it is a simple design, no moving parts results in a robust system [78].

[76] focused on the addition of an electro–magnetic actuator between the centre of the body and a secondary mass (of one tonne) with the objective of suppressing the first symmetrical flexible mode. The main disadvantages are that they tend to be large in size and heavy in weight and can be challenging to package between two bodies of the vehicle. [88, 89] show there are some additional problems, air gap variations between the magnets can produce an unstable system this can be counteracted with proper force feedback.

In primary suspension measurements required for the sensors and actuators can be an issue in terms of selecting a practical sensor with the appropriate cost and reliability. Therefore, sensors and actuators are significantly important when selecting a choice of concept, control strategy and improving of performance which can be obtained by the implementation of active control. In addition, actuation requirements are high, particularly considering controlling force, torque or bandwidth subject to stability control require to use in active primary control application. Therefore, design and chose of an actuator to cover all these requirement is critical [28, 29, 76, 77].

[78] Servo-pneumatic actuator is a type of actuator which is commonly utilized in secondary suspension in trains. Air pressure is controlled in an active servo-pneumatic system, which gives rise to desired suspension characteristics. This study shows that the air pressure

[90] a hydraulic actuator was selected instead of a pneumatic actuator as its able to control up to a 12 Hz frequency range when compared to the 2–3 Hz for a pneumatic actuator. Performance was good, vibration was reduced. However, disadvantages of hydraulic actuation such as the risk of oil leakage, maintainability and maintenance costs need to be considered.

[72, 84] A screw mechanism converts rotational torque into linear motion. Gearboxes can also be used to connect the motor to actuate the wheelset in an angular direction. It is noticeable the study has been done with actuated solid axel wheelset. [91] investigated the control implications of speed fluctuation between wheels on the active steering of an independently rotating wheelset, using in hub wheel motors

[85, 92] Electromagnetic actuators have the advantage of an operational bandwidth that is higher than the wheelset bandwidth. In addition to this a compact design, low maintenance cost and linear behaviour for the operational range of force (0 – 5 kNm) required for wheelset control. Recent studies examined the use of Electromagnetic actuators in a skyhook damping

configuration [74,75] Electromagnetic actuators perform well with a frequency of 10 Hz in secondary suspensions

[86, 87] Electromagnetic actuators are made from of two pairs of electromagnets mounted back to back and functioning in attraction mode. The magnets produce a force in both directions between along the actuator.

[76]examined methods of improving ride quality. In this case the addition of an electromagnetic actuator between the centre of the car body and an auxiliary mass of one tonne in order to suppress the first symmetrical flexible mode of vibration. An electromagnetic actuator is preferred due to a large operational frequency bandwidth up to 50 Hz, electromagnetic actuators are a robust and reliable device due to minimal moving parts [78].

Electromagnetic actuators are relatively large devices and can be heavy. Designers will need to consider how to fit them in the small spaces available. [88, 89] examined the effect of air gap variations between the magnets inside the electromagnetic actuators results in an unstable system. This can be addressed with proper force feedback.

2.7 Sensing

Sensing is a vital part of active control, as feedback is fundamental to achieve active control. Under real world circumstances where actual measurements cannot be obtained sometimes, model– based solutions can be used to estimate the required measurements. These models are based on the other measurements which can be obtained easily and the dynamic relationships between states can be calculated or simulated as needed.

There have been previous studies conducted into the use of estimators on railway vehicles using actively controlled suspension systems to gain feedback measurements for the controllers as well as for other applications [58]. In [80] a kalman filter is used to provide estimated state feedback for an optimal control scheme for wheelsets, where track features such as cant angles and curve radius are also included in the estimation.

In [93], the use of kalman–bucy filter was investigated to predict the creep forces in the contact area. Inertial sensor measurements are used in this process while the estimations are further analysed to allow them to be applied to estimate usable traction levels, even at low level of tractive forces.

[94] This paper explored an enhanced virtual reference model for semi-active suspension to coordinate the vehicle ride comfort and handling stability. The reference model combines the virtues of skyhook with ground-hook control logic, and the hybrid coefficient was tuned according to the longitudinal and lateral acceleration to improve the vehicle stability in high-speed travel. Suspension state observer based on unscented Kalman filter was designed. A sliding mode controller (SMC) was developed to track the states of the reference model. The stability of the SMC strategy was confirmed by means of Lyapunov function considering the nonlinear damper characteristics and sprung mass variation of the vehicle. The proposed control system offers improved coordination between vehicle ride comfort and stability.

[95] studied state estimation techniques, state observers were used to provide crucial feedback parameters required for active control with IRW, based on a full model of the vehicle and available measurements such as yaw velocity, lateral acceleration of wheelsets, bogie and vehicle, to avoid the use of expensive sensors and complex instrumentation.

2.8 Semi-active Devices

One of the common devices used for semi-active controllers is the variable hydraulic dampers with an orifice that contains a fast-acting throttle valve as described in reference [19], which have been used in semi-active suspensions in railway vehicles [44, 96, 97]. Damping ratio in a variable hydraulic damper may be controlled through the use of solenoid valves [98] attempted to improve ride quality with semi-active systems through the use of solenoid valves to control the damping rate. In reference [44], they indicated that Semi-active dampers are hydraulic dampers with an orifice that contains a fast-acting throttle valve. Reference [14] described ride quality improvements through the use of semi-active suspension. It is worth noting that these kinds of semi-active suspension systems were manufactured using oil cylinders and mechanical valves, so their performance could decrease over time and maintenance could clearly be costly. In addition, the use of a mechanical elements to produce the valve time delay could also reduce the performance of the system.

Another type of semi-active device uses controllable fluids. The essential characteristic of a controllable fluid is the capability to reversibly change from a free-flowing viscous fluid to a semi-solid in a controllable manner on a millisecond timescale when exposed to an electric or magnetic field [14]. The use of smart (controllable) fluids can help overcome the drawbacks of

other systems and improve performance through changes to the fluid properties instead of the flow geometry [19].

Advantages of using controllable fluids include much faster time responses of typically less than 10 ms, no moving parts (apart from the pistons of the damper) which makes them simple and reliable [19] and reversible control of the fluid properties through the use of a low-power electrical source [99].

Smart fluids are divided into two groups:

1. Magnetorheological dampers, which achieve shock absorption through rheological fluids whose physical properties can be changed through application of a magnetic field.
2. Electrorheological dampers, which are essentially identical to magnetorheological dampers, but control is effected by changing an electric field [35, 99].

2.8.1 Magnetorheological Damper

A scaled half-size railway vehicle model with a stabilised suspension system was comprised of an MR damper (Modified Bouc-Wen model) with a semi-active control strategy to improve ride quality [100]. Research has been conducted into semi-active controllers with MR dampers for railway vehicles in order to improve ride quality and stability. In reference [98], the authors applied a different control strategy for their railway vehicle simulation. Their results showed that a system with a semi-active controller using MR dampers could improve ride quality. Also, the authors of reference [101] discussed semi-active controllers utilizing MR dampers in the secondary suspension of a locomotive. Their results indicated that semi-active suspension has a better performance than passive systems in this regard.

An MR damper was applied to a semi-active suspension to improve ride quality in vertical secondary suspension. The purpose of the study was to reduce the lateral and yaw vibration of the railway vehicle [45].

References [14, 36] presented a model of a full-scale railway vehicle developed with a semi-active control system integrated with MR damper (Modified Bouc-Wen model) for secondary suspension with 17 degrees of freedom, the aim of which was to improve the lateral, yaw, and roll motions of the car body, trucks and wheelsets. The system controller measuring

the acceleration feedback and measurable accelerations. Evaluation of the semi-active suspension with MR dampers, random and periodical track irregularities were modelled with a uniform state-space origin conforming to the test data. A mixture of the dynamic behaviours of a railway vehicle fitted with MR dampers and rail track irregularities were established and given as the state-space formulation. The simulation and analysis of a full-scale vehicle showed the significance of vehicle dynamic equations to semi-active suspension systems utilizing MR damper presented in the closed and open loops. The results suggested that a semi-active suspension system integrated with an MR damper is effective and useful compared to the passive model. A reduction in acceleration of the car body in a Semi-active system with MR damper was observed when compared with the passive system.

In [102], a high-speed railway with 15 DOFs was developed. The damping ratio utilized to investigate the sensitivity of the critical speed as pertaining to the suspension parameters. The results of this study showed that the secondary lateral damping rate is the most sensitive of the parameters affecting critical speed. It was shown that the semi-active secondary lateral suspension installed with an MR damper had the ability to increase the railway vehicle's stability and critical speed.

The experimental study reported in reference [103] gave an account of an investigation into the performance of a semi-active controller including MR damper on a roller rig when compared to the latter's existing passive suspension system. The equations for the dynamic behaviour of a railway vehicle with a 15 degrees-of-freedom semi-active system was developed to show the lateral, yaw and roll motions of the car body, bogie and wheelset. With derived mathematical model of Semi-active system, the calculation of the MR damper parameters was feasible to apply in a real scale railway vehicle. Damping force characteristics were evaluated experimentally. In addition, a skyhook control system with a Kalman filter was designed and developed in order to evaluate the ride quality of the vehicle. This indicated that a semi-active controller with skyhook controller system integrated with an MR damper effectively reduced vibrations in the critical frequency range of 1.0-1.5 Hz that can have a direct effect on the ride quality of the vehicle.

A novel MR damper for a semi-active railway vehicle suspension system was proposed in [104]. It was developed through designing and testing to ensure the suitability of the railway vehicle suspension.

Reference [105] described the design of a new damping technology to improve performance in terms of the stability and ride quality of the railway vehicle. To achieve this, a choice of the secondary suspension and different controllers such as Skyhook, Dynamic Compensation and a Sliding Mode Controller were studied. A semi-active damper in a high-speed train was used to evaluate the ride quality. The best performance could be seen from the feedback compensation control method.

The authors of reference [106] used a Bingham MR damper model to investigate the design of a two-degree of freedom system and its associated stability analysis. The Circle Criterion was used to inspect the MR system stability, which illustrated that for any random sequential time-varying input current, the origin of the state space was stable. In addition, a nonlinear inverse control law (feedback linearizing control law) was designed.

Research has been carried out for semi-active controllers using MR dampers for railway vehicles with regards to improving the vibration characteristics of such systems. In reference [107], an attempt to investigate suitable semi-active control methods for MR dampers (Modified Bouc-Wen model) with seven degree-of-freedom tracked vehicle suspensions. These consisted of the Skyhook, Hybrid and Fuzzy-Hybrid control methods. Simulink simulations were run for each control method for different inputs, such as bumps and sinusoidal roads for several vehicle speeds, to compare the performances of these three methods in the time and frequency domains against conventional suspension. The results indicated that a system with an MR damper showed significantly better performance; furthermore, of the three control methods, Fuzzy-Hybrid showed the best performance in terms of reducing the wheel bounce response and body acceleration. In summary, Ata, W. and A. Salem aim was to prove that a semi-active controller integrated with an MR damper could control the vibration of a vehicle suspension system.

Reference [108] proposed a nine degree-of-freedom railway vehicle system. The dynamic and mathematical model of the system was developed. The MR damper (Modified Bouc-Wen model) was manufactured at full size and its characteristics evaluated through experiment. Different control algorithms such as Skyhook and LQR were used to improve the vibrations within the system. Kim, H.-C., et al work indicated that vibration performance of the lateral motion of the car body improved.

Studies were completed in [109] for different control strategies for a semi-active integrated MR damper for the secondary suspension system. It was shown that the skyhook method was appropriate for MR damper suspension railway vehicles.

The experimental work presented in reference [110] indicated that by reducing the vibration, an accurate mechanical model of an MR damper is as important as a good control algorithm. In order to clarify this matter, a semi-active control system with a different controller integrated with an MR damper for a quarter-car was investigated. By utilizing a hyperbolic tangent model, the mechanical characteristics of the MR damper were modelled through experiment. Moreover, a new Hybrid Fuzzy and Fuzzy Proportional-Integral-Derivative (HFFPID) controller mixture with Fuzzy Proportional-Integral-Derivative (Fuzz-PID) and Fuzzy controller were expanded to increase the performance of the semi-active system. As for the numerical simulation result, the acceleration of the body with a semi-active suspension was best controlled using a HFFPID controller by reducing 58.9% and subsequently controller HFPID and Fuzzy-PID by condensing 42.1% and 37.3% compared to passive suspension.

Reference [111] investigated the modelling and Simulink of two control algorithms for a semi-active controller equipped with an MR damper as applied to a quarter-vehicle. The control algorithms used were Skyhook and a new control strategy based on the inversion of the Energetic Macroscopic Representation (EMR) of the MR suspension. The results showed that of the two, EMR had a better performance.

The aim of reference [112] was to present the response of a quarter-car model using an MR damper in a bumpy road at constant velocity. The MR damper was modelled using the Bingham and Bouc-Wen model. MR characteristics were obtained using a multi-objective optimization technique called the Non-dominated Sorting Genetic Algorithm II (NSGA II). An LRQ controller was employed as the active controller. The result showed that an optimal MR damper could perform as well as active suspension. Reference [113] experimentally assessed the efficiency of the performance of an MR damper. Reference [114] used a H_∞ controller for a system employing an MR damper to validate the performance of the system through simulation. References [115, 116] constructed a MR damper for a passenger vehicle and clarified the control characteristics of the associated damping forces. In addition, by using hardware in the loop simulation, Choi, S.-B., S.-K. Lee, and Y.-P. Park, developed their study to calculate control performance of the MR damper.

Reference [117] considered a semi-active controller integrated with an MR damper for a 1/5-scale railway vehicle application through numerical analysis and experimental tests (on a roller rig) to demonstrate reduced lateral vibration of the car body in terms of ride quality of the railway vehicle. Simulations suggested better performance that was actually found in experimental testing, but both sets of results showed significant improvement compared to conventional passive suspension.

Reference [118] investigated two semi-physical damper models of the semi-active damper of the DLR robotic electric vehicle ROboMObil (ROMO). They also attempted to compare their accuracy by mimicking real damper dynamic performance. By adapting and developing a Bouc-Wen model, the system became more accurate, particularly for higher control input. Likewise, in simulation results, the graph of the force related to the MR damper, expressed a better compatibility for real time. [75] Baiasu, D., G. Ghita, and I. Sebesan, developed a 17 degree-of-freedom railway vehicle according to lateral, yaw and rolling motions, to control the lateral vibration. They were presented that control system can be more trustable and cost effective with using electro-hydraulic devices.

Reference [119] reported experimental tests performed on a linear MR damper (Bouc-Wen model). According to dynamic conditions encountered, an attempt to discover how the effects of the displacement, frequency and magnetic field altered the mechanical state of the MR damper was made through various experiments. Experimental studies were conducted with an INSTRON test machine. Damping force was found to increase slowly with magnetic field saturation as well as the damping force increasing with increasing displacement. Furthermore, it was seen that for small frequency intervals less than 2.0 Hz, there was no existence of any inertial effect on the damping force; moreover, damping force was not dependent on oscillation frequency. Nonetheless, for frequencies greater than 4.0 Hz, there exists nonlinearity due to fluid inertial effect. To define the performance of an MR damper, a viscoelastic-plastic model according to pre-yield and post-yield mechanism was designed. The consequence of this experimental study of force vs. displacement and force vs. velocity cycles illustrated that the model can predict MR has a worthy performance.

Reference [99] presented the design of an MR damper suitable for an on- and off-highway vehicle suspension system. The authors demonstrated the ability of a magnetic fluid to control damping force through experiment. In reference [120], the damping force of an MR damper was predicted and dynamic model of MR damper was investigated. As a result, they have been

compared to predicted damping force results with measured damping force in time domain. Reference [121] proposed an MR lag model damper in a semi-active suspension. They developed a dynamic model of the system and validated it by comparing the predicted damping force to the measured one. Reference [122] presented hysteretic compensator (a retardation of an effect when the forces acting upon a body are changed) of MR damper. Kamath, G.M. and N.M. Werely, investigated nonlinear Preisach hysteresis model and hysteretic compensator. In addition, indicated damping force control performance.

In an experimental paper [100], a semi-active controller with an MR damper (modified Bouc-Wen) has been studied for a half-scale train model. An MR damper was designed and produced. Parameters for this damper were determined based on experimental results. Furthermore, it was demonstrated that the MR damper was able to change the damping force under a wide range of magnetic field; also, the increase in damping coefficient with electric current was investigated. The simulation results showed that the system could be controlled more effectively with a semi-active suspension system including MR damper when compared to a passive system.

Reference [123] studied and developed a 17 degree-of-freedom model for a full-scale railway vehicle. A semi-active controller with an H_∞ system controller including yaw and rolling pendulum motions integrated with forward MR damper (Modified Bouc-Wen) as well as an ANFIS inverse MR model as the damper controller was designed to consider lateral, yaw and roll acceleration of car body, bogies and wheelsets of the full-sale railway vehicle. Random track irregularities as input to the simulation were modelled. Pursuant to the Simulink results, the semi-active system that included an MR damper reduced lateral, yawing and rolling motions of the car body. Reference [124] combined a theoretical and experimental study. The experimental study used an INSTRON machine utilizing an MR damper in flow mode, which indicated that damping force increased with electric current, but it was notable that it reduced with excitation amplitude. However, the damping force in the MR damper was able to change over a wide range of magnitudes of magnetic field. For a specific value of the current, the MR damper tended to be saturated, but below this specific value the MR damper could not be considered a viscous damper. The simulation for a semi-active system conducted for a quarter car with the use of an MR damper (Bouc–Wen model) demonstrated that the acceleration of the sprung mass, suspension travel and wheel deflection all showed superior (better) control of the body resonance.

Reference [125] developed and determined the nonlinear stiffness of an MR damper model via Simulink.

Finally, it may be noted that MR dampers provide for a greater dynamic range force than ER dampers [99, 126].

2.8.2 Other Variable Dampers

Maneetham, in [127], presented the modelling of a hydraulic servo system. This study attempted to design and implement a control system for hydraulic systems. The mathematical model of the damper was developed, a PD controller was utilized to control the system. The model and controller were simulated in Matlab Simulink. [128] In an experimental study, a reverse continuous variable damper was designed and expanded for use in the semi-active suspension of passenger cars, and its performance determined experimentally.

[129] presented a variable stiffness system included two helical springs and a variable fluid damper for a two degree of freedom quarter car model, where the damping and stiffness constants are varied to adapt to changes in operating conditions.

There have been studies on the use of Electrorheological (ER) dampers. Reference [130] defined a ground-vehicle suspension system by using an ER fluid damper to control the lateral vibrations of the rail vehicle. However, it may be noted that a system that uses ER dampers requires high voltage control and, as such, its application is limited for safety reasons [126, 131].

Reference [132] attempted to compare ride quality and handling performance of a passive system with semi-active suspension and active suspension that use an MR damper (Bingham Model) in a two degree-of-freedom quarter car for random road excitations. The results indicated that active suspension gives better ride quality and stability than semi-active suspension.

Also, reference [46] notes that active-suspension performs better in terms of ride quality but it is remarkable that semi-active suspension can positively present better performance through the vehicle.

2.9 Summary

This chapter has presented the literature review for a diverse range of active/semi-active suspension concepts. Active technology in rail vehicles is categorised into two main classes: the first is the primary active suspension, which improves running stability and/or wheelset guidance; and the second is the active secondary suspension, which helps to improve passenger ride comfort.

From the literature review, it is clear that with the application of a full-active control suspension system, levels of dynamic performance can be obtained that are not possible with a passive suspension system.

Practical issues have to be considered in the development of active suspension. For instance, the controller developed must be robust against parameter variations, some feedback signals are costly and problematic to measure and thus it ultimately becomes essential to use alternative and cheaper methods.

In dynamic models of railway vehicles, the order is high, and the system is very interactive between different motions. Hence, some form of dynamic simplification needs to be employed in the development of active control systems.

The trade-off between curving and stability is a particularly critical issue, where the main benefits are expected to result through the use of semi-active solutions.

The performance of the lateral secondary suspension in a high-speed railway vehicle is more important than in conventional railway vehicles in terms of both comfort and stability.

Most semi-active control strategies are fixed structure controls and are based on matching the force demanded to the extent this is feasible within the limits imposed by the minimum and maximum damper settings. These limitations restrict the performance of semi-active suspension systems.

CHAPTER 3: MODELLING OF THE VEHICLE DYNAMIC SYSTEMS

3.1 Introduction

In this chapter, the models for the study are developed, which include the Single independently rotating wheelsets, a Two-Axle Vehicle with independently rotating wheelsets and a conventional bogie railway vehicle. Correspondingly, the mathematical models of a modified Bouc–Wen model for the magnetorheological damper and an inverse MR damper controller has been built using the lookup table technique.

3.2 Analysis of the Model

The railway vehicle dynamics are complex due to the fact it is a multi-body system. Each body in the system has six degrees of freedom, these are lateral, longitudinal, vertical (displacement), yaw, pitch and roll (rotational). Second order differential equation is applied to every individual degree of freedom. Therefore $6*N$ differential equation is essential to present the dynamic of the system. N is the number of masses, which for this case study will be 7 masses covering, one railway vehicle body, two bogies and four wheelsets. Thus, eventually a total of 42 second order differential equations are needed to represent the system completely [4]. However, study of all elements is not essential as inclusion of all the degrees of freedom will make the dynamic/mathematic study of the system more complex and not relevant to this study. In this study just lateral, yaw and relative rotation motion will be included. It is due to longitudinal creep force effects on wheelset yaw motion and because wheelset is independently rotating wheelsets, so it effect on relative rotation of the two wheels too. Also, lateral force impacts the lateral motion. The numerical Simulation has been modelled in Matlab/Simulink for the system with different input track irregularities.

3.3 Modelling of Independently Rotating Wheelset

The structure of a wheelset comprised of independently rotating wheels (IRW), where each wheel can rotate independently of the other shows in figure 3-1.

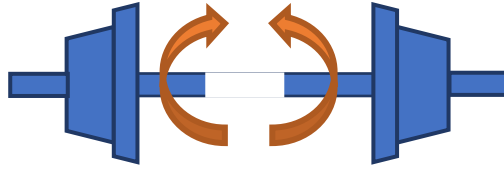


Figure 3-1- Independently Rotating Wheels (IRW)

A side perspective view of a wheelset is depicted in Figure 3-2. As the wheelset is moving forward at a constant speed V_s , the rotational speed of each wheel is determined by:

$$\omega = \frac{V_s}{r_0} \quad (3-1)$$

When the wheelset is travelling along a track in the longitudinal direction, both the track curvature ($1/R$) and the wheelset yaw motion (ψ) can affect the forward speed of the wheelset, and invariably the longitudinal creepage.[71]



Figure 3-2- Side view of the left and right wheels

However, to permit the rotation of the independent wheels (ϕ) without the subsequent representation of the longitudinal motion (which is usually assumed to have a constant speed), an extra state $\frac{d\phi}{dt}$ is presented which denotes the differential angular velocity of the rotation between each wheel, and is defined as [5]:

$$\frac{d\phi}{dt} = \frac{\frac{d\phi_R}{dt} - \frac{d\phi_L}{dt}}{2} \quad (3-2)$$

where the angular velocities w_R and w_L of the right and left wheels are given by:

$$\omega_L = \frac{v_s}{r_0} + \frac{d\phi_R}{dt} \quad (3-3)$$

$$\omega_R = \frac{v_s}{r_0} + \frac{d\phi_L}{dt} \quad (3-4)$$

The relationship between creep and creep force can be considered to be linear and therefore linear coefficients can be used for its evaluation. Where f_{1l} and f_{1R} are left and right wheelset longitudinal contact forces and f_{2l} , f_{2R} represent left and right wheelset lateral forces and f_{11} and f_{22} represent the longitudinal and lateral coefficients, respectively. In addition, γ_1 correspond to creepage in the longitudinal direction and γ_2 is creepage in the lateral direction [71].

$$F_{1l} = -f_{11}\gamma_{1l} \quad (3-5)$$

$$F_{2l} = -f_{22}\gamma_{2l} \quad (3-6)$$

$$F_{1R} = -f_{11}\gamma_{1R} \quad (3-7)$$

$$F_{2R} = -f_{22}\gamma_{2R} \quad (3-8)$$

$$\gamma_1 = \frac{\text{actual forward velocity} - \text{pure rolling forward velocity}}{\text{forward velocity due to rolling}} \quad \begin{array}{l} \text{Longitudinal} \\ \text{Creepage} \end{array}$$

$$\gamma_2 = \frac{\text{actual lateral velocity} - \text{pure rolling lateral velocity}}{\text{forward velocity due to rolling}} \quad \text{Lateral Creepage}$$

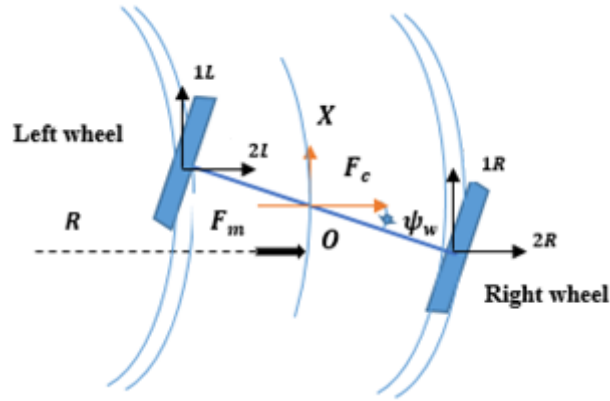


Figure 3-3- Forces action on wheelset in plan view

The longitudinal creep force can be found as [5]:

$$F_x = -f_{11}\gamma_{1l} + f_{11}\gamma_{1R} = -\frac{2L_g f_{11}}{v_s} \dot{\psi} - \frac{2\lambda f_{11}}{r_0} (y_w - y_t) + \frac{2L_g f_{11}}{R} - \frac{2r_0 f_{11}}{v_s} \dot{\phi} \quad (3-9)$$

In addition, the wheelset lateral creep force can be found as:

$$F_y = -f_{22}\gamma_{2l} - f_{22}\gamma_{2R} = -2f_{22} \left(\frac{\dot{y}}{v_s} - \psi \right) \quad (3-10)$$

Figure 3-3 shows that the contact force F_{1L} , contributes to the yaw motion of the wheelset in the direction akin to clockwise, whereas F_{1R} has the effect in the opposite, that is, the anticlockwise, direction.

Where L_g is half wheelset axle length. While the wheelset moves on a curve and canted track with a cant angle θ_t depicted in Figure 3-4, a component F_m of the force due to gravity $m_w \cdot g$ will act on the wheelset in lateral direction, which can be defined as:

$$F_m = -m_w \cdot g \cdot \sin \theta_t \quad (3-11)$$

Given that θ_t is usually small in practical cases, therefore, $\sin\theta_t$ can approximately be equal to θ_t , yielding:

$$F_m = -m_w \cdot g \cdot \theta_t \quad (3-12)$$

The centrifugal force F_c acting on the wheelset also needs to be taken into consideration. Since

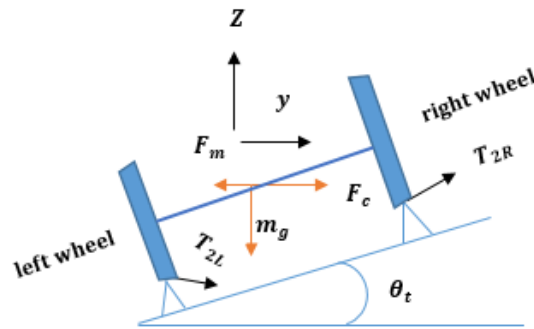


Figure 3-4- Forces action on wheelset in plan view

a synchronous local reference Oxy is used in the assessment of its dynamic, as shown in Figure 3-5, F_c can be derived from:

$$F_c = \frac{m_w \cdot v_s^2}{R} \quad (3-13)$$

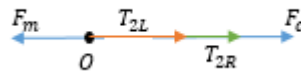


Figure 3-5- Forces combining in the lateral direction

Considering Newton's second law, the subsequent dynamic equation of lateral motion of the wheelset can be expressed by equation 3.14:

$$m_w \ddot{y}_w = F_y + F_c + F_m \quad (3-14)$$

The dynamic equation of the yaw motion of the wheelset, according to the law of angular moments, can be expressed as:

$$J_w \cdot \ddot{\psi}_w = F_x L_g \quad (3-15)$$

Where I_w is the moment of inertia of the wheelset. Also, the dynamic equation of the relative rotation between the two wheels of the wheelset describe as:

$$J_\phi \ddot{\phi}_R = r_0 F_R \quad (3-16)$$

$$J_\phi \ddot{\phi}_L = r_0 F_L \quad (3-17)$$

From equations 3-16 and 3-17

$$J_\phi \ddot{\phi} = \frac{r_0}{2} (F_R - F_L) \quad (3-18)$$

By combining the centrifugal force and the creep forces on the curves, an unconstrained wheelset can be expressed in terms of its lateral, yaw motion and the relative rotation between the two wheels of a wheelset as follows, where y_t represents the track irregularities in the lateral displacement:

$$\ddot{y} = -\frac{2f_{22}}{m_w v_s} \dot{y} + \frac{2f_{22}}{m_w} \psi + \frac{v_s^2}{R} - g\theta \quad (3-19)$$

$$\ddot{\psi} = -\frac{2f_{11} L_g \lambda}{J_w r_0} (y - y_t) - \frac{2f_{11} L_g^2}{J_w v_s} \dot{\psi} - \frac{2f_{11} L_g r_0}{J_w v_s} \dot{\phi} + \frac{2f_{11} L_g^2}{J_w R} \quad (3-20)$$

$$\ddot{\phi} = -\frac{f_{11} \lambda}{J_\phi} (y - y_t) - \frac{f_{11} L_g r_0}{J_\phi v_s} \dot{\psi} - \frac{f_{11} r_0^2}{J_\phi v_s} \dot{\phi} + \frac{f_{11} L_g r_0}{J_\phi R} \quad (3-21)$$

The wheelset dynamics are dictated by creepage. The first term in the lateral equation arises as a result of the pure lateral velocity; the second term, however, is that induced by wheelset

yaw. The third and fourth terms are to permit a moving axis system, i.e., the effects of track cant (θ) and curvature ($1/R$). The first term in the yaw equation is the longitudinal creep brought on by the conicity, and the second is that induced by the yaw velocity. The third term, where $\dot{\phi}$ is the difference in the variation of the rotating angular velocity between the right and left wheels, and is defined as [5, 7, 133]:

The last term is thus a correction to permit a moving axis system, this time to denote the dynamics in the rail speed, as initiated by the curvature [5, 12].

Table 3-1 shows the eigenvalue of the single independently rotating wheelsets.

The first two lines of the table represent the unstable modes of the independently rotating wheelset (equation 3-20). Third line of the table represents the eigenvalue at the origin (mean $S=0$) that indicates the lack of guidance action due to two wheels wheelset rotating independently (equation 3-21). The four and fifth line give the eigenvalues of the wheelset high frequency mode. Therefore, it is essential to stabilize the wheelset as well as provide guidance control for the wheelset to follow the track.

Table 3-1- Eigenvalues of single independently rotating wheelset

	Pole	Damping	Frequency (Hz/Time Unit)
1	$5.99e+00 + 4.06e+01i$	$-1.46e-01$	6.54
2	$5.99e+00 - 4.06e+01i$	$-1.46e-01$	6.54
3	0		0
4	$-4.34e+02$	$1.00e+00$	69.07
5	$-2.08e+02$	$1.00e+00$	33.1

For many years, the use of wheelsets with independently rotating wheels (IRW) has been the interest of railway engineers. IRW reduces creep forces, but it is not without its own disadvantages. One of the most common disadvantages of IRW is that it does not have natural

curving ability, and hence the system is unstable without control. In other words, the natural steering action of the wheelset is lost, which means that some kind or type of steering action is required to keep the wheelset appropriately aligned on a curve.

3.4 Modelling of a Two-Axle Railway Vehicle with Independently Rotating Wheelsets (IRW)

Active control technology provides much effective solution than the passive solutions and therefore offer the potential to simplify the mechanical configuration of rail vehicles. In this study, a simple two axle vehicle is first used. Figure 3-6 shows plan view of the two-axle vehicle used for modelling. The parameters used for this vehicle model are based on the requirements for future high-speed passenger vehicles that are intended to travel at 300 km/h. As the common practice for the study of vehicle dynamics the railway vehicle speed is constant but in case of study at a different speed value of the parameter V_s can be changed in the model. The vehicle model includes a vehicle body and two wheelsets, in which the wheelsets are connected to the body through springs and dampers in the lateral direction. In practical case some form of longitudinal connection also exists due to the need to transmit traction and breaking forces from the wheels to the vehicle body. They can be arranged such that the yaw dynamics, are not affected and therefore do not need to be considered in this study.

There is also vertical suspension as well as roll suspension which are not included in this model as this study is focused on active steering of the wheelset for which only the plan view dynamics of the vehicle are considered.

On each wheelset, between wheelset and body, an actuator is mounted in the yaw or longitudinal direction for active control applications as shown in figure 3-6. It should be noted that actuator can be mounted in either yaw or lateral direction. However, the comparison of different structure shown that by mounting the actuator in yaw direction can provide the effective control of the wheelsets. It is because placing an actuator in lateral direction, wheelset controlling force is applied directly to the vehicle body and it has a negative affect of the body modes [6].

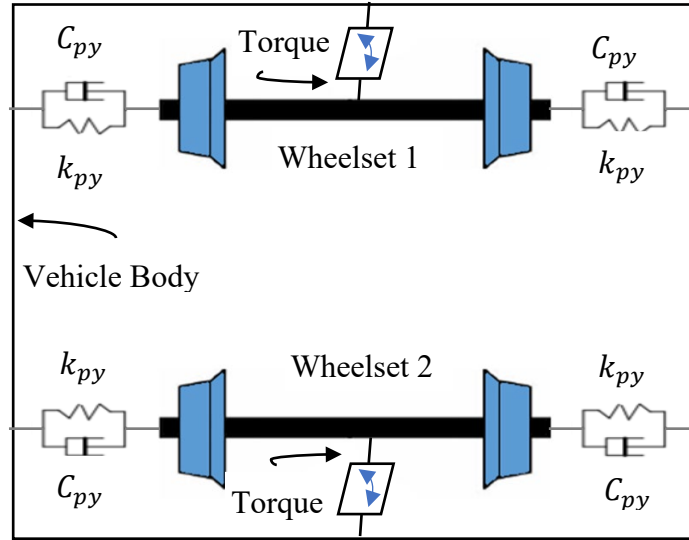


Figure 3-6- Plan view of a two axles vehicle

The linearized model with eight degrees of freedom presented in equations 3-28 to 3-47, which is developed based on the idea that an active steering controller improves the performance on the curve in such a way as to significantly decrease the effect of nonlinearities. It is noteworthy that the nonlinearities of the railway vehicle model are significantly related with nonlinear wheel-rail profiles and contact forces, and mainly it becomes an issue when the wheel-rail contact point approaches the wheel flange. However, it is possible to overcome this issue by utilizing an active steering control to allow the wheelset to operate at the linear region of the wheel and rail surfaces [134].

The reference directions in Figure 3-6 are from left to right for the lateral movements and clockwise for the yaw movements. The positive reference for the relative rotation between the two wheels of each wheelset is in the direction that makes the wheelset yaw in the positive direction.

Equations 3-22 and 3-23 represent suspension forces of the primary suspension system in lateral direction, Equations 3-24 and 3-25 represent the lateral creep forces and Equations 3-26 and 3-27 represent the longitudinal creep forces.

$$F_{pyw1} = -K_{py}(-y_v - L_v\psi_v + y_{w1}) - C_{py}(-\dot{y}_v - L_v\dot{\psi}_v + \dot{y}_{w1}) \quad (3-22)$$

$$F_{pyw2} = -K_{py}(-y_v + L_v\psi_v + y_{w2}) - C_{py}(-\dot{y}_v + L_v\dot{\psi}_v + \dot{y}_{w2}) \quad (3-23)$$

$$F_{y1} = -2f_{22}\left(\frac{\dot{y}_{w1}}{v_s} - \psi_{w1}\right) \quad (3-24)$$

$$F_{y2} = -2f_{22}\left(\frac{\dot{y}_{w2}}{v_s} - \psi_{w2}\right) \quad (3-25)$$

$$F_{x1} = -\frac{2L_g f_{11}}{v_s}\dot{\psi}_{w1} - \frac{2\lambda f_{11}}{r_0}y_{w1} + \frac{2L_g f_{11}}{R_1} - \frac{2r_0 f_{11}}{v_s}\dot{\phi}_{w1} \quad (3-26)$$

$$F_{x2} = -\frac{2L_g f_{11}}{v_s}\dot{\psi}_{w2} - \frac{2\lambda f_{11}}{r_0}y_{w2} + \frac{2L_g f_{11}}{R_2} - \frac{2r_0 f_{11}}{v_s}\dot{\phi}_{w2} \quad (3-27)$$

As previously explained a two-axle railway vehicle includes two wheelsets, which are connected to the body. The dynamics of the railway vehicle can be characterised by the lateral, y_w , and yaw, ψ_w , motion as well as the relative rotation between two wheels of a wheelset, ϕ_w . The governing equations of motion for wheelset one in lateral motion presented in Equations 3-28 to 3-30, yaw motion in Equations 3-31 and 3-32 and the relative rotation between two wheels of a wheelset in Equations 3-33 and 3-34. Subsequently Equations 3-35 to 3-41 presented the dynamics of wheelset 2.

However, longitudinal absolute forward rotation of the wheels is not modelled as they are not of concern or relevance to railway vehicle dynamics because of the large time constants of the forward motion.

$$m_w\ddot{y}_{w1} = F_{pyw1} + F_{y1} \quad (3-28)$$

By substituting 3-22 and 3-24 into 3-28 gives:

$$m_w \ddot{y}_{w1} = -K_{py}(-y_v - L_v \psi_v + y_{w1}) - C_{py}(-\dot{y}_v - L_v \dot{\psi}_v + \dot{y}_{w1}) \quad (3-29)$$

$$-2f_{22} \left(\frac{\dot{y}_{w1}}{v_s} - \psi_{w1} \right) + F_m + F_c$$

By substituting 3-12 and 3-13 into 3-29 gives:

$$m_w \ddot{y}_{w1} + \left(\frac{2f_{22}}{v_s} + C_{py} \right) \dot{y}_{w1} + K_{py} y_{w1} - 2f_{22} \psi_{w1} - C_{py} \dot{y}_v - K_{py} y_v - C_{py} L_v \dot{\psi}_v \quad (3-30)$$

$$-K_{py} L_v \psi_v = m_w \left(\frac{v_s^2}{R_1} - g \theta_{c1} \right)$$

$$J_w \cdot \ddot{\psi}_{w1} = F_{x1} L_g + T_{w1} \quad (3-31)$$

By substituting 3-26 into 3-31 gives:

$$J_w \ddot{\psi}_{w1} + \left(\frac{2f_{11} L_g^2}{v_s} \right) \dot{\psi}_{w1} + \frac{2f_{11} \lambda L_g}{r_0} y_{w1} + \frac{2r_0 f_{11} L_g}{v_s} \dot{\phi}_{w1} = \frac{2f_{11} L_g^2}{R_1} + \frac{2f_{11} \lambda L_g}{r_0} y_{t1} \quad (3-32)$$

$$+ T_{w1}$$

$$J_\phi \ddot{\phi}_{w1} = \frac{r_0}{2} (F_{x1}) \quad (3-33)$$

By substituting 3-26 into 33 gives:

$$J_\phi \ddot{\phi}_{w1} + \frac{r_0^2 f_{11}}{v_s} \dot{\phi}_{w1} + f_{11} \lambda y_{w1} + \frac{r_0^2 f_{11} L_g}{v_s} \dot{\psi}_{w1} = \frac{r_0 f_{11} L_g}{R_1} + f_{11} \lambda y_{t1} \quad (3-34)$$

Rear wheelset:

$$m_w \ddot{y}_{w2} = F_{pyw2} + F_{y2} \quad (3-35)$$

By substituting 3-23 and 3-25 into 3-35 gives:

$$m_w \ddot{y}_{w2} = -K_{py}(-y_v + L_v \psi_v + y_{w2}) - C_{py}(-\dot{y}_v + L_v \dot{\psi}_v + \dot{y}_{w2}) \quad (3-36)$$

$$-2f_{22} \left(\frac{\dot{y}_{w2}}{v_s} - \psi_{w2} \right) + F_m + F_c$$

By substituting 3-12 and 3-13 into 3-36 gives:

$$m_w \ddot{y}_{w2} + \left(\frac{2f_{22}}{v_s} + C_{py} \right) \dot{y}_{w2} + K_{py} y_{w2} - 2f_{22} \psi_{w2} - C_{py} \dot{y}_v - K_{py} y_v + C_{py} L_v \dot{\psi}_v \quad (3-37)$$

$$+ K_{py} L_v \psi_v = m_w \left(\frac{v_s^2}{R_2} - g \theta_{c2} \right)$$

$$J_w \ddot{\psi}_{w2} = F_{x2} L_g + T_{w2} \quad (3-38)$$

By substituting 3-27 into 3-38 gives:

$$J_w \ddot{\psi}_{w2} + \left(\frac{2f_{11} L_g^2}{v_s} \right) \dot{\psi}_{w2} + \frac{2f_{11} \lambda L_g}{r_0} y_{w2} + \frac{2r_0 f_{11} L_g}{v_s} \dot{\phi}_{w2} = \frac{2f_{11} L_g^2}{R_2} + \frac{2f_{11} \lambda L_g}{r_0} y_{t2} \quad (3-39)$$

$$+ T_{w2}$$

$$J_\phi \ddot{\phi}_{w2} = \frac{r_0}{2} (F_{x2}) \quad (3-40)$$

By substituting 3-27 into 3-40 gives:

$$J_\phi \ddot{\phi}_{w2} + \frac{r_0^2 f_{11}}{v_s} \dot{\phi}_{w2} + f_{11} \lambda y_{w2} + \frac{r_0^2 f_{11} L_g}{v_s} \dot{\psi}_{w2} = \frac{r_0 f_{11} L_g}{R_2} + f_{11} \lambda y_{t2} \quad (3-41)$$

Body railway vehicle dynamics can be characterised by the lateral, y_v , and yaw, ψ_v , motions, which are given by the following equations:

$$m_v \ddot{y}_v = -F_{pyw1} - F_{pyw2} + F_m + F_c \quad (3-42)$$

By substituting 3-22 and 3-23 into 3-42 gives:

$$\begin{aligned} m_v \ddot{y}_v = & K_{py}(-y_v + L_v \psi_v + y_{w1}) + C_{py}(-\dot{y}_v + L_v \dot{\psi}_v + \dot{y}_{w1}) + K_{py} \\ & (-y_v - L_v \psi_v + y_{w2}) + C_{py}(-\dot{y}_v - L_v \dot{\psi}_v + \dot{y}_{w2}) + F_m + F_c \end{aligned} \quad (3-43)$$

By substituting 3-12 and 3-13 into 3-43 gives:

$$\begin{aligned} m_v \ddot{y}_v + 2C_{py} \dot{y}_v + 2K_{py} y_v - C_{py} \dot{y}_{w1} - K_{py} y_{w1} - C_{py} \dot{y}_{w2} - K_{py} y_{w2} \\ = \frac{m_w v_s^2}{2} \left(\frac{1}{R_1} + \frac{1}{R_2} \right) - \frac{m_w g}{2} (\theta_{c1} + \theta_{c2}) \end{aligned} \quad (3-44)$$

$$J_v \ddot{\psi}_v = -F_{pyw1} L_v + F_{pyw2} L_v - (T_{w1} + T_{w2}) \quad (3-45)$$

By substituting 3-22 and 3-23 into 3-45 gives:

$$\begin{aligned} J_v \ddot{\psi}_v = & K_{py} L_v (-y_v - L_v \psi_v + y_{w1}) + C_{py} L_v (-\dot{y}_v - L_v \dot{\psi}_v + \dot{y}_{w1}) - \\ & K_{py} L_v (-y_v + L_v \psi_v + y_{w2}) - C_{py} L_v (-\dot{y}_v + L_v \dot{\psi}_v + \dot{y}_{w2}) \end{aligned} \quad (3-46)$$

$$\begin{aligned} J_v \ddot{\psi}_v + 2L_v^2 C_{py} \dot{\psi}_v + 2L_v^2 K_{py} \psi_v - L_v C_{py} \dot{y}_{w1} + L_v C_{py} \dot{y}_{w2} - L_v K_{py} y_{w1} + L_v K_{py} y_{w2} \\ = -(T_{w1} + T_{w2}) \end{aligned} \quad (3-47)$$

There are two different types of railway track input, deterministic and random. Deterministic input includes curve radius R_1, R_2 (for front and rear wheelset) and cant angles θ_1, θ_2 (for front and rear wheelset) which represent the design alignment. These characteristics are designed to provide passenger comfort. In addition, y_{t1}, y_{t2} (for front and rear wheelset)

are random inputs which are track irregularities that represent unintended deviations from the intended alignment.

Table 3-2 shows the eigenvalues of the two-axle railway vehicle for an uncontrolled model. The first four lines of the table present the unstable kinematic modes of the wheelset (equation 3-39). Fifth and sixth line of the table represent the eigenvalue at the origin (mean $S=0$) that is shown lack of guidance action due to two wheels of the wheelset rotating independently (equation 3-41). The seventh to tenth line give the eigenvalue of the wheelset high frequency mode and subsequently eleventh to fourteen lines presented the eigenvalue of the wheelset low frequency mode (equations 3-45 and 3-47). Thus, it is absolutely necessary to stabilize the wheelset kinematic as well as provide guidance control for wheelset to follow the track.

Table 3-2- Eigenvalues of Two- Axle railway vehicle without controller

	Pole	Damping	Frequency (Hz/Time Unit)
1	$4.16 + 38.2j$	-1.08e-01	6.11
2	$4.16 - 38.2j$	-1.08e-01	6.11
3	$4.17 + 38.2j$	-1.08e-01	6.11
4	$4.17 - 38.2i$	-1.08e-01	6.11
5	$-1.29e-14 + 3.30e-14j$	3.64e-01	$5.6e^{-15} \approx 0$
6	$-1.29e-14 - 3.30e-14j$	3.64e-01	$5.6e^{-15} \approx 0$
7	-416	1.00	66.2
8	-416	1.00	66.2
9	-239	1.00	38
10	-239	1.00	38
11	$-1.33 + 5.96j$	2.18e-01	0.9
12	$-1.33 - 5.96j$	2.18e-01	0.9
13	$-1.22 + 5.72j$	2.09e-01	0.93

14	-1.22 - 5.72j	2.09e-01	0.93
----	---------------	----------	------

3.5 Modelling of a Conventional Bogie Railway Vehicle with Independently Rotating Wheelsets (IRW)

A conventional bogie vehicle is also used in the study. Figure 3-7 shows a simplified plan view of the

conventional bogie vehicle which is used for modelling. The parameters used for this vehicle model are not the same as the two-axle railway vehicle. Also, by adding a bogie to the model an extra parameter is added to the system.

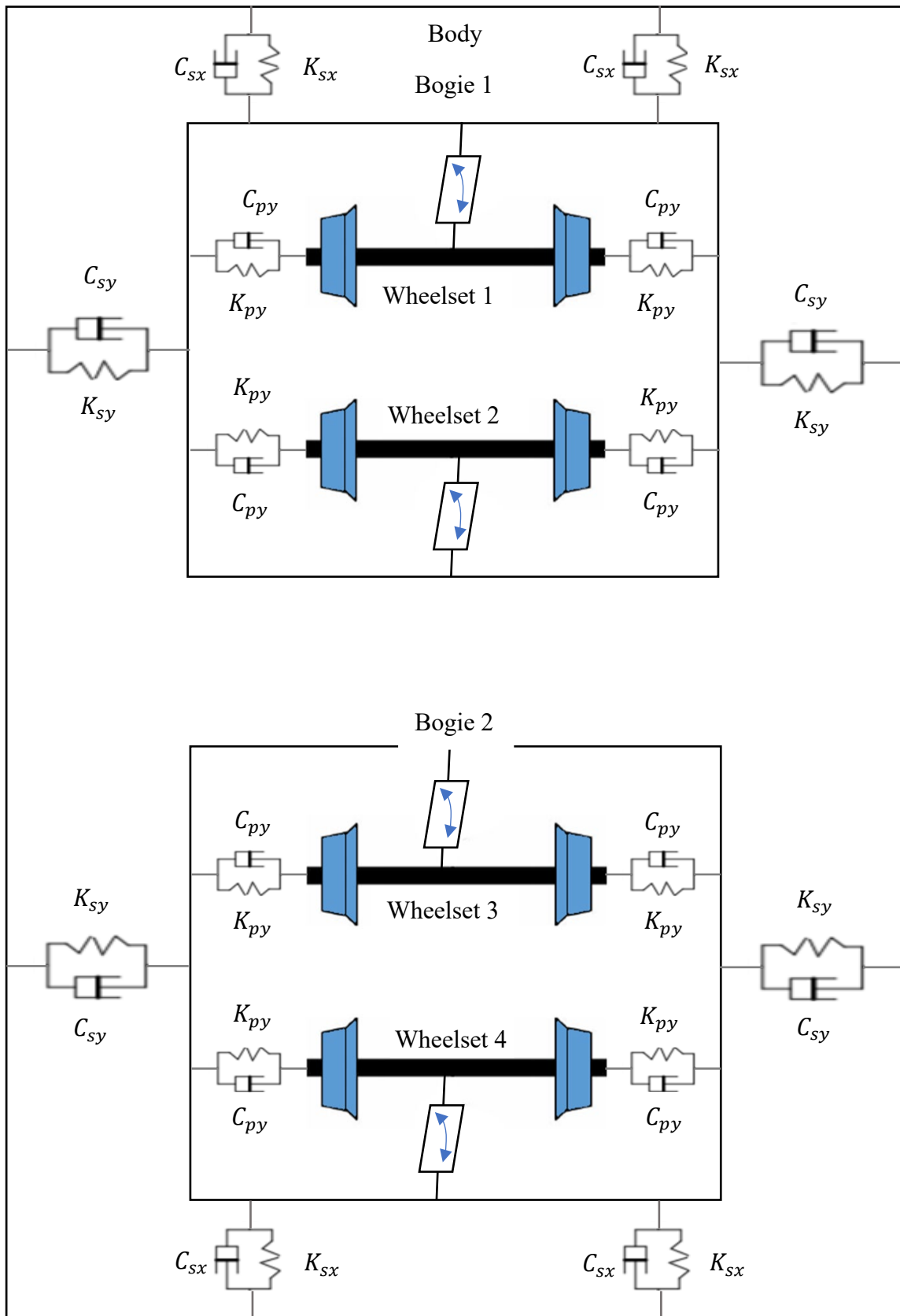


Figure 3-7- Plan view diagram of conventional bogie vehicle

It is notable that fundamental features of the model such as speed, inputs are the same as two axle railway vehicle model.

The vehicle model includes a vehicle body, two bogie (front and rear) and four wheelsets. Each two wheelsets are connected to a bogie, wheelsets 1 and 2 are connected to the front bogie and wheelsets 3 and 4 are connected to rear bogie, through springs and dampers in the lateral direction. On each wheelset, between wheelset and bogie an actuator is mounted in the yaw direction for active control application as it shown in figure 3-7. Also, each bogie connected to the body through springs and dampers in lateral and yaw direction.

The linearized model with 32 degrees of freedom is presented in equations 3.64 to 3.81.

Equations 3-48 to 3-51 represent suspension forces of the primary suspension system in lateral direction. Equations 3-52 to 3-55 represent suspension forces of the secondary suspension system in lateral and longitudinal direction. Equations 3-56 to 3-59 represent the lateral creep forces Equations 3-60 to 3-63 represent longitudinal creep forces causing the wheelset yaw motion.

$$F_{pyw1} = -K_{py}(-y_{b1} - L_v\psi_{b1} + y_{w1}) - C_{py}(-\dot{y}_{b1} - L_v\dot{\psi}_{b1} + \dot{y}_{w1}) \quad (3-48)$$

$$F_{pyw2} = -K_{py}(-y_{b1} + L_v\psi_{b1} + y_{w2}) - C_{py}(-\dot{y}_{b1} + L_v\dot{\psi}_{b1} + \dot{y}_{w2}) \quad (3-49)$$

$$F_{pyw3} = -K_{py}(-y_{b2} - L_v\psi_{b2} + y_{w3}) - C_{py}(-\dot{y}_{b2} - L_v\dot{\psi}_{b2} + \dot{y}_{w3}) \quad (3-50)$$

$$F_{pyw4} = -K_{py}(-y_{b2} + L_v\psi_{b2} + y_{w4}) - C_{py}(-\dot{y}_{b2} + L_v\dot{\psi}_{b2} + \dot{y}_{w4}) \quad (3-51)$$

$$F_{syb1} = -K_{sy}(-y_c - L\psi_c + y_{b1}) - C_{sy}(-\dot{y}_c - L\dot{\psi}_c + \dot{y}_{b1}) \quad (3-52)$$

$$F_{syb2} = -K_{sy}(-y_c + L\psi_c + y_{b2}) - C_{sy}(-\dot{y}_c + L\dot{\psi}_c + \dot{y}_{b2}) \quad (3-53)$$

$$F_{sxb1} = -K_{sx}(\psi_c - \psi_{b1})b_2 - C_{sx}(\dot{\psi}_c - \dot{\psi}_{b1})b_2 + K_{sx}b_2L\frac{R_1R_2}{R_1+R_2} \quad (3-54)$$

$$F_{sxb2} = -K_{sx}(\psi_c - \psi_{b2})b_2 - C_{sx}(\dot{\psi}_c - \dot{\psi}_{b2})b_2 - K_{sx}b_2L \frac{R_3R_4}{R_3+R_4} \quad (3-55)$$

$$F_{y1} = -2f_{22} \left(\frac{\dot{y}_{w1}}{v_s} - \dot{\psi}_{w1} \right) \quad (3-56)$$

$$F_{y2} = -2f_{22} \left(\frac{\dot{y}_{w2}}{v_s} - \dot{\psi}_{w2} \right) \quad (3-57)$$

$$F_{y3} = -2f_{22} \left(\frac{\dot{y}_{w3}}{v_s} - \dot{\psi}_{w3} \right) \quad (3-58)$$

$$F_{y4} = -2f_{22} \left(\frac{\dot{y}_{w4}}{v_s} - \dot{\psi}_{w4} \right) \quad (3-59)$$

$$F_{x1} = -\frac{2L_g f_{11}}{v_s} \dot{\psi}_{w1} - \frac{2\lambda f_{11}}{r_0} y_{w1} + \frac{2L_g f_{11}}{R_1} - \frac{2r_0 f_{11}}{v_s} \dot{\phi}_{w1} \quad (3-60)$$

$$F_{x2} = -\frac{2L_g f_{11}}{v_s} \dot{\psi}_{w2} - \frac{2\lambda f_{11}}{r_0} y_{w2} + \frac{2L_g f_{11}}{R_2} - \frac{2r_0 f_{11}}{v_s} \dot{\phi}_{w2} \quad (3-61)$$

$$F_{x3} = -\frac{2L_g f_{11}}{v_s} \dot{\psi}_{w3} - \frac{2\lambda f_{11}}{r_0} y_{w3} + \frac{2L_g f_{11}}{R_3} - \frac{2r_0 f_{11}}{v_s} \dot{\phi}_{w3} \quad (3-62)$$

$$F_{x4} = -\frac{2L_g f_{11}}{v_s} \dot{\psi}_{w4} - \frac{2\lambda f_{11}}{r_0} y_{w4} + \frac{2L_g f_{11}}{R_4} - \frac{2r_0 f_{11}}{v_s} \dot{\phi}_{w4} \quad (3-63)$$

The dynamics of the conventional bogie railway vehicle is characterised by the lateral, y_w , yaw, ψ_w , motion and the relative rotation between two wheels of a wheelset, ϕ_w . The governing equations of motion for wheelset one lateral motion is presented in Equations 3-64, yaw motion in Equations 3-65 and the relative rotation between two wheels of a wheelset in Equations 3-66. Subsequently Equations 3-67 to 3-69 represent the dynamic of wheelset 2, 3-

70 to 3-72 represent the dynamic of wheelset 3 and 3-73 to 3-75 represent the dynamic of wheelset 4.

However, as mentioned earlier in practice to transmit the traction and braking forces to the vehicle some sort of longitudinal connection is required, this is not included in this model as it is not the concern of the current study.

Applying the forces in equation 3-48 to 3-63 to the wheelsets, bogies and body frames using the newtons second laws gives:

Wheelset 1:

$$m_w \ddot{y}_{w1} + \left(\frac{2f_{22}}{v_s} + C_{py} \right) \dot{y}_{w1} - 2f_{22} \psi_{w1} + K_{py} y_{w1} - K_{py} y_{b1} - K_{py} L_v \psi_{b1} \quad (3-64)$$

$$-C_{py} \dot{y}_{b1} - C_{py} L_v \dot{\psi}_{b1} = m_w \left(\frac{v_s^2}{R_1} - g \theta_{c1} \right)$$

$$J_w \ddot{\psi}_{w1} + \left(\frac{2f_{11} L_g^2}{v_s} \right) \dot{\psi}_{w1} + \frac{2f_{11} \lambda L_g}{r_0} y_{w1} + \frac{2r_0 f_{11} L_g}{v_s} \dot{\phi}_{w1} = \frac{2f_{11} L_g^2}{R_1} + \frac{2f_{11} \lambda L_g}{r_0} y_{t1} \quad (3-65)$$

$$+ T_{w1}$$

$$J_\phi \ddot{\phi}_{w1} + \frac{r_0^2 f_{11}}{v_s} \dot{\phi}_{w1} + f_{11} \lambda y_{w1} + \frac{r_0^2 f_{11} L_g}{v_s} \dot{\psi}_{w1} = \frac{r_0 f_{11} L_g}{R_1} + f_{11} \lambda y_{t1} \quad (3-66)$$

Wheelset 2:

$$m_w \ddot{y}_{w2} + \left(\frac{2f_{22}}{v_s} + C_{py} \right) \dot{y}_{w2} - 2f_{22} \psi_{w2} + K_{py} y_{w2} - K_{py} y_{b1} + K_{py} L_v \psi_{b1} \quad (3-67)$$

$$-C_{py} \dot{y}_{b1} + C_{py} L_v \dot{\psi}_{b1} = m_w \left(\frac{v_s^2}{R_2} - g \theta_{c2} \right)$$

$$J_w \ddot{\psi}_{w2} + \left(\frac{2f_{11}L_g^2}{v_s} \right) \dot{\psi}_{w2} + \frac{2f_{11}\lambda L_g}{r_0} y_{w2} + \frac{2r_0 f_{11}L_g}{v_s} \dot{\phi}_{w2} = \frac{2f_{11}L_g^2}{R_2} + \frac{2f_{11}\lambda L_g}{r_0} y_{t2} \quad (3-68)$$

+T_{w2}

$$J_\phi \ddot{\phi}_{w2} + \frac{r_0^2 f_{11}}{v_s} \dot{\phi}_{w2} + f_{11}\lambda y_{w2} + \frac{r_0^2 f_{11}L_g}{v_s} \dot{\psi}_{w2} = \frac{r_0 f_{11}L_g}{R_2} + f_{11}\lambda y_{t2} \quad (3-69)$$

Wheelset 3:

$$m_w \ddot{y}_{w3} + \left(\frac{2f_{22}}{v_s} + C_{py} \right) \dot{y}_{w3} - 2f_{22}\psi_{w3} + K_{py}y_{w3} - K_{py}y_{b2} - K_{py}L_v\psi_{b2} \quad (3-70)$$

$$-C_{py}\dot{y}_{b2} - C_{py}L_v\dot{\psi}_{b2} = m_w \left(\frac{v_s^2}{R_3} - g\theta_{c3} \right)$$

$$J_w \ddot{\psi}_{w3} + \left(\frac{2f_{11}L_g^2}{v_s} \right) \dot{\psi}_{w3} + \frac{2f_{11}\lambda L_g}{r_0} y_{w3} + \frac{2r_0 f_{11}L_g}{v_s} \dot{\phi}_{w1} = \frac{2f_{11}L_g^2}{R_3} + \frac{2f_{11}\lambda L_g}{r_0} y_{t3} \quad (3-71)$$

+T_{w3}

$$J_\phi \ddot{\phi}_{w3} + \frac{r_0^2 f_{11}}{v_s} \dot{\phi}_{w3} + f_{11}\lambda y_{w3} + \frac{r_0^2 f_{11}L_g}{v_s} \dot{\psi}_{w3} = \frac{r_0 f_{11}L_g}{R_3} + f_{11}\lambda y_{t3} \quad (3-72)$$

Wheelset 4:

$$m_w \ddot{y}_{w4} + \left(\frac{2f_{22}}{v_s} + C_{py} \right) \dot{y}_{w4} - 2f_{22}\psi_{w4} + K_{py}y_{w4} - K_{py}y_{b2} + K_{py}L_v\psi_{b2} \quad (3-73)$$

$$-C_{py}\dot{y}_{b2} + C_{py}L_v\dot{\psi}_{b2} = m_w \left(\frac{v_s^2}{R_4} - g\theta_{c4} \right)$$

$$J_w \ddot{\psi}_{w4} + \left(\frac{2f_{11}L_g^2}{v_s} \right) \dot{\psi}_{w4} + \frac{2f_{11}\lambda L_g}{r_0} y_{w4} + \frac{2r_0 f_{11}L_g}{v_s} \dot{\phi}_{w4} = \frac{2f_{11}L_g^2}{R_4} + \frac{2f_{11}\lambda L_g}{r_0} y_{t4} \quad (3-74)$$

+T_{w4}

$$J_\phi \ddot{\phi}_{w4} + \frac{r_0^2 f_{11}}{v_s} \dot{\phi}_{w4} + f_{11}\lambda y_{w4} + \frac{r_0^2 f_{11}L_g}{v_s} \dot{\psi}_{w4} = \frac{r_0 f_{11}L_g}{R_4} + f_{11}\lambda y_{t4} \quad (3-75)$$

Dynamics of each bogie can be characterised by the lateral, y_b , and yaw, ψ_b , motions, which are given by the following equations, equations 3-76 present lateral motion and equations 3-77 present yaw motion of front bogie. Moreover equations 3-78 and 3-79 present lateral and yaw motion in rear bogie.

Front bogie:

$$m_b \ddot{y}_{b1} - K_{sy}(y_c + L\psi_c - y_{b1}) - C_{sy}(\dot{y}_c + L\dot{\psi}_c - \dot{y}_{b1}) - K_{py}(y_{w1} + y_{w2} - 2y_{b1}) \quad (3-76)$$

$$-C_{py}(\dot{y}_{w1} + \dot{y}_{w2} - 2\dot{y}_{b1}) = \frac{m_b v_s^2}{2} \left(\frac{1}{R_1} + \frac{1}{R_2} \right) - \frac{m_b g}{2} (\theta_{c1} + \theta_{c2})$$

$$J_b \ddot{\psi}_{b1} - K_{sx} b_2^2 \left(\psi_c - \psi_{b1} + \frac{LR_1 R_2}{b_2(R_1 + R_2)} \right) - C_{sx} b_2^2 (\dot{\psi}_c - \dot{\psi}_{b1}) \quad (3-77)$$

$$-2K_{py} L_v (y_{w1} - y_{w2} - 2L_v \psi_{b1}) - 2C_{py} L_v (\dot{y}_{w1} - \dot{y}_{w2} - 2L_v \dot{\psi}_{b1})$$

$$= -(T_{w1} + T_{w2})$$

Rear bogie:

$$m_b \ddot{y}_{b2} - K_{sy}(y_c + L\psi_c - y_{b2}) - C_{sy}(\dot{y}_c + L\dot{\psi}_c - \dot{y}_{b2}) - K_{py}(y_{w3} + y_{w4} - 2y_{b2}) \quad (3-78)$$

$$-C_{py}(\dot{y}_{w3} + \dot{y}_{w4} - 2\dot{y}_{b2}) = \frac{m_b v_s^2}{2} \left(\frac{1}{R_3} + \frac{1}{R_4} \right) - \frac{m_b g}{2} (\theta_{c3} + \theta_{c4})$$

$$J_b \ddot{\psi}_{b2} - K_{sx} b_2^2 \left(\psi_c - \psi_{b2} + \frac{LR_3 R_4}{b_2(R_3 + R_4)} \right) - C_{sx} b_2^2 (\dot{\psi}_c - \dot{\psi}_{b2}) \quad (3-79)$$

$$-2K_{py} L_v (y_{w3} - y_{w4} - 2L_v \psi_{b2}) - 2C_{py} L_v (\dot{y}_{w1} - \dot{y}_{w2} - 2L_v \dot{\psi}_{b2})$$

$$= -(T_{w3} + T_{w4})$$

Equations 3-80 and 3-81 describe lateral, y_c , and yaw, ψ_c , motions of vehicle body.

$$m_c \ddot{y}_c - K_{sy} (y_{b1} + y_{b2} - 2y_c) - C_{sy} (\dot{y}_{b1} + \dot{y}_{b2} - 2\dot{y}_c) \quad (3-80)$$

$$= \frac{m_c v_s^2}{4} \left(\frac{1}{R_1} + \frac{1}{R_2} + \frac{1}{R_3} + \frac{1}{R_4} \right) - \frac{m_c g}{4} (\theta_{c1} + \theta_{c2} + \theta_{c3} + \theta_{c4})$$

$$J_c \ddot{\psi}_c - K_{sx} b_2^2 \left(\psi_{b1} + \psi_{b2} - 2\psi_c + \frac{LR_1 R_2}{2(R_1 + R_2)} - \frac{LR_3 R_4}{2(R_3 + R_4)} \right) + C_{sx} b_2^2 (\dot{\psi}_{b1}$$

$$+ \dot{\psi}_{b2} - 2\dot{\psi}_c) - K_{sy} L (-2L\psi_c - y_{b2} + y_{b1}) - C_{sy} L (-2L\dot{\psi}_c - \dot{y}_{b2} + \dot{y}_{b1})$$

$$= (T_{w1} + T_{w2} + T_{w3} + T_{w4})$$

Table 3-3 shows the eigenvalues of the conventional bogie railway vehicle without controller. The first eight lines of the table present the unstable kinematic modes of the wheelset (equations 3-65, 3-68, 3-71-and 3-74). Lines nine to twelve of the table represent the eigenvalue at the origin (mean $S=0$) that is shown lake of guidance action due to two wheels of the wheelset rotating independently (equations 3-66, 3-69, 3-72 and 3-75). The lines thirteen to twenty give the eigenvalue of the wheelset high frequency mode and lines twenty-one to twenty-eight give the eigenvalue of the bogies (equations 3-76 to 3-79) subsequently twenty-nine to thirty-two presented the eigenvalue of the body vehicle (equations 3-80 and 3-81). Thus, same as two axle vehicle it is essential to stabilize the wheelset kinematic as well as provide guidance control for wheelset to follow the track.

Table 3-3- The eigenvalue of the conventional bogie railway vehicle without controller model

	Pole	Damping	Frequency (Hz/Time Unit)
1	$4.83 + 26.7j$	-1.78e-01	4.31
2	$4.83 - 26.7j$	-1.78e-01	4.31
3	$4.81 + 26.7j$	-1.77e-01	4.31
4	$4.81 - 26.7j$	-1.77e-01	4.31
5	$1.08 + 23.8j$	-4.55e-02	3.78
6	$1.08 - 23.8j$	-4.55e-02	3.78
7	$1.16 + 23.8j$	-4.89e-02	3.78
8	$1.16 - 23.8j$	-4.89e-02	3.78
9	-2.06e-14	1.00	≈ 0
10	2.95e-14	-1.00	≈ 0
11	1.13e-13	-1.00	≈ 0
12	2.13e-13	-1.00	≈ 0
13	-410	1.00	65.25
14	-410	1.00	65.25
15	-410	1.00	65.25
16	-410	1.00	65.25
17	-183	1.00	29.1
18	-183	1.00	29.1
19	-183	1.00	29.1
20	-183	1.00	29.1
21	$-98.2 + 136j$	5.85e-01	26.7
22	$-98.2 - 136j$	5.85e-01	26.7
23	$-26.8 + 118j$	2.22e-01	19.25

24	-26.8 – 118j	2.22e-01	19.25
25	-26.8 + 118j	2.23e-01	19.25
26	-26.8 - 118j	2.23e-01	19.25
27	-111	1.00	17.66
28	-111	1.00	17.66
29	-2.09 + 4.62j	4.12e-01	0.8
30	-2.09 - 4.62j	4.12e-01	0.8
31	-1.60 + 4.39j	3.42e-01	0.74
32	-1.60- 4.39j	3.42e-01	0.74

3.6 Magnetorheological Damper

An MR damper can be categorised as a controllable fluid damper where the viscosity properties changes in the presence of an induced magnetic field. By changing the field intensity around the fluid, the yield stress can be controlled to very high accuracy. Changing the field intensity can produce an adjustable damping force [13]. MR fluids can be made up of micro-sized ferromagnetic grains, like as iron particles, which are suspended in a carrier oil (non-magnetisable liquid) such as mineral oil, synthetic oil, water or glycol [15, 17].

MR fluids graduate change in their rheological behaviour under the influence of an induced magnetic field. MR fluids can reversibly and rapidly switch from free-flowing liquids to semi-solid in a millisecond. It is noticeable that MR fluids have controllable yield strength while exposed to a magnetic field [135]. Without applying magnetic field, MR fluids are moving in the steady stream in a comparable manner to any other fluid of similar viscosity. In this situation, the ferrous particles have not any form state, as shown in Figure 3-8. When a magnetic field is induced, the ferrous particles align parallel to the flux path, as shown in Figure 3-9, and finally particles will appear and form in the fluid, as shown in Figure 3-10 [13]. In addition, it is important to note that, as a result, a yield stress increase in the field and the degree of the change will affect the intensity of the induced magnetic field [136].

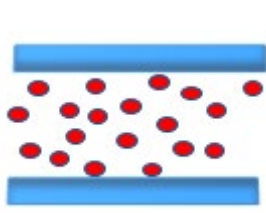


Figure3-8- No magnetic field applied

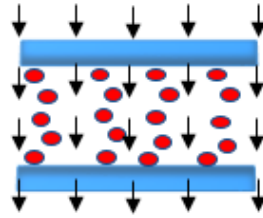


Figure 3-9- Magnetic field applied

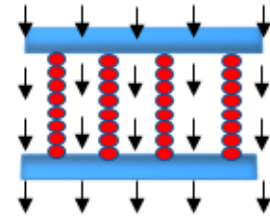


Figure 3-10- Chains have formed

An MR damper is a nonlinear device, which means the output is not directly proportional to the input. It is also a hysteretic device, which means that the output is dependent on history of the output as well as the instantaneous values of the input [137]. The inputs of the MR damper include an electrical input, which can be a current or voltage, and a mechanical input, which is the displacement of one end of the damper relative to the other and/or the corresponding velocity, and/or acceleration [13]. Subsequently, the input for the inverse dynamics of the model is current or voltage, which is required to produce the desired force for a given machine input.

The most basic mathematical model is that of Bingham [13]. This model was first used to study the dynamic behaviour of ER dampers [138] and then subsequently utilized for MR dampers [120]. It is notable that the model cannot produce a force-velocity hysteresis loop. The model is presented in Figure 3-11.

The Bouc-Wen model is shown in Figure 3-12. This model is able to mimic different hysteretic behaviour, but it is not very accurate.

The Modified Bouc-Wen model is shown in Figure 3-13. This model is able to mimic a different hysteretic behaviour, and it can be a much more accurate model [13, 139].

In this research a Modified Bouc-Wen model of MR damper is used for semi-active controller.

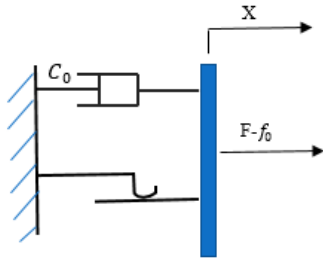


Figure 3-11- Bingham model

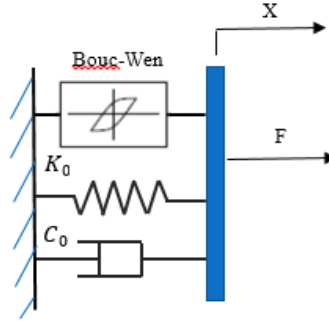


Figure 3-12- Bouc-Wen model

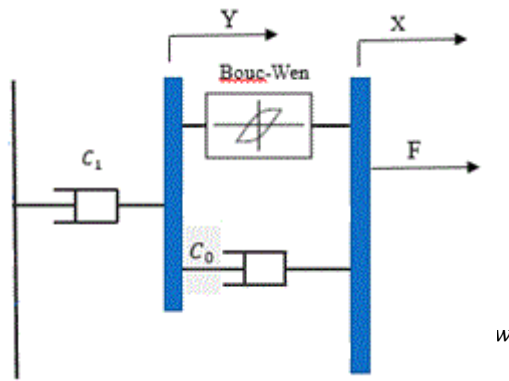


Figure 3-13- Modified Bouc-Wen

A mathematical model for the MR damper model Modified Bouc- Wen is presented to demonstrate vibrational control performance. The nonlinear equations below define the Modified Bouc-Wen model [123].

$$F = C_1 \dot{y} \tag{3-82}$$

$$\dot{y} = \frac{1}{C_0 + C_1} [\alpha z + C_0 \dot{x}] \tag{3-83}$$

$$\dot{z} = -\gamma |\dot{x} - \dot{y}| z |z|^{n-1} - \beta (\dot{x} - \dot{y}) |z|^n + A (\dot{x} - \dot{y}) \tag{3-84}$$

Where F is the damping force, C_1 display viscous damping at low velocities, C_0 represents viscous damping at high velocities, x is the piston's relative displacement, y is the damper internal displacement and z is the evolutionary variable. In addition, α is a scaling value for the Bouc–Wen hysteresis loop, and β , A , and n are parameters used to adjust the scale and shape of the hysteresis loop. The parameters γ , β , A and n are constants. Also, to complete the MR damper model equations it is essential to determine the function which depends on the current. The parameters C_0 , C_1 and α , are utilised to be functions of the applied current I as follow [123]:

$$\alpha = \alpha_a + \alpha_b I + \alpha_c I^2 \quad (3-85)$$

$$C_0 = C_{0a} + C_{0b} I \quad (3-86)$$

$$C_1 = C_{1a} + C_{1b} I \quad (3-87)$$

The optimum value of the 10 parameters, C_{0a} , C_{0b} , α_a , α_b , α_c , C_{1a} , C_{1b} , γ , β , A , and n , for the modified Bouc–Wen model of Mr damper presented in table 3-4.

Table 3-4- Parameter values of the Modified Bouc-Wen model [123].

parameter	value
C_{0a}	1000 Nsmm^{-1}
C_{0b}	$1103 \text{ Nsmm}^{-1} \text{A}^{-1}$
α_a	10441 Nmm^{-1}
α_b	$14930 \text{ Nmm}^{-1} \text{A}^{-1}$
C_{1a}	8649 Nsmm^{-1}
C_{1b}	$10622 \text{ Nsmm}^{-1} \text{A}^{-1}$
n	parameters used to adjust the scale and shape of the hysteresis loop (2)
γ	parameters used to adjust the scale and shape of the hysteresis loop (96320 mm^{-2})
β	parameters used to adjust the scale and shape of the hysteresis loop (96320)
A	parameters used to adjust the scale and shape of the hysteresis loop (470 mm^{-2})

The model is first examined in Simulink in a range of operating conditions without any control applied.

Figures 3-14 and 3-15 show damping force vs. velocity of MR damper at frequency 1 and 5 Hz. Parameter I is the control current, that can be varied between 0~2A, and the velocity inputs (sinewave) applied across the MR damper. Damping force increases with increases in the relative velocity. Damping force determined by relevant current and velocity input to the MR damper. This means that there are upper and lower bounds to the force that can be applied.

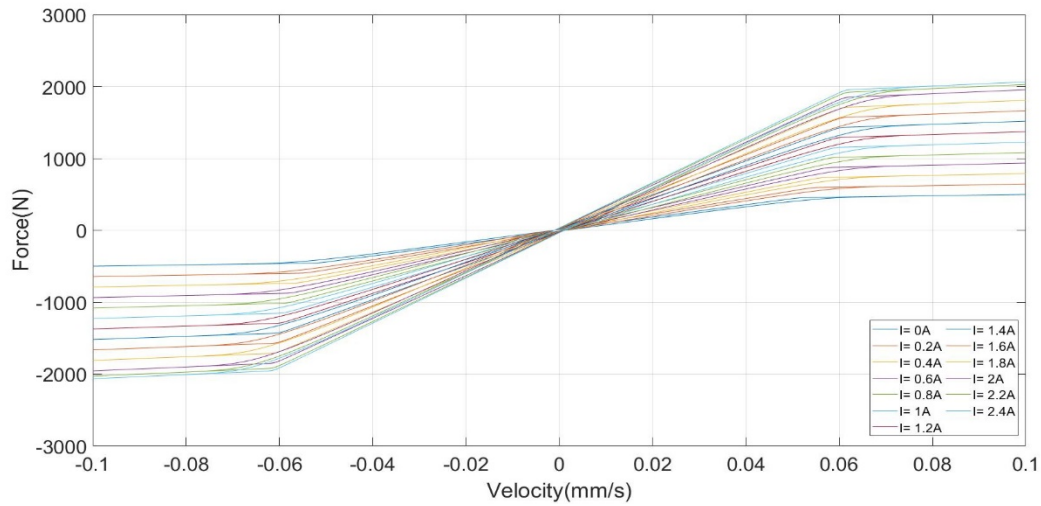


Figure 3-14- Damping force vs. velocity of Modified Bouc-Wen model (1Hz,0.1mm/s)

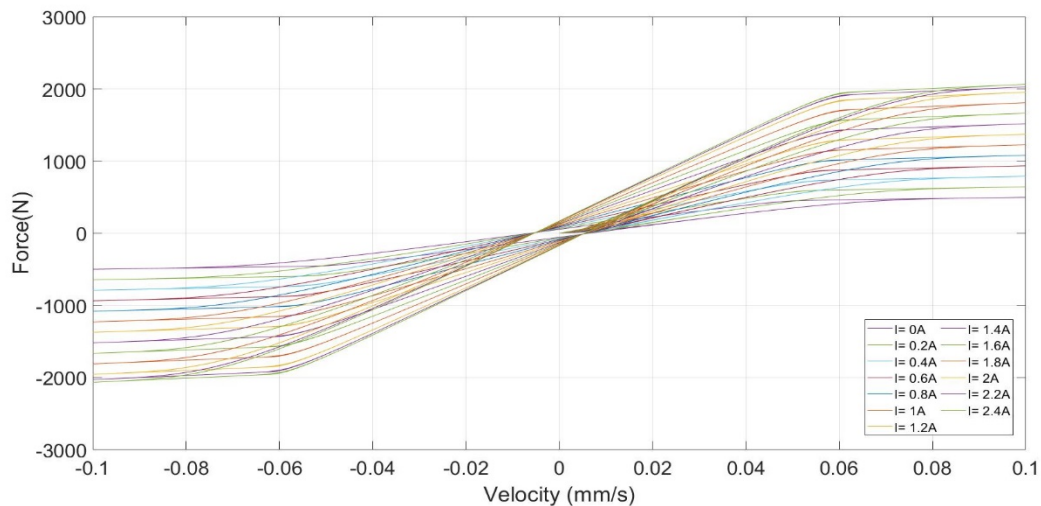


Figure 3-15- Damping force vs. velocity of Modified Bouc-Wen model (5Hz,0.1mm/s)

It is clear that force and velocity (for lower velocity) have nonlinear relationship. However, as show in figure 3-14 and 3-15 for high velocity the relationship between force and velocity becomes more linear. This relation between force and small velocity is due to bleed of MR fluid between the cylinder and the piston, which is necessary to rectify harshness of the MR damper. Also, increasing the frequency leads to an increase in nonlinearity [33].

Between 0 A to 2 A, the absorbing energy can be seen to increase but for currents greater than 2 A the absorbed energy produced relatively little variance, which means for currents

above 2 A the magnetic field has become saturated. Therefore, an effective magnetic field for this damper would be less than 2 A.

3.7 Summary

In this chapter mathematical models of single independently rotating wheelsets, the Two-Axle Vehicle with Independently Rotating Wheelsets and conventional bogie railway vehicle have been developed. Also, a mathematical model of the modified Bouc-Wen model (prototype of magnetorheological dampers) was developed to represent the dynamic behaviour of a magnetorheological dampers.

Magnetorheological dampers can change the damping ratio by changing magnetic fields. Magnetorheological dampers are an interesting object for semi-active controllers in suspension usage due to properties such as fast response time, large damping force range, low power consumption and safe-mode operation in case of failure.

Magnetorheological dampers have been used to control vibration. However, a controller is essential to control current in order for MR dampers to generate the desired force. Due to complexity of mathematical models and highly nonlinear magnetorheological damper inverse model method has been used as a local magnetorheological damper controller. The technique used in this study for inverse model is Lookup table. The lookup table has been used to attain controlled current regarding to demanded damping force, the controlled current is fed to the magnetorheological damper.

Chapter 4: Active Control

4.1 Introduction

Active primary suspension is designed to increase the quality of running stability on a straight track as well as to improve curving performance. That is a very difficult trade-off for passive suspensions. An active controller can be used for either independently rotating wheels (IRW) or a solid axle [26-28]

Control strategies are different for independently rotating wheels and solid axle wheelsets. Independently rotating wheels use the approach of active control to increase stability and improve guidance control on curving and straight track. The main aim of active control for solid axle wheelsets is to provide effective stabilization for hunting as the conventional solid axle wheelsets are kinematically unstable. In addition, it is essential to provide steering for solid axle wheelset on the curve if the yaw stiffness in vehicle (passive) suspensions severely interferes with curving.

In the literature review chapter, a wide range of control methods for full active primary suspensions have been examined to provide the technical background for this study. This study is focussed on the use of independently rotating wheelsets based on two different vehicle configurations: a two-axle vehicle and a conventional bogie railway vehicle. By analyzing the effects of the active controller on both vehicle configurations, improved understanding of dynamics between the vehicle and the active wheelset control can also be achieved.

This study is built upon previous studies on the full active steering control systems for independently rotating wheelset, based on measured relative rotation speed of the two wheels on the same axle, and the relative yaw velocity between the wheelset and vehicle body as the required feedback. The full active control laws are first designed and examined in order to aid the investigation into the feasibility of a semi-active control approach and provide the basis for the development of such a new control scheme as presented in the next chapter.

4.2 Active Control Scheme

According to past literature, there is a general trend to design active control systems as per control architecture shown in Figure 4-1 with actuated independently rotation wheelsets (AIRW).

Figure 4-1 shows a conventional bogie railway vehicle and a similar scheme, consisting of only two wheelsets and a body frame, may be applied to a two-axle vehicle. Front and rear bogies can be seen, where IRW 1 and IRW 2 (independently rotation wheelsets) are connected to the front bogie and IRW 3 and IRW 4 (independently rotation wheelsets) are connected to the rear bogie.

Each wheelset has a feedback loop, which consists of a controller, sensors and an actuator, although the controllers for the wheelsets are not necessarily independent from one another and it is possible that an integrated design may be used to provide the control of all individual actuators at the system level.

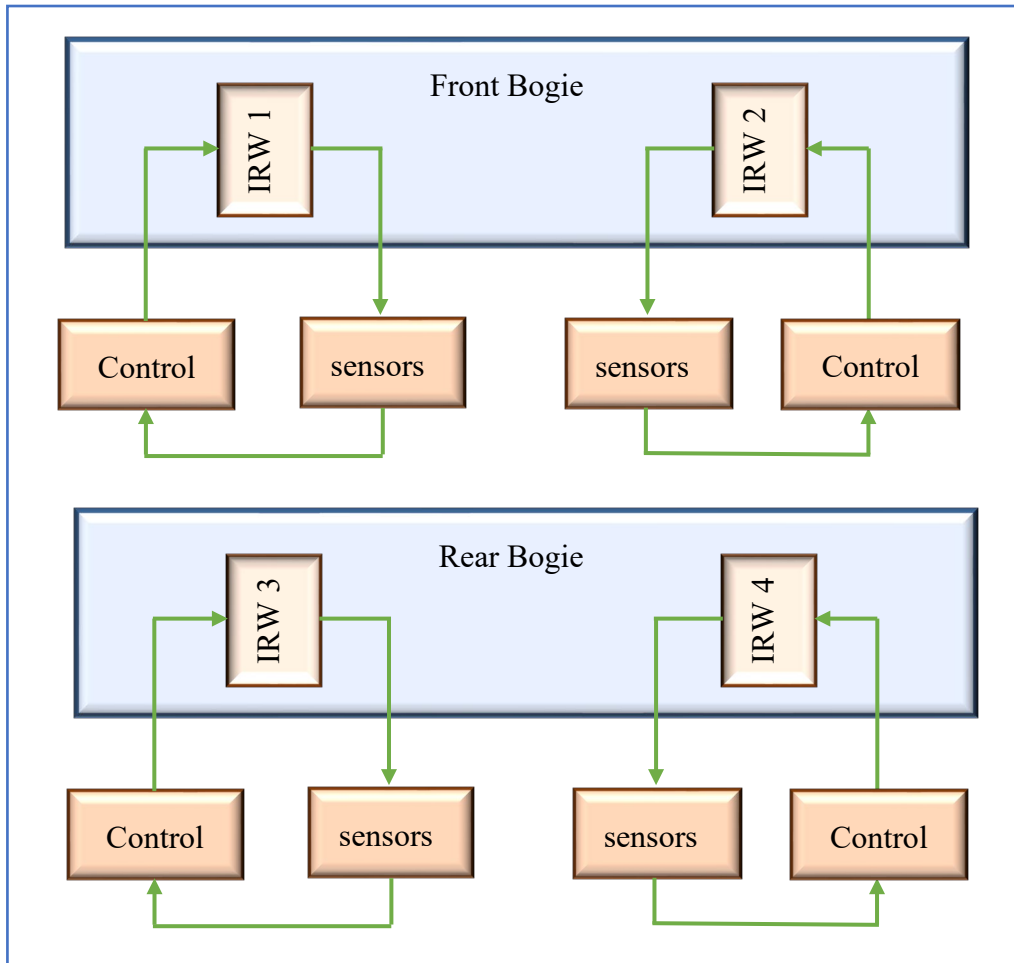


Figure 4-1- Active control scheme of conventional bogie vehicle with IRWs

4.3 Wheelset Controller

For an independently rotating wheelset, the two wheels on the same axle rotate independently of each other and therefore they are not able to provide natural self-curving and/or to follow the track without making flange contact [6, 8, 9]. Therefore, the control of independently rotating wheelset has an essential requirement for some form of guidance action to deliver stability on curves.

In addition, analysing the dynamics of independently rotating wheelset shows that there is also an issue of instability. Therefore it is also essential to provide some kind of stabilization [12].

It is noticeable that the vehicle dynamic model is of very high order 14th order for a two-axle vehicle of plan view motions and 32th order for the conventional bogie vehicle. There are interactions between different motions such as yaw, lateral and rotation motion within each wheelset as well as interactions between the wheelsets (2 /4) through the body/bogie motions. Also, two different track input, deterministic and random track, impact differently on the vehicle behaviours and therefore it is critical to manage the two different track features effectively in the control design. In addition, it is desirable in the control design to abstain from complex state estimate due to expensive or impractical requirement or measurement such that, active control systems are cost effective and less complicated. And finally, as the wheelset dynamics are dependent of vehicle speed, the controller needs to be adaptive to the vehicle travelling speed, with some kind of gain scheduling for example [7].

The design and tuning of the active control laws are first carried out for the two-axle vehicle. In order to reduce the complexity of the control design, the model can be decoupled into two separate independent subsystems as it shows in figure 4-2 [134]. The derivations from the basic mathematical model of the vehicle to the independent modes are presented as follows.

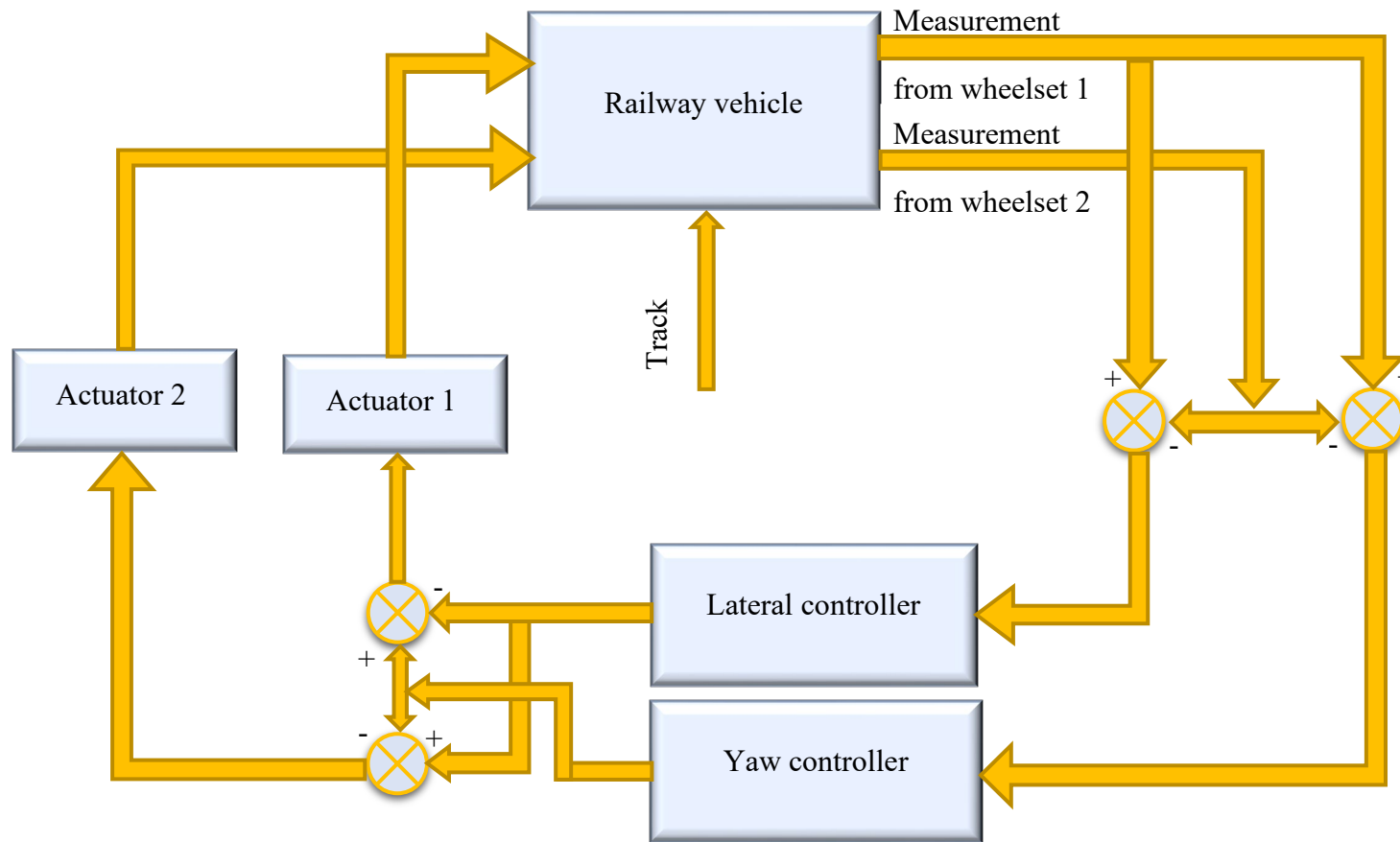


Figure 4-2- Modal control diagram

Equations 4-1 to 4-8 show a linearised representation of the plan view model of the vehicle. Compensation terms must be included in the equations for the accelerations of the reference axes as all variables are related to the local track references.

The equations indicate strong interconnections between the six motions of the vehicle: lateral and yaw motions of each wheelset are coupled via wheel/rail contact forces; the lateral and yaw motions of the body are coupled via the lateral movement of the two wheelsets; consequently the two wheelsets are coupled via the vehicle body [134].

Front wheelset

$$m_w \ddot{y}_{w1} + \left(\frac{2f_{22}}{v_s} + C_{py} \right) \dot{y}_{w1} + K_{py} y_{w1} - 2f_{22} \psi_{w1} - C_{py} \dot{y}_v - K_{py} y_v C_{py} L_v \dot{\psi}_v \quad (4-1)$$

$$-K_{py} L_v \psi_v = m_w \left(\frac{v_s^2}{R_1} - g \theta_{c1} \right)$$

$$J_w \ddot{\psi}_{w1} + \left(\frac{2f_{22} L_g^2}{v_s} \right) \dot{\psi}_{w1} + \frac{2f_{11} \lambda L_g}{r_0} y_{w1} + \frac{2r_0 f_{11} L_g}{v_s} \dot{\phi}_{w1} \frac{2f_{11} L_g^2}{R_1} + \frac{2f_{11} \lambda L_g}{r_0} y_{t1} \quad (4-2)$$

$$+ T_{w1}$$

$$J_\phi \ddot{\phi}_{w1} + \frac{r_0^2 f_{11}}{v_s} \dot{\phi}_{w1} + f_{11} \lambda y_{w1} + \frac{r_0 f_{11} L_g}{v_s} \dot{\psi}_{w1} = \frac{2r_0 f_{11} L_g}{R_1} + f_{11} \lambda y_{t1} \quad (4-3)$$

Rear wheelset

$$m_w \ddot{y}_{w2} + \left(\frac{2f_{22}}{v_s} + C_{py} \right) \dot{y}_{w2} + K_{py} y_{w2} - 2f_{22} \psi_{w2} - C_{py} \dot{y}_v - K_{py} y_v + C_{py} L_v \dot{\psi}_v \quad (4-4)$$

$$+ K_{py} L_v \psi_v = m_w \left(\frac{v_s^2}{R_2} - g \theta_{c2} \right)$$

$$J_w \ddot{\psi}_{w2} + \left(\frac{2f_{11}L_g^2}{v_s} \right) \dot{\psi}_{w2} + \frac{2f_{11}\lambda L_g}{r_0} y_{w2} + \frac{2r_0 f_{11}L_g}{v_s} \dot{\phi}_{w2} = \frac{2f_{11}L_g^2}{R_2} + \frac{2f_{11}\lambda L_g}{r_0} y_{t2} \quad (4-5)$$

$$+T_{w2}$$

$$J_\phi \ddot{\phi}_{w2} + \frac{r_0^2 f_{11}}{v_s} \dot{\phi}_{w2} + f_{11}\lambda y_{w2} + \frac{r_0 f_{11}L_g}{v_s} \dot{\psi}_{w2} = \frac{2r_0 f_{11}L_g}{R_2} + f_{11}\lambda y_{t2} \quad (4-6)$$

Body

$$\begin{aligned} m_v \ddot{y}_v + 2C_{py} \dot{y}_v + 2K_{py} y_v - C_{py} \dot{y}_{w1} - K_{py} y_{w1} - C_{py} \dot{y}_{w2} - K_{py} y_{w2} \\ = \frac{m_w v_s^2}{2} \left(\frac{1}{R_1} + \frac{1}{R_2} \right) - \frac{m_v g}{2} (\theta_{c1} + \theta_{c2}) \end{aligned} \quad (4-7)$$

$$\begin{aligned} J_v \ddot{\psi}_v + 2L_v^2 C_{py} \dot{\psi}_v + 2L_v^2 K_{py} \psi_v - L_v C_{py} \dot{y}_{w1} + L_v C_{py} \dot{y}_{w2} - L_v K_{py} y_{w1} + L_v K_{py} y_{w2} \\ = -(T_{w1} + T_{w2}) \end{aligned} \quad (4-8)$$

Corresponding motion equations for the wheelsets can be added or subtracted. i.e. lateral, yaw and rotation motion equations for one wheelset are added or subtracted from the corresponding equations relating to the other wheelset.

The new equations can be obtained by adding and subtracting equation 4-1 and 4-3 to/from equation 4-4 and 4-6 to obtain equations 4-9 to 4-11 and adding and subtracting equation 4-2 and 4-3 to/from equation 4-5 and 4-6 to obtain equations 4-13 to 4-15:

Lateral mode equations

$$m_w \ddot{y}_{wa} + \left(\frac{2f_{22}}{v_s} + C_{py} \right) \dot{y}_{wa} + K_{py} y_{wa} - 2f_{22} \psi_{wa} - 2C_{py} \dot{y}_v - 2K_{py} y_v = m_w \ddot{y}_{ra} \quad (4-9)$$

$$J_w \ddot{\psi}_{wa} + \frac{2f_{22}L_g^2}{v_s} \dot{\psi}_{wa} + \frac{2f_{11}\lambda L_g}{r_0} y_{wa} + \frac{2r_0 f_{11} L_g}{v_s} \dot{\phi}_{wa} = \frac{2f_{11}L_g^2}{R_{ta}} + \frac{2f_{11}\lambda L_g}{r_0} y_{ta} \quad (4-10)$$

$$+ T_{wa}$$

$$J_\phi \ddot{\phi}_{wa} + \frac{r_0^2 f_{11}}{v_s} \dot{\phi}_{wa} + f_{11}\lambda y_{wa} + \frac{r_0 f_{11} L_g}{v_s} \dot{\psi}_{wa} = \frac{2r_0 f_{11} L_g}{R_a} + f_{11}\lambda y_{ta} \quad (4-11)$$

$$m_v \ddot{y}_v + 2C_{py} \dot{y}_v + 2K_{py} y_v - C_{py} \dot{y}_{wa} - K_{py} y_{wa} = \frac{m_w}{2} \ddot{y}_{ra} \quad (4-12)$$

Yaw mode equations

$$m_w \ddot{y}_{wb} + \left(\frac{2f_{22}}{v_s} + C_{py} \right) \dot{y}_{wb} + K_{py} y_{wb} - 2f_{22} \psi_{wb} - 2C_{py} L_v \dot{\psi}_v - 2K_{py} L_v \psi_v \quad (4-13)$$

$$= m_w \ddot{y}_{rb}$$

$$J_w \ddot{\psi}_{wb} + \frac{2f_{22}L_g^2}{v_s} \dot{\psi}_{wb} + \frac{2f_{11}\lambda L_g}{r_0} y_{wb} + \frac{2r_0 f_{11} L_g}{v_s} \dot{\phi}_{wb} = \frac{2f_{11}L_g^2}{R_{tb}} + \frac{2f_{11}\lambda L_g}{r_0} y_{tb} \quad (4-14)$$

$$+ T_{wb}$$

$$J_\phi \ddot{\phi}_{wb} + \frac{r_0^2 f_{11}}{v_s} \dot{\phi}_{wb} + f_{11}\lambda y_{wb} + \frac{r_0 f_{11} L_g}{v_s} \dot{\psi}_{wb} = \frac{2r_0 f_{11} L_g}{R_b} + f_{11}\lambda y_{tb} \quad (4-15)$$

$$J_v \ddot{\psi}_v + 2C_{py} L_v^2 \dot{\psi}_v + 2K_{py} L_v^2 \psi_v - C_{py} L_v \dot{y}_{wb} - K_{py} L_v y_{wb} = \frac{J_v}{2} \ddot{\theta}_{rb} - T_{wb} \quad (4-16)$$

This results in a subsystem that can be treated as an IRW joined to a mass of the body lateral motion, this is known as lateral mode as seen in figure 4-3. The other IRW is attached to a mass of the body yaw motion, this is known as yaw mode as seen in figure 4-4.

To supply feedback signals that are required by the yaw and lateral controller the output measurement from two wheelsets are decomposed. Therefore, to control the two wheelsets the output signals from the two controllers are re-combined.

The entire variables which are represented in equations 4-17 to 4-32 are either the summation or differences between correlate with variable of the track geometric or two wheelsets at the two wheelsets.

Modal variables

$$y_{wa} = y_{w1} + y_{w2} \quad (4-17)$$

$$y_{wb} = y_{w1} - y_{w2} \quad (4-18)$$

$$\psi_{wa} = \psi_{w1} + \psi_{w2} \quad (4-19)$$

$$\psi_{wb} = \psi_{w1} - \psi_{w2} \quad (4-20)$$

$$\phi_{wa} = \phi_{w1} + \phi_{w2} \quad (4-21)$$

$$\phi_{wb} = \phi_{w1} - \phi_{w2} \quad (4-22)$$

$$T_{wa} = T_{w1} + T_{w2} \quad (4-23)$$

$$T_{wb} = T_{w1} - T_{w2} \quad (4-24)$$

Track inputs

$$\frac{1}{R_{ta}} = \frac{1}{R_1} + \frac{1}{R_2} \quad (4-25)$$

$$\frac{1}{R_{tb}} = \frac{1}{R_1} - \frac{1}{R_2} \quad (4-26)$$

$$y_{ta} = y_{t1} + y_{t2} \quad (4-27)$$

$$y_{tb} = y_{t1} - y_{t2} \quad (4-28)$$

Reference axis accelerations

$$\ddot{y}_{ra} = v_s^2 \left[\frac{1}{R_1} + \frac{1}{R_2} \right] - g(\theta_{c1} + \theta_{c2}) \quad (4-29)$$

$$\ddot{y}_{rb} = v_s^2 \left[\frac{1}{R_1} - \frac{1}{R_2} \right] - g(\theta_{c1} - \theta_{c2}) \quad (4-30)$$

$$\ddot{\theta}_{ra} = v_s \left[\frac{1}{R_1} + \frac{1}{R_2} \right] \quad (4-31)$$

$$\ddot{\theta}_{rb} = v_s \left[\frac{1}{R_1} - \frac{1}{R_2} \right] \quad (4-32)$$

Where \ddot{y}_{ra} and \ddot{y}_{rb} are the lateral centrifugal force due to track curve and cant angle. Also $\ddot{\theta}_{ra}$ and $\ddot{\theta}_{rb}$ represented angular accelerations dur to curve transitions of the track.

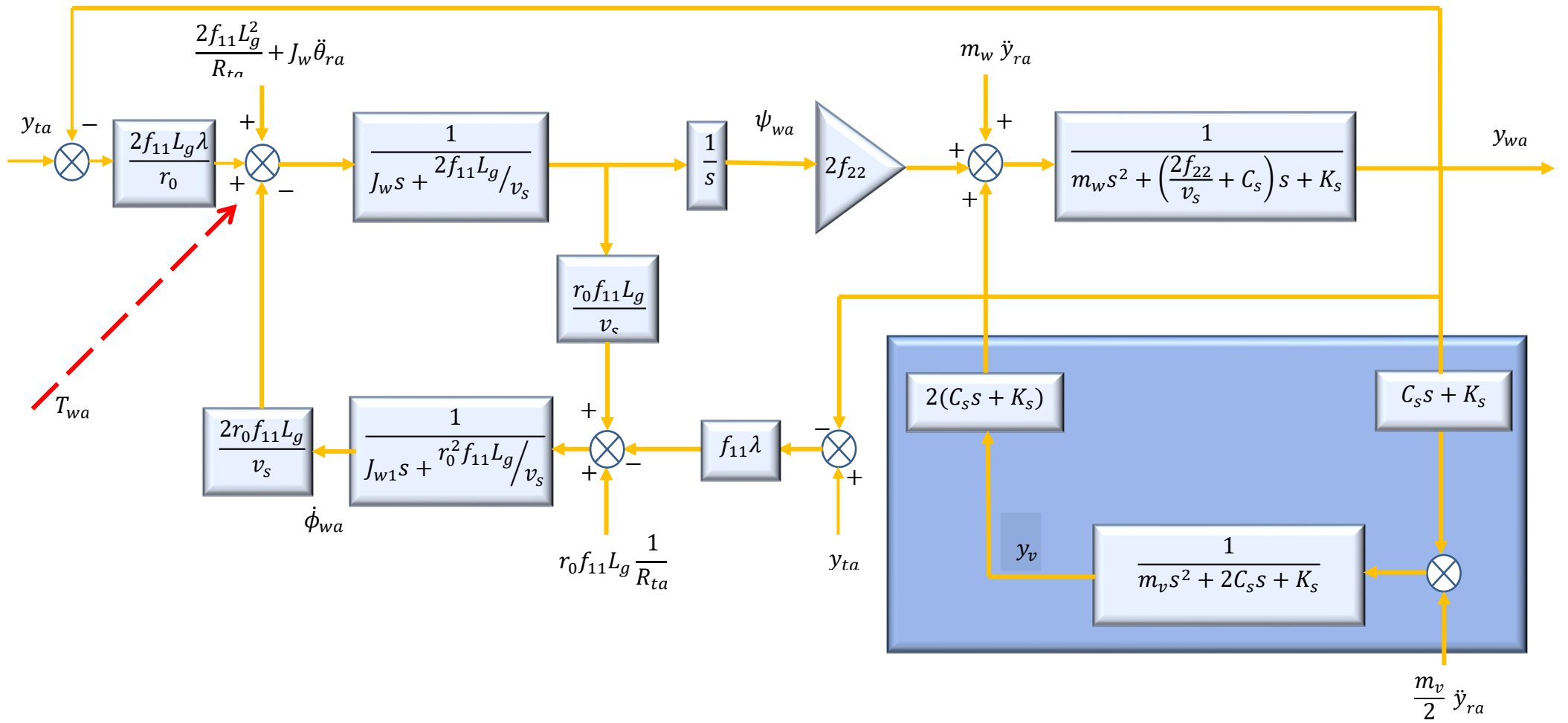


Figure 4-3- Lateral mode

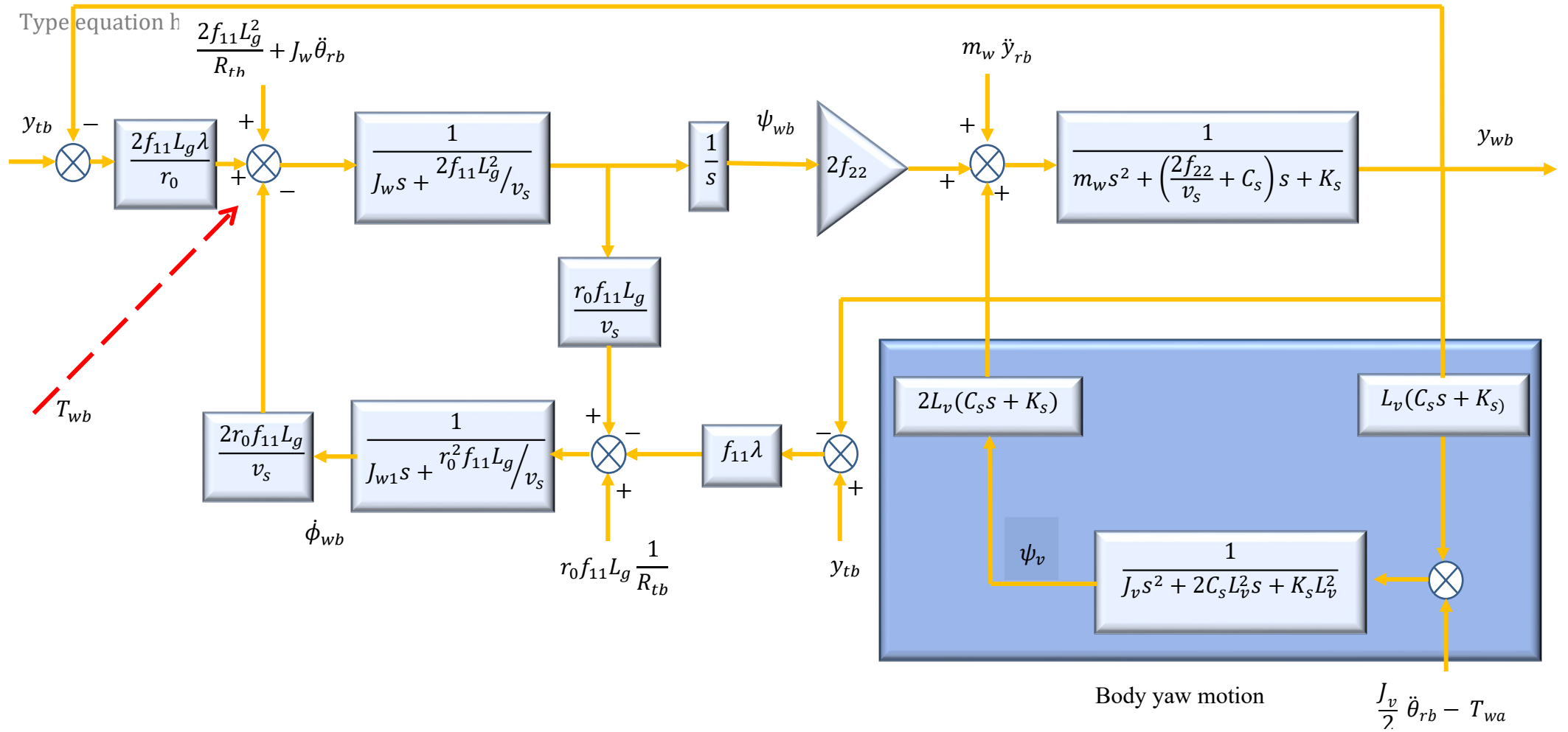


Figure 4-4-Yaw mode

Wheelset Stability Control Design

Previous studies show that stabilization of wheelset can be obtained by yaw velocity as feedback. However, the control gain is carefully chosen using the classical root locus design technique, considering decoupling the model into two independent subsystems. IRW attached to a mass of the body lateral motion and the other one as IRW attached to a mass of the body yaw motion. In addition, the body yaw rate has been used for sensing consideration. Therefore by adding the body yaw rate in the controllers, stabilization can be provided by relative yaw velocity between the body and each wheelset by measuring the actuator movement directly [7].

Wheelset Guidance Control Design

To provide the essential guidance action for the IRW to follow the track some sort of feedback is required. The relative displacement between the wheelset and the track would be an obvious choice to provide the required feedback for guidance control, but a direct measurement of the wheel and rail deflection is not easy and is expensive in real application. On the other hand, estimation methods can be used to estimate the signals from other practical sensors, but the control design will be more complicated with higher order and it will be very complicated and hard to observe if working effectively in the presence of large parameter variations [140].

However, if two wheels may be controlled to rotate at the same speed, the independently rotating wheelset would behave in a similar way to its solid axle counterpart and the restoration of self-curving would then be possible. Therefore, a control action can be designed such that the actuator will steer the axle to achieve a zero-speed difference between the two wheels on of the independently rotating wheelset.

Control Gain G_s & G_g for Two axle Vehicle

A state space for the lateral mode given in 4-33 to 4-40 are delivered from 4-9 to 4-12 for stability and guidance control. Also, the state space presented in 4-41 to 4-48 obtain from 4-13 to 4-16 for stability and guidance control in yaw mode.

Latera mode

$$\dot{X} = AX + Bu \quad (4-33)$$

$$y = CX + Du \quad (4-34)$$

$$\dot{X}_a = \begin{bmatrix} \dot{y}_{wa} \\ y_{wa} \\ \dot{\psi}_{wa} \\ \psi_{wa} \\ \dot{\phi}_{wa} \\ \dot{y}_{va} \\ y_{va} \end{bmatrix} \quad (4-35)$$

$$A = \begin{bmatrix} -\frac{2f_{22}}{m_w v_s} - \frac{C_{py}}{m_w} & -\frac{K_{py}}{m_w} & 0 & \frac{2f_{22}}{m_w} & 0 & \frac{2C_{py}}{m_w} & \frac{2K_{py}}{m_w} \\ 1 & 0 & 0 & 0 & 0 & 0 & 0 \\ 0 & -\frac{2f_{11}\lambda L_g}{J_w r_0} & -\frac{2f_{22}L_g^2}{J_w v_s} & 0 & -\frac{2r_0 f_{11}L_g}{J_w v_s} & 0 & 0 \\ 0 & 0 & 1 & 0 & 0 & 0 & 0 \\ 0 & -\frac{f_{11}\lambda}{J_\phi} & -\frac{f_{11}L_g r_0}{J_\phi v_s} & 0 & -\frac{f_{11}r_0^2}{J_\phi v_s} & 0 & 0 \\ \frac{C_{py}}{m_v} & \frac{K_{py}}{m_v} & 0 & 0 & 0 & -\frac{2C_{py}}{m_v} & -\frac{2K_{py}}{m_v} \\ 0 & 0 & 0 & 0 & 0 & 1 & 0 \end{bmatrix} \quad (4-36)$$

$$B = [0; 0; \frac{1}{J_w}; 0; 0; 0; 0] \quad (4-37)$$

$$C_1 = [0 \ 0 \ 1 \ 0 \ 0 \ 0 \ 0] \quad (4-38)$$

$$C_2 = [0 \ 0 \ 0 \ 0 \ -1 \ 0 \ 0] \quad (4-39)$$

$$D = [0] \quad (4-40)$$

Yaw mode

$$\dot{X} = AX + Bu \quad (4-41)$$

$$y = CX + Du \quad (4-42)$$

$$\dot{X}_b = \begin{bmatrix} \dot{y}_{wb} \\ y_{wb} \\ \dot{\psi}_{wb} \\ \psi_{wb} \\ \dot{\phi}_{wb} \\ \psi_{vb} \\ \dot{\psi}_{vb} \\ \psi_{vb} \end{bmatrix} \quad (4-43)$$

$$A \quad (4-44)$$

$$= \begin{bmatrix} -\frac{2f_{22}}{m_w v_s} - \frac{C_{py}}{m_w} & -\frac{K_{py}}{m_w} & 0 & \frac{2f_{22}}{m_w} & 0 & \frac{2C_{py}L_v}{m_w} & \frac{2K_{py}L_v}{m_w} \\ 1 & 0 & 0 & 0 & 0 & 0 & 0 \\ 0 & -\frac{2f_{11}\lambda L_g}{J_w r_0} & -\frac{2f_{22}L_g^2}{J_w v_s} & 0 & -\frac{2r_0 f_{11}L_g}{J_w v_s} & 0 & 0 \\ 0 & 0 & 1 & 0 & 0 & 0 & 0 \\ 0 & -\frac{f_{11}\lambda}{J_\phi} & -\frac{f_{11}L_g r_0}{J_\phi v_s} & 0 & -\frac{f_{11}r_0^2}{J_\phi v_s} & 0 & 0 \\ \frac{C_{py}L_v}{m_v} & \frac{K_{py}L_v}{m_v} & 0 & 0 & 0 & -\frac{2C_{py}L_v^2}{m_v} & -\frac{2K_{py}L_v^2}{m_v} \\ 0 & 0 & 0 & 0 & 0 & 1 & 0 \end{bmatrix}$$

$$B = [0; 0; \frac{1}{J_w}; 0; 0; 0; 0] \quad (4-45)$$

$$C_1 = [0 \ 0 \ 1 \ 0 \ 0 \ 0 \ 0] \quad (4-46)$$

$$C_2 = [0 \ 0 \ 0 \ 0 \ -1 \ 0 \ 0] \quad (4-47)$$

$$D = [0] \quad (4-48)$$

Where A is the state matrix, X is the state variable, U is the torque input, C_1 is the output for the stability control feedback, C_2 is the output for the guidance control feedback and D, the output which is 0.

Figures 4-5 to 4-8 give the locus diagrams for the design of the stability gain for the lateral and yaw modes respectively, using the wheelset yaw velocity as the feedback.

To design the control gain for the stability control used lateral mode, equations 4-33 to 4-40, to produce the root locus diagram for the stability control gain. However, C_1 have been used because the feedback is yaw velocity. From figures 4-5 and 4-6 it is quite clear how the unstable poles are moved towards because of the feedback C_1 and increase of the control gain. For the yaw mode the process is the same however used the yaw model, equation 4-41 to 4-48, instead.

As it was shown in the previous chapter in the modelling of two axle vehicle, there are a pair of unstable poles for each wheelset, in this case $4.16 \pm 38.2j$ at the beginning of the locus. Those two unstable poles are clearly being moved towards the stable region on the left-hand side as the control gain increases. The control gains are then selected for the closed loop poles to have a minimum damping of about 0.2, which is a commonly used requirement for the design of railway vehicles.

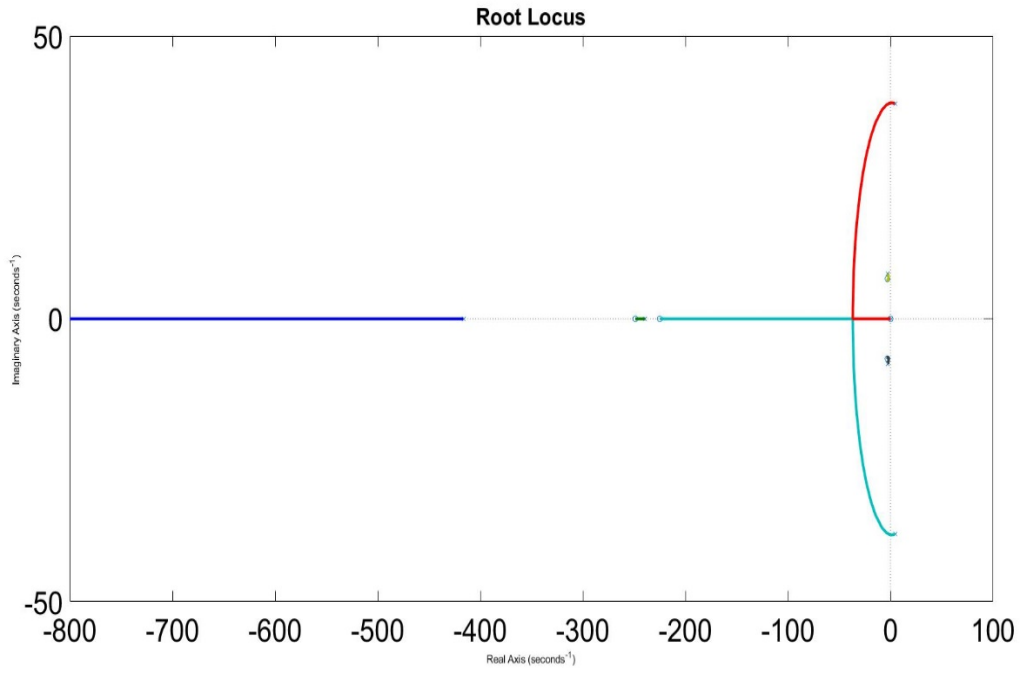


Figure 4-5- Root locus for the design of the stability controller for lateral mode

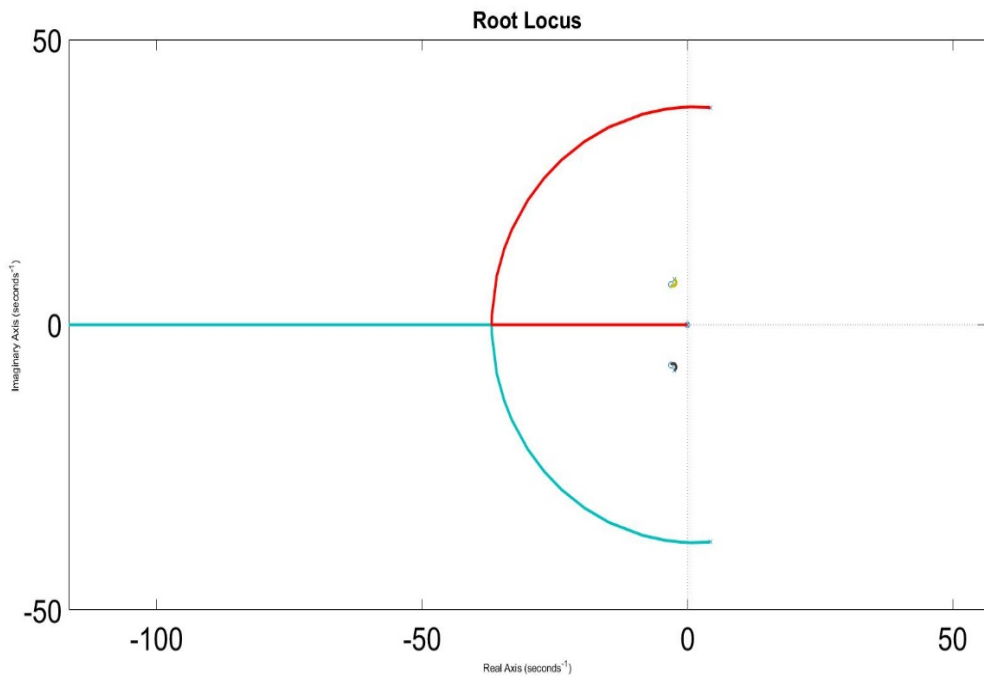


Figure 4-6- Zoom in version

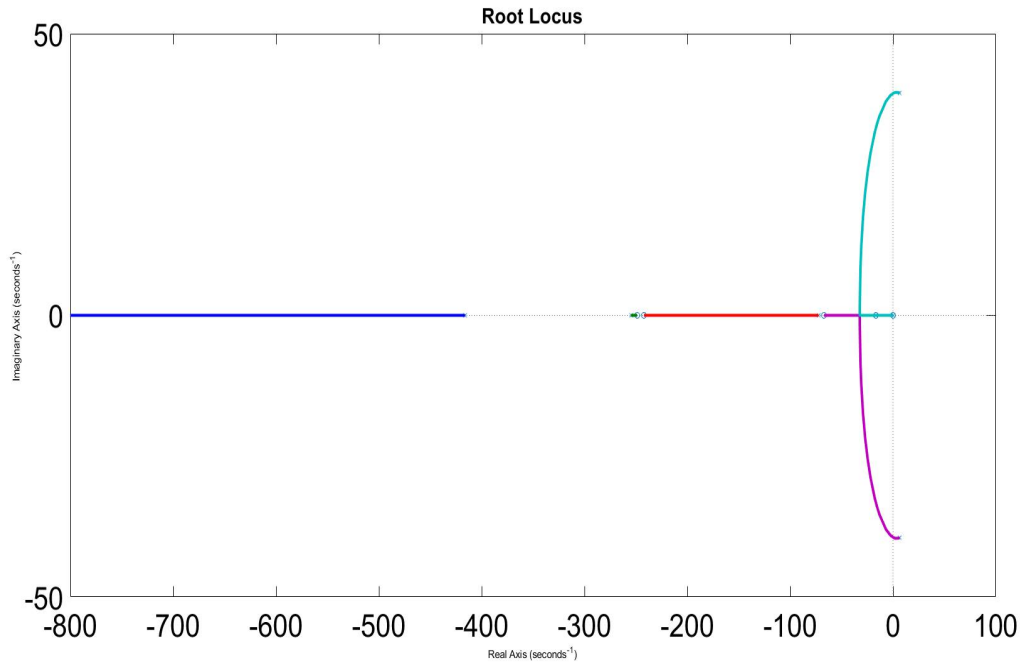


Figure 4-7- Root locus for the design of the stability controller for yaw mode

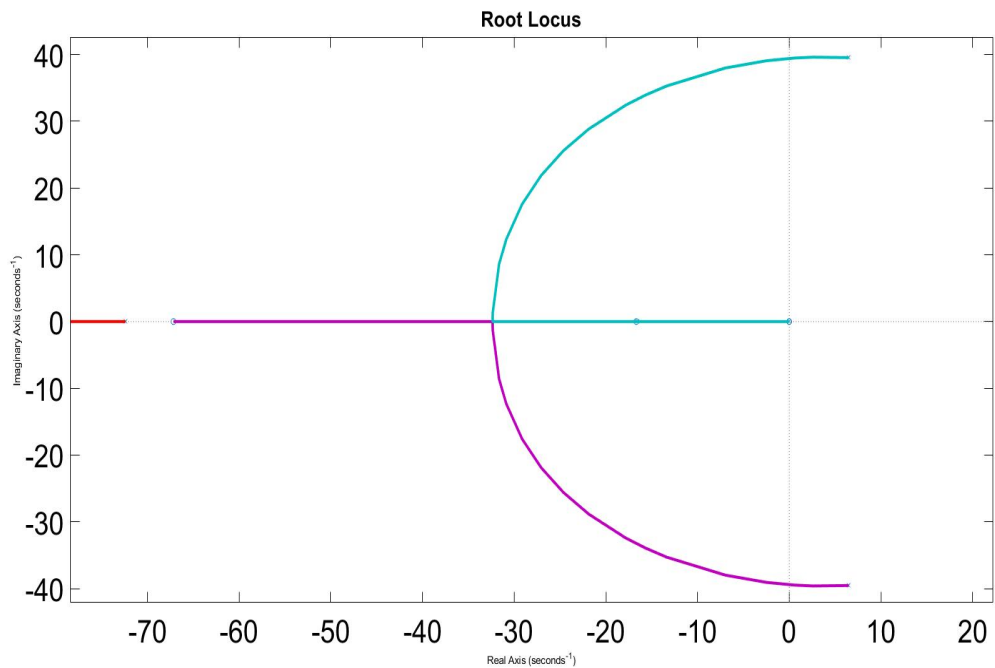


Figure 4-8- Zoom in version

For the two-axle vehicle used in the study, the lateral and yaw modes are very similar and therefore the same control gains are selected for simplicity. It is obvious that the first four rows

of the table 3-2 (chapter 3) which presented the unstable kinematic modes of the wheelset (Table shows the eigenvalues of the two-axle railway vehicle for an uncontrolled model) now are amended by choosing $G_s = 34545$.

The state-space models for the lateral and yaw modes of the vehicle are then modified to include the stability control gains as selected and also the relative rotational speed of the wheelset as the feedback to carry out the design for the steering control.

The lack of guidance action of the independently rotating wheelsets is indicated by the pole at 0 as discussed in the previous chapter. Figures 4-9 to 4-12 show how the pole may be moved towards the left-hand side by using the relative rotational velocity as the feedback.

To design the control gain for the guidance control used lateral mode, equations 4-33 to 4-40, to produce the root locus diagram for the guidance control gain. However, C_2 have been used because the feedback is rotational speed. From figures 4-9 and 4-12 it is quite clear that the guidance can now provide by the rotational feedback, as indicated by the poles $S=0$ being moved to towards the left. For the yaw mode the process is the same however used the yaw model, equation 4-41 to 4-48, instead.

The selection of the guidance control gains must be careful, as it has also a de-stabilising effect on the other two poles. A trade-off between the response of the guidance and level of the stability is made, with the selection of $G_g = 1992$.

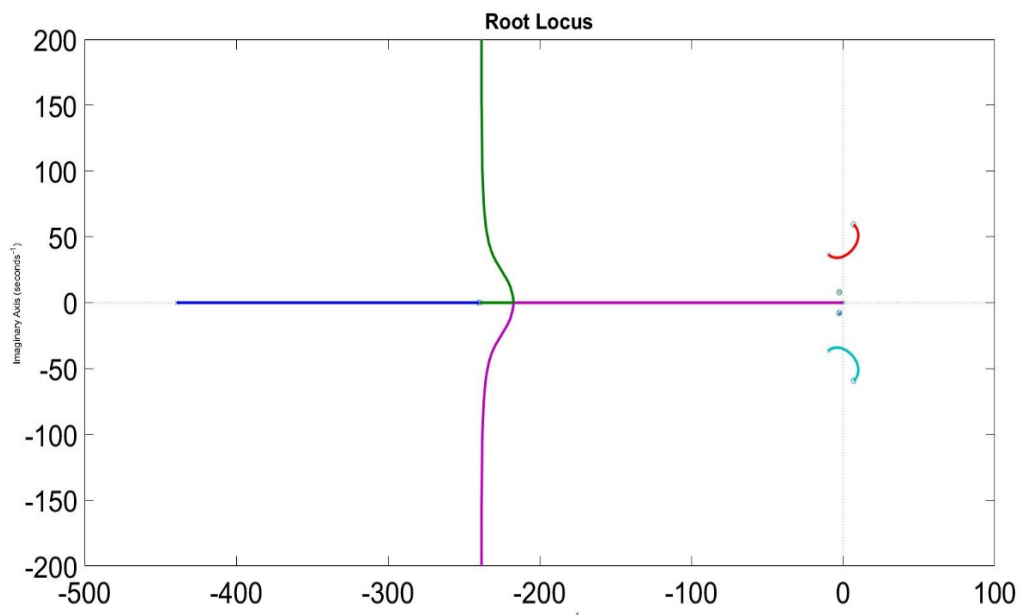


Figure 4-9- Root locus of two axle vehicle with guidance controller for lateral mode

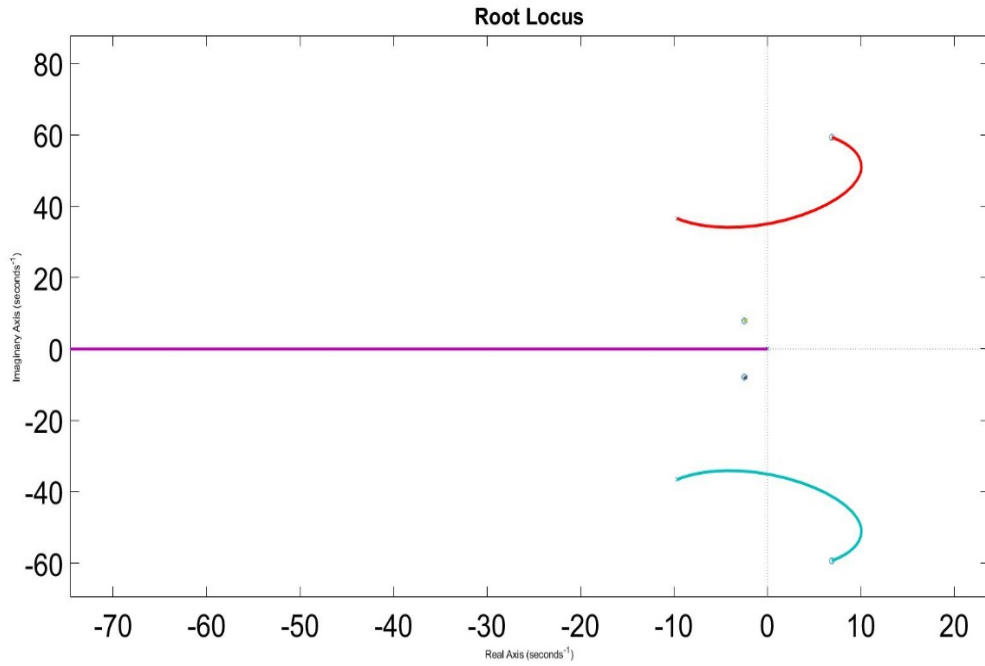


Figure 4-10- Zoom in version

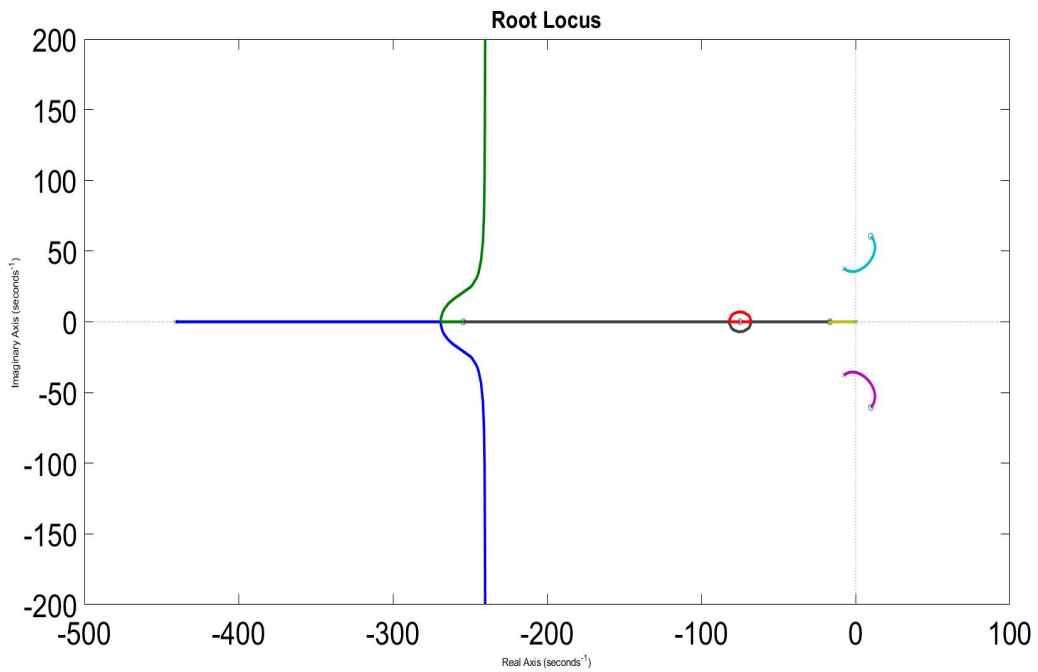


Figure 4-11- Root locus of two axle vehicle with guidance controller for yaw mode

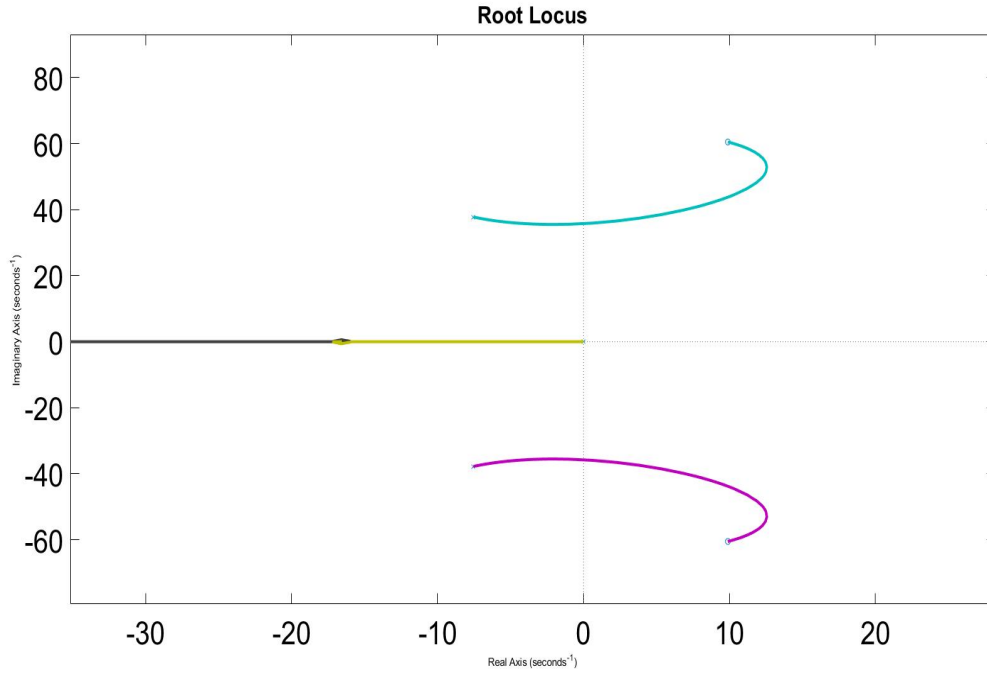


Figure 4-12- Zoom in version

Therefore, equations 4-51 and 4-52 represent the final control law consisting of guidance and stability terms for front and rear wheelsets:

$$T_a = G_s \dot{\psi}_a x + G_g \dot{\phi}_a x \quad (4-49)$$

$$T_b = G_s \dot{\psi}_b x - G_g \dot{\phi}_b x \quad (4-50)$$

After converting T_a and T_b to final control laws, T_{w1} and T_{w2} are

$$T_{w1} = G_s \dot{\psi}_{w1} x + G_g \dot{\phi}_{w1} x \quad (4-51)$$

$$T_{w2} = G_s \dot{\psi}_{w2} x + G_g \dot{\phi}_{w2} x \quad (4-52)$$

With the design of both stability and guidance controllers, equations 3-30, 3-32, 3-34, 3-37, 3-39 and 3-41 will change to equation 4-53 to 4-58.

Front wheelset:

$$m_w \ddot{y}_{w1} + \left(\frac{2f_{22}}{v_s} + C_{py} \right) \dot{y}_{w1} + K_{py} y_{w1} - 2f_{22} \psi_{w1} - C_{py} \dot{y}_v - K_{py} y_v - C_{py} L_v \dot{\psi}_v \quad (4-53)$$

$$-K_{py} L_v \psi_v = m_w \left(\frac{v_s^2}{R_1} - g \theta_{c1} \right)$$

$$J_w \ddot{\psi}_{w1} + \left(\frac{2f_{11} L_g^2}{v_s} \right) \dot{\psi}_{w1} + \frac{2f_{11} \lambda L_g}{r_0} y_{w1} + \frac{2r_0 f_{11} L_g}{v_s} \dot{\phi}_{w1} = \frac{2f_{11} L_g^2}{R_1} + \frac{2f_{11} \lambda L_g}{r_0} y_{t1} \quad (4-54)$$

$$+ G_s \dot{\psi}_{w1} + G_g \dot{\phi}_{w1}$$

$$J_\phi \ddot{\phi}_{w1} + \frac{r_0^2 f_{11}}{v_s} \dot{\phi}_{w1} + f_{11} \lambda y_{w1} + \frac{r_0^2 f_{11} L_g}{v_s} \dot{\psi}_{w1} = \frac{r_0 f_{11} L_g}{R_1} + f_{11} \lambda y_{t1} \quad (4-55)$$

Rear wheelset:

$$m_w \ddot{y}_{w2} + \left(\frac{2f_{22}}{v_s} + C_{py} \right) \dot{y}_{w2} + K_{py} y_{w2} - 2f_{22} \psi_{w2} - C_{py} \dot{y}_v - K_{py} y_v + C_{py} L_v \dot{\psi}_v \quad (4-56)$$

$$+ K_{py} L_v \psi_v = m_w \left(\frac{v_s^2}{R_2} - g \theta_{c2} \right)$$

$$J_w \ddot{\psi}_{w2} + \left(\frac{2f_{11} L_g^2}{v_s} \right) \dot{\psi}_{w2} + \frac{2f_{11} \lambda L_g}{r_0} y_{w2} + \frac{2r_0 f_{11} L_g}{v_s} \dot{\phi}_{w2} = \frac{2f_{11} L_g^2}{R_2} + \frac{2f_{11} \lambda L_g}{r_0} y_{t2} \quad (4-57)$$

$$+ G_s \dot{\psi}_{w2} + G_g \dot{\phi}_{w2}$$

$$J_\phi \ddot{\phi}_{w2} + \frac{r_0^2 f_{11}}{v_s} \dot{\phi}_{w2} + f_{11} \lambda y_{w2} + \frac{r_0^2 f_{11} L_g}{v_s} \dot{\psi}_{w2} = \frac{r_0 f_{11} L_g}{R_2} + f_{11} \lambda y_{t2} \quad (4-58)$$

Table 4-1 show the all the unstable poles in table 3-2 are stable now after designing the stability control and also the lack of guidance amended in this table by designing guidance control gain, it is noticeable that the poles from table 4-1 are from equation 4-53 to 4-58.

Table 4-1- The eigenvalue of the two-axle railway vehicle for controlled model

	Pole	Damping	Frequency (Hz/Time Unit)
1	-7.65+35.2j	2.12e-01	5.7
2	-7.65-35.2j	2.12e-01	5.7
3	-7.58+35j	2.11e-01	5.6
4	-7.58-35j	2.11e-01	5.6
5	-7.12	1.00e+00	1.1
6	-6.96	1.00e+00	1.1
7	-436	1.00e+00	69.39
8	-436	1.00e+00	69.39
9	-239	1.00e+00	38
10	-239	1.00e+00	38
11	-1.29+5.94j	2.12e-01	0.9
12	-1.29-5.94j	2.12e-01	0.9
13	-1.14+5.73j	1.95e-01	0.9
14	-1.14-5.73j	1.95e-01	0.9

Principally in a railway vehicle stabilization for high-speed application will continue to be stable at low speed. However, guidance performance can be significantly reduced due to noticeable wheel-rail lateral movement on both curved and random tracks. Therefore, it was essential that different control gains need to be used for different speed operations. However, the change of vehicle speed is relatively slow compared with the yaw and lateral dynamics and gain scheduling has been studied previously by tuning the control gains for different speed

ranges to address the issue [quote a reference here]. The speed adaptation is not the focus of the study, so control gains are simply tuned for different speed operations.

Wheelset Controller for Conventional Bogie Vehicle

Similarly, the same control design approach may be applied for the bogie vehicle. By considering the two bogies being largely decoupled (as the secondary suspensions are much softer) and designing the controllers for the two bogies independently – each bogie is just like a two-axle vehicle, so the process above can be repeated. Therefore, the design process is not presented to avoid unnecessary duplication, but the final outcome of the design is provided as below.

Equations 3-64 to 3-75 will change to equation 4-59 to 4-70.

Wheelset 1:

$$m_w \ddot{y}_{w1} + \left(\frac{2f_{22}}{v_s} + C_{py} \right) \dot{y}_{w1} - 2f_{22} \psi_{w1} + K_{py} y_{w1} - K_{py} y_{b1} - K_{py} L_v \psi_{b1} \quad (4-59)$$

$$-C_{py} \dot{y}_{b1} - C_{py} L_v \dot{\psi}_{b1} = m_w \left(\frac{v_s^2}{R_1} - g \theta_{c1} \right)$$

$$J_w \ddot{\psi}_{w1} + \left(\frac{2f_{11} L_g^2}{v_s} \right) \dot{\psi}_{w1} + \frac{2f_{11} \lambda L_g}{r_0} y_{w1} + \frac{2r_0 f_{11} L_g}{v_s} \dot{\phi}_{w1} = \frac{2f_{11} L_g^2}{R_1} + \frac{2f_{11} \lambda L_g}{r_0} y_{t1} \quad (4-60)$$

$$+ G_s \dot{\psi}_{w1} + G_g \dot{\phi}_{w1}$$

$$J_\phi \ddot{\phi}_{w1} + \frac{r_0^2 f_{11}}{v_s} \dot{\phi}_{w1} + f_{11} \lambda y_{w1} + \frac{r_0^2 f_{11} L_g}{v_s} \dot{\psi}_{w1} = \frac{r_0 f_{11} L_g}{R_1} + f_{11} \lambda y_{t1} \quad (4-61)$$

Wheelset 2:

$$m_w \ddot{y}_{w2} + \left(\frac{2f_{22}}{v_s} + C_{py} \right) \dot{y}_{w2} - 2f_{22} \psi_{w2} + K_{py} y_{w2} - K_{py} y_{b1} + K_{py} L_v \psi_{b1} \quad (4-62)$$

$$-C_{py} \dot{y}_{b1} + C_{py} L_v \dot{\psi}_{b1} = m_w \left(\frac{v_s^2}{R_2} - g \theta_{c2} \right)$$

$$J_w \ddot{\psi}_{w2} + \left(\frac{2f_{11} L_g^2}{v_s} \right) \dot{\psi}_{w2} + \frac{2f_{11} \lambda L_g}{r_0} y_{w2} + \frac{2r_0 f_{11} L_g}{v_s} \dot{\phi}_{w2} = \frac{2f_{11} L_g^2}{R_2} + \frac{2f_{11} \lambda L_g}{r_0} y_{t2} \quad (4-63)$$

$$+ G_s \dot{\psi}_{w2} + G_g \dot{\phi}_{w2}$$

$$J_\phi \ddot{\phi}_{w2} + \frac{r_0^2 f_{11}}{v_s} \dot{\phi}_{w2} + f_{11} \lambda y_{w2} + \frac{r_0^2 f_{11} L_g}{v_s} \dot{\psi}_{w2} = \frac{r_0 f_{11} L_g}{R_2} + f_{11} \lambda y_{t2} \quad (4-64)$$

Wheelset 3:

$$m_w \ddot{y}_{w3} + \left(\frac{2f_{22}}{v_s} + C_{py} \right) \dot{y}_{w3} - 2f_{22} \psi_{w3} + K_{py} y_{w3} - K_{py} y_{b2} - K_{py} L_v \psi_{b2} \quad (4-65)$$

$$-C_{py} \dot{y}_{b2} - C_{py} L_v \dot{\psi}_{b2} = m_w \left(\frac{v_s^2}{R_3} - g \theta_{c3} \right)$$

$$J_w \ddot{\psi}_{w3} + \left(\frac{2f_{11} L_g^2}{v_s} \right) \dot{\psi}_{w3} + \frac{2f_{11} \lambda L_g}{r_0} y_{w3} + \frac{2r_0 f_{11} L_g}{v_s} \dot{\phi}_{w1} = \frac{2f_{11} L_g^2}{R_3} + \frac{2f_{11} \lambda L_g}{r_0} y_{t3} \quad (4-66)$$

$$+ G_s \dot{\psi}_{w3} + G_g \dot{\phi}_{w3}$$

$$J_\phi \ddot{\phi}_{w3} + \frac{r_0^2 f_{11}}{v_s} \dot{\phi}_{w3} + f_{11} \lambda y_{w3} + \frac{r_0^2 f_{11} L_g}{v_s} \dot{\psi}_{w3} = \frac{r_0 f_{11} L_g}{R_3} + f_{11} \lambda y_{t3} \quad (4-67)$$

Wheelset 4:

$$m_w \ddot{y}_{w4} + \left(\frac{2f_{22}}{v_s} + C_{py} \right) \dot{y}_{w4} - 2f_{22} \psi_{w4} + K_{py} y_{w4} - K_{py} y_{b2} + K_{py} L_v \psi_{b2} \quad (4-68)$$

$$-C_{py} \dot{y}_{b2} + C_{py} L_v \dot{\psi}_{b2} = m_w \left(\frac{v_s^2}{R_4} - g \theta_{c4} \right)$$

$$J_w \ddot{\psi}_{w4} + \left(\frac{2f_{11} L_g^2}{v_s} \right) \dot{\psi}_{w4} + \frac{2f_{11} \lambda L_g}{r_0} y_{w4} + \frac{2r_0 f_{11} L_g}{v_s} \dot{\phi}_{w4} = \frac{2f_{11} L_g^2}{R_4} + \frac{2f_{11} \lambda L_g}{r_0} y_{t4} \quad (4-69)$$

$$+ G_s \dot{\psi}_{w4} + G_g \dot{\phi}_{w4}$$

$$J_\phi \ddot{\phi}_{w4} + \frac{r_0^2 f_{11}}{v_s} \dot{\phi}_{w4} + f_{11} \lambda y_{w4} + \frac{r_0^2 f_{11} L_g}{v_s} \dot{\psi}_{w4} = \frac{r_0 f_{11} L_g}{R_4} + f_{11} \lambda y_{t4} \quad (4-70)$$

Table 4-2 show the all the unstable poles in table 3-3 are stable now after designing the stability control and also the lack of guidance amended in this table by designing guidance control gain, it is noticeable that the poles from table 4-2 are from equation 4-59 to 4-70.

Table 4-2- The eigenvalue of the conventional bogie railway vehicle with controller model

	Pole	Damping	Frequency (Hz/Time Unit)
1	-4.71+27.2j	1.71e-01	4.4
2	-4.71-27.2j	1.71e-01	4.4
3	-4.64+27.1j	1.69e-01	4.4
4	-4.64-27.1j	1.69e-01	4.4
5	-14.6+13.1j	7.44e-01	3
6	-14.6-13.1j	7.44e-01	3
7	-14.5+12.7j	7.50e-01	3
8	-14.5-12.7j	7.50e-01	3

9	-3.96	1.00e+00	0.63
10	-3.96	1.00e+00	0.63
11	-6.73	1.00e+00	1.07
12	-6.62	1.00e+00	1.07
13	-367	1.00e+00	58
14	-367	1.00e+00	58
15	-359	1.00e+00	57
16	-359	1.00e+00	57
17	-235	1.00e+00	37
18	-235	1.00e+00	37
19	-99.9+113j	6.63e-01	24
20	-99.9-113j	6.63e-01	24
21	-99.9+113j	6.63e-01	24
22	-99.9-113j	6.63e-01	24
23	-26.8+118j	2.21e-01	19
24	-26.8-118j	2.21e-01	19
25	-26.7+118j	2.21e-01	19
26	-26.7-118j	2.21e-01	19
27	-117	1.00e+00	18
28	-117	1.00e+00	18
29	-2.07+4.68j	4.05e-01	0.8
30	-2.07-4.68j	4.05e-01	0.8
31	-1.55+4.42j	3.31e-01	0.74

32	-1.55-4.42j	3.31e-01	0.74
----	-------------	----------	------

4.4 Simulation and Result

Simulation is carried out for the two-axle vehicle and the bogie vehicle on deterministic and random track inputs to validate the control design and to evaluate the performance of the actively controlled vehicles. Two curved tracks are used to evaluate the curving dynamics, one tight curve for the low speed of 20m/s (72km/h) with curve radius of 200m and the other a large curve for the high speed of 83.3m/s (300km/h) with the curve radius of 3470m – in both cases a cant angle of 6° is used [141]. Figures 4-13 to 4-30 show the lateral displacement, angel of attack (yaw angle), the wheel-rail contact forces in the longitudinal and latera directions, the control force and power on curve under the different track input conditions.

For a railway vehicle with independently rotating wheelsets, the longitudinal creep force will be much lower due as two wheels on the same axle can rotate freely. However, a suitable guidance action is required to ensure the wheelsets follow the track and flange contact is avoided. Figures 4-13 and 4-15 demonstrates how the actively controlled IRW would behave on curve and straight track. Figures 4-13 and 4-14 show that the two wheelsets have a displacement when approaching the curve. This behaviour is to give the outer wheel a larger contact wheel radius and the inner wheel a smaller contact radius, to account for the different distance between the outer and inner rails on curves. Also figure 4-16 shows the vehicles lateral displacement between wheelset and straight track with irregularity with delay between wheelsets and pick less than 10mm. Hence, wheelsets typically have a typical range of +/- 10mm before the undesirable flange contact occurs then the wheelsets are not running on the flanges.

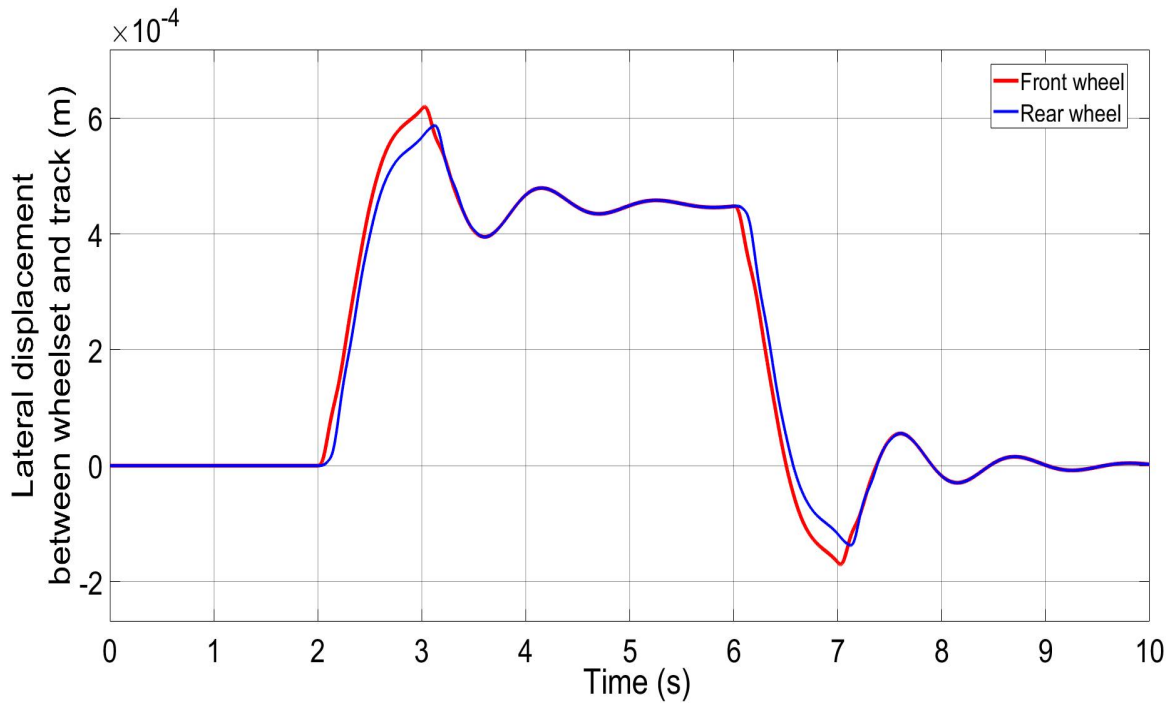


Figure 4-13- Two axle vehicles lateral displacement between wheelset and track on curve, 83 m/s

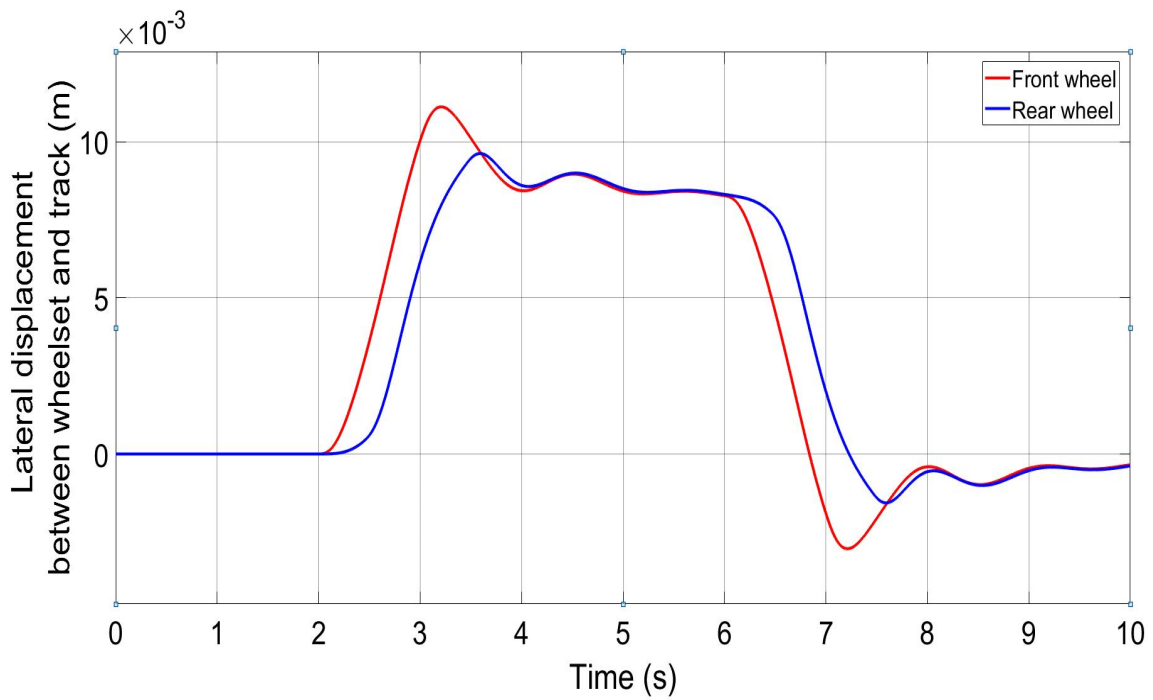


Figure 4-14- Two axle vehicles lateral displacement between wheelset and track on curve, 20 m/s

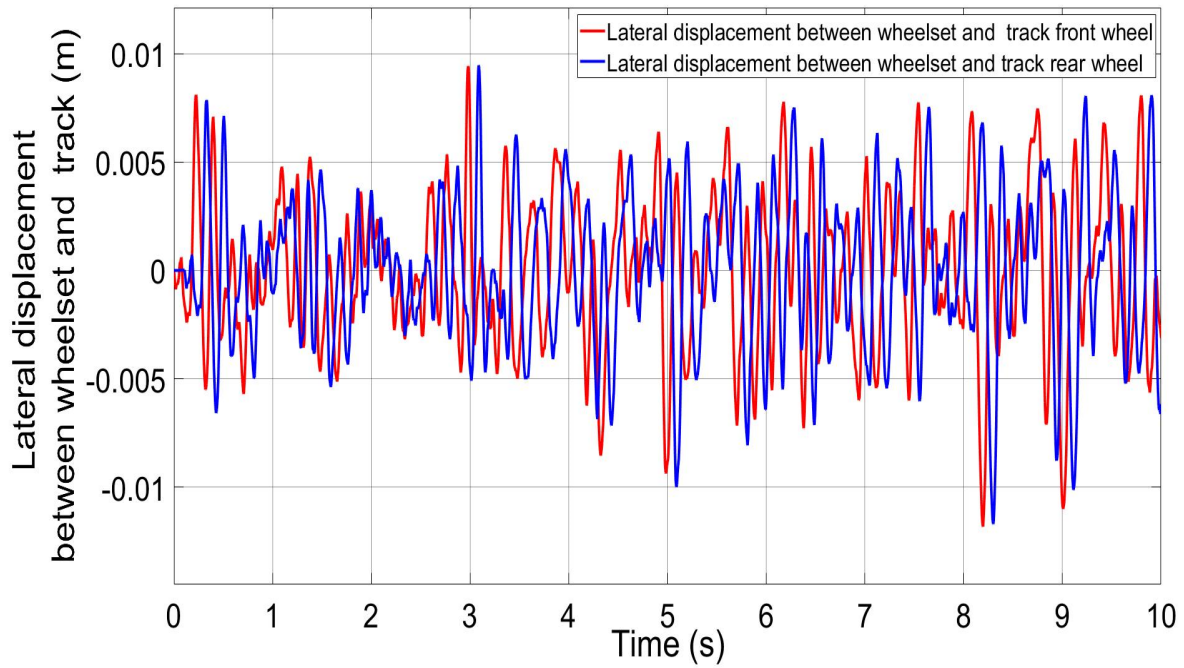


Figure 4-15- Two axle vehicles lateral displacement between wheelset and straight track with irregularity, 83 m/s

Figures 4-16 and 4-18 show the angles of attack for the two wheelsets on curve and straight track. The actively controlled wheelsets have an equal angle of attack when running around a steady curve, to provide the appropriate lateral creep force for the cant deficiency. Figure 4-18 shows that the wheelsets have similar angle of attack with time delay between them.

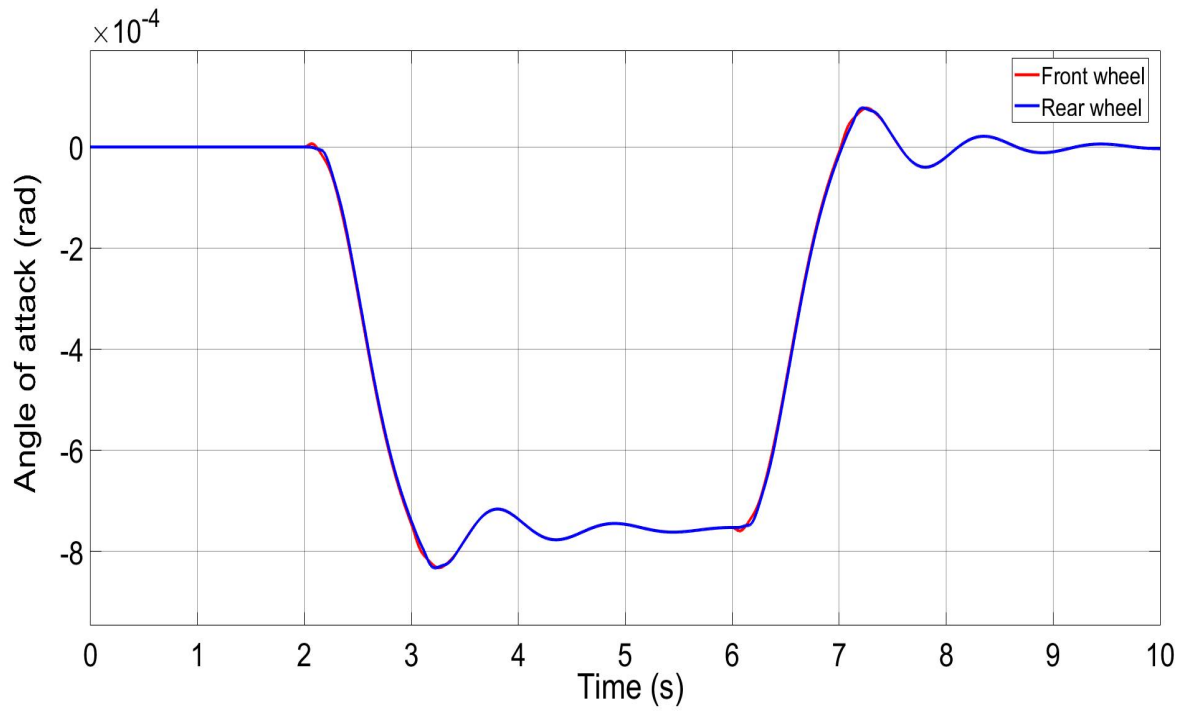


Figure 4-16- Two axle vehicles angle of attack on curve, 83 m/s

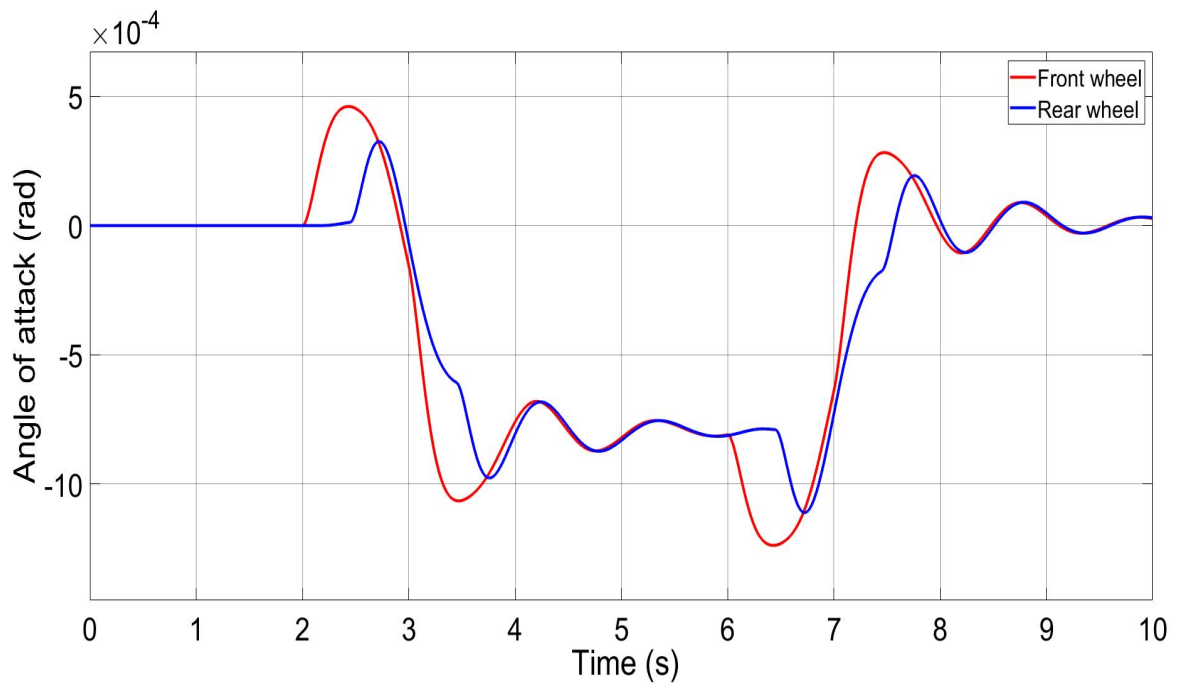


Figure 4-17- Two axle vehicles angle of attack on curve, 20 m/s

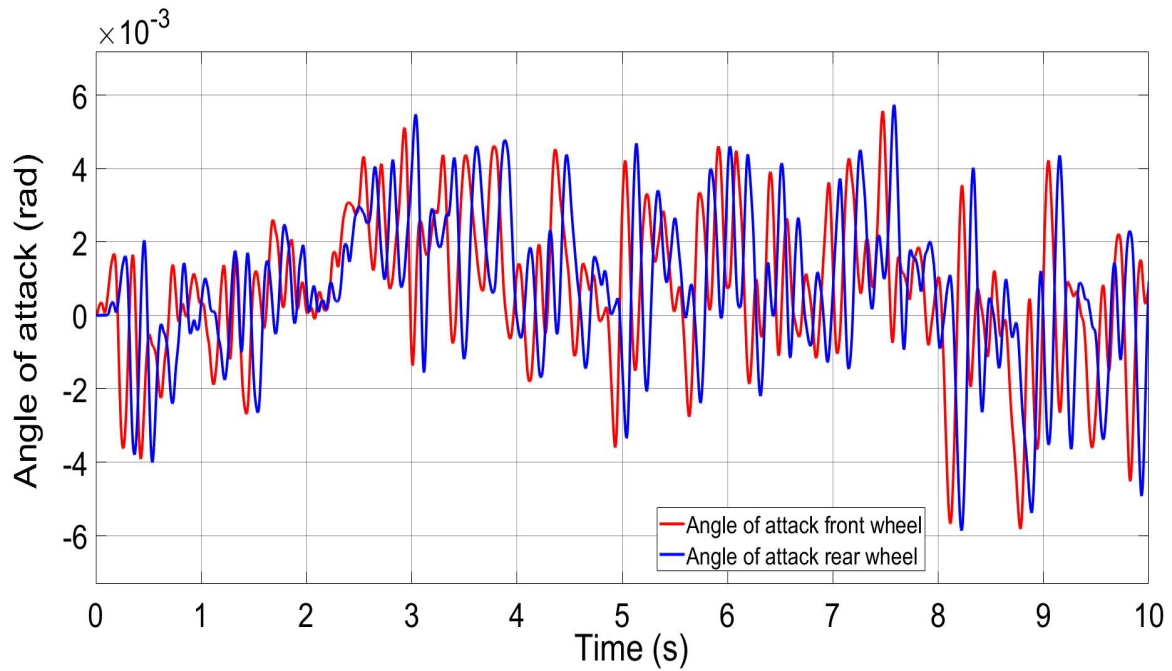


Figure 4-18- Two axle vehicles angle of attack on straight track with irregularity, 83 m/s

Figures 4-19 and 4-21 show the longitudinal creep forces for the two axle wheelsets on curve and straight track. longitudinal creep forces are very low because the two-wheelset rotating freely therefore the longitudinal on a steady curve is almost zero. Also, the result for straight track show that the longitudinal creep forces for the front and rear wheelset follow the same pattern with delay between them.

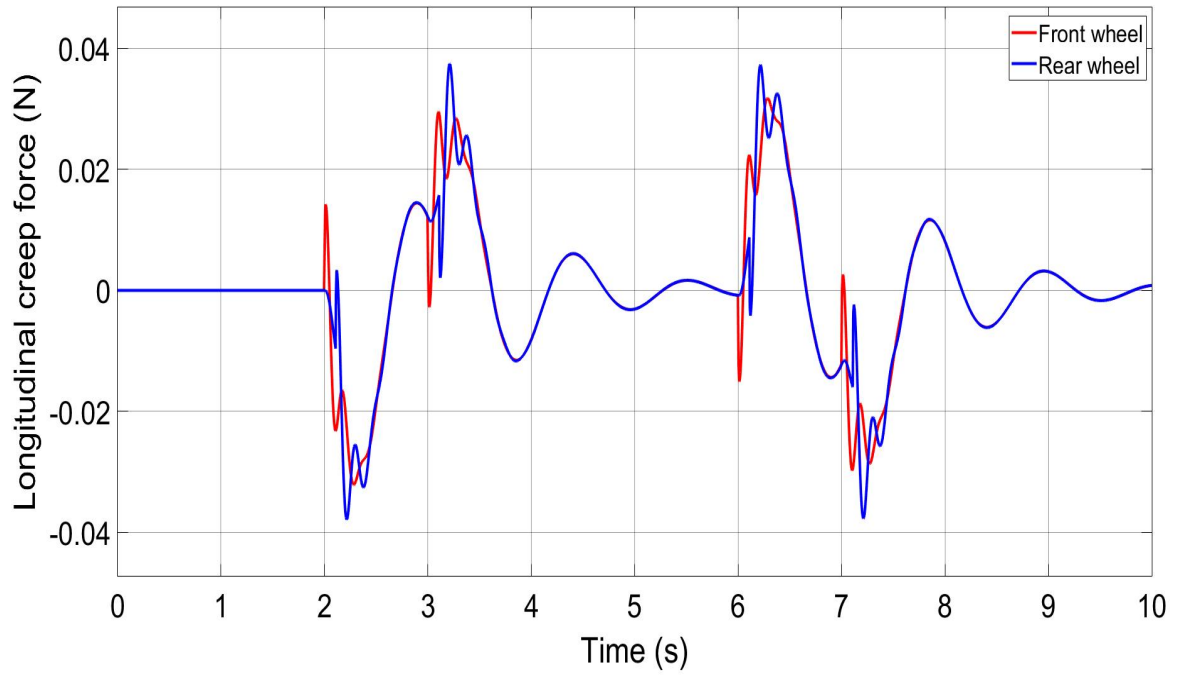


Figure 4-19- Longitudinal creep force on curve track, 83 m/s

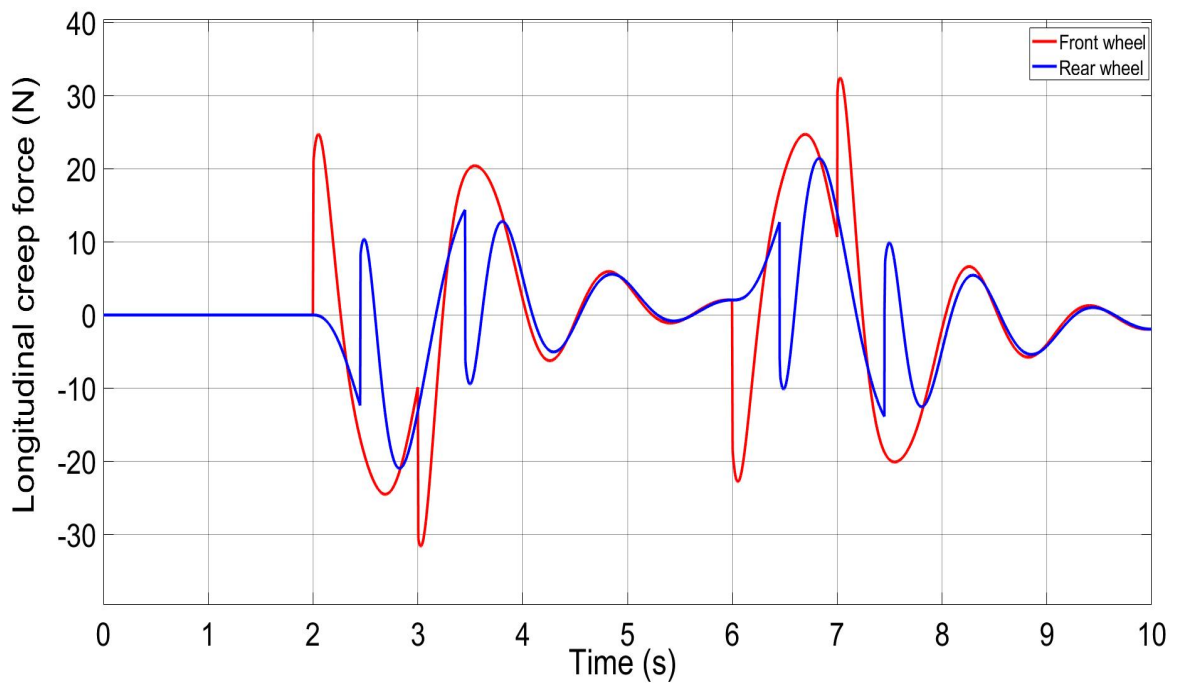


Figure 4-20- Longitudinal creep force on curve track, 20 m/s

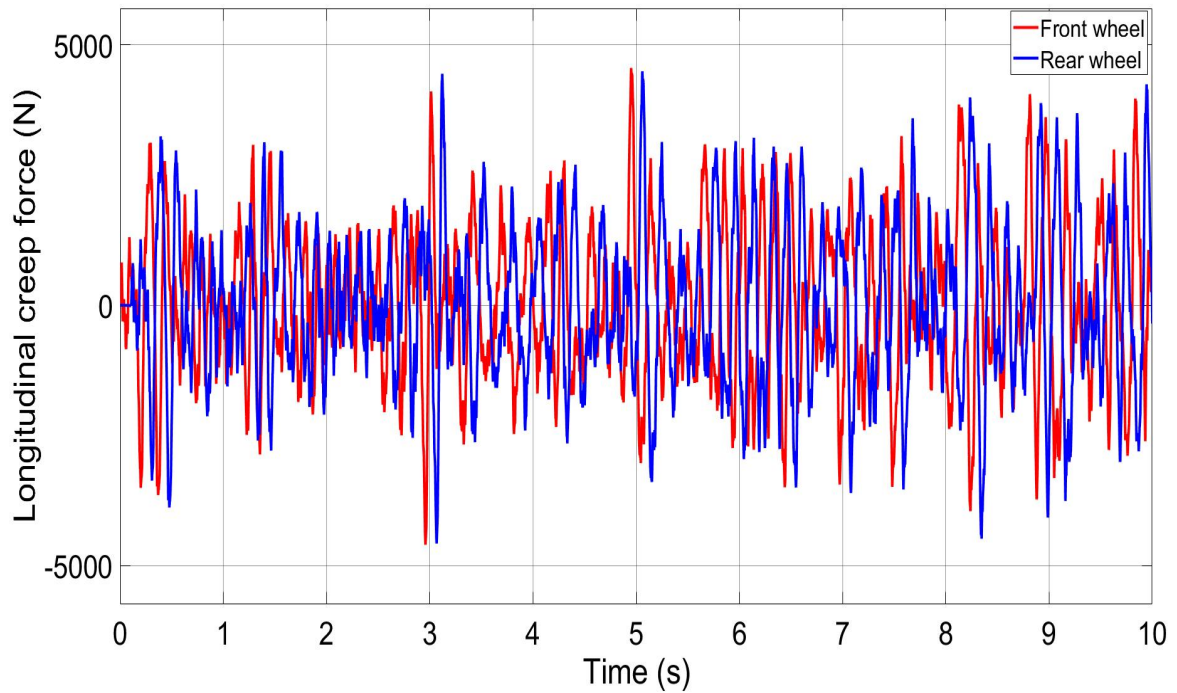


Figure 4-21- Longitudinal creep force on straight track, 83 m/s

Figures 4-22 and 4-24 shows lateral creep forces on the curve and straight tracks. These lateral creep forces occur as a reaction force to the centrifugal force which the vehicle is experiencing during the curved track and the total of lateral creep forces in the wheelsets are equal to the centrifugal force. Also, the result for straight track show that the lateral creep force is more effected by the angle of attack rather than the lateral velocity.

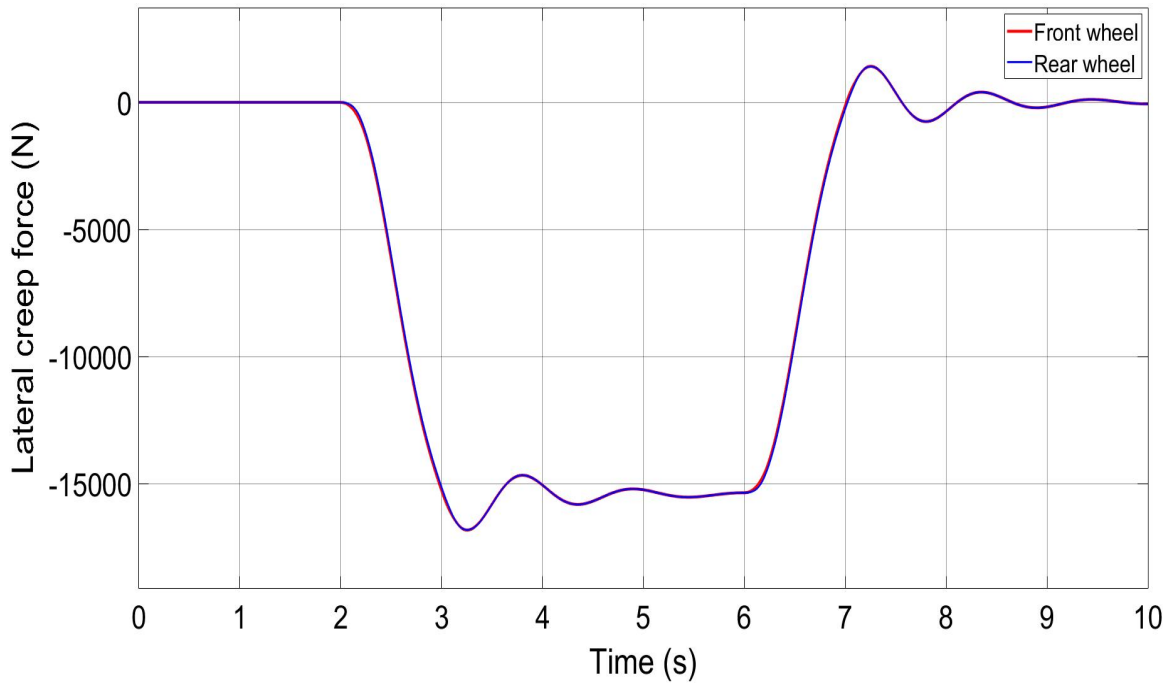


Figure 4-22- Lateral creep force on curve track, 83 m/s

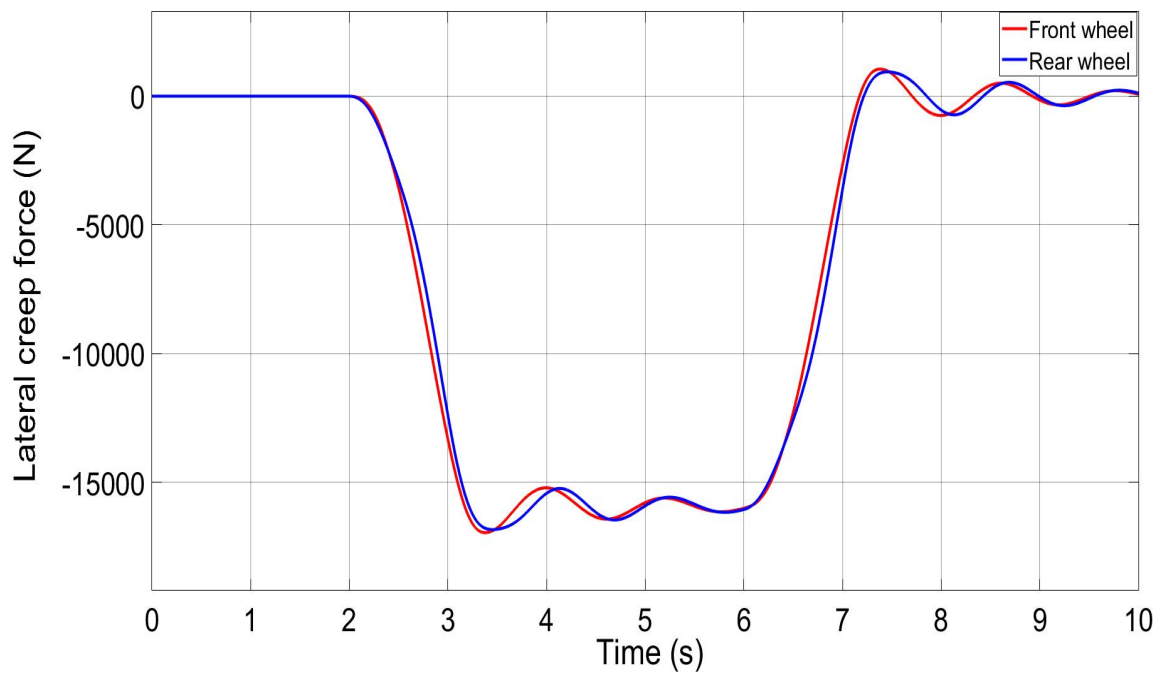


Figure 4-23- Lateral creep force on curve track, 20 m/s

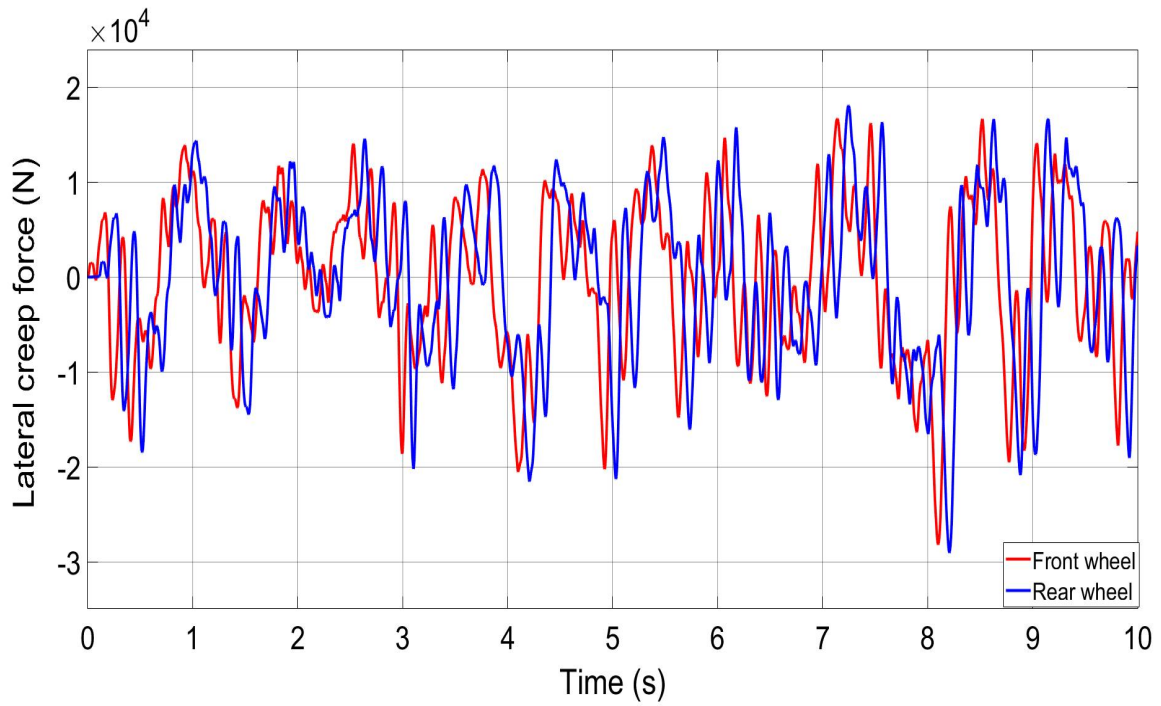


Figure 4-24- Lateral creep force on straight track, 83 m/s

Figures 4-25 to 4-27 shows the power requirement for the active control independently rotating wheelset for both curve track and straight track with irregularity at different speeds. In all cases, the results show that the active control laws only dissipate power – indicating that the application of semi-active methods is viable as there is no requirement to provide any additional energy.

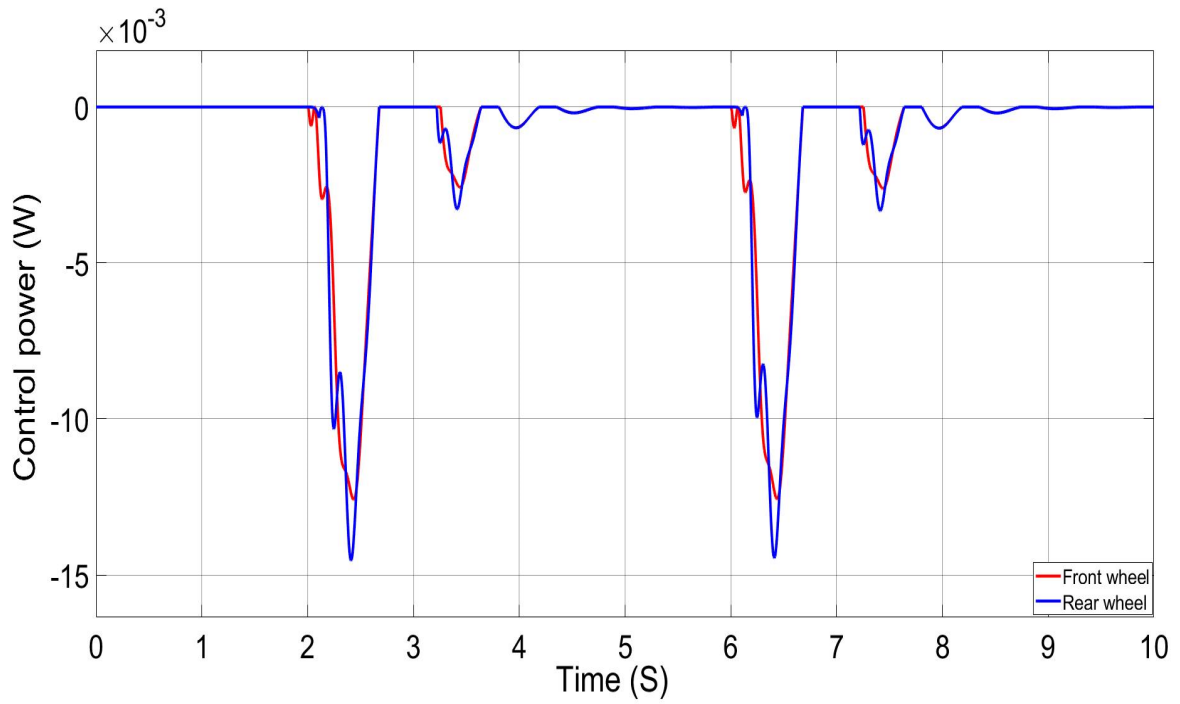


Figure 4-25- Active control power on curved track, speed 83.3 m/s

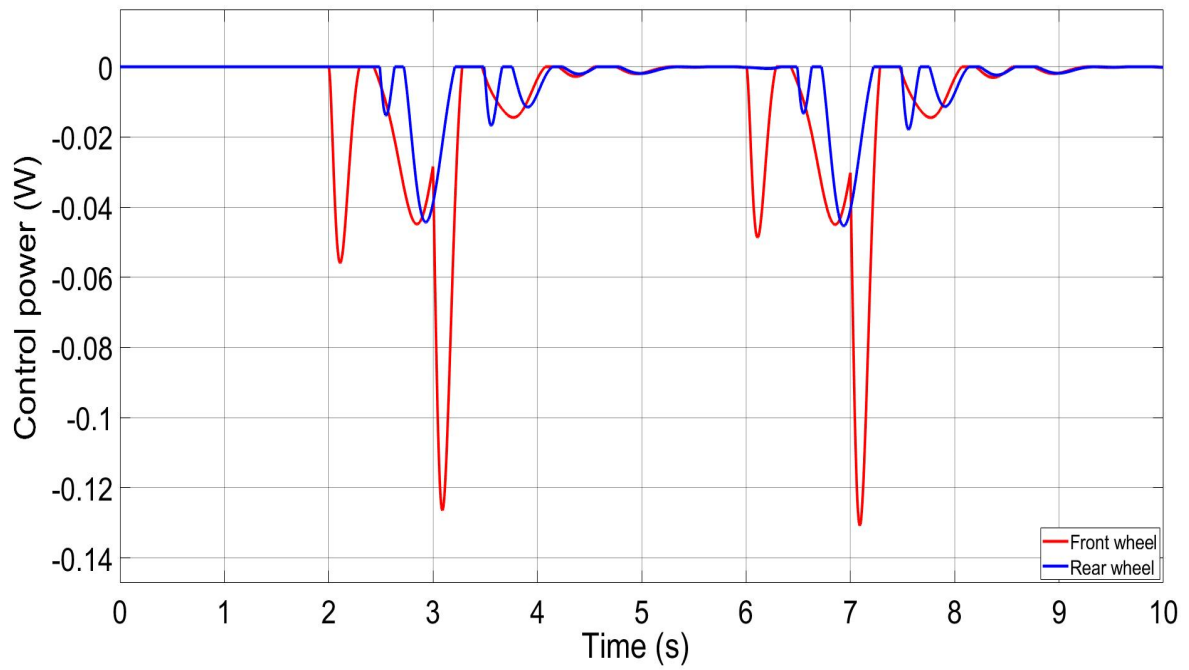


Figure 4-26- Active control power on curved track, speed 20 m/s

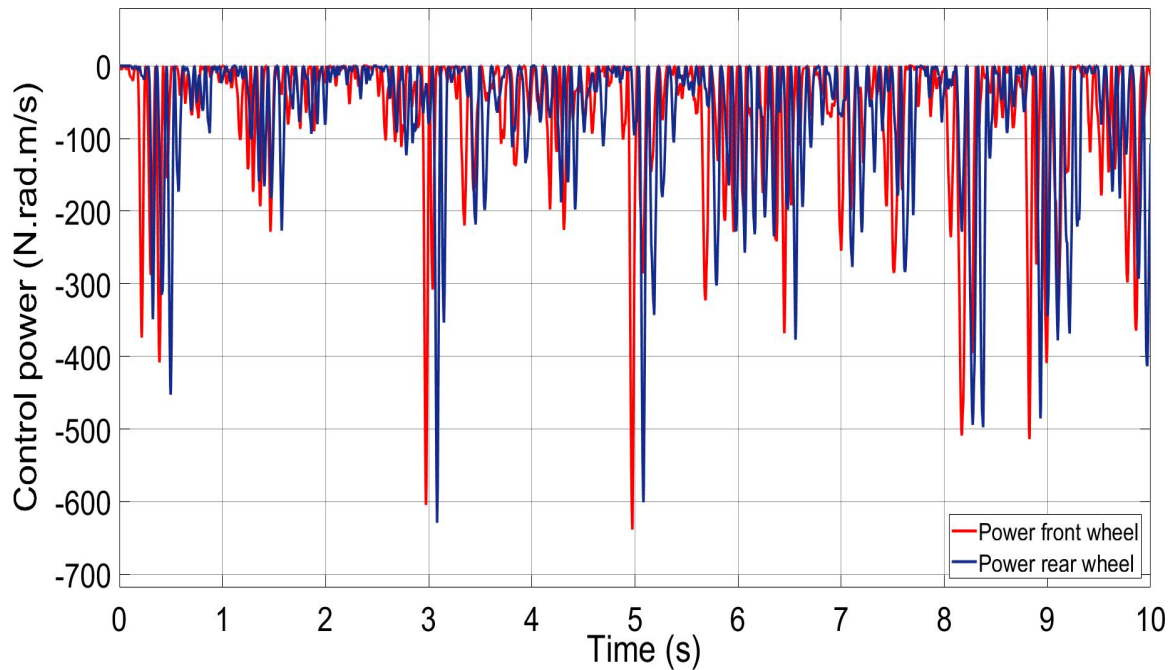


Figure 4-27- Active control power on straight track with irregularities, speed 83.3 m/s

The control force required to steer the independently rotating wheelset on pure curved track is relatively small. Figures 4-28 and 4-30 shows control force on a pure curved track at vehicle speed of 83.3 m/s. For speed of 83.3 m/s the required force of approximately 1150N.m which is significantly lower than solid-axle wheelsets [6, 142].

It is because when the two wheels are free to rotate separately, and active control reduces the longitudinal creep forces at the wheel/rail contact points. Therefore, the controller does not have to 'struggle' against the creep forces, when compared to solid axle vehicle.

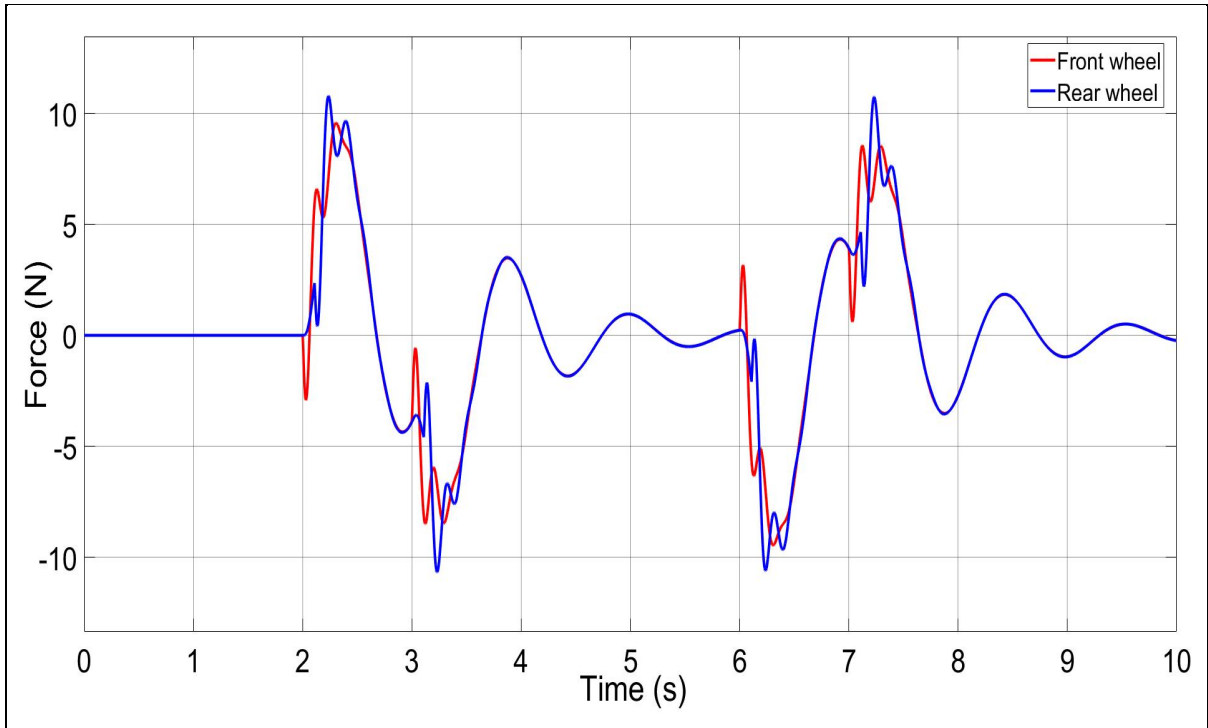


Figure 4-28- Active Control force on curved track, speed 83.3 m/s

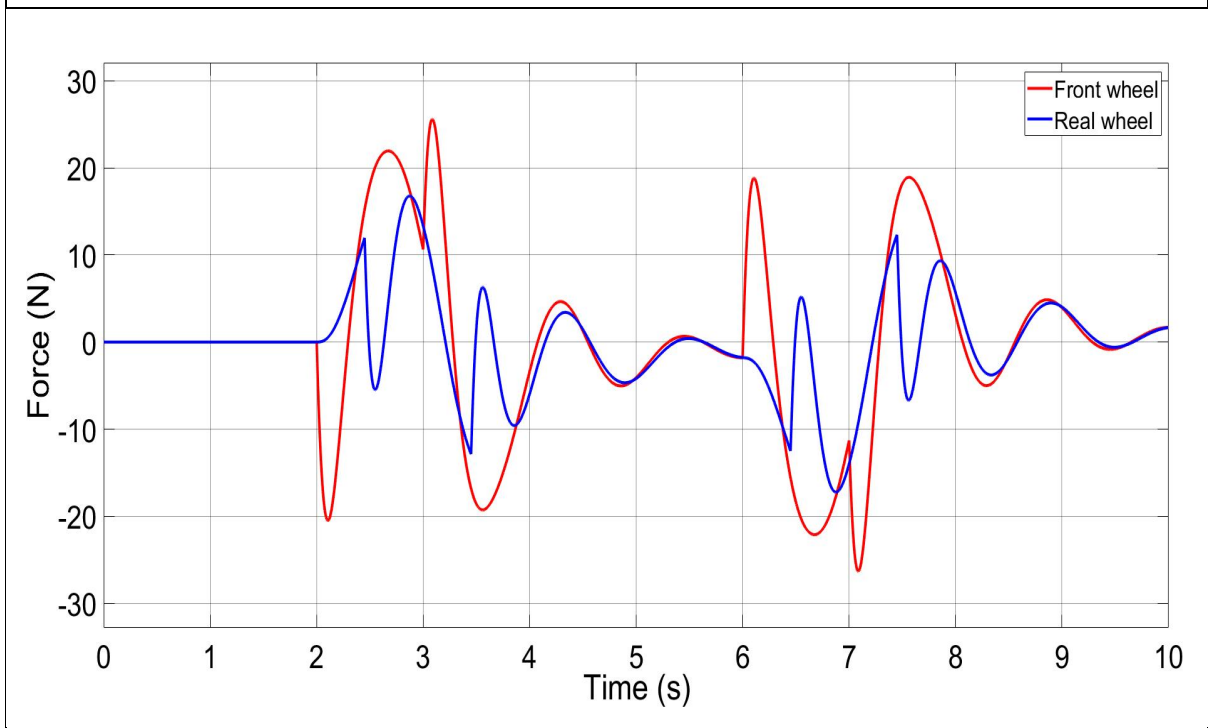


Figure 4-29- Active Control force on curved track, speed 20 m/s

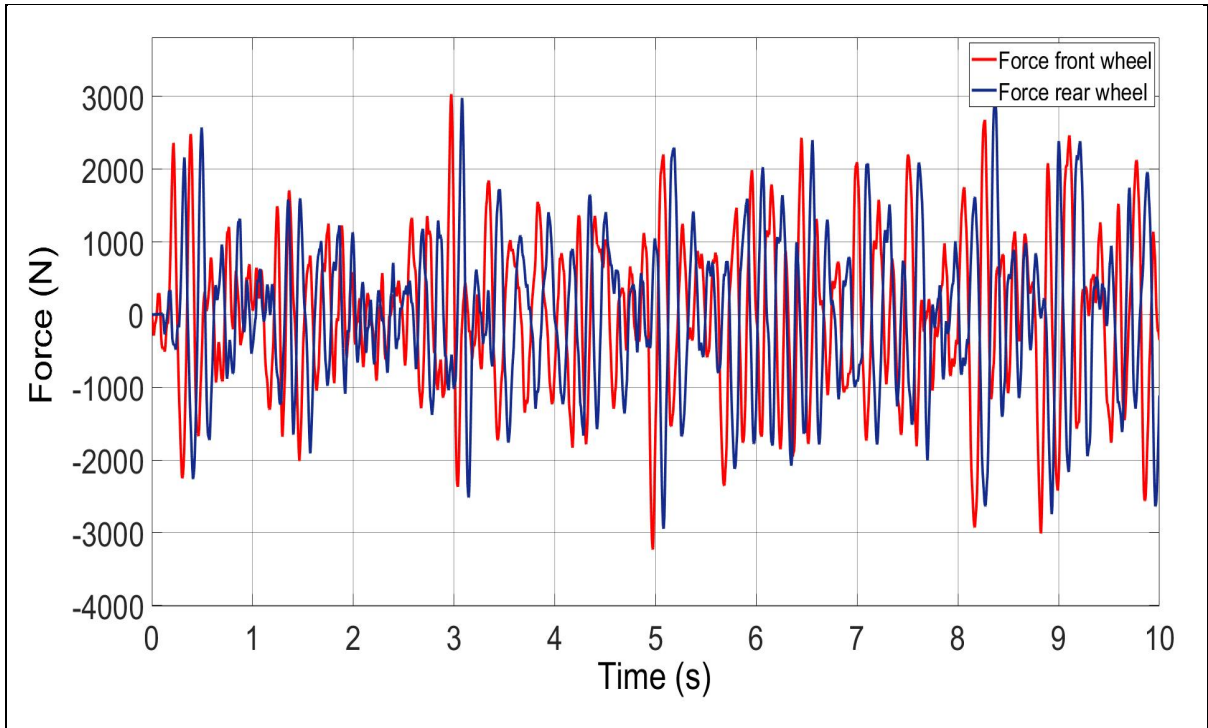


Figure 4-30-Active control force on straight track with irregularities, speed 83.3 m/s

Table 4-3 show the active control quantitative performance in different track with different speeds.

Table 4-3 Active control quantitative performance in different track with different speeds

Two axle vehicles	Curve Track 83 m/s	Curve Track 20 m/s	Straight track 83 m/s
Lateral displacement between wheelset and track, front wheel	4.4×10^{-4} (m)	8.7×10^{-3} (m)	0.0086 (m)
Angle of attack, front wheel	-7.7×10^{-4} (rad)	-7.6×10^{-4} (rad)	5.9×10^{-3} (rad)
Longitudinal creep force, front wheel	Almost 0 (N)	5 (N)	4640 (N)
Lateral creep force, front wheel	-15000 (N)	-15130 (N)	1.82×10^4 (N)
Active control power, front wheel	-12.6×10^{-3} (W)	-0.12.4 (W)	-600 (W)
Active Control force, front wheel	9.8 (N)	28 (N)	3000 (N)

4.5 Summary

Active suspensions, with the use of actuators and sensors, can be used to control the railway wheelsets by injecting or dissipating energy into/from the system in order to reduce vibrations, using control strategies that cannot be readily achieved with passive devices. However, it is obvious that such a system needs an external source to generate power to activate different components[23]. An active controller can deliver much improved performance over a large frequency range compared with passive suspensions and in the long term can be used to help and bring about revolutionary changes in the design of future railway vehicles [13, 15, 28, 29].

However, active suspension systems have a few disadvantages, such as they are bulky in size which can be challenging to install in tight space bogie frames, high cost, complicated design and also the requirement for high power therefore safety critical and the use of hardware redundancies (e.g. duplication of actuators) [24].

It is noticeable that this chapter is built upon previous studies on the full active steering control systems for independently rotating wheelset, based on measured relative rotation speed of the two wheels on the same axle, and the relative yaw velocity between the wheelset and vehicle body as the required feedback.

Chapter 5: Semi-Active Control

5.1 Introduction

This chapter presents the development of a novel semi-active approach for the control of independently rotating wheelsets (IRW), using magnetorheological (MR) dampers to provide the necessary stabilization and guidance control. Magnetorheological (MR) dampers are used to replace the actuators in the full active control, leading to a solution that would be cheaper in costs and smaller in size than the full active control systems. Because the semi-active control devices such as MR dampers can only dissipate energy, one of the keys focuses of the study is to develop and verify the control strategy that does not require the injection of power into the system in the provision of the stability control and guidance/steering. Figure 5-1 shows the overall scheme for the semi-active control system with the MR fluid dampers.

There are two stages of control. The system controller (i.e., the wheelset control) for the wheelsets is used to provide the stability and guidance for the wheelsets based on the feedback measurements of the yaw velocity and relative rotation of the wheelsets, but the controller needs to be formulated in semi-active mode as the actuation device (the MR damper) can only dissipate energy. There is also a local controller for the MR damper which needs to be designed to provide the necessary damping force as demanded by the wheelset controller.

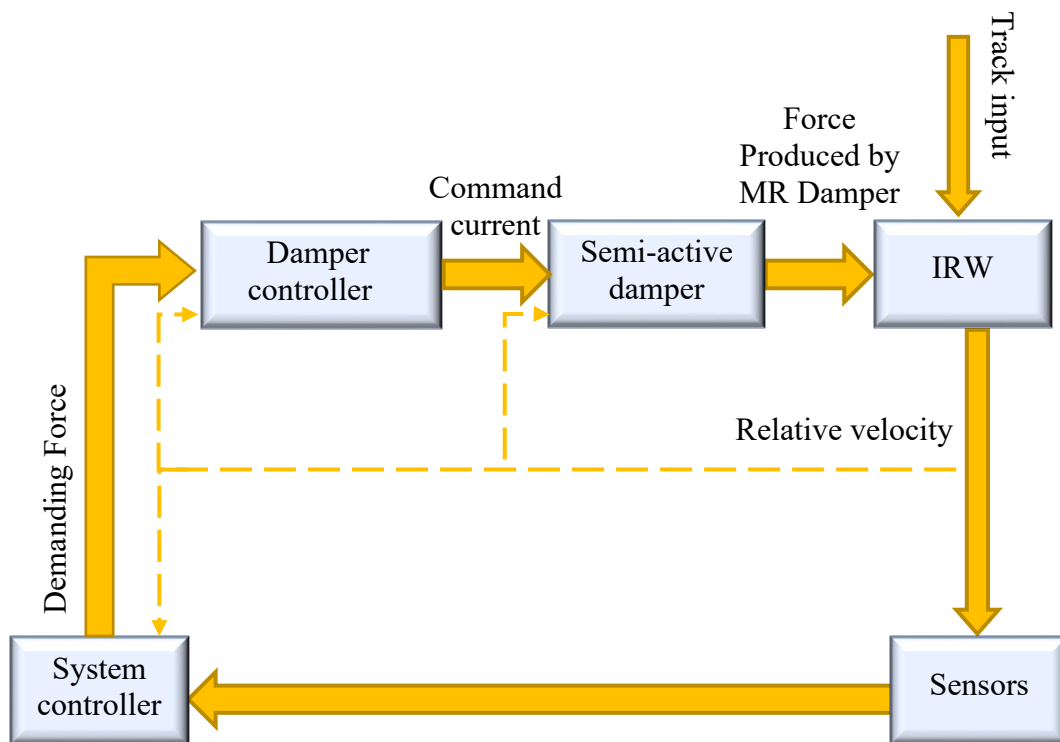


Figure 5-1- Schematic of the semi-active control system with the MR damper

5.2 Semi-Active Controller

An ideal semi-active damper is a non-linear device with a force/velocity coefficient that can be varied instantly up to a maximum defined value. However, this is not the case for the semi-active device in practice. Figure 5-2 provides a generalised characteristic which illustrates that it is constrained to operate in a relatively small area of the graph. Operation in the upper left and lower right quadrants is not possible, limitations can also be seen in the other two quadrants as a result of the minimum and maximum damping rates provided. This demonstrates the fundamentally non-linear nature of all semi-active suspensions [46].

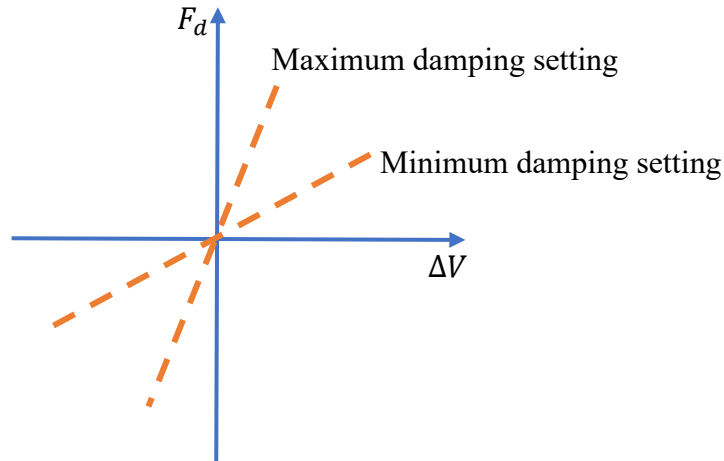


Figure 5-2- Semi-active minimum and maximum damping forces

Desired Damping Force Semi-Active Controller

This section discusses the formulation of the semi-active control based on the active control strategy presented in chapter 4. As it was demonstrated in the previous chapter, the active controller does not require the power injection and is well suited for implementation using the semi-active approach. However, there are still practical constraints due to the limitations of semi-active devices so the aim is to provide a damping force, F_{MR} , to match the desired control force, $F_{Controller}$ as closely as possible.

$$F_{MR} = C_{MR} \cdot \Delta V \quad (5-1)$$

$$C_{MR} = \begin{cases} \frac{F_{Controller}}{\Delta V} & \text{If } \begin{cases} \frac{F_{Controller}}{\Delta V} > 0 \\ \frac{F_{Controller}}{\Delta V} \leq 0 \end{cases} \end{cases} \quad (5-2)$$

Equation 5-2 indicates that C_{MR} (damping setting) is zero if MR damper relevant velocity ΔV and the control system damping force, $F_{Controller}$, are not in the same direction and it is set to provide a control effort only if MR damper relevant velocity and the control system damping force, $F_{Controller}$, are in the same direction (both positive or negative), i.e the desired damping

force will be proportional of C_{MR} if control system damping force and MR damper relevant velocity have the same sign.

The ideal and simplified characteristics of an MR damper are presented in equations 5-3 and 5-4. It should be noted that the semi-active damper used in this study is a MR damper and the damping coefficient of this type of damper is directly controlled by the input current going through the MR damper coil as shown in equation 5-3, where I is current supplied to the coils which must be between $I = 0$ and $I = I_{max}$.

$$F_{MR} = \alpha \cdot I \tag{5-3}$$

$$0 \leq I \leq I_{max} \tag{5-4}$$

In the case of MR dampers, the force vs. velocity characteristics are of strong nonlinearity as shown in Figure 5-3 and there is no direct/linear relationship between the input current and output force. Therefore, it is necessary to include a local control for the MR damper such that the appropriate damping force is produced to match the control force as demanded by the wheelset controller.

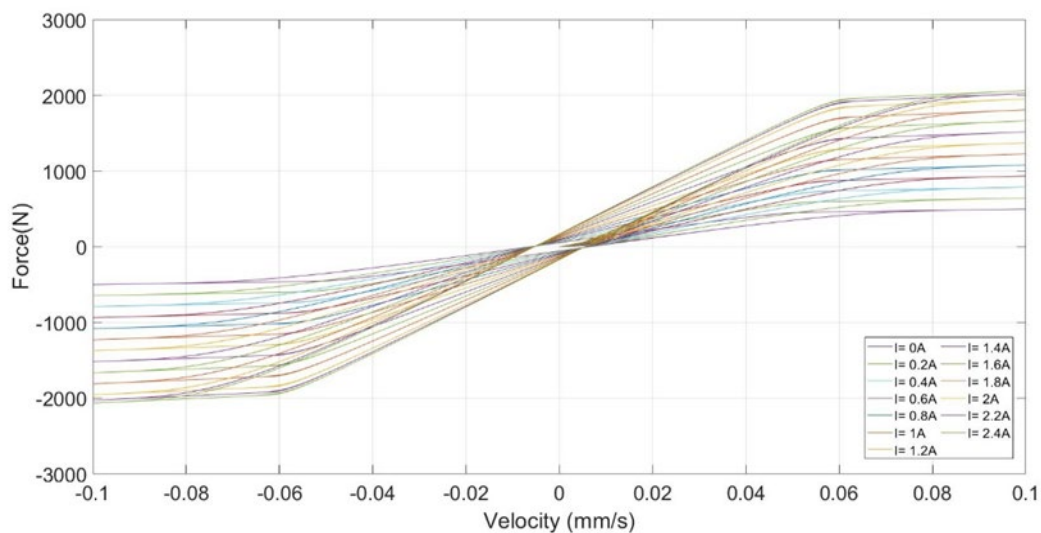


Figure 5-3- Damping force vs. velocity of Modified Bouc-Wen model

5.3 Magnetorheological Damper Controllers

In this research a combination of a lookup table based on the inverse MR damper model and a local feedback is used to control the current input (to the MR damper) the former is to produce the desire force as precisely as possible and the latter is providing the necessary robustness to account for the effect of uncertainties in the lookup table.

The MR damper can only track the damping force when the control force falls between the two limits as shown in figure 5-2. The possible zones in the first and third quadrants are obtained for positive and negative values, otherwise the damping force is set to either the lower level (F_{min}) or upper level (F_{max}) by setting the input current at either the minimum ($I=0A$) or the maximum ($I=2 A$ in this study) possible level, respectively. Above the upper limit of current, it is not possible to further increase the output force by increasing the current. Also, the force produced from the MR damper is also limited by the travelling velocity of the damper. Therefore, the force controller is designed to determine the desired damping force regards to active control force (demanded force) and suspension velocity, which is governed by:

$$F_{desire} = \begin{cases} F_{max}, & F_{active} \geq F_{max} \\ F_{active}, & F_{max} \geq F_{active} > F_{min} \\ F_{min}, & F_{active} \leq F_{min} \end{cases} \quad (5-5)$$

where F_{max} and F_{min} are the maximum and minimum forces that can be generated by the MR damper. F_{active} is the active control force (demanded force) which can be determined by the active control system, F_{desire} is the desired damping force that can be tracked by the MR damper [123].

while:

$$F_{max} = C_{max} \overbrace{(\dot{y}_{v1} - \dot{y}_{w1})}^{\Delta_{v1}} \quad (5-6)$$

$$\dot{y}_{v1} - \dot{y}_{w1} = \Delta_{v1} \quad (5-7)$$

By substituting 5-7 into 5-6 gives:

$$F_{max} = C_{max} \Delta_{v1} \quad (5-8)$$

And

$$F_{min} = C_{min} \overbrace{(\dot{y}_{v2} - \dot{y}_{w2})}^{\Delta_{v2}} \quad (5-9)$$

$$\dot{y}_{v2} - \dot{y}_{w2} = \Delta_{v2} \quad (5-10)$$

By substituting 5-10 into 5-9 gives:

$$F_{min} = C_{min} \Delta_{v2} \quad (5-11)$$

A look up table using the inverse model of the MR damper is used to calculate the current input from required force and relative velocity of the device. However, it is not possible to have precise knowledge of MR parameters and it is also difficult to account for the hysteresis present in MR dampers in the lookup table. Therefore, an additional local PI feedback controller is also used to improve the robustness for the MR control.

Figure 5-4 shown the structure of the design. The force demanded by the system controller and the force produced by the MR damper are fed to the PI controller and the output of the PI controller is added to the current generated by the lookup table as the total current demand for the MR damper.

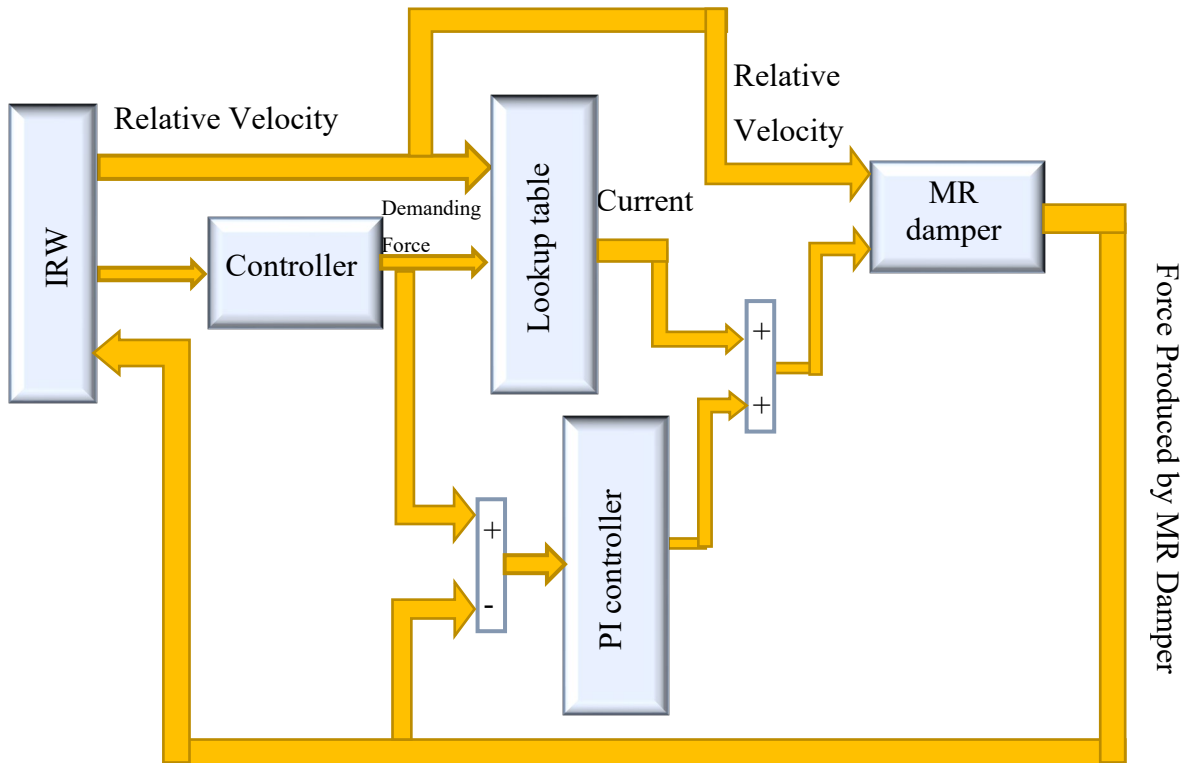


Figure-5-4- Semi active controller includes Lookup table and MR damper, robust with PI controller

5.4 Inverse Dynamics (Feedforward) Design

Inverse MR damper models were used to determine the input current in order to track the desired force. A lookup table used is applied to build the inverse MR damper model in this study to control the current input and provide the appropriate output force for the semi-active controller

As shown in Figure 5-5 the inputs for the inverse model are the damping force (demanded force) and relative velocity (of MR damper, which is also directly related to the relative yaw velocity between the wheelset and the vehicle body frame), and the output is the current demand. In general, with an increasing number of data points (force and velocity) in the lookup table, the accuracy of the inverse model increases. However, by increasing the number of the force and velocity points the inverse model can become very large.

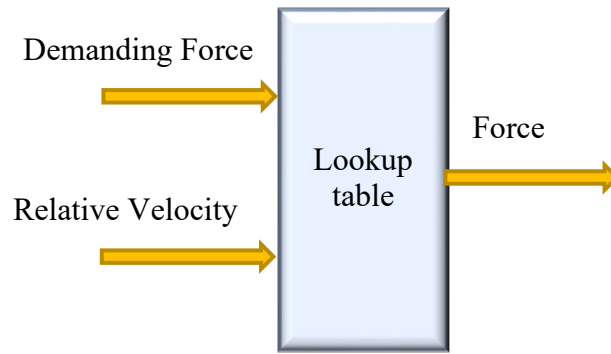


Figure 5-5- Look up table

To design an accurate lookup table model, 29 different relative velocity and 2003 different currents were fed into the model of the MR damper to generate different forces for each instance (as illustrated in Figure 5-6).

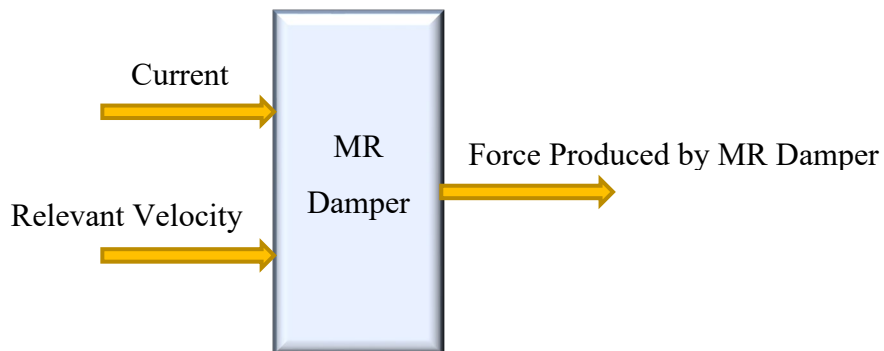


Figure 5-6-MR damper

The relative velocity to design this controller is from 0 to 0.1 m/s (the maximum amplitude of difference yaw velocity between wheelset and body is 0.1 m/s) and the current is from 0 A to 2 A (for the dampers used in the study as explained in section 3.6).

With this data, a 29*2003 table was generated (as illustrated in table 5-1), and from this table a smaller table 19*22 is formed for the inverse lookup mode (as shown in table 5-2). It is noticeable to mention that the table 5-1 was a big table due to see how force is change with a

very small change in either current or velocity. However, eventually to make it less complicated while get a very accurate result made a smaller table from table 5-1 which result is table 5-2.

Table 5-1- Force generated by MR damper

		Δ Velocity(m/s)				
		$\Delta V_1=0\text{m/s}$	$\Delta V_2=0.003\text{m/s}$	$\Delta V_{29}=0.1\text{m/s}$
Current(A)	$i_1 = 0A$					
	$i_1 = 0.001A$					
	$i_1 = 0.002A$					
					
					
	$i_{2003} = 2 A$					

Table 5-2- Look up table

		Force (N)				
		$F_1=0 N$	$F_1=N$	$F_{22} = N$
Velocity(m/s)	$\Delta V_1=0 \text{ m/s}$					
	$\Delta V_2=0.003 \text{ m/s}$					
					
					
					
	$\Delta V_{19}=0.1\text{m/s}$					

1

Eventually, the output of the inverse controller model (current) and the different yaw velocity between wheelset and body are given to the MR damper as input, and the desired damping force for the system is expected in return as it shown in Figure 5-7.

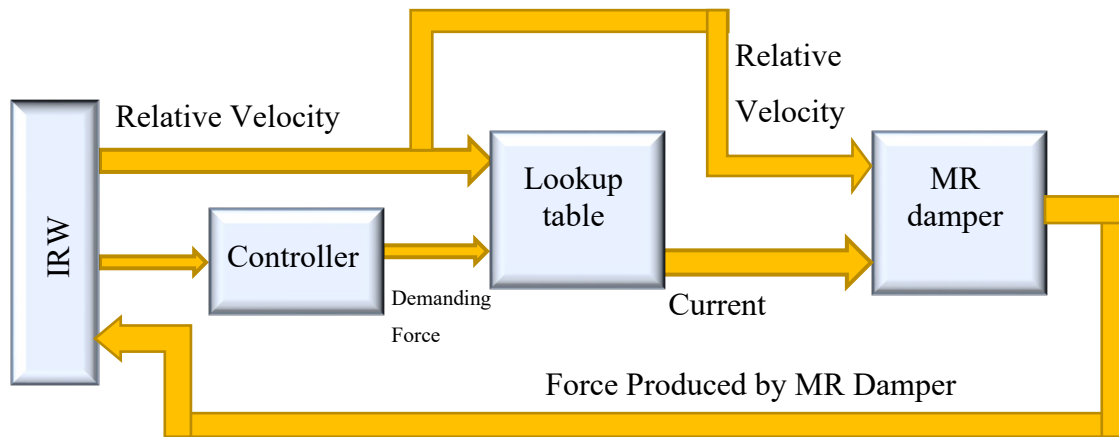


Figure 5-7- Semi active system structure with Look up table and MR damper

5.5 Feedback (PI) Controller

As already described in section 5.3, a PI controller for the local feedback control is also used to overcome the problem of damper uncertainty and ensure the systems is robust. Equation 5-12 represent the PI controller.

$$u(t) = K_p e(t) + K_i \int_0^t e(\tau) d\tau \quad (5-12)$$

$$e(t) = F_{desired} - F_{MR} \quad (5-13)$$

Where $u(t)$ is the control variable (control current), $e(t)$ is the error defined as $e = F_{desired} - F_{MR}$, k_p is the proportional feedback gain, k_i is the integral feedback gain, F_{MR} is the generated MR force and $F_{desired}$ is the desired damping force that generated by the system

controller. Control gain for the local controller is tuned to match the output to the input at the best possible level for the control of the primary suspension.

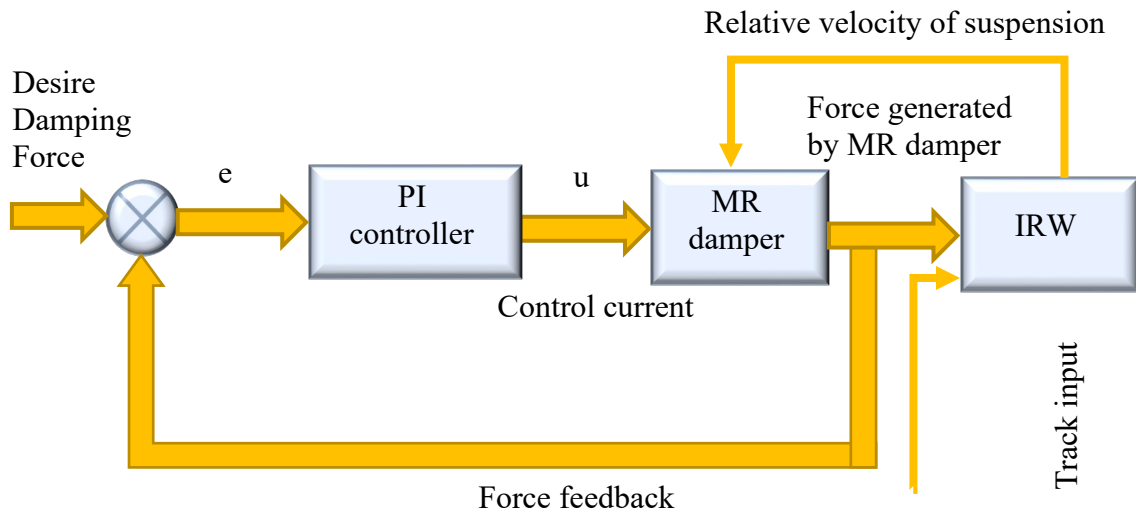


Figure 5-8- The PI local controller for the MR damper

The control gains of the PI controller are tuned with the help of the MR model and computer simulation, including the feedforward lookup table. It is assumed that the feedback signal of the output force can be measured by using a loadcell. A comprehensive assessment of the MR controller is carried out to validate the control design as presented in the next section.

5.6 Evaluation of Control Performance

Computer simulations are used to assess the performance of the local MR control, with different force demand and relative velocity of the MR damper.

In Figure 5-9, the velocity and desired force have the same frequency and in phase, and therefore the MR damper force adequately followed the desired force.

When the frequencies of the velocity and force demand are different, the MR damper can only deliver the output as required when the force and velocity are both positive or negative.

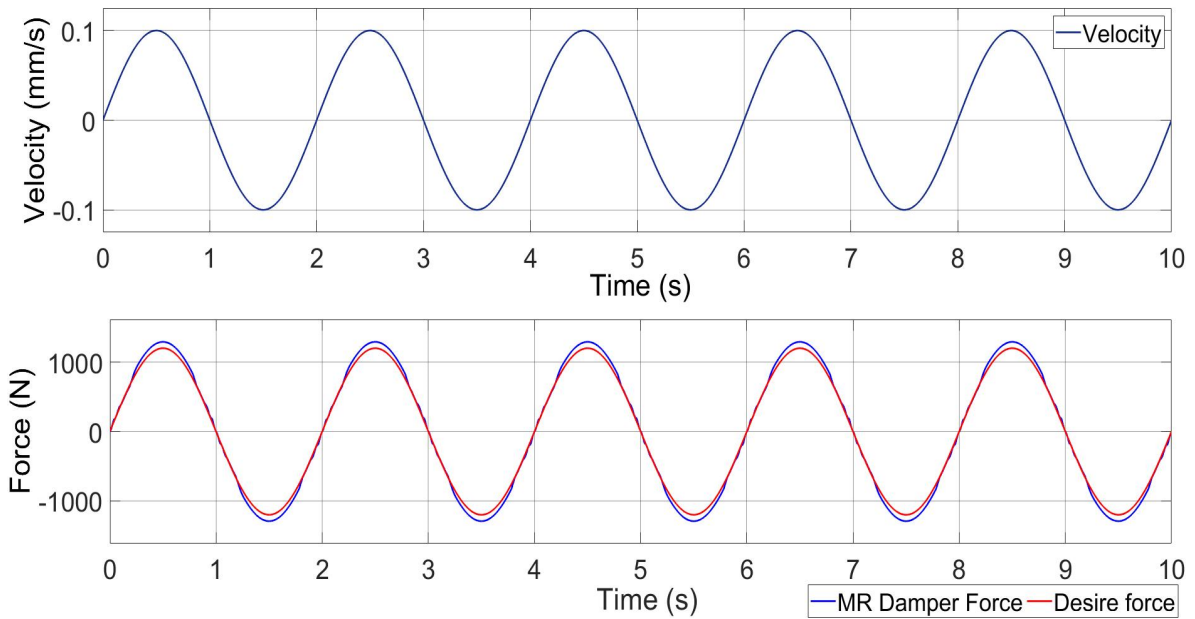


Figure 5-9- Validity of inverse MR damper (0.5 Hz, Amplitude=0.1mm)-sin input

In Figure 5-10, the velocity has one cycle between 0 to 1 seconds, and the desire force completed a cycle between 0 to 2 seconds. Between 0 and 0.5 seconds, when both velocity and desire force are greater than zero, the MR damping force follows the desired force, whereas between 0.5 to 1 seconds the velocity was negative and the desire force was greater than zero, in which instance the MR damping force followed the velocity as already noted in equation 5-1, as $F = cy$.

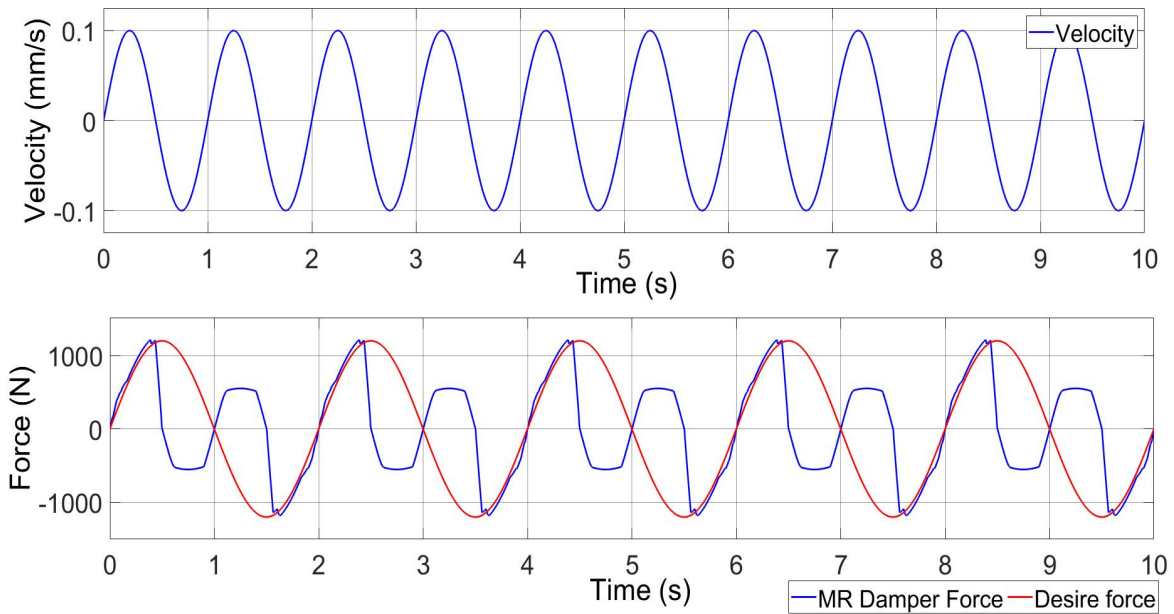


Figure 5-10- Validity of inverse MR damper (0.5 Hz, Amplitude=0.1mm)-sin input

Figure 5-11 shows a step input for the velocity and sinusoidal demand for the desire force. Before 1 second, the velocity is 0 therefore the force produced by the MR damper is zero (refer to equation 5-1). From 1 second, the MR damper follow the force demand where the desired force and the velocity are both greater than zero and it follows the pattern of the velocity where force is negative while velocity is positive.

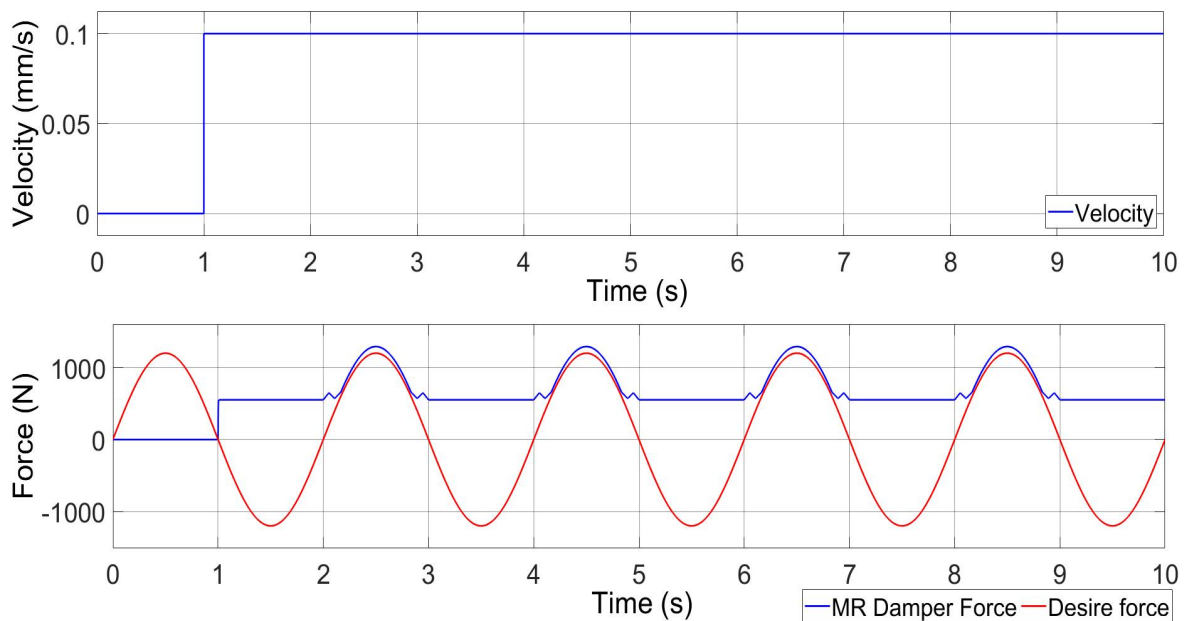


Figure 5-11- Validity of inverse MR damper (0.5 Hz, Amplitude=0.1mm)-step input

The behaviour of Figure 5-11 is very similar to figure 5-10, where the difference is velocity is sinusoidal and the desired force is a step input.

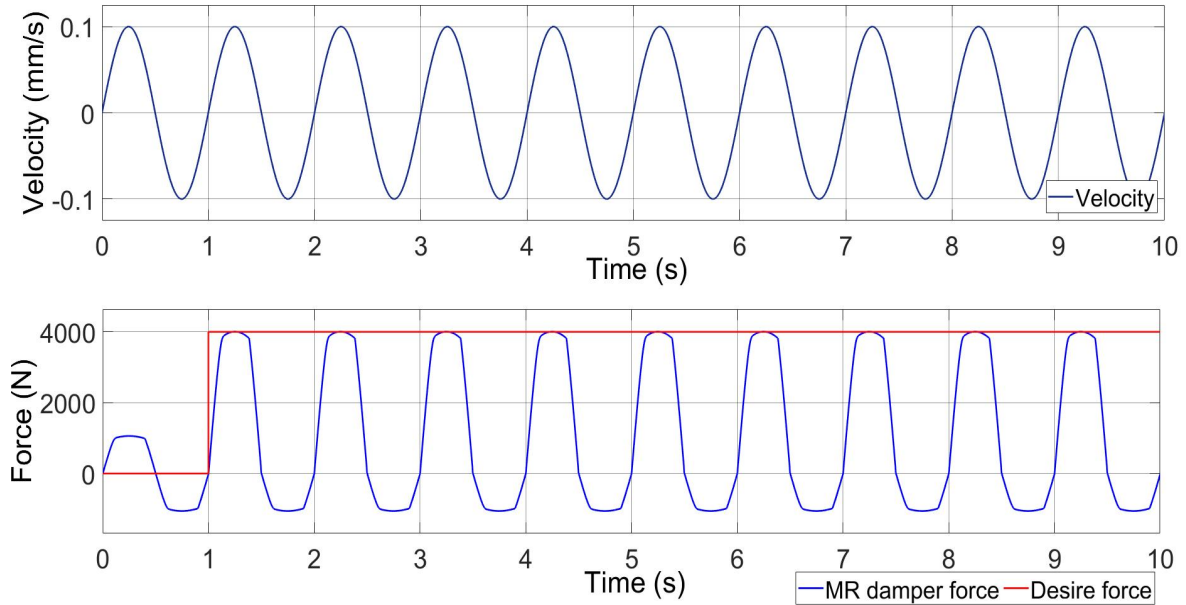


Figure 5-12- Validity of inverse MR damper, Amplitude=0.1mm, step input

Simulations are also run to assess the robustness of the MR control. Figures 5-13 to 5-16 show the comparison between the desired force, the force produced by MR damper with the lookup table set by 6% tolerance, with and without the PI feedback control included.

In figure 5-13, the peak desired force is 1200 N, the force generated by the MR damper with the lookup table only is 1285 N and the force produced by MR damper with both lookup table and the PI controller is 1203 N an control error of 7.01% and 0.25% respectively. In Figure 5-14, the peak demanded force is 1125N while the force generated by the MR damper with the lookup table only is 1214 N and the force produced by MR damper with both lookup table and the PI controller is 1128 N an control error of 7.91% and 0.27% respectively.

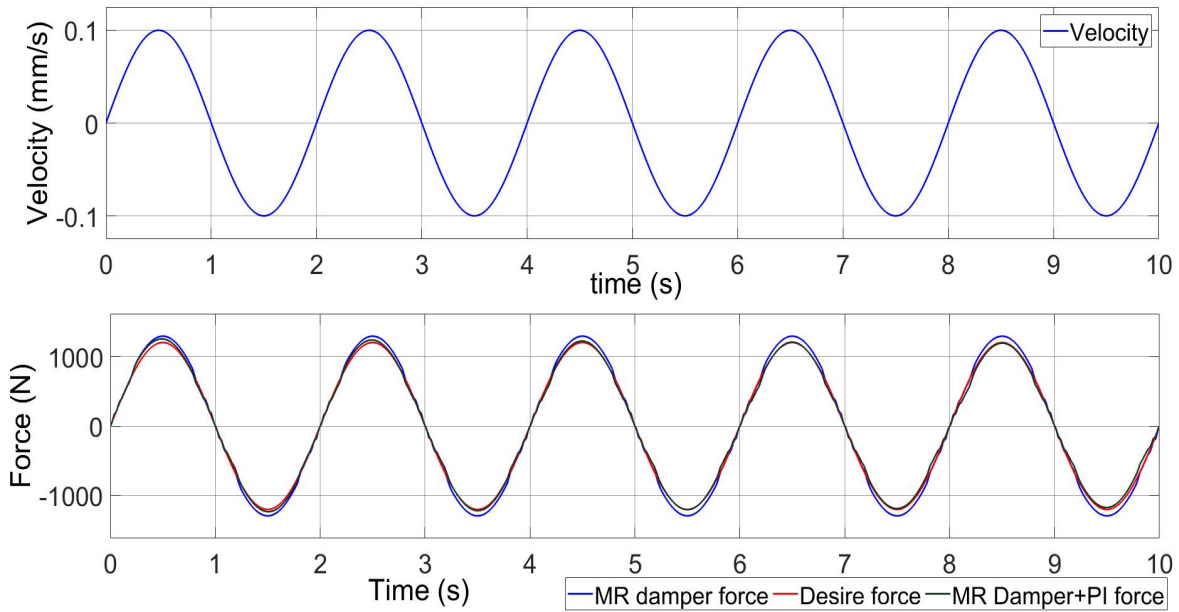


Figure 5-13- Validity of inverse MR damper + PI controller (0.5 Hz, Amplitude=0.1mm)-sin input

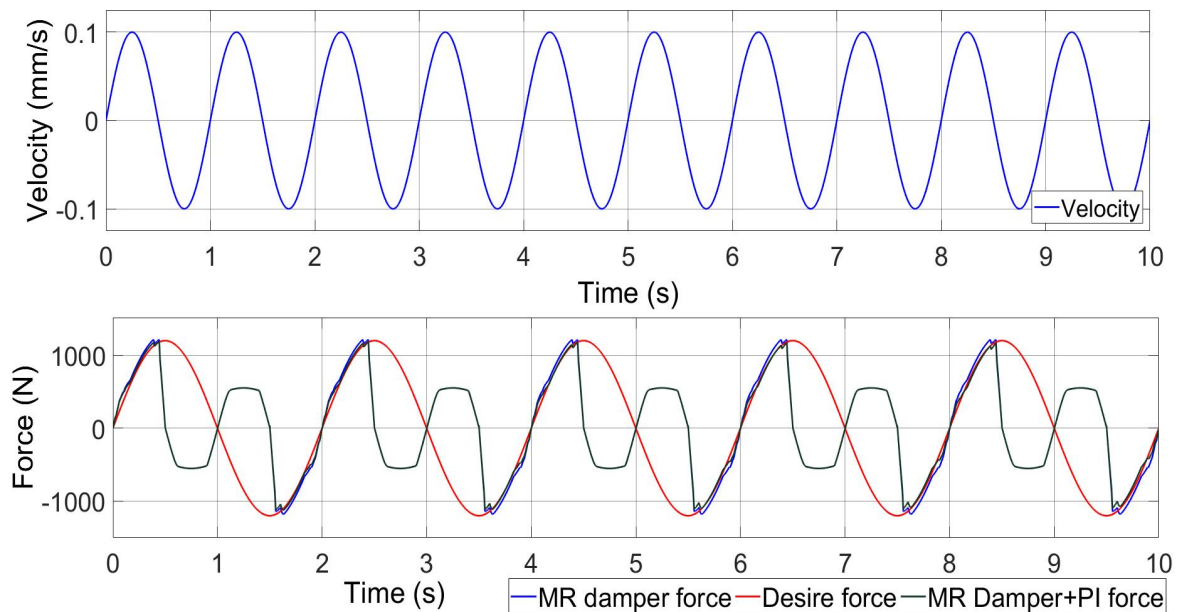


Figure 5-14- Validity of inverse MR damper + PI controller (0.5 Hz, Amplitude=0.1mm)-sin input

In Figure 5-15, the peak demanded force is 1200N while force generated by MR damper is 1292 N and the force produced by the MR damper and PI controller is 1192 N - an control error of 7.67% and 0.67% respectively. In Figure 5-16, the peak demanded force is 1200N while the force generated by MR damper with the lookup table only is 1292 N and the force

produced by MR damper with the both lookup table and the PI controller is 1201 N an control error of 7.67% and 0.08% respectively.

It is therefore the additional feedback control enhances the performance of the MR dampers considerably in conditions where the lookup table does not have a perfect representation.

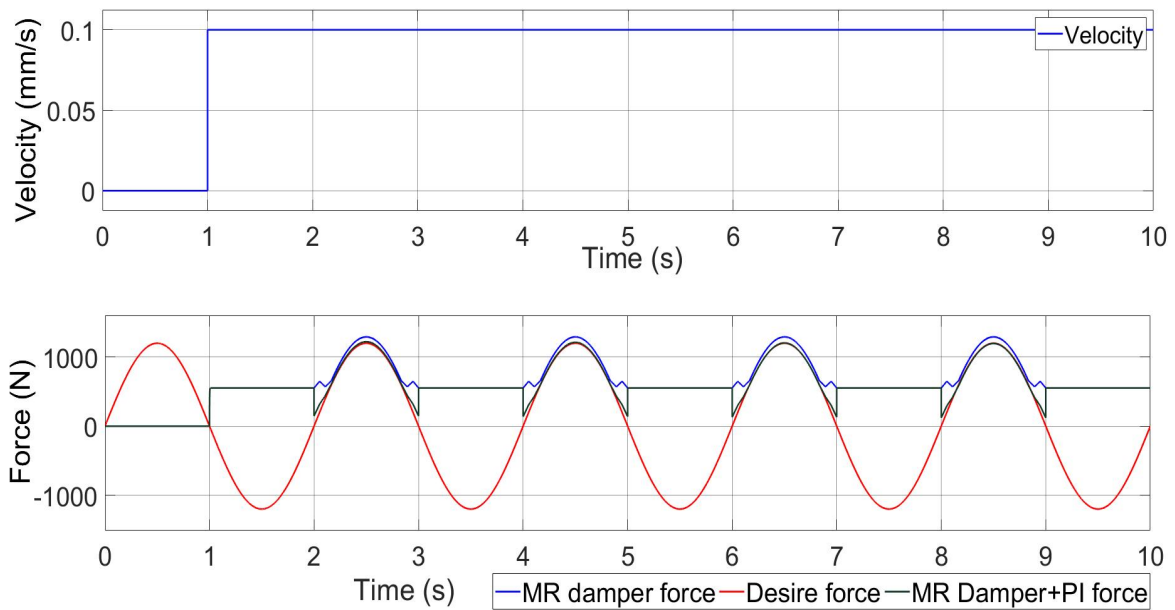


Figure 5-15- Validity of inverse MR damper + PI controller (0.5 Hz, Amplitude=0.1mm)-step input

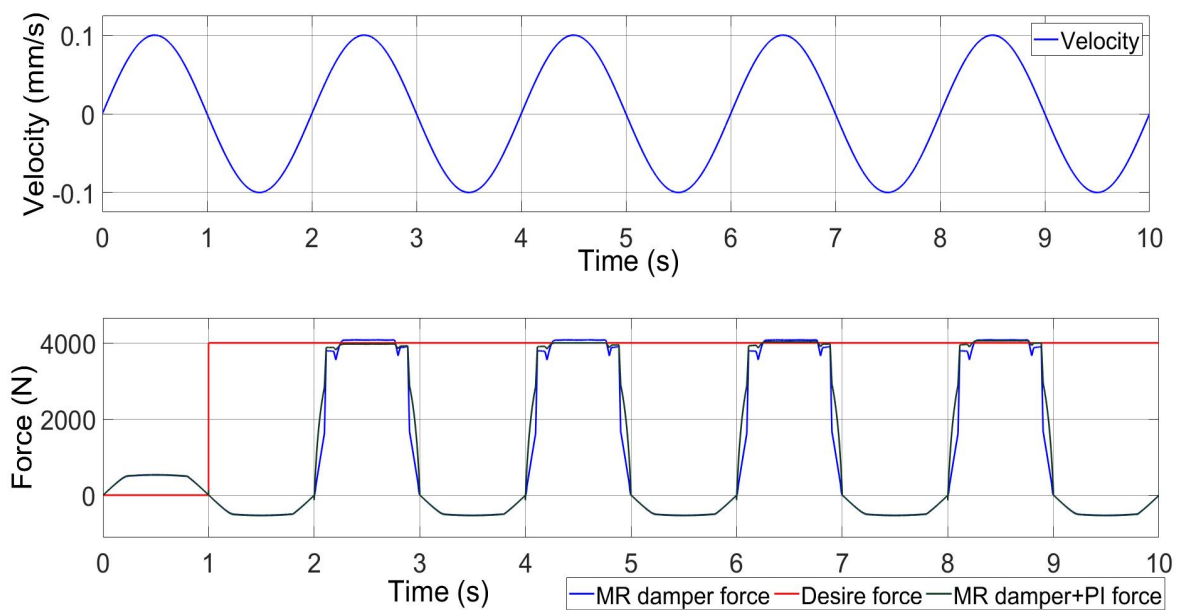


Figure 5-16- Validity of inverse MR damper+ PI controller, Amplitude=0.1mm, step input

5.7 Summary

The main finding of this chapter is the design details of a novel semi-active scheme for the control of independently rotating wheelsets (IRW) in railway vehicles, using magnetorheological (MR) dampers to provide the necessary stabilization and guidance control. Magnetorheological (MR) dampers are used to replace the actuators in the full active control, leading to a solution that would be cheaper in costs and smaller in size than the full active control systems. Because the semi-active control devices such as MR dampers can only dissipate energy, one of the keys focuses of the study is to develop and verify the control strategy that does not require the injection of power into the system in the provision of the stability control and guidance/steering. To ensure that the MR dampers will produce the control force as demanded by the wheelset control, a lookup table for the inverse MR damper model is used in this study to obtain the control current according to the desired damping force, whereas a local PI control is also used to improve the robustness of the MR damper control. Computer simulations are used to demonstrate that the MR dampers with the combination of the local feedforward and feedback controls are capable of producing the output forces in semi-active control conditions.

Chapter 6: Simulation Results and Assessments

6.1 Introduction

This chapter presents the simulation results and evaluation of the vehicle performance of the proposed semi-active control strategy applied to two different railway vehicles, a two-axle vehicle, and a conventional bogie vehicle. The control scheme used in the simulation include the semi-active control laws, the MR damper and also, the local control of the MR damper. The results of the full active control strategy are also included for comparison. Vehicle responses on both track curves and straight track with irregularities are assessed.

6.2 Track Input

In railway vehicle the dynamic behaviour of vehicle is closely related to the wheel-rail interaction therefore track excitations/geometry has a direct effect on wheelsets response and the performance of the railway vehicle needs to be evaluated through track input.

In the railway industry, railway track input characteristics can be divided to two types:

- Deterministic (low-frequency signals)
- Random track inputs (high-frequency signals).

The deterministic tracks inputs typically consist of curves (R), cant angle (θ) and transition time that a train takes to connect the straight track to a curved/gradient track. Random tracks are track irregularities showing the deflection from intended alignment in lateral and vertical directions. Only lateral irregularities are used in this study as the study is focusing on the stability and guidance control of primary suspensions and only plan-view dynamics are relevant [58, 143].

Low Speed Curve

In this study, both high speed and low speed of the vehicle operations are considered. Figures 6-1 and 6-2 show a curved track with radius of 200 (m) and a cant angle of 6° , and transition

time of 1 (s) , this is used for assessing the curving performance for a low vehicle speed of 72 Kmh^{-1} (or 20m/s).

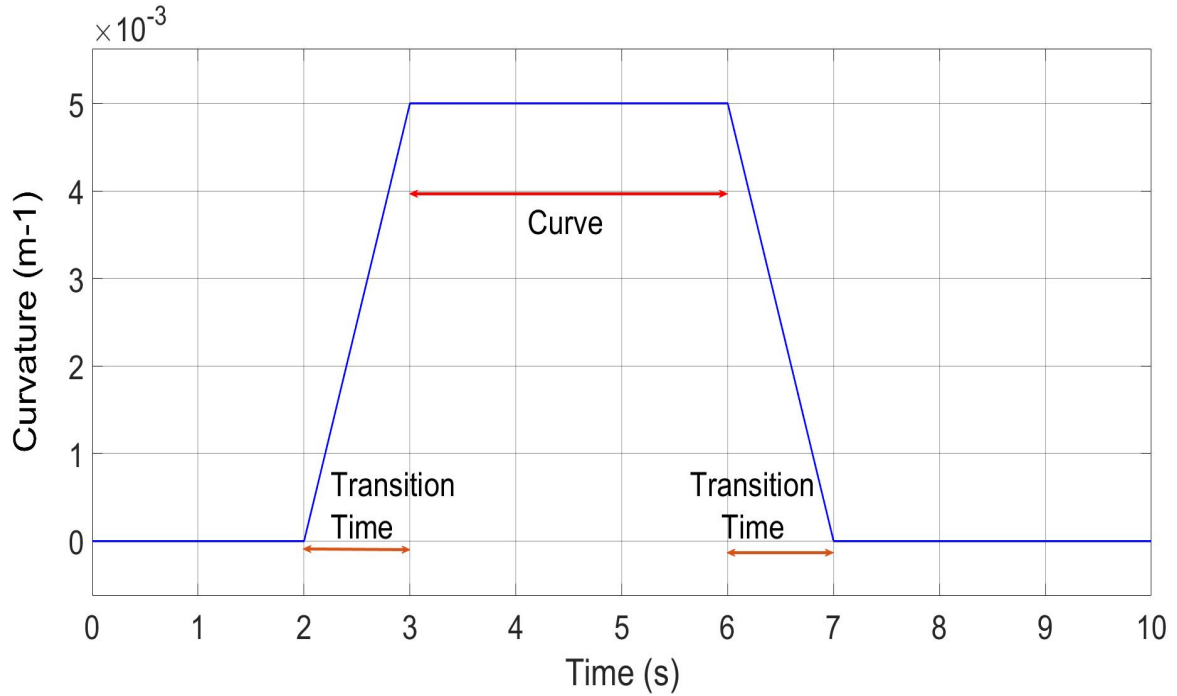


Figure 6-1- Curve track input at 20 (m/s)

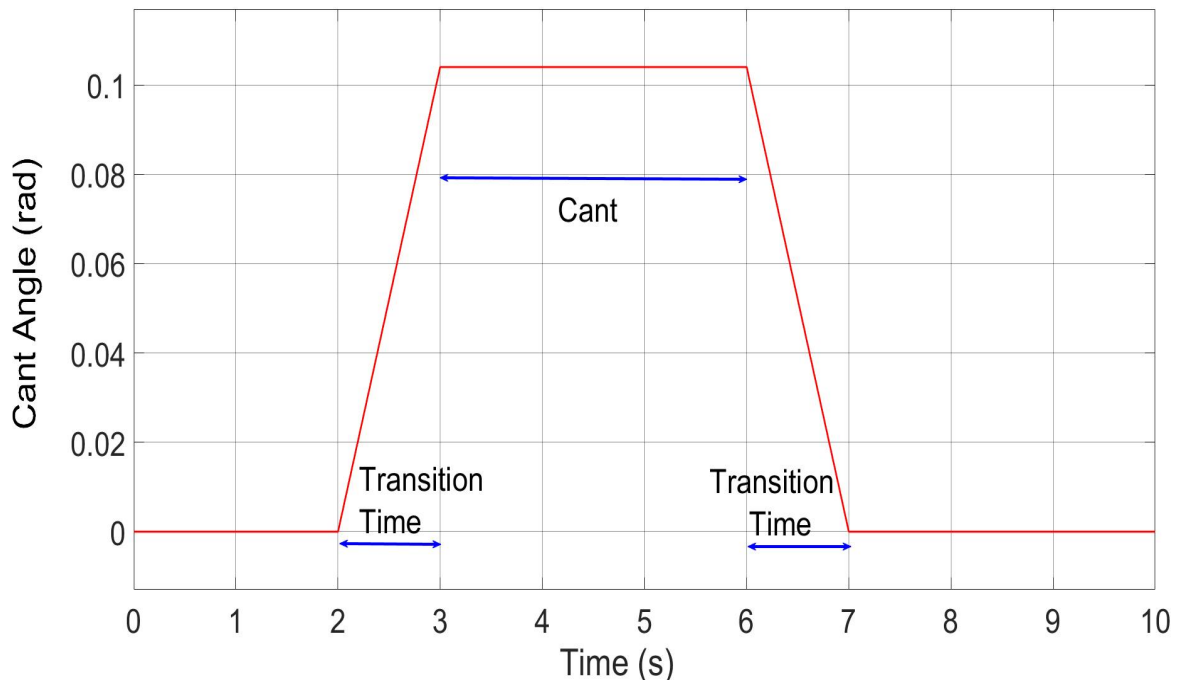


Figure 6-2- Cant Angle Input ($\theta = 6^\circ$)

High Speed Curve

Figures 6-3 and 6-4 show a curved track with radius of 3470 (m) and a cant angle of 6° , and transition time of 1 (s) – this is used for assessing the curving performance for a high vehicle speed of 300 Km h^{-1} (or 83m/s).

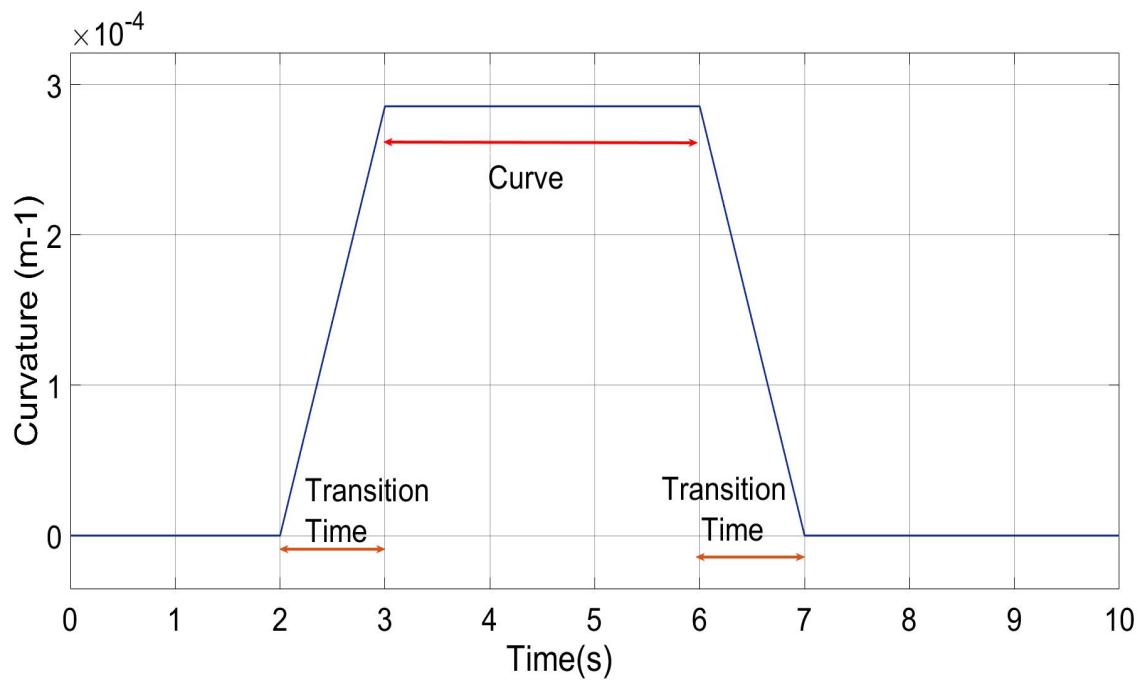


Figure 6-3- Curvature track Input ($R= 3470 \text{ m}$)for 83m/s , 300 Km h^{-1}

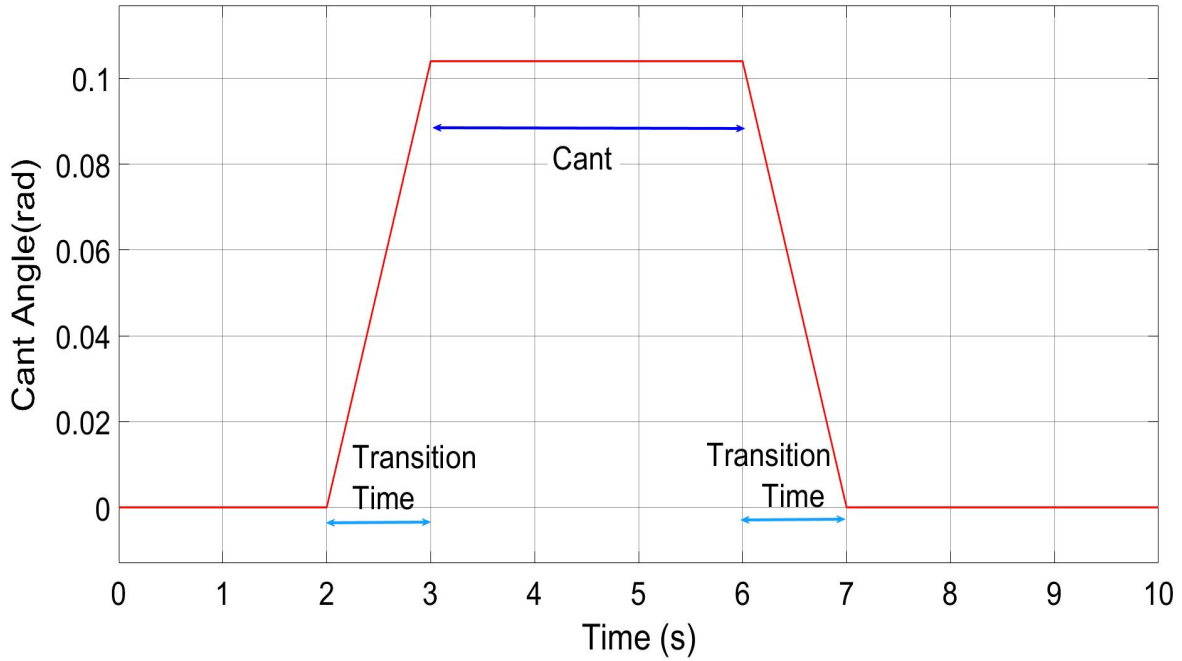


Figure 6-4- Cant Angle Input ($\theta = 6^\circ$)

Track Irregularities – Generic Track Data at The Speed of 83m/s, 300 Km h^{-1}

The lateral track irregularities used in this study represent the track roughness due to engineering imperfection. A set of generic generated lateral irregularity data is generated from filtered white-noise in order to provide a broad frequency spectrum with a relatively high level of irregularities [144] as illustrated in Fig 6-5.

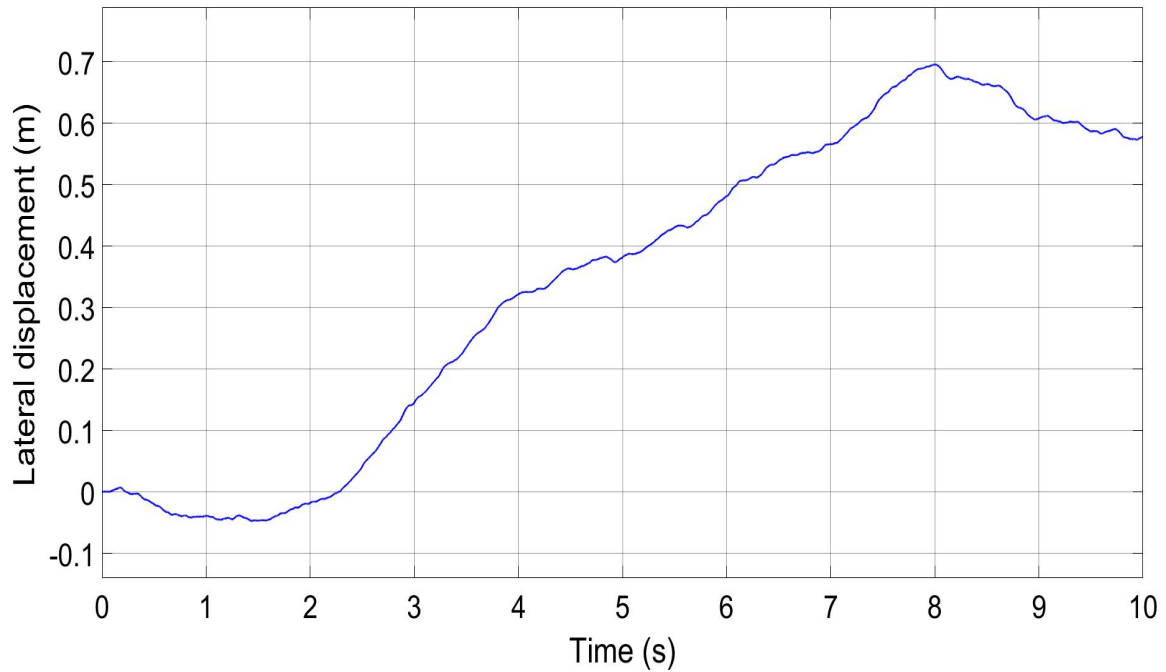


Figure 6-5- Generic track data at the speed of 83m/s, 300 Kmh^{-1}

Track Irregularities – Measured Track Data at The Speed of 50m/S

A set of measured data from a real section of railway track is also used to evaluate the performance of the proposed control scheme. This data is measured from for a UK mainline, with the speed up to 50m/s or 180 km/h. Note that the data as shown in Fig 6-6 does not contain low frequency components as in the case of the generic track data – this is due to the constraint of the measurement vehicles that are not able to measure long wave irregularities.

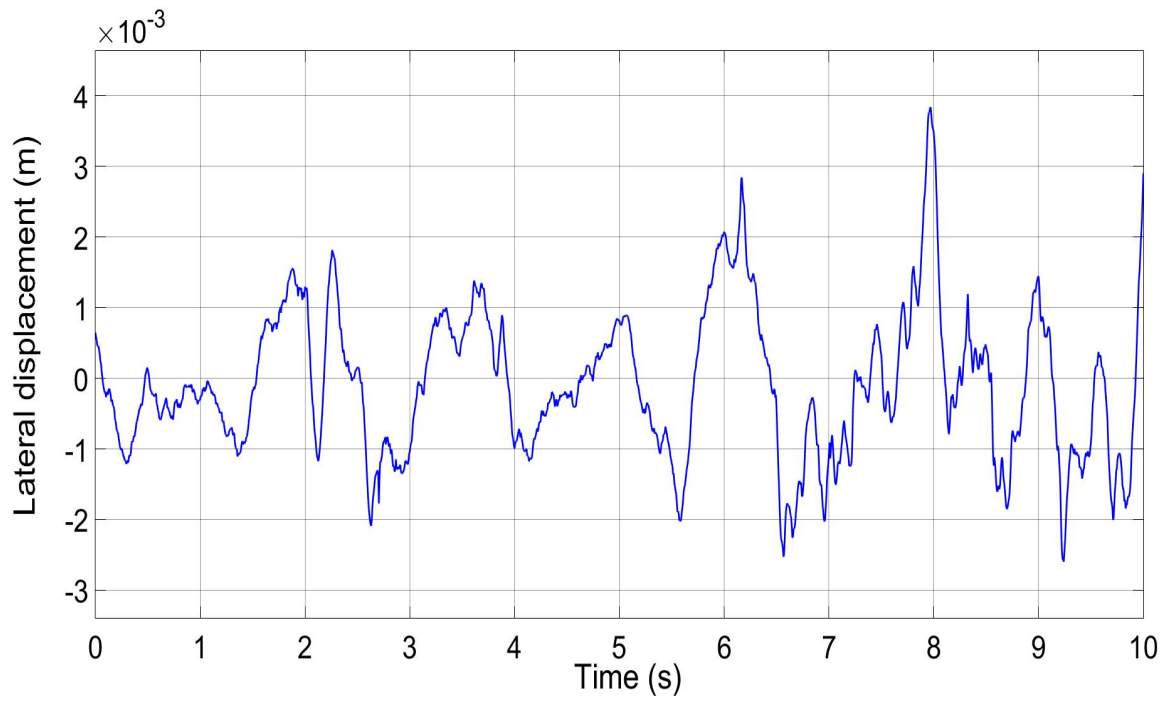


Figure 6-6- Measured Track Data at The Speed of 50m/S

6.3 Two axle Vehicle

6.3.1 In curve track Curve track at the speeds of 83m/s, 300 Km^h⁻¹ and 20 m/s, 72 Km^h⁻¹

This section presents the simulation results of the two-axle vehicle at the vehicle speeds of 83 and 20 m/s on curve tracks. Typical vehicle performances are presented, including angle of attack, lateral deflection, lateral creep force, longitudinal creep force, control force and control power for the front and rear wheelsets.

Figures 6-7 to 6-10 compare the angle of attack (yaw motion) for full active controller and semi-active controller. The semi active controller at 83m/s produces an equal angle of attack between the two wheelsets on the steady curve, to provide the appropriate lateral creep forces for the cant deficiency similar to that of the full active control. The angles of attack for semi active controller at 20m/s also match those of the full active control, with a small but more noticeable deviation. More importantly, however, the same angle of attack for the two wheelsets is formed on the steady curve to provide equal lateral forces that balance the centrifugal force of the vehicle on curves.

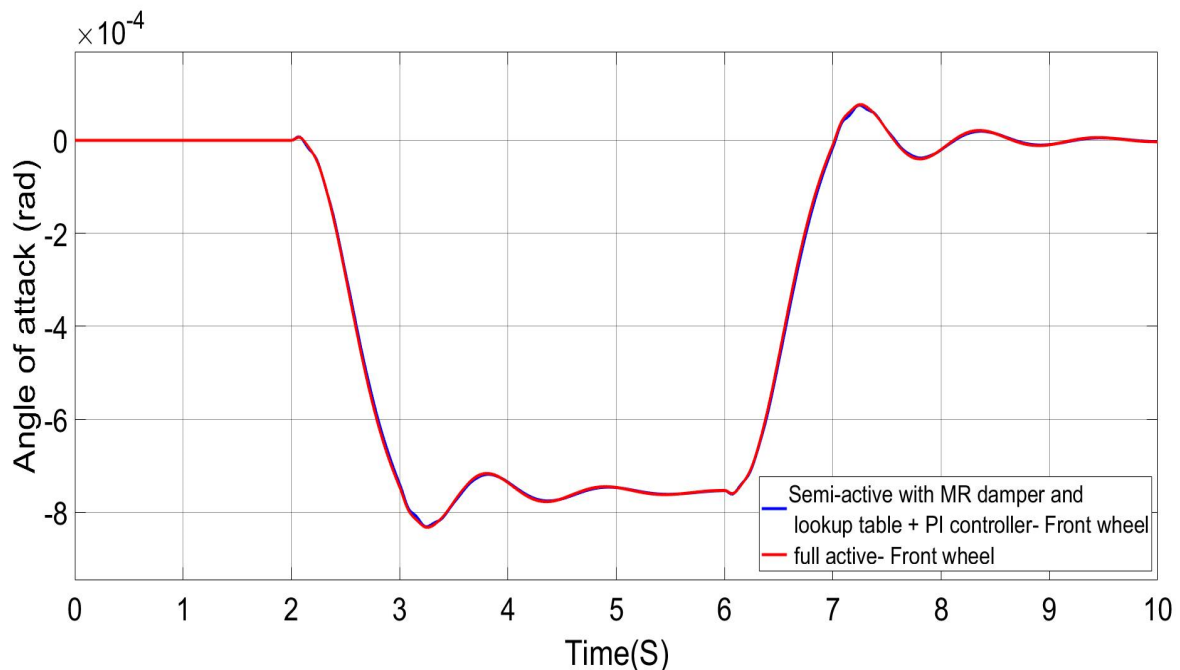


Figure 6-7- Two axle vehicle angle of attack on curve, 83 m/s- Front wheelset

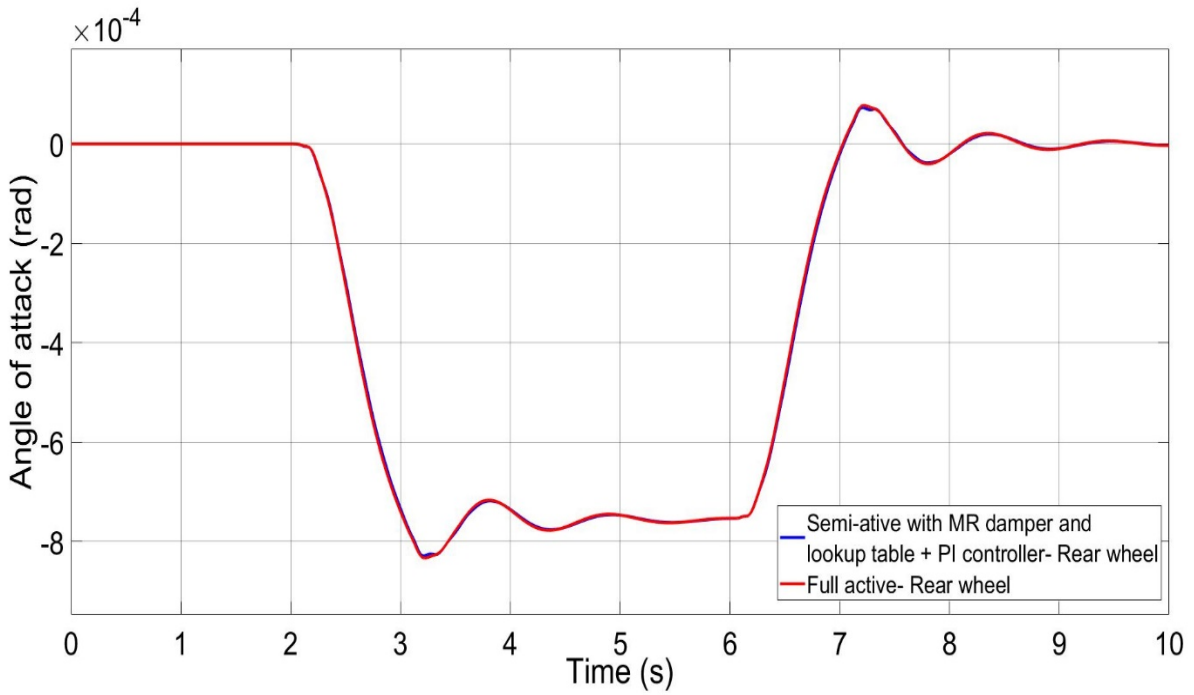


Figure 6-8- Two axle vehicle angle of attack on curve, 83 m/s- Rear wheelset

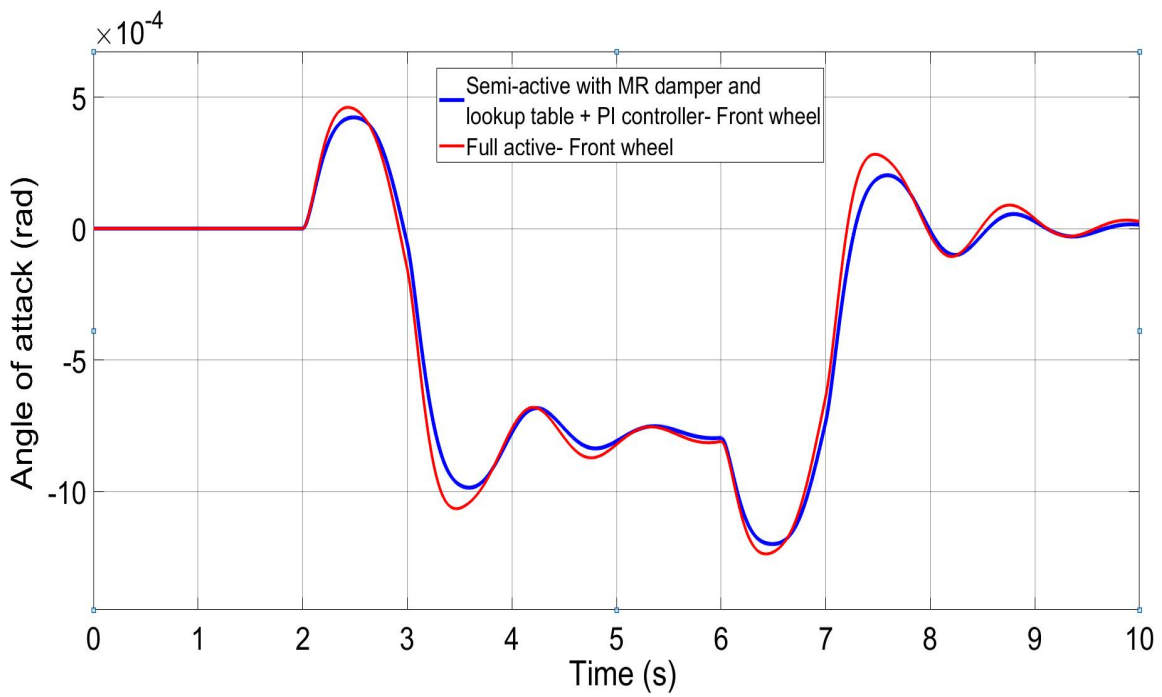


Figure 6-9- Two axle vehicle angle of attack on curve, 20 m/s- Front wheelset

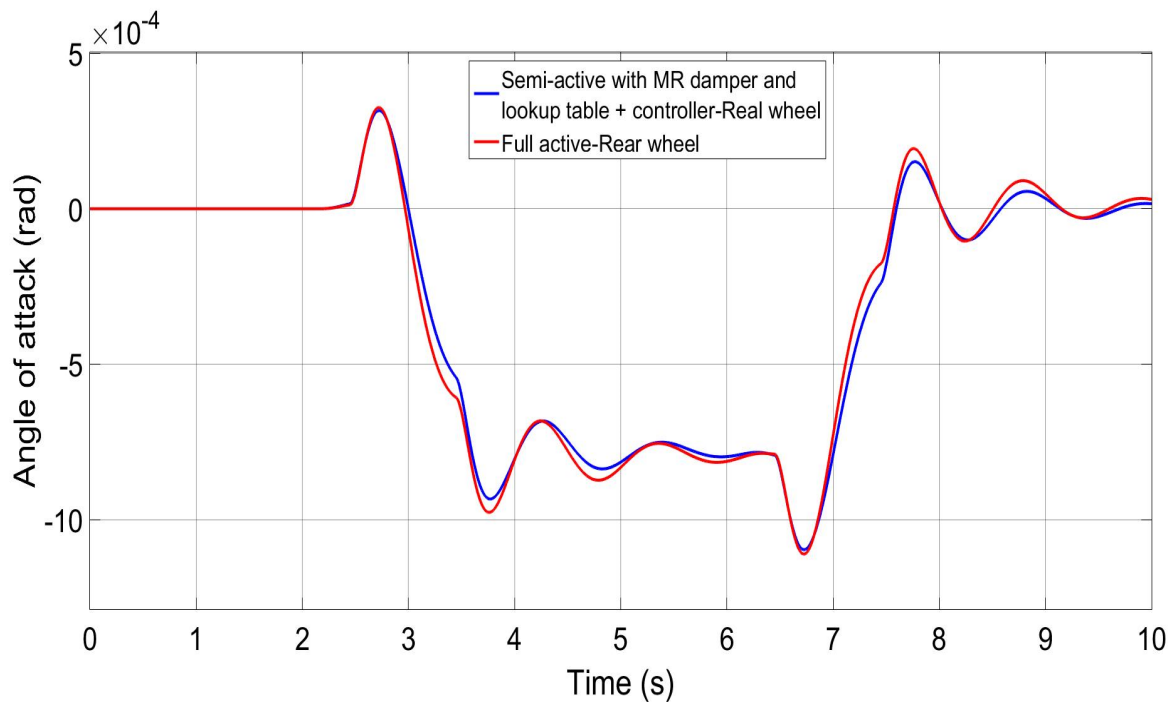


Figure 6-10- Two axle vehicle angle of attack on curve, 20 m/s- Rear wheelset

Figures 6-11 to 6-14 illustrate the lateral displacements between wheelset and track for full active controller and semi-active controller in the front and rear wheelsets.

Figures shows that wheelsets have a displacement when approaching the curve however this lateral displacement is just enough to allow the natural curving on the curve. This occurs due to the independently rotating wheelsets are controlled (by the steering action in the control algorithms) to behave similarly to the solid-axle wheelsets and therefore to restore the curving ability, with the wheelsets moving outwards to have the difference in contact radius.

Achieving a pure rolling action for the independently rotating wheelset is not as crucial as for the solid-axle wheelset, as the two wheels on the same axle can rotate freely and the longitudinal creep force will be much lower. Therefore, it is not an issue of concern that the lateral displacement of the front and rear wheelset at speed of 83m/s is approximately 0.4 mm for the semi active controller and 0.43mm for the active controller - a small difference, but both are small compared to the clearance of the wheel-profiles. On the low speed (of 20m/s) and tighter curve, the lateral displacements for the full active and semi-active controllers are 8 mm and 8.8 mm respectively, still within the flange contact limits.

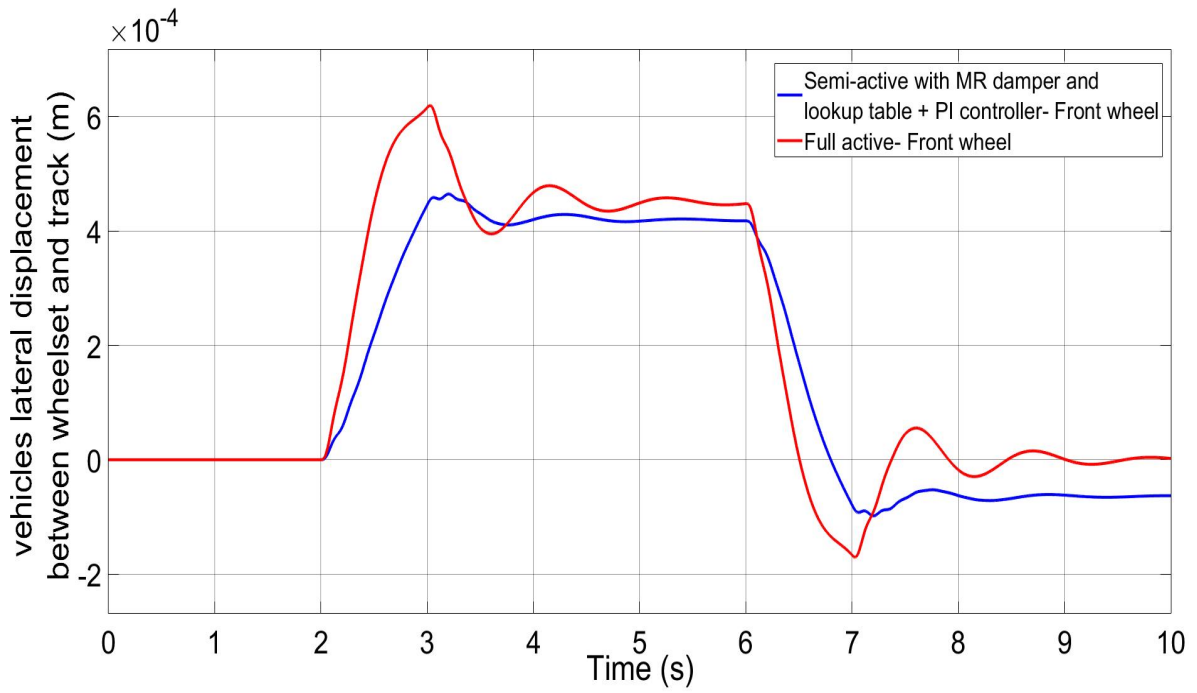


Figure 6-11- Two axle vehicle lateral displacement between wheelset and track on curve, 83 m/s- Front wheelset

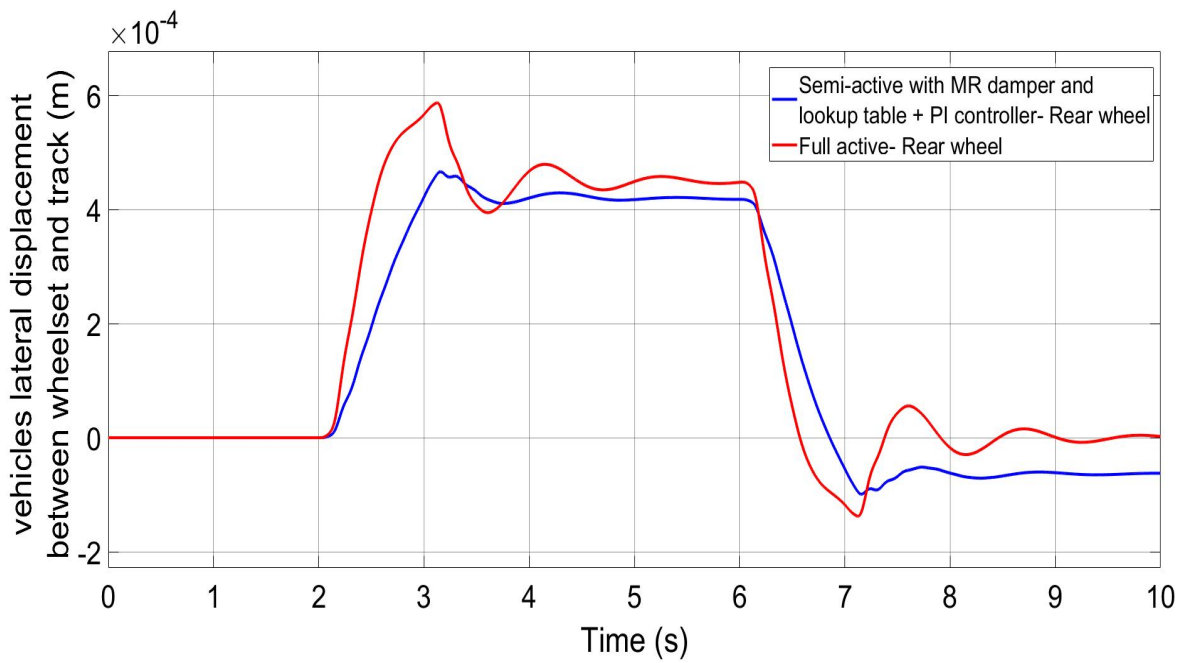


Figure 6-12- Two axle vehicle lateral displacement between wheelset and track on curve, 83 m/s- Rear wheelset

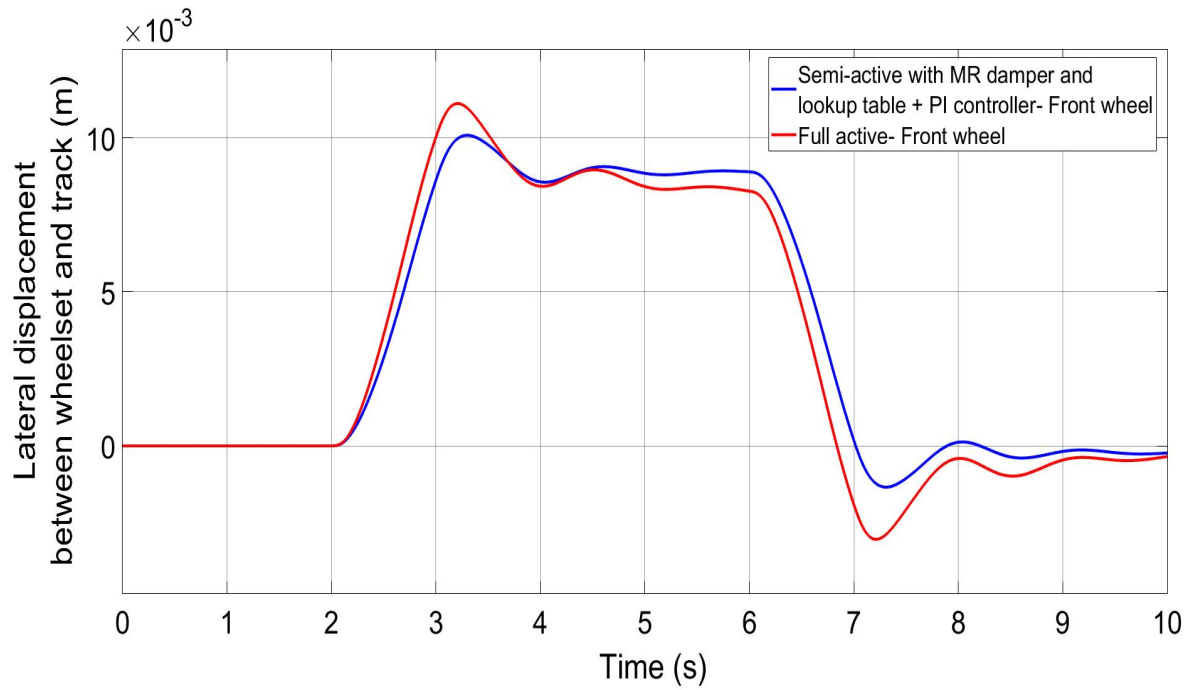


Figure 6-13- Two axle vehicle lateral displacement between wheelset and track on curve, 20 m/s- Front wheelset

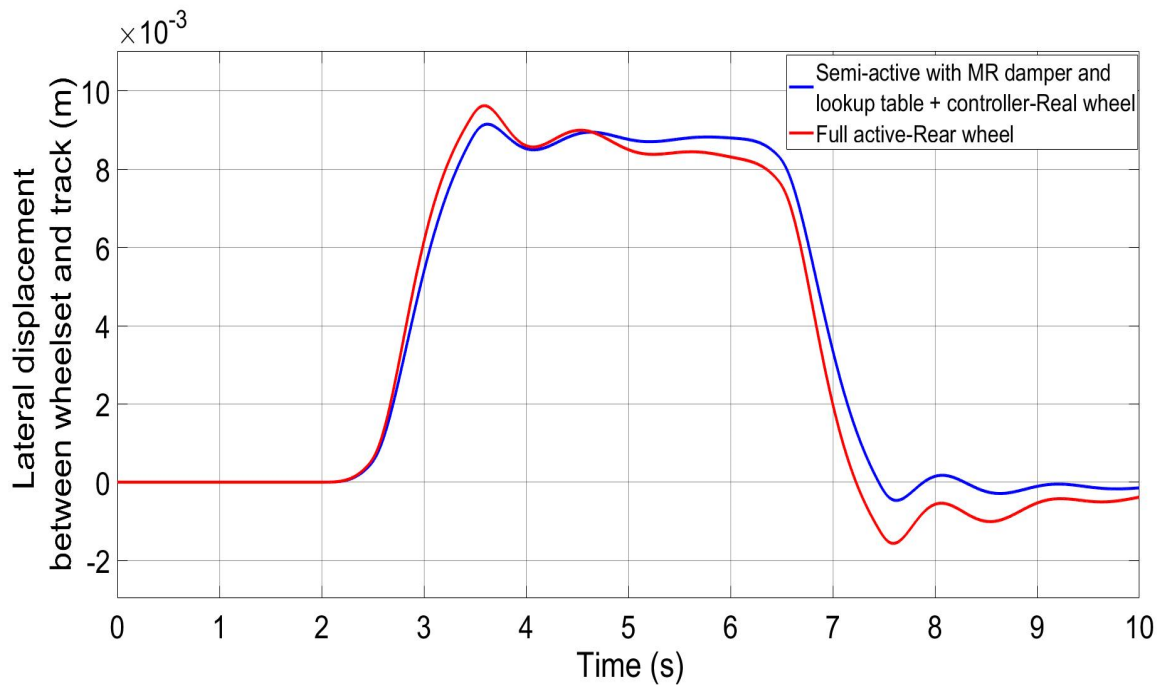


Figure 6-14- Two axle vehicle lateral displacement between wheelset and track on curve, 20 m/s- Rear wheelset

Figures 6-15 to 6-18 demonstrate the lateral creep forces for full active controller and semi-active controller in the front and rear wheelset.

In the lateral direction, some creep forces will be required to provide the necessary curving force to compensate for any cant deficiency. As the result presented, the lateral creep force in full active controller and semi-active controller are similar.

These lateral creep forces occur as a reaction force to the centrifugal force which the vehicle is experiencing during the curved track and the total of lateral creep forces in the wheelsets are equal to the centrifugal force.

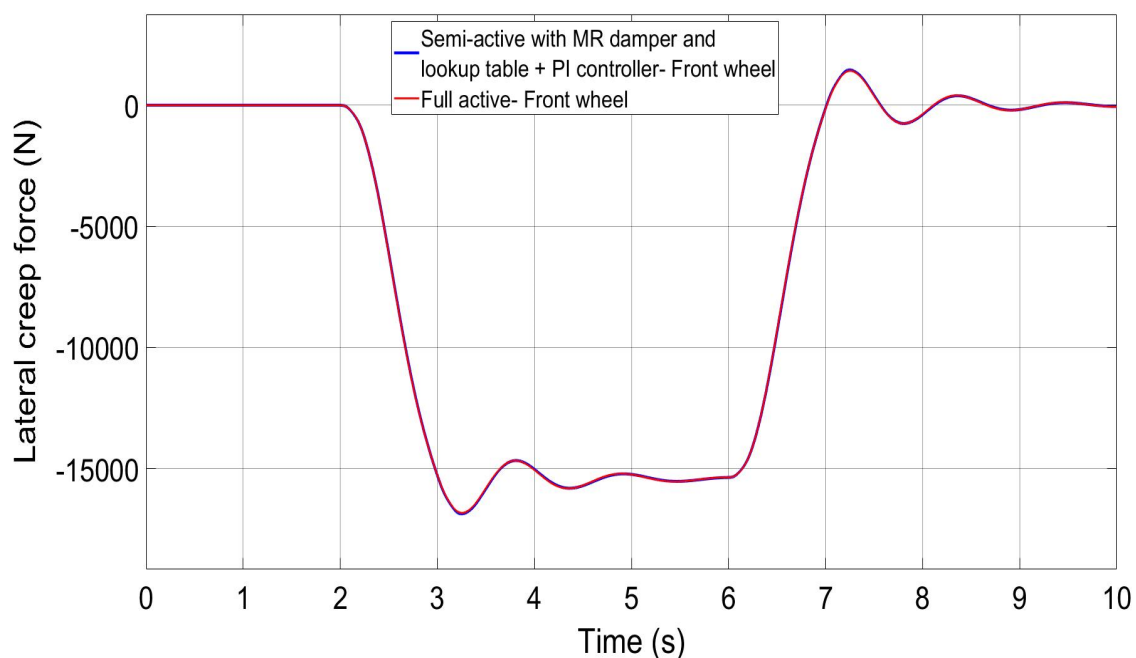


Figure 6-15- Two axle vehicle lateral creep force on curve track, 83 m/s- Front wheelset

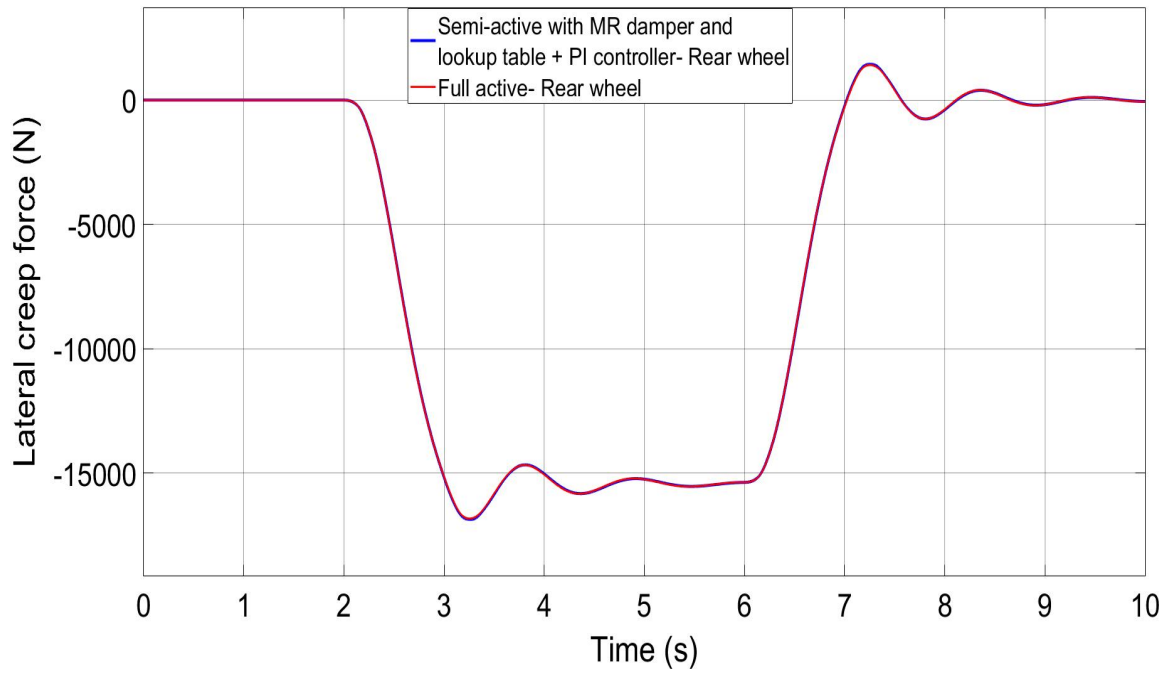


Figure 6-16- Two axle vehicle lateral creep force on curve track, 83 m/s- Rear wheelset

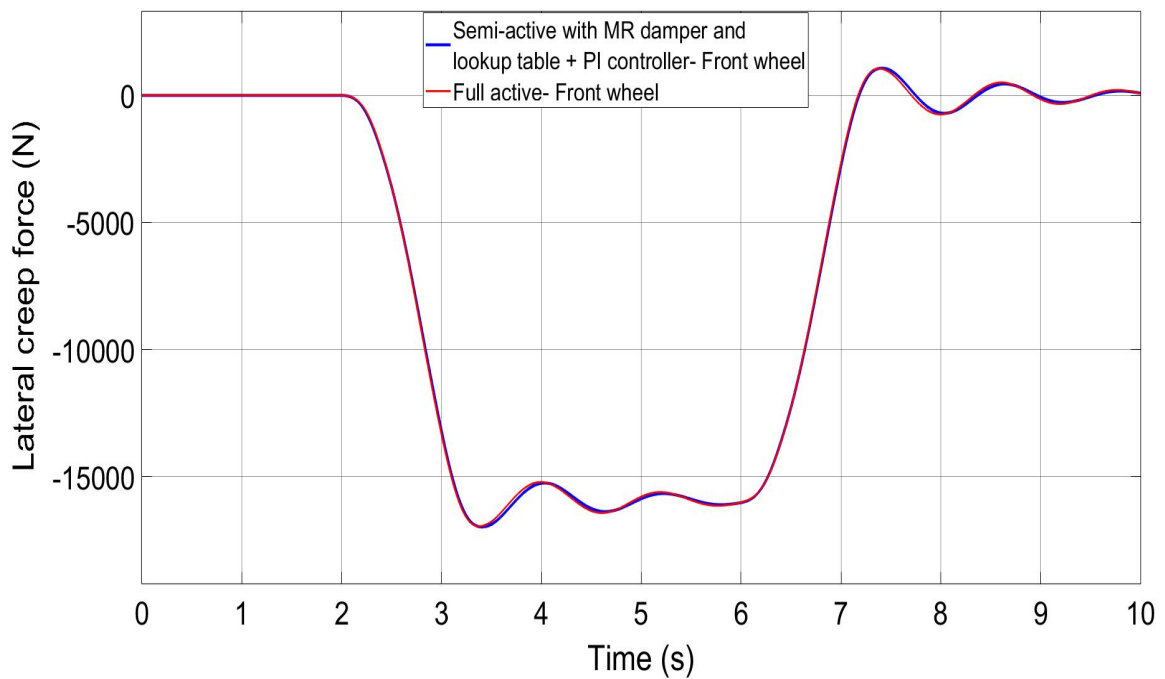


Figure 6-17- Two axle vehicle lateral creep force on curve track, 20 m/s- Front wheelset

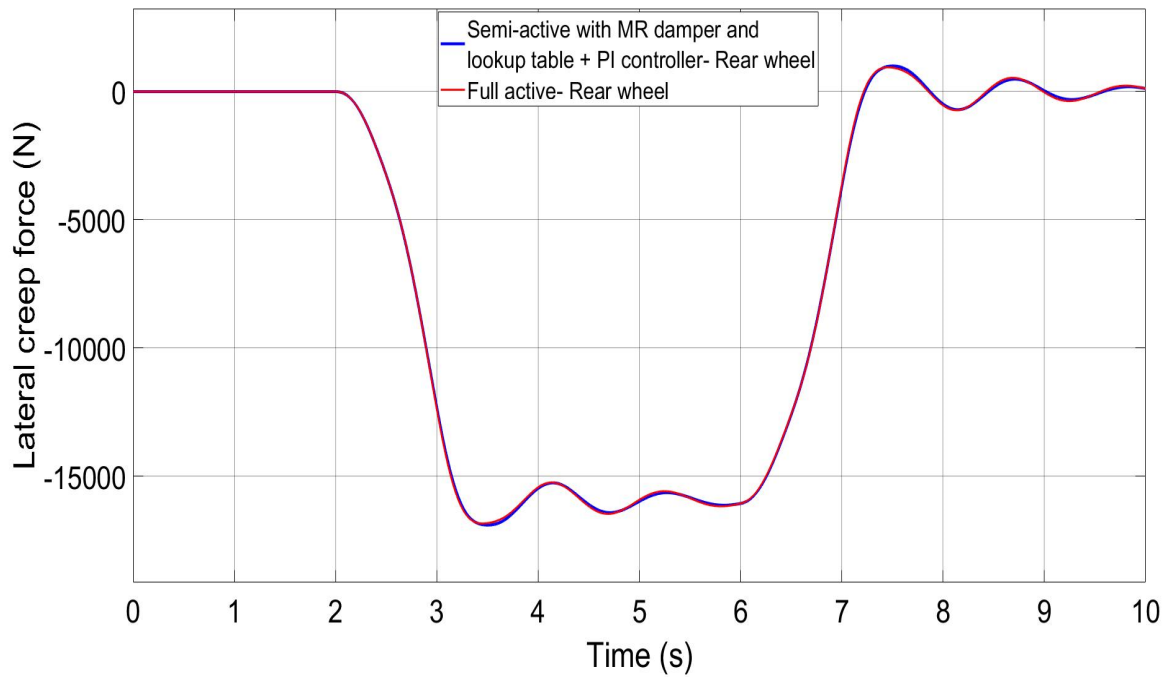


Figure 6-18- Two axle vehicle lateral creep force on curve track, 20 m/s- Rear wheelset

Figures 6-19 and 6-20 confirm that the lateral creep forces are balancing total centrifugal forces due to cant-deficiency at speed of 83 m/s and 20 m/s for front wheelset.

At the speeds of 83m/s and 20 m/s, the centrifugal forces are 15420 N and 15940 N respectively, which are closely matched the lateral creep forces in both full active and semi control cases.

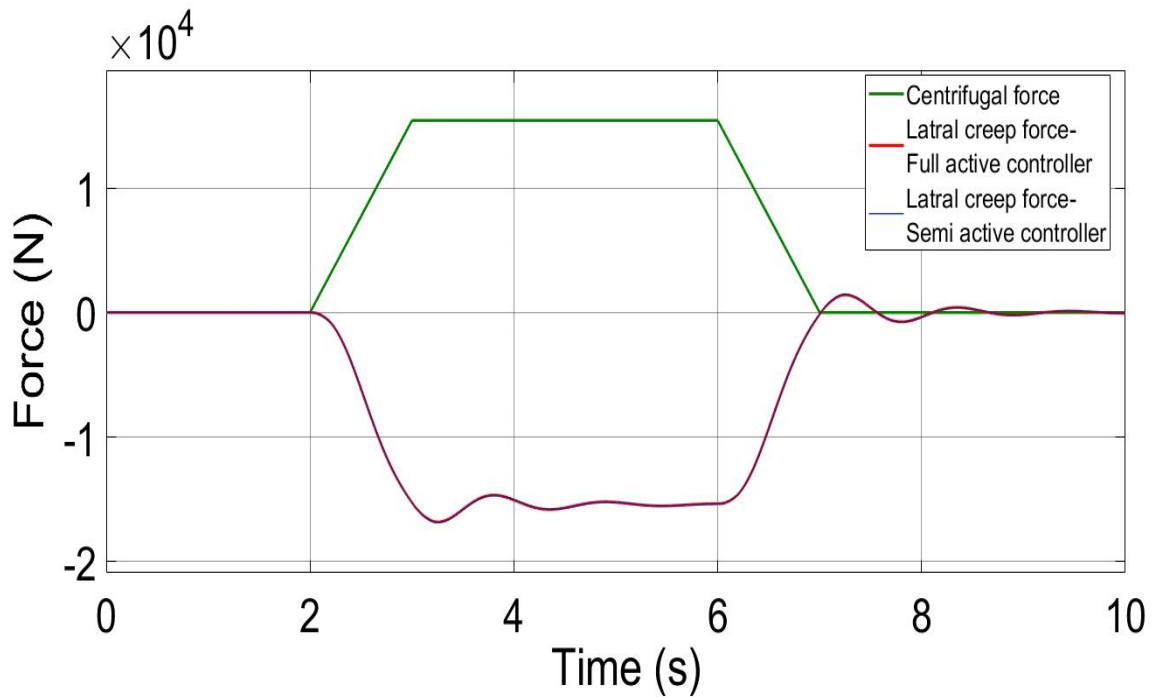


Figure 6-19- Comparison of lateral creep force and centrifugal force on curve track, 83 m/s- Front wheelset

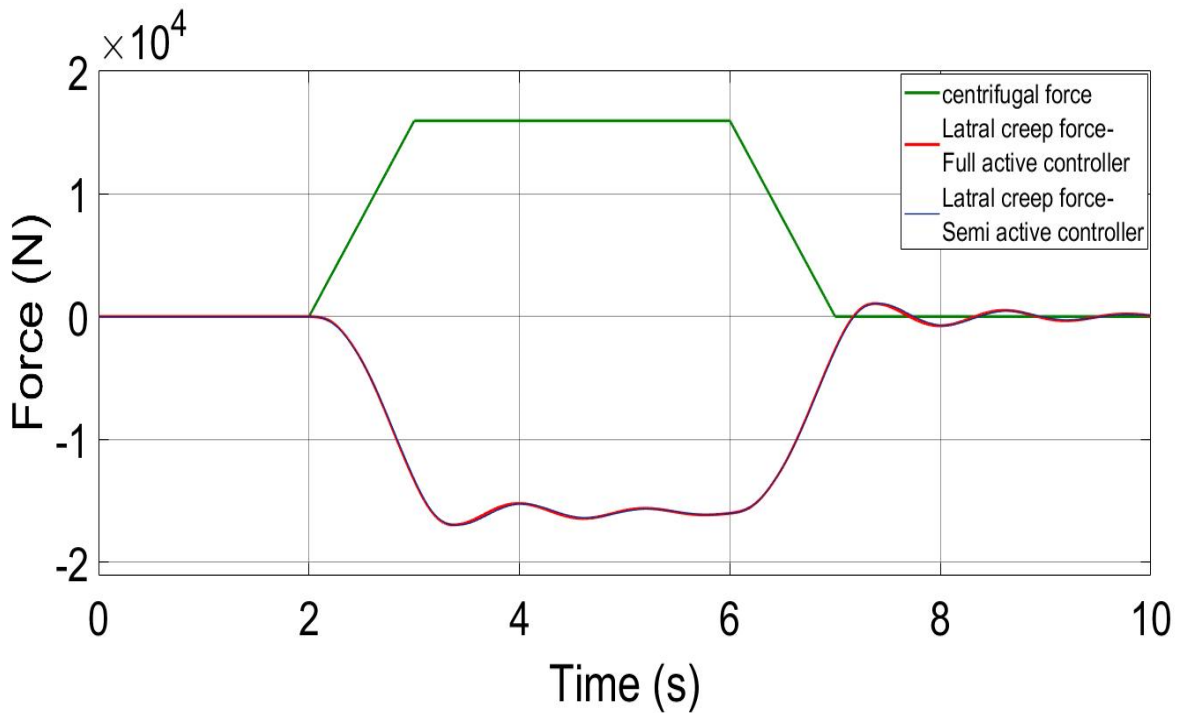


Figure 6-20- Comparison of lateral creep force and centrifugal force on curve track, 20 m/s- Front wheelset

Figures 6-21 to 6-24 show the longitudinal creep forces for full active controller and semi-active controller in the front and rear wheelset.

Due to the free rotation of the two wheels of the independently rotating wheelsets, the longitudinal creep forces are very low, where the longitudinal contact forces on a steady curve are nearly zero. However, the simulation analysis shows that there is some difference of longitudinal creep force between the full active and semi active controller, which are likely caused by the dynamics and non-linearity of the MR dampers used in the semi-active control scheme.

The maximum and minimum longitudinal creep forces in the front wheelset for full active controller are 11.12 N, -11.24 N and 14.52 N and -9.4 N for semi active controller at speed of 83 m/s. Also, the biggest difference between longitudinal with different controller in the front wheelset is 10.4 N at 6.824 second when the longitudinal force for semi active controller is 5.9 N and longitudinal force for active controller is -4.5 N.

At the speed of 20 m/s, the maximum and minimum longitudinal creep forces in the front wheelset for the full active controller are 32.43 N, -31.64 N and 41.68 N and -40.74 N for semi active controller. Furthermore, the largest difference between longitudinal with different controller in the front wheelset is 9 N at 7.029 second when longitudinal force for semi active controller is 41.43 N and longitudinal force for active controller is 32.43 N.

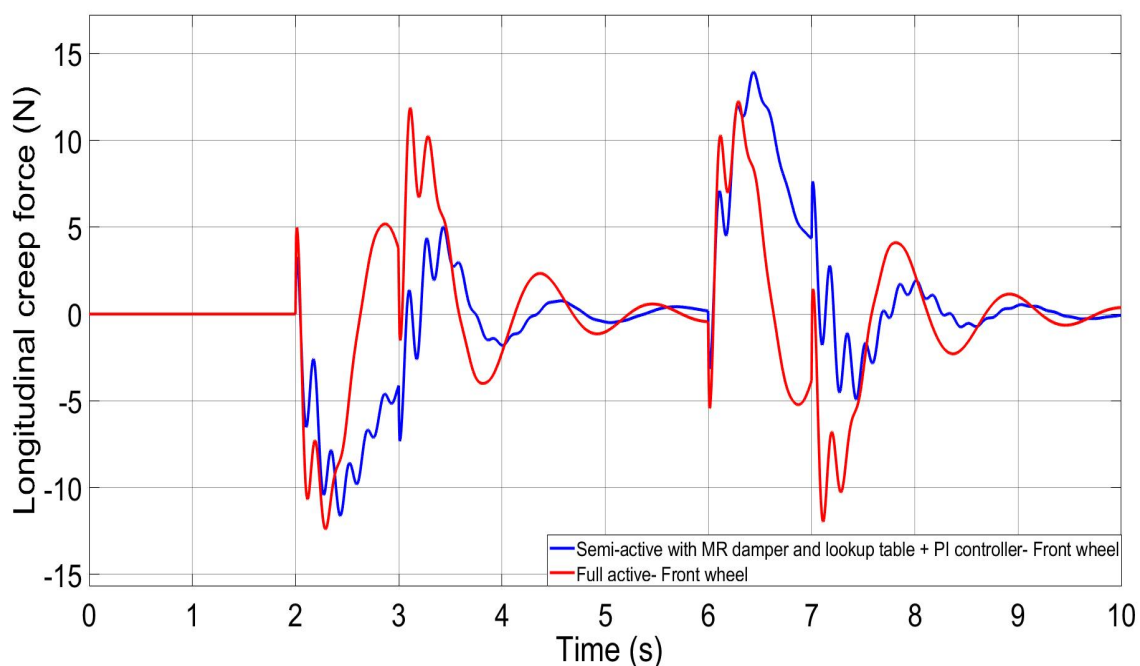


Figure 6-21- Two axle vehicle longitudinal creep force on curve track, 83 m/s- Front wheelset

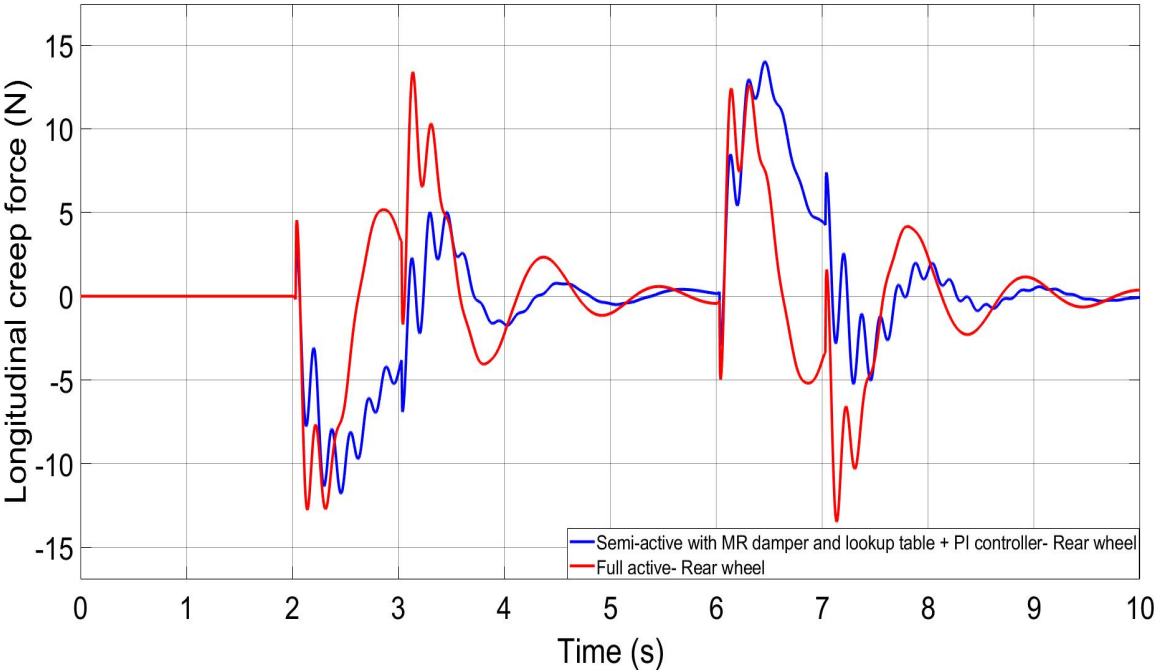


Figure 6-22- Two axle vehicle longitudinal creep force on curve track, 83 m/s- Rear wheelset

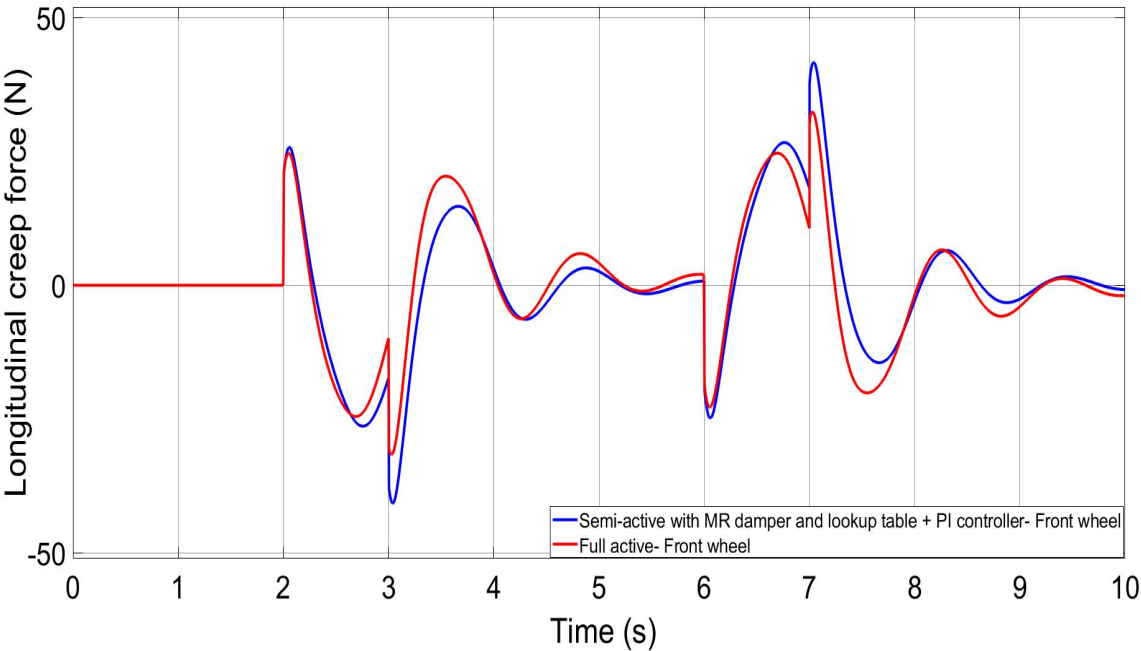


Figure 6-23- Two axle vehicle longitudinal creep force on curve track, 20 m/s- Front wheelset

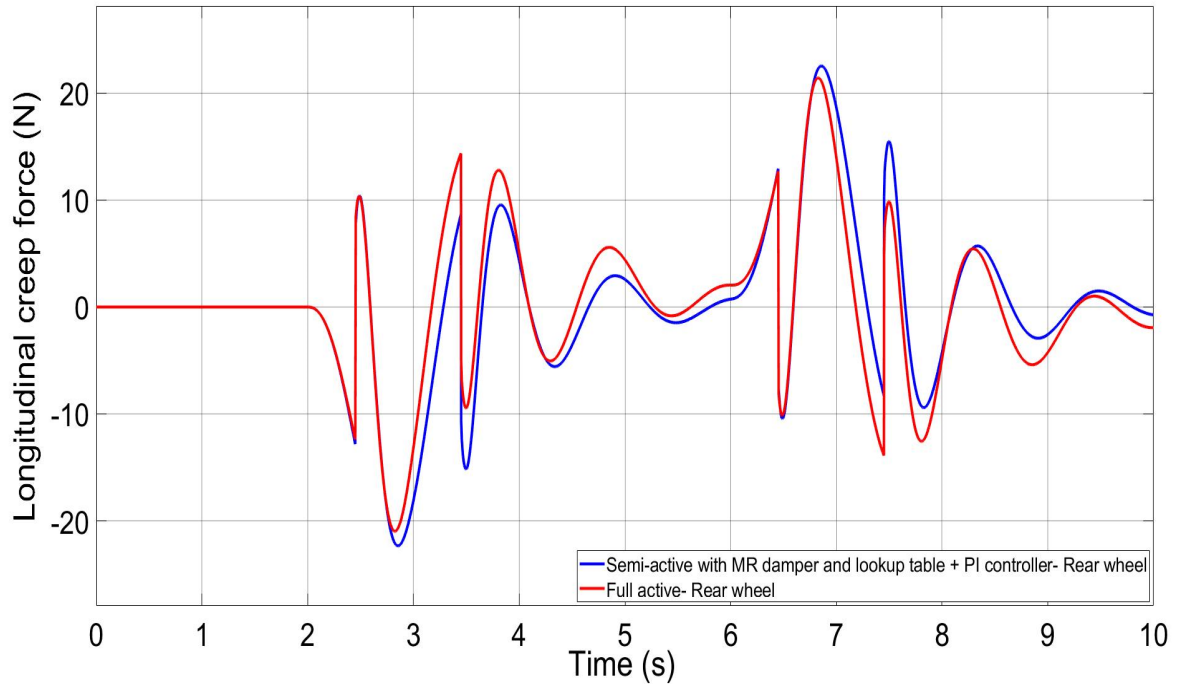


Figure 6-24- Two axle vehicle longitudinal creep force on curve track, 20 m/s- Rear wheelset

Figures 6-25 to 6-28 show the control effort generated by full active controller and semi-active controller in the front and rear wheelset.

The longitudinal creep forces (as shown in figure 6-21 to 6-24) need to be balanced by control effort in the actuators (for the full active control) or the MR dampers (for the semi-active control). It can be seen from Figure 6-25 to 6-28 that controller forces in both semi active controller and the full active controller cases follow the pattern of the longitudinal creep forces.

The maximum and minimum control forces generated in the front wheelset for full active controller are 9.572 N, -9.465 N and 9.526 N and -12 N for semi active controller at speed of 83 m/s. At speed of 20 m/s, the maximum and minimum longitudinal creep forces in the front wheelset for the full active controller are 25.6 N, -26.33 N and 31.47 N and -32.32 N for semi active controller.

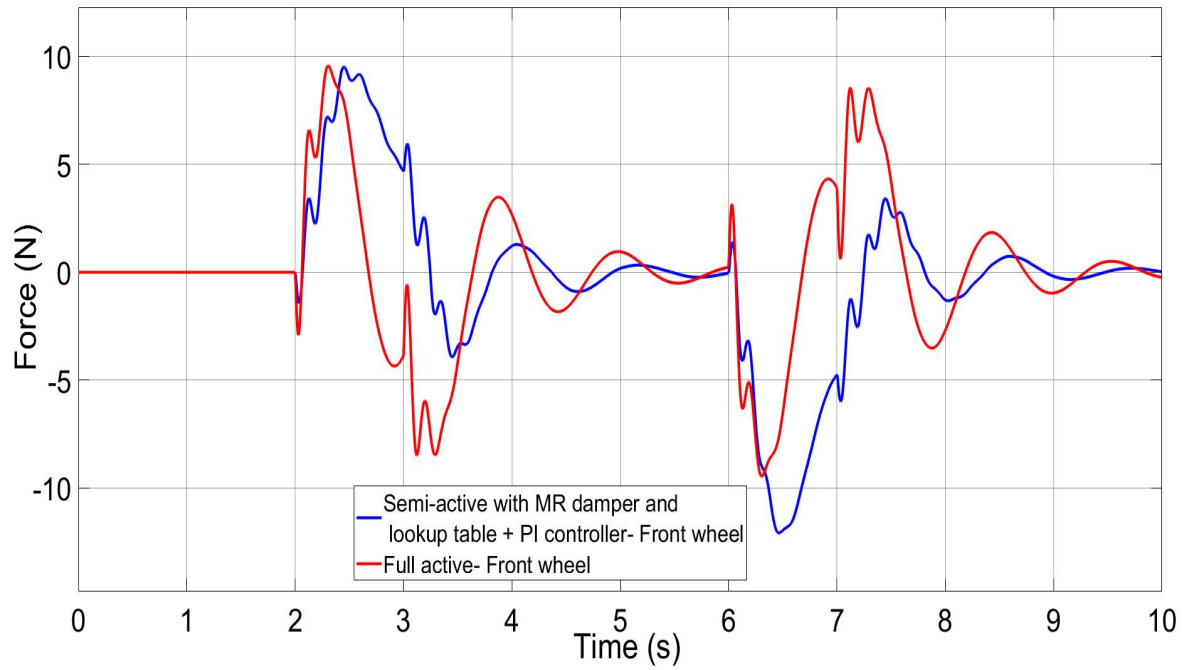


Figure 6-25- Two axle vehicle control force on curved track, speed 83.3 m/s- Front wheelset

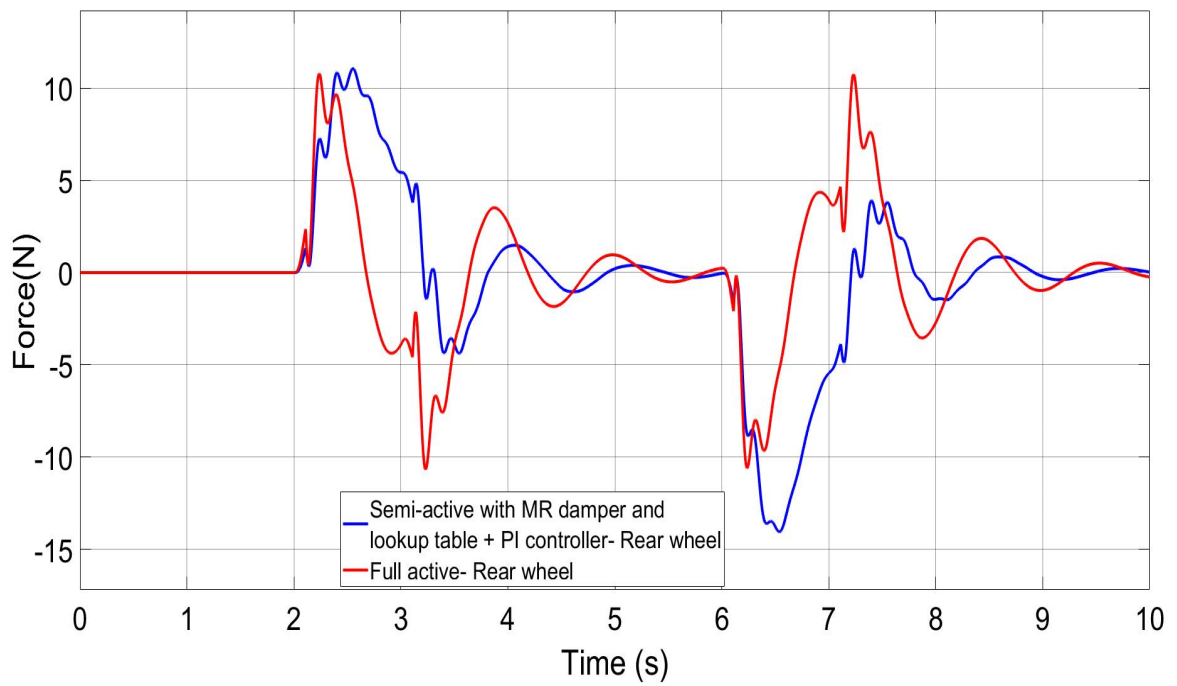


Figure 6-26- Two axle vehicle control force on curved track, speed 83.3 m/s- Rear wheelset

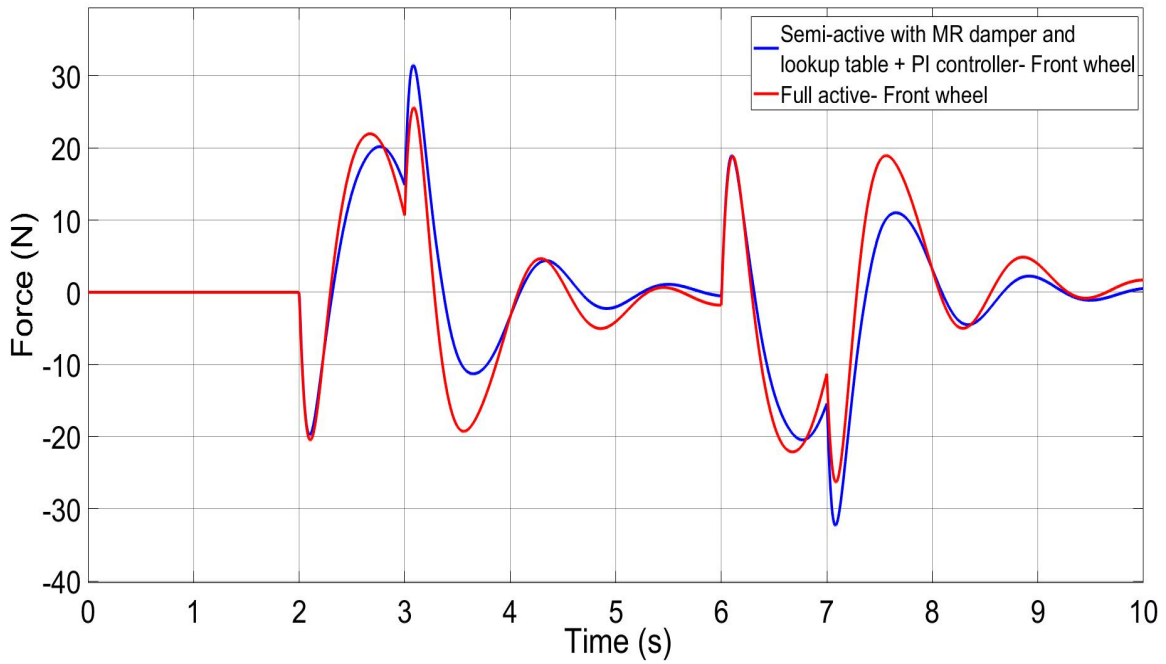


Figure 6-27- Two axle vehicle control force on curved track, speed 20 m/s- Front wheelset

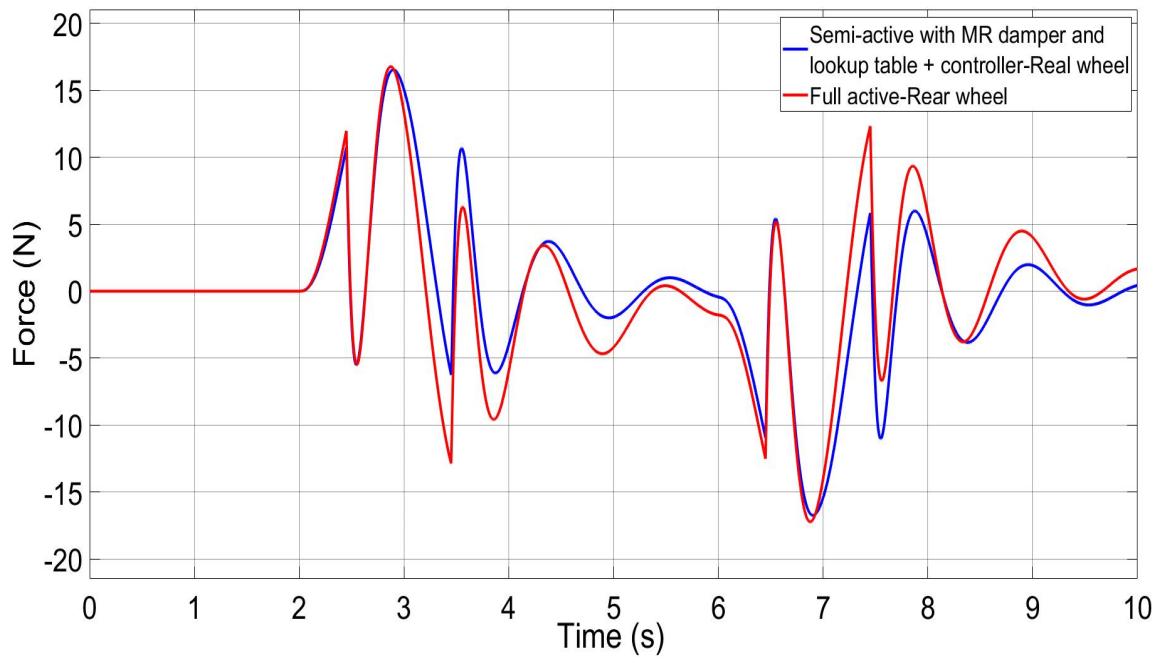


Figure 6-28- Two axle vehicle control force on curved track, speed 20 m/s- Rear wheelset

Figures 6-29 to 6-32 shows the control power generated by full active controller and semi-active controller in the front and rear wheelset.

As shown in figures, the control power is reduced to almost zero when the vehicle is travelling on the steady curved of the track. Also, it is clear both controllers only dissipate the energy from the wheelset and there is no requirement to provide any additional energy.

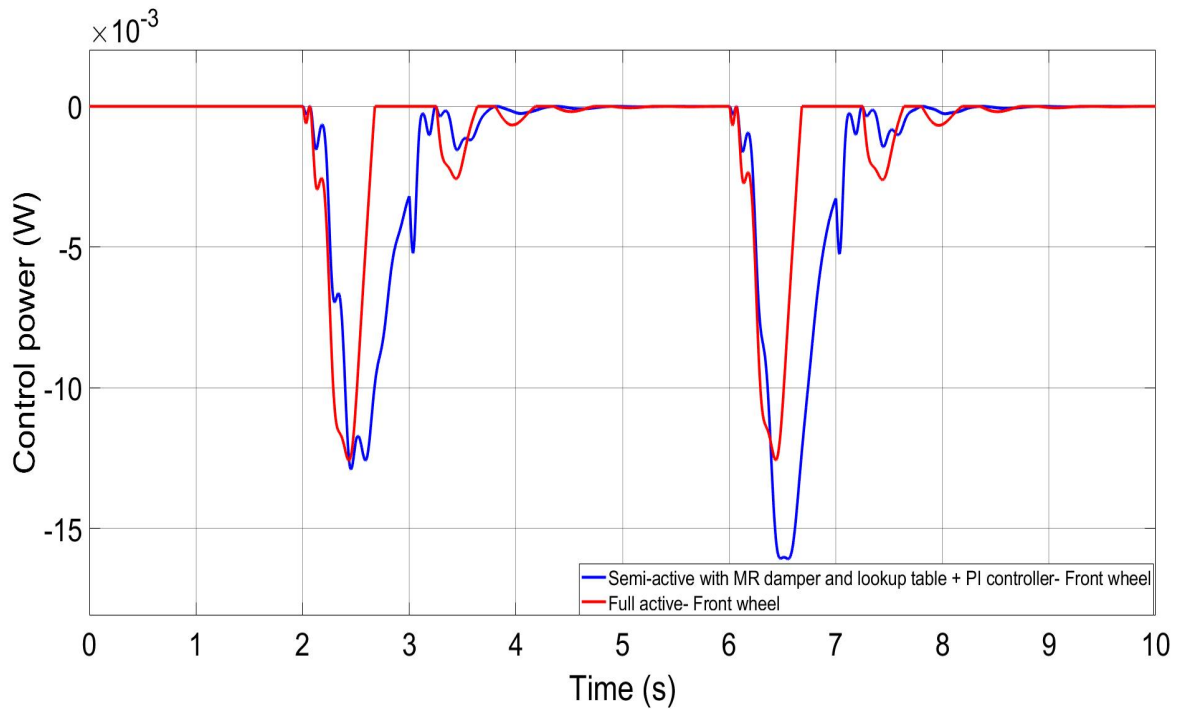


Figure 6-29- Two axle vehicle control power on curved track, speed 83.3 m/s- Front wheelset

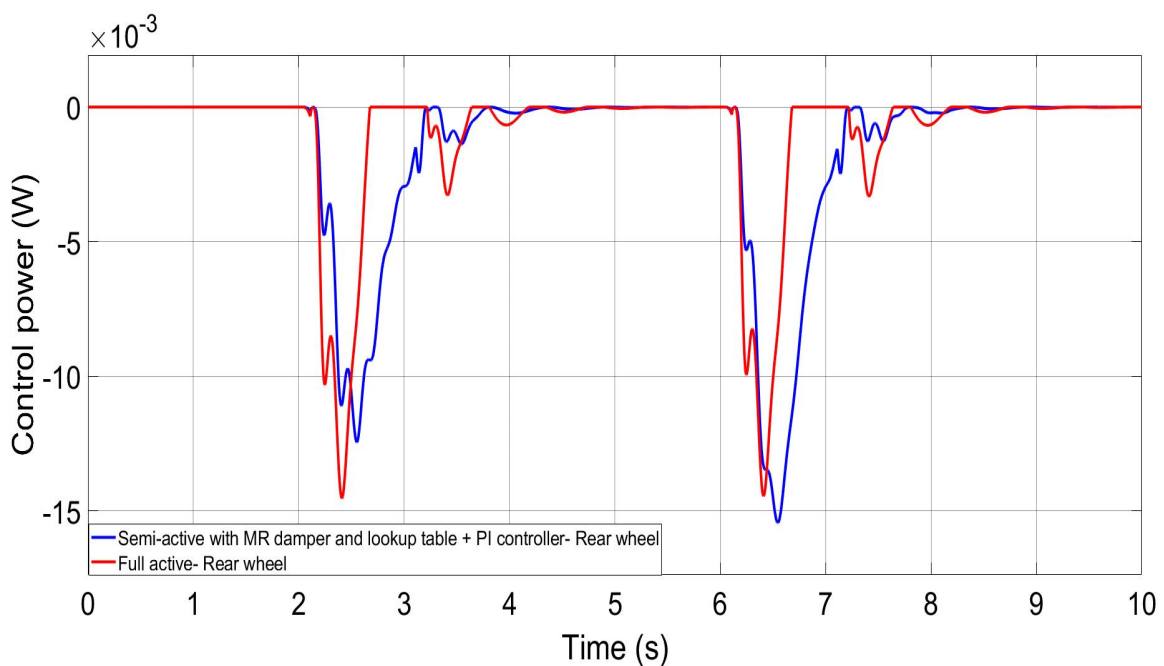


Figure 6-30- Two axle vehicle control power on curved track, speed 83.3 m/s- Rear wheelset

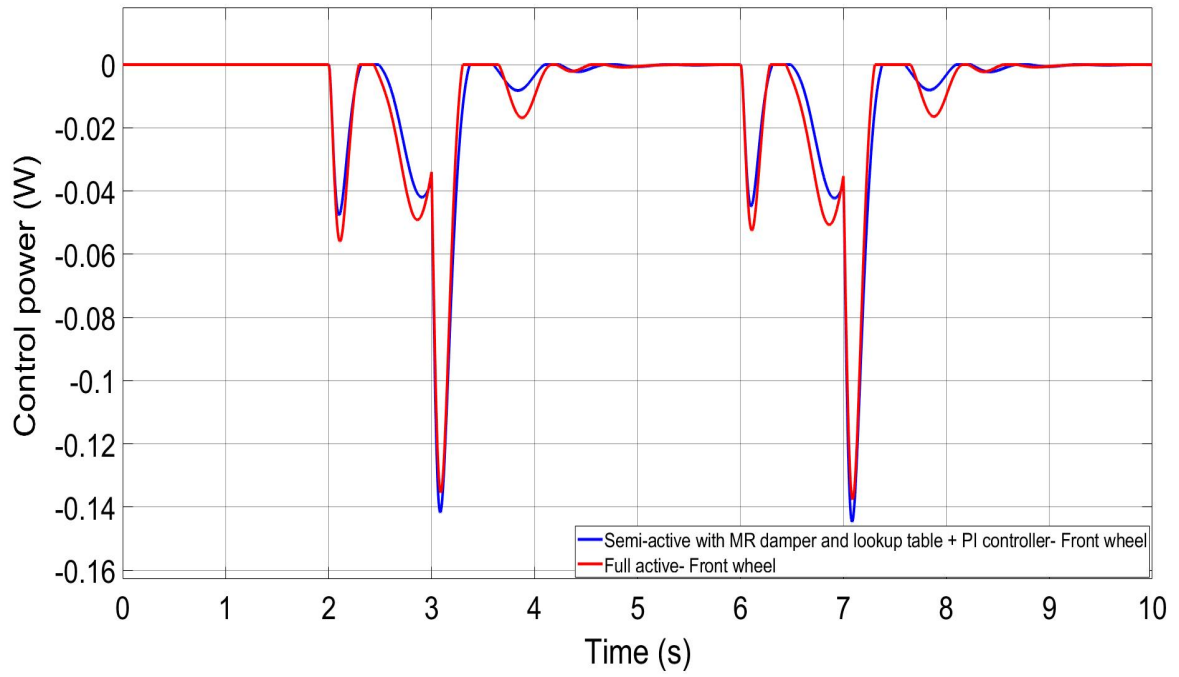


Figure 6-31- Two axle vehicle control power on curved track, speed 20 m/s- Front wheelset

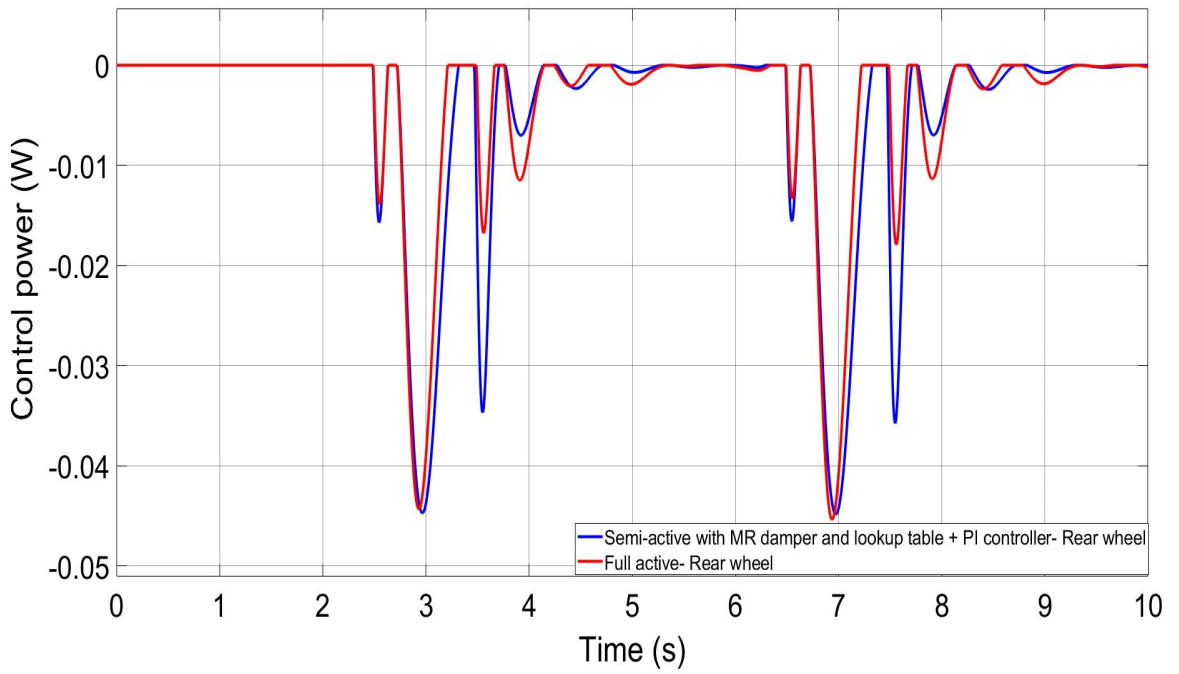


Figure 6-32- Two axle vehicle control power on curved track, speed 20 m/s- Rear wheelset

6.3.2 Straight Track with Track Irregularities (Generic Track Data Irregularity at The Speed of 83m/s, 300 Km^h⁻¹)

This section presents the simulation results of the two-axle vehicle at the speed of 83 m/s using generic random track input. Again, the angle of attack, lateral deflection, lateral creep force, longitudinal creep force, control force, control power and torque for the front and rear wheelsets are assessed.

Figures 6-33 and 6-34 show the angle of attack for active controller and semi-active controller in the front and rear wheelset. As the figures show, the angle of attack for semi-active controller is very similar to the result of full active controller with the time delay between wheelsets. It is worth to mention that the angle of attack is caused by the dynamic response of the wheelset to track input/geometry changes, especially at high frequencies.

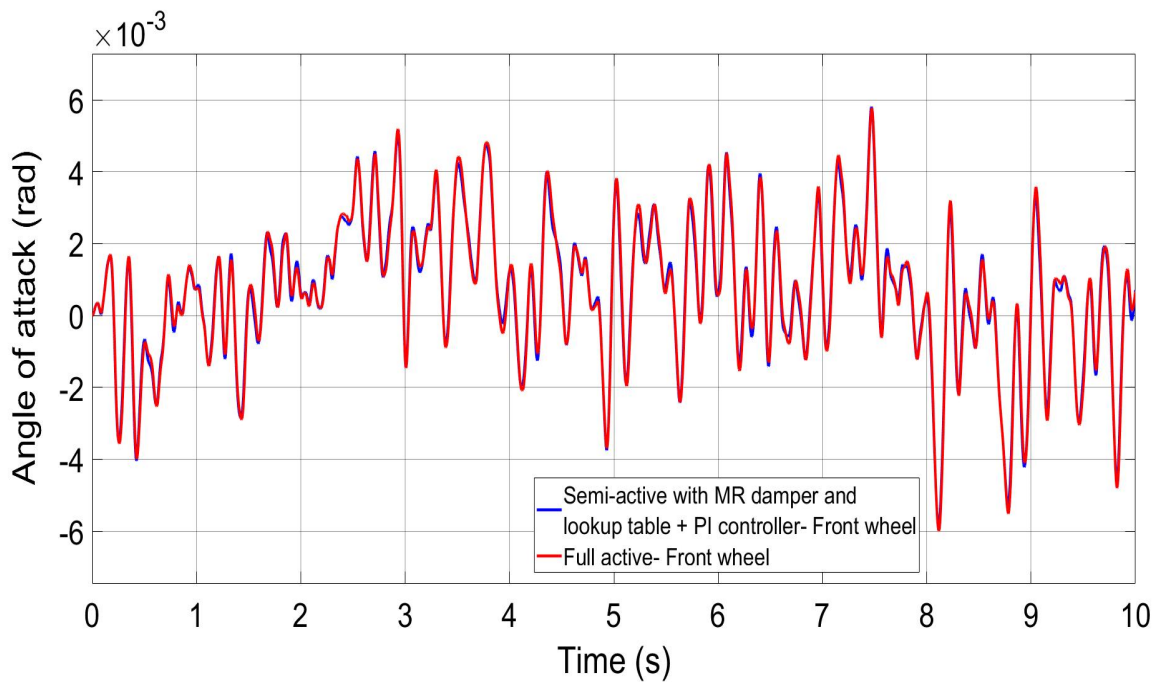


Figure 6-33- Two axle vehicle angle of attack on computer generic track, 83 m/s- Front wheelset

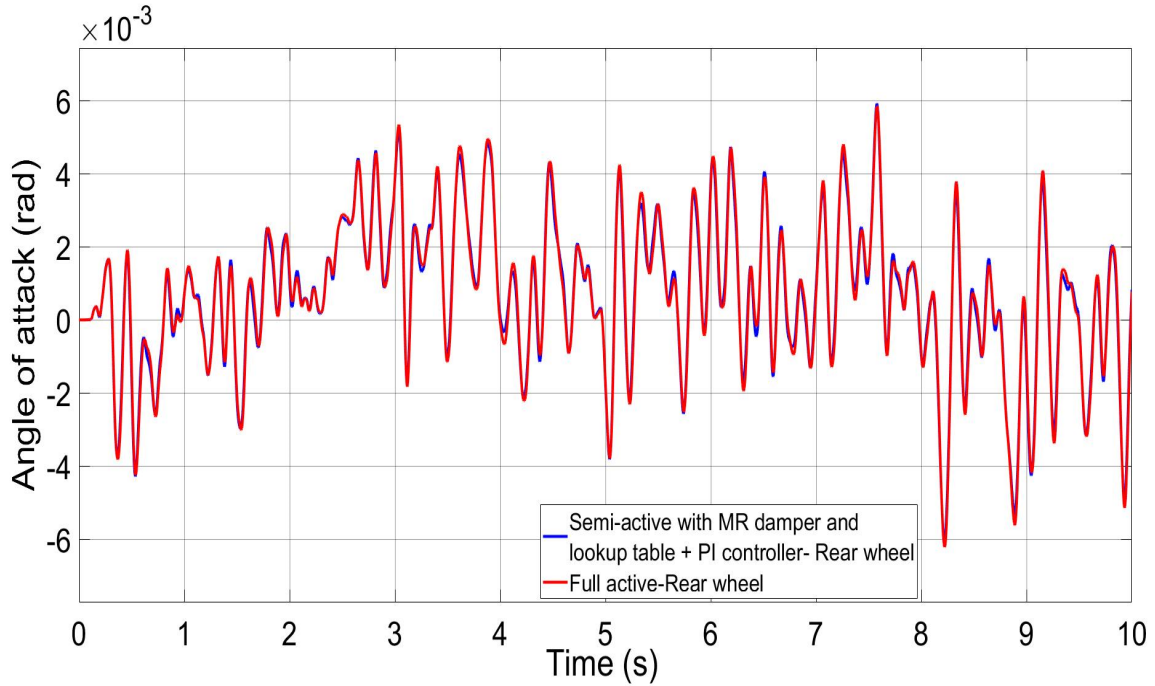


Figure 6-34- Two axle vehicle angle of attack on computer generic track, 83 m/s -Rear wheelset

Figures 6-35 and 6-36 show the lateral deflection for the active controller and semi-active controller in the front and rear wheelset. As the results show, the semi active controller lateral displacement is very close to the result of full active controller with delay between the wheelset with the peak less than 10mm. Therefore, it shows that wheelsets are not running on the flanges, as wheelsets typically have a typical range of +/-10mm before the undesirable flange contact occurs. The lateral displacement is also caused by the dynamic response of the wheelset to track geometry changes, especially at high frequencies.

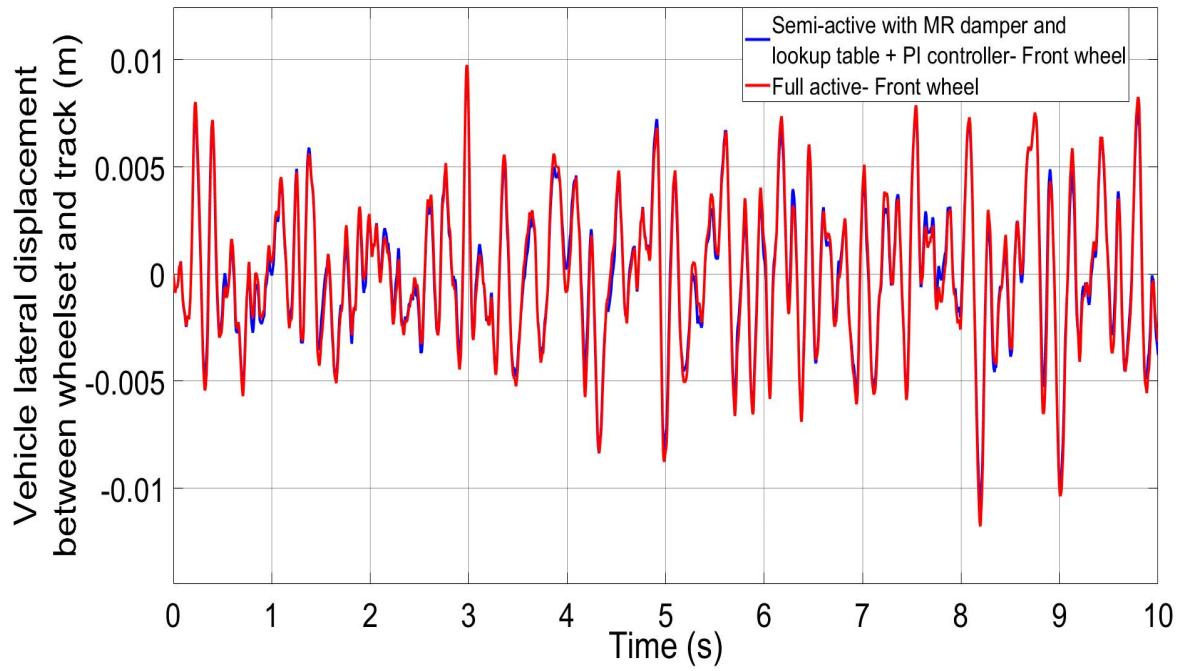


Figure 6-35- Two axle vehicle lateral displacement between wheelset and track on computer generic track, 83 m/s- Front wheelset

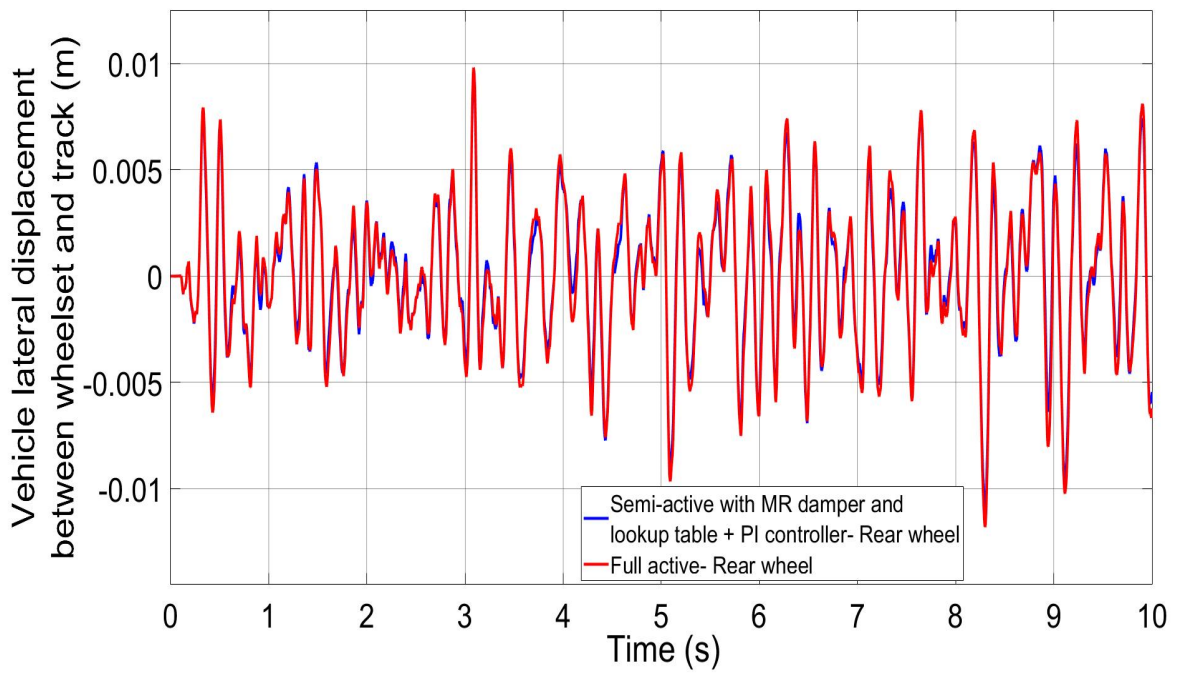


Figure 6-36- Two axle vehicle lateral displacement between wheelset and track on computer generic track, 83 m/s- Rear wheelset

Figures 6-37 and 6-38 show the lateral creep forces for the active controller and semi-active controller in the front and rear wheelset.

The lateral creep forces here are caused by the angle of attack and the lateral velocity of the wheelset, with the angle of attack being more dominant than the lateral velocity.

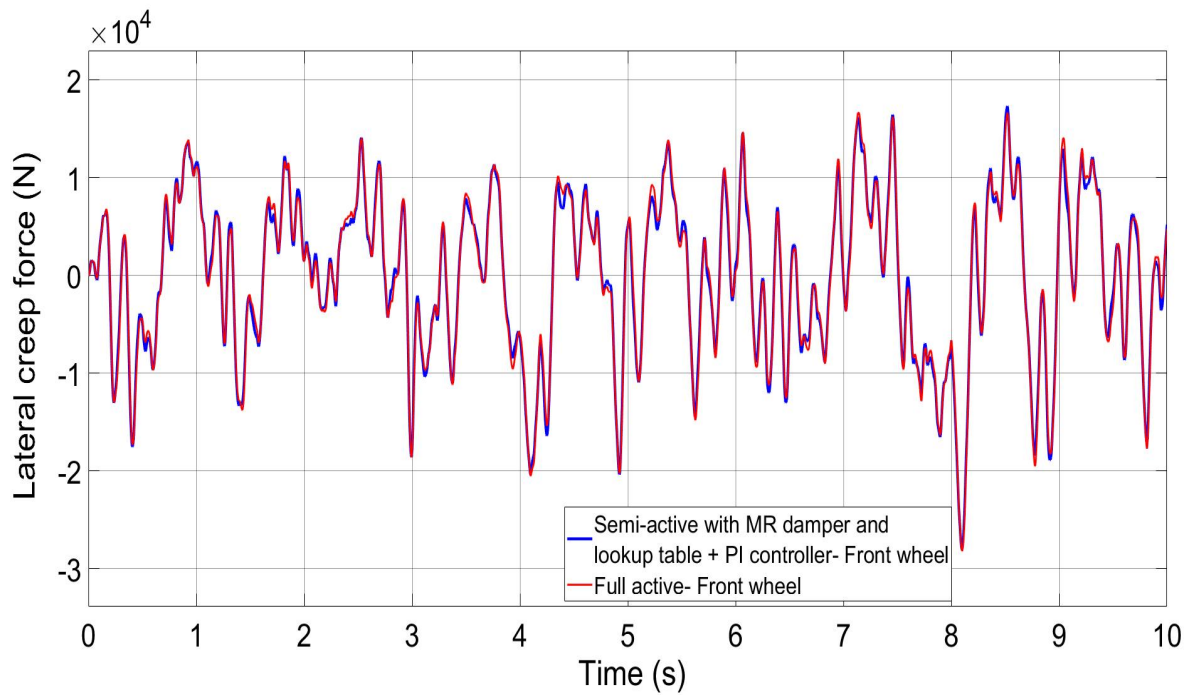


Figure 6-37- Two axle vehicle lateral creep force on computer generic track, 83 m/s- Front wheelset

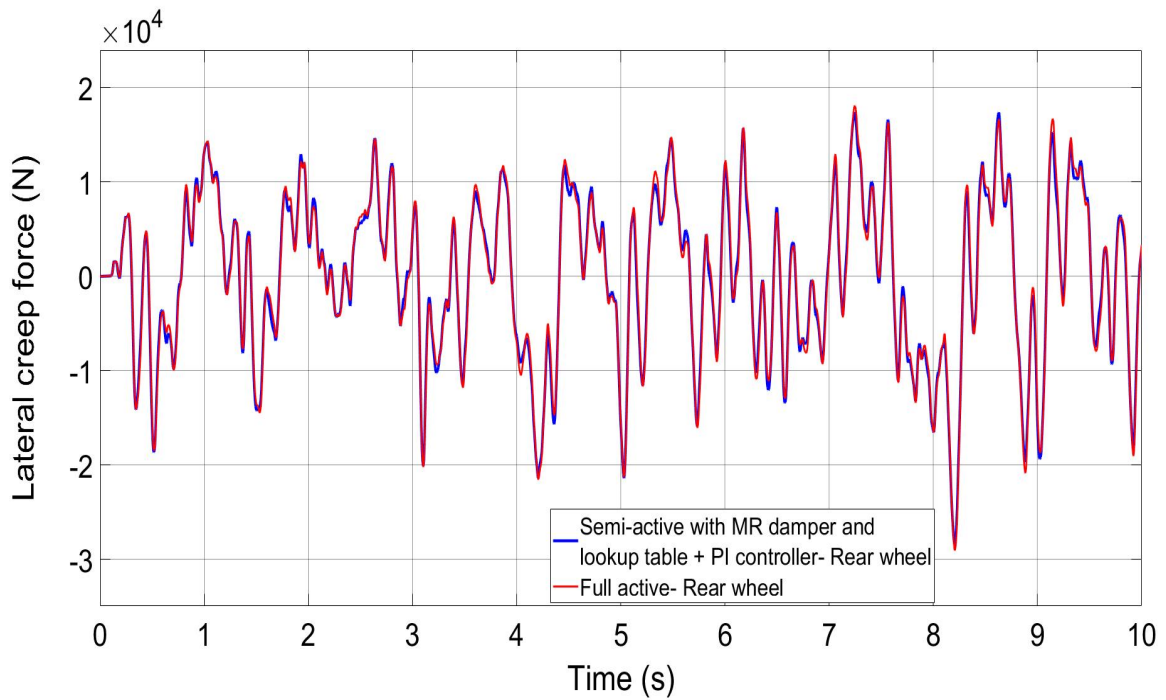


Figure 6-38- Two axle vehicle lateral creep force on computer generic track, 83 m/s- Rear wheelset

Figures 6-39 and 6-40 show the longitudinal creep force for active controller and semi-active controller in the front and rear wheelset.

The figures indicate that the longitudinal creep forces for the front and rear wheelset follow the same pattern. The longitudinal creep forces here are caused by the wheel-rail displacement/deflection and the yaw velocity of the wheelset, with the lateral displacement between wheelset having a more dominant effect than angle of attack.

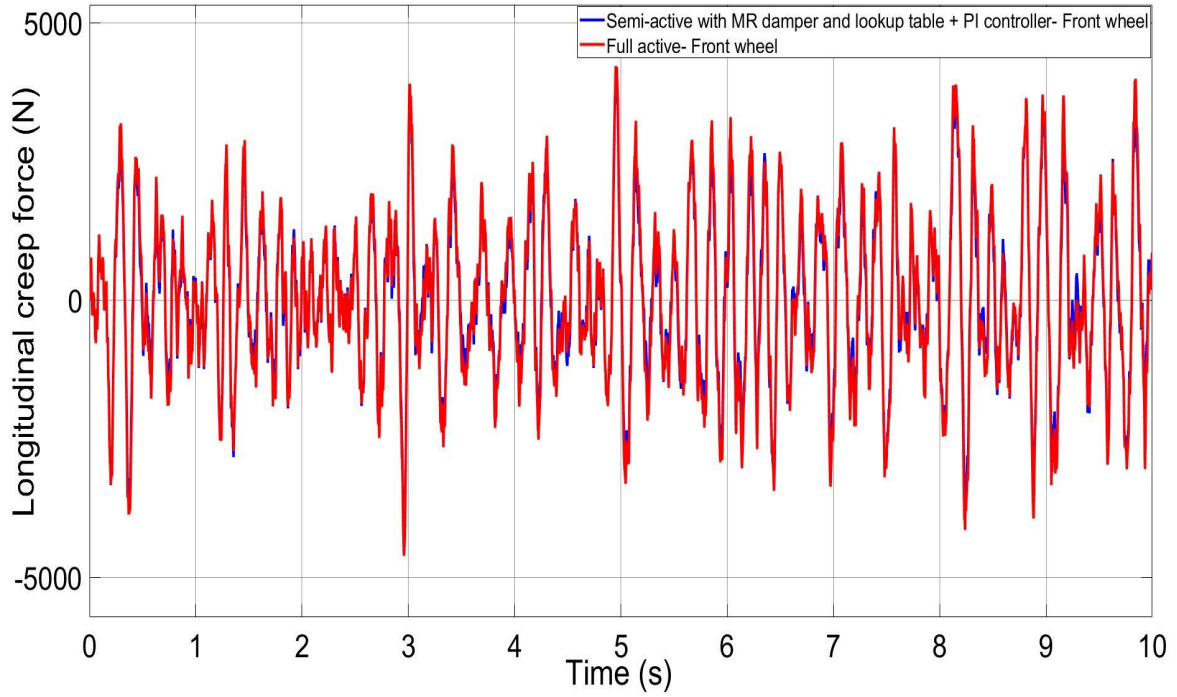


Figure 6-39- Two axle vehicle longitudinal creep force on computer generic track, 83 m/s- Front wheelset

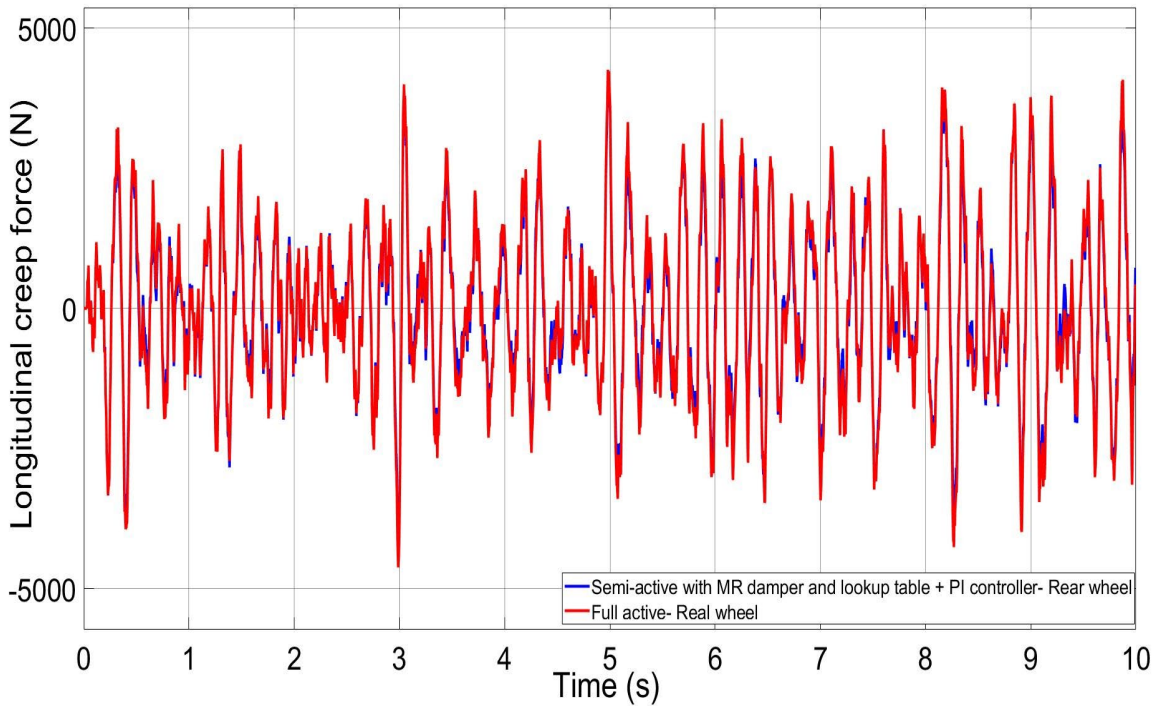


Figure 6-40- Two axle vehicle longitudinal creep force on computer generic track, 83 m/s- Rear wheelset

Figures 6-41 and 6-42 show the control force generated by active controller and semi-active controller in the front and rear wheelset.

The result shows that the force generated by semi active controller is a close match to the force generated by full active controller.

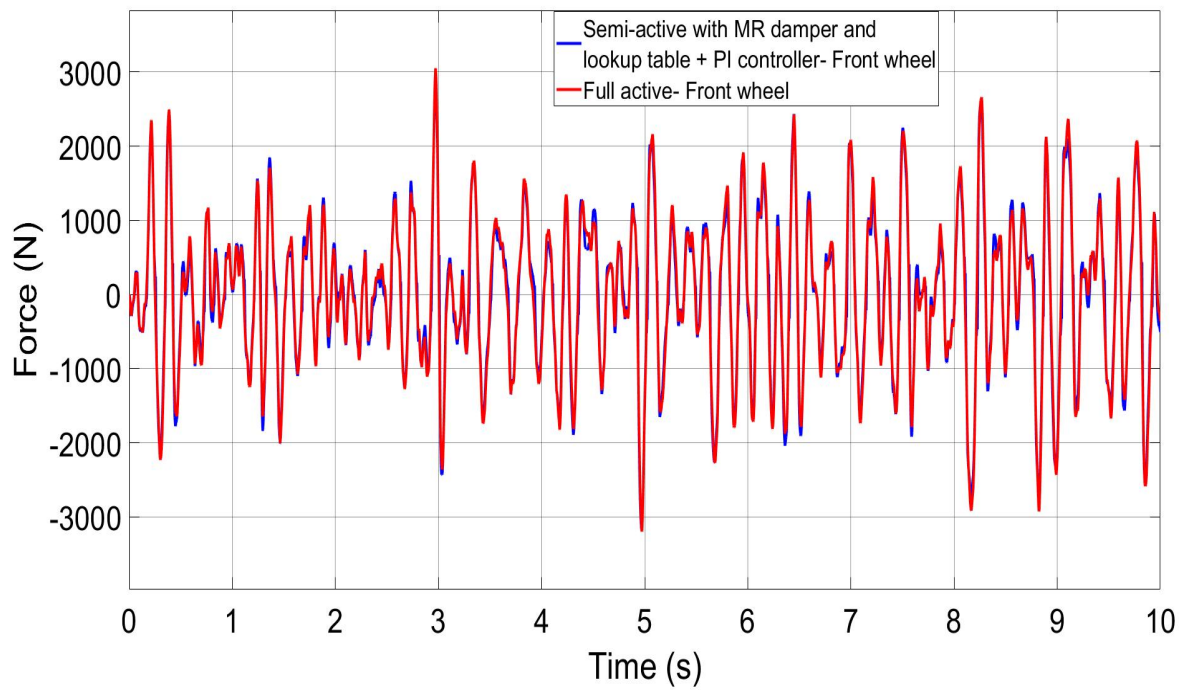


Figure 6-41- Two axle vehicle control force on computer generic track, 83 m/s- Front wheelset

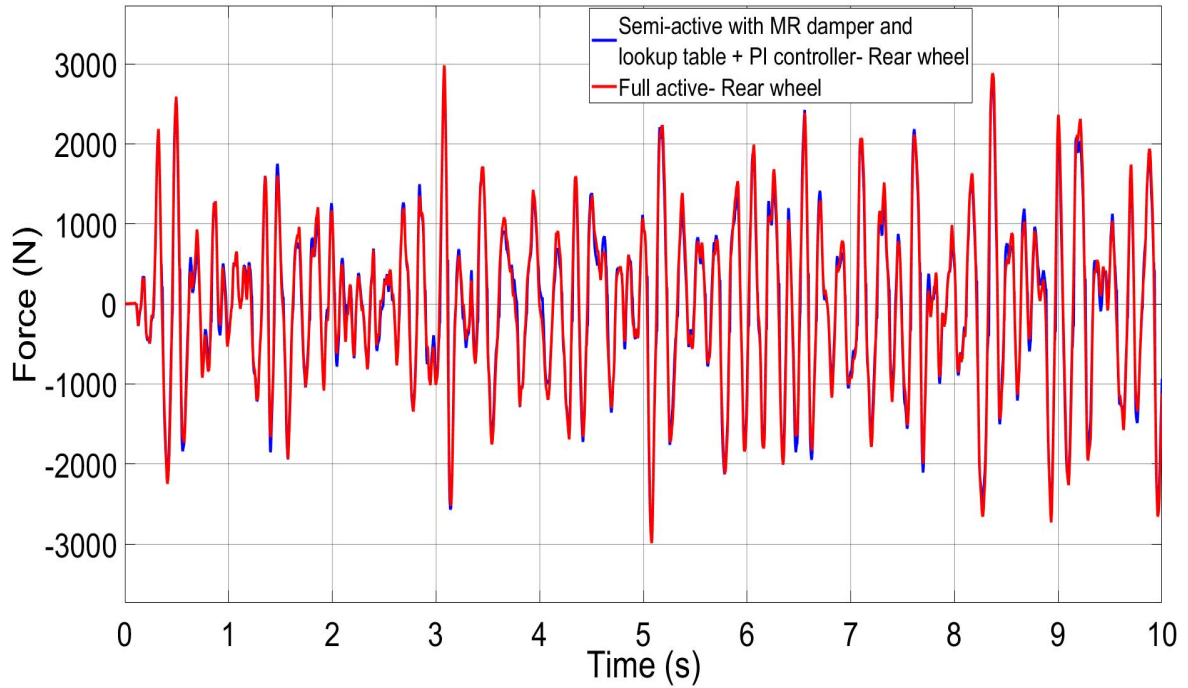


Figure 6-42- Two axle vehicle control force on computer generic track, 83 m/s- Rear wheelset

Figures 6-43 and 6-44 present the control power for the full active controller and semi-active controller in the front and rear wheelset. The result shows that the power generated by the semi active controller is slightly higher than the full active control power. However, it is clear both controllers only dissipate the energy from the wheelset and there is no requirement to provide any additional energy.

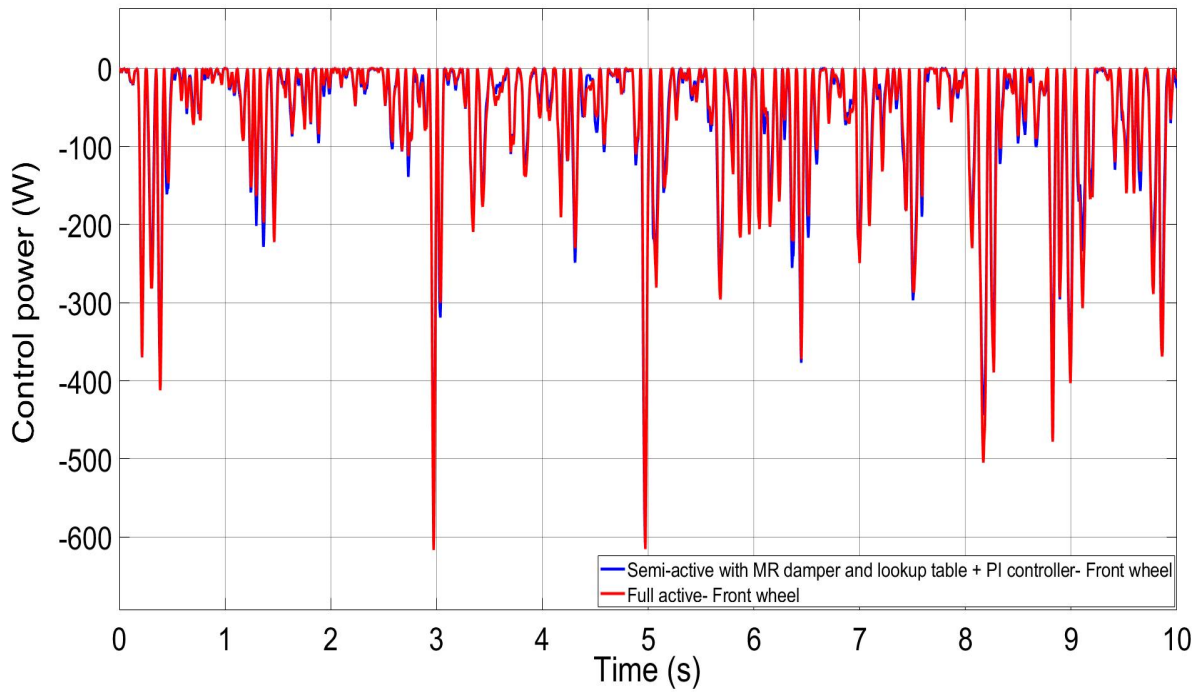


Figure 6-43- Two axle vehicle control power on computer generic track, 83 m/s- Front wheelset

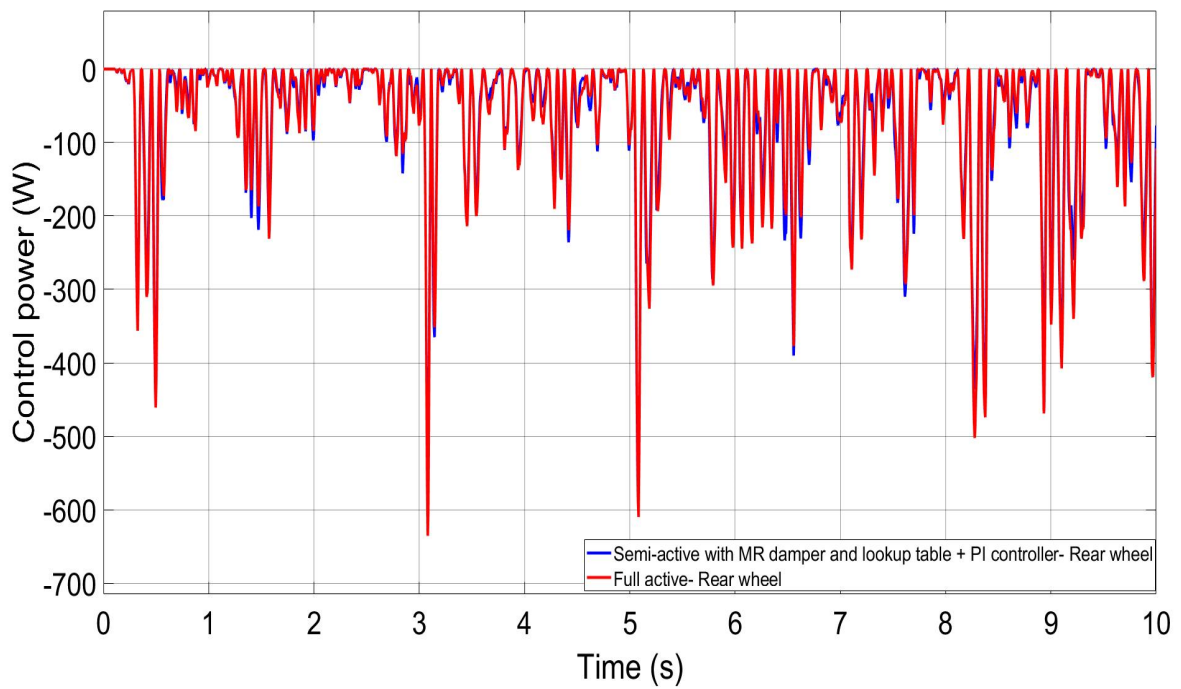


Figure 6-44- Two axle vehicle control power on computer generic track, 83 m/s- Rear wheelset

6.3.3 Straight Track with Irregularity (Measured Track Data at The Speed of 50m/S, 180 Km⁻¹)

This section presents the simulation result of two axle vehicle at 50 m/s in Measured Track Data.

Figures 6-45 and 6-46 shows the angle of attack for active controller and semi-active controller in the front and rear wheelset on measured track. As it shows in figures, the angle of attack in the semi-active controller is lower than that of the active controller. Since the yaw angle has effect on lateral creep force so in this case the semi-active controller appears to have a less lateral creep force than the full active controller.

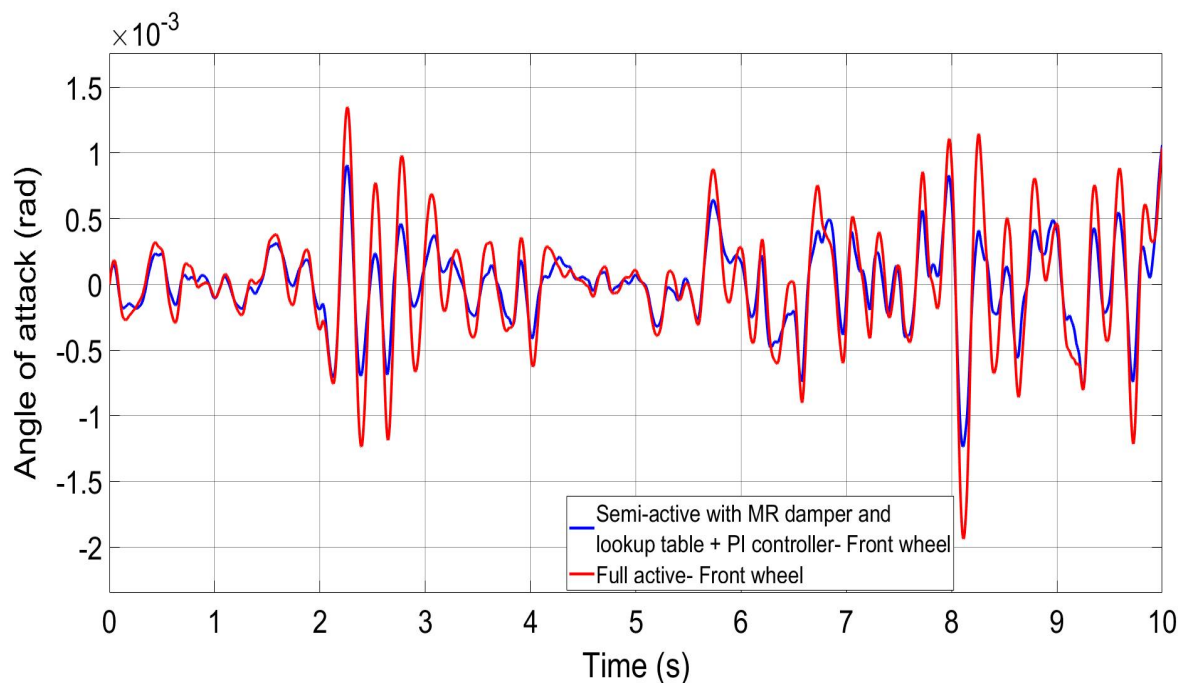


Figure 6-45- Two axle vehicles angle of attack on measured track, 50 m/s- Front wheelset

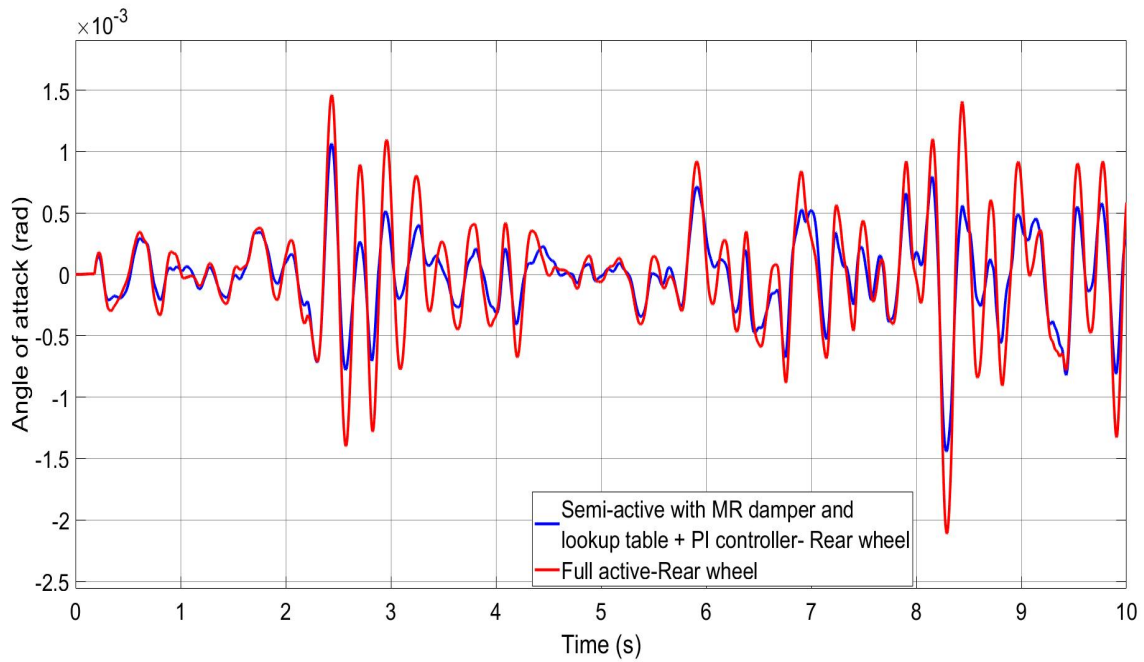


Figure 6-46- Two axle vehicles angle of attack on measured track, 50 m/s- Rear wheelset

Figures 6-47 and 6-48 show the lateral displacement between wheelset and track on measured track for the active controller and the semi-active controller in the front and rear wheelset. As shown in the figures, the semi-active controller appears to produce better track following ability than the full active controller, although in both cases, the lateral displacements are well within the flange clearance.

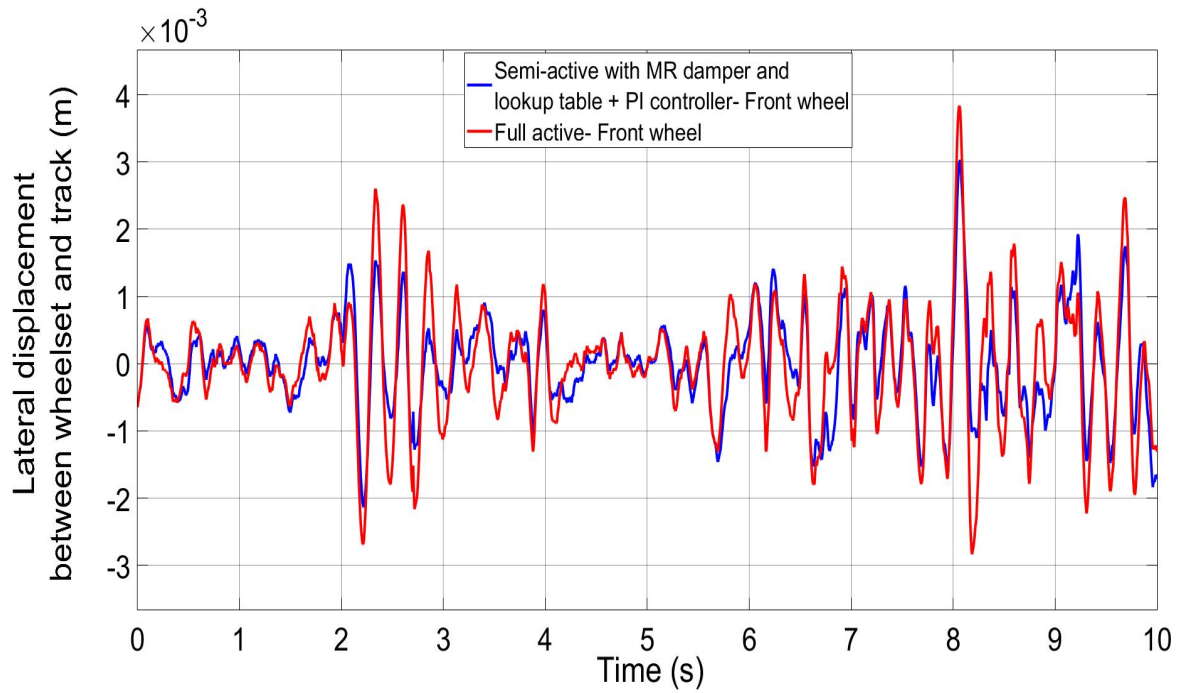


Figure 6-47- Two axle vehicles lateral displacement between wheelset and track on measured track, 50 m/s- Front wheelset

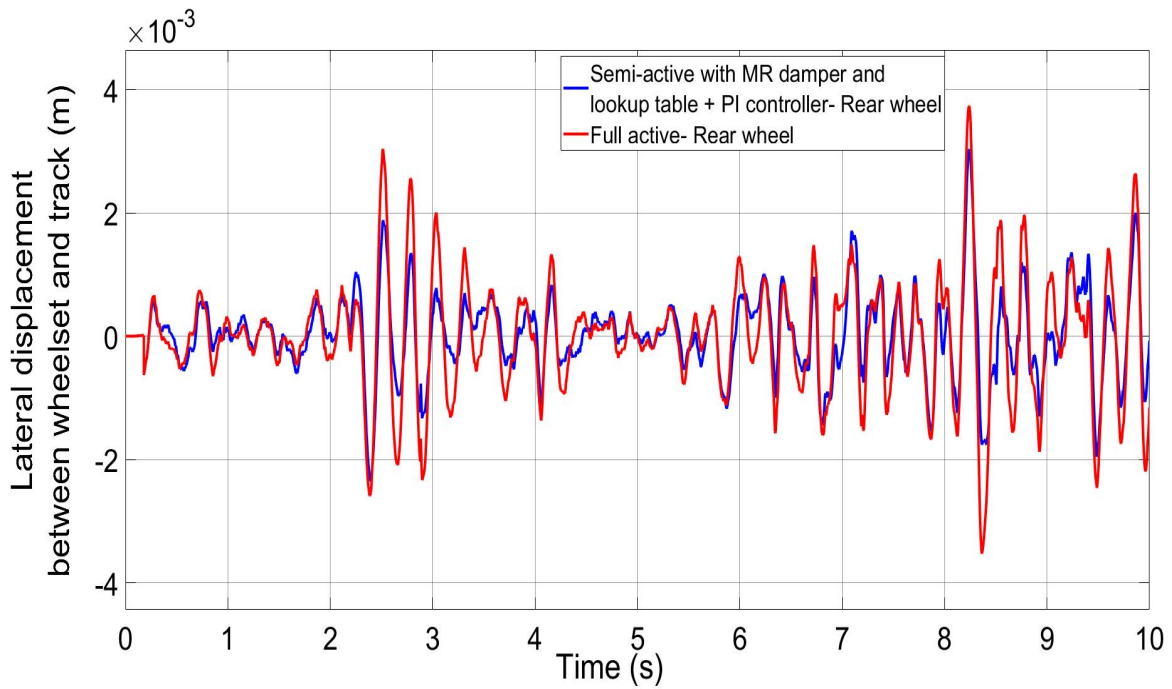


Figure 6-48- Two axle vehicles lateral displacement between wheelset and track on measured track, 50 m/s- Rear wheelset

Figures 6-50 and 6-51 depicts lateral creep forces of the wheelsets on measured track. The lateral creep force values for both wheelsets (front and rear) have a very similar outline of the forces, due to the similarities in the wheelset lateral displacement and angle of attack behaviour in response to track irregularities.

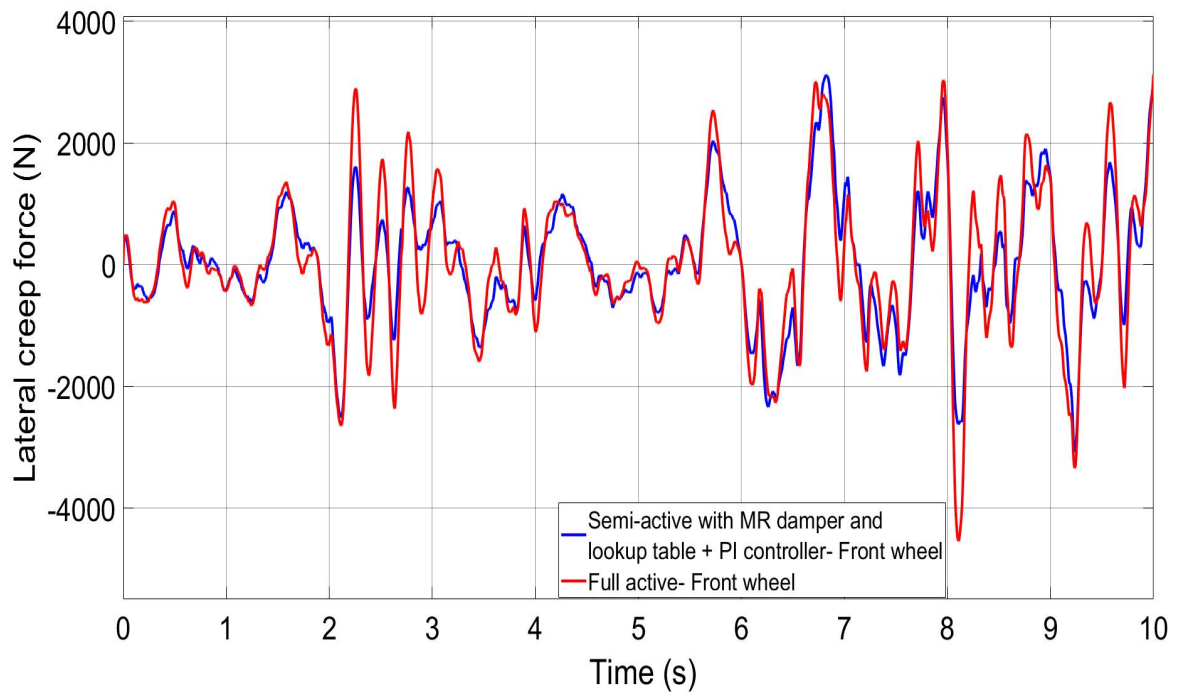


Figure 6-49- Two axle vehicle lateral creep force on measured track, 50 m/s- Front wheelset

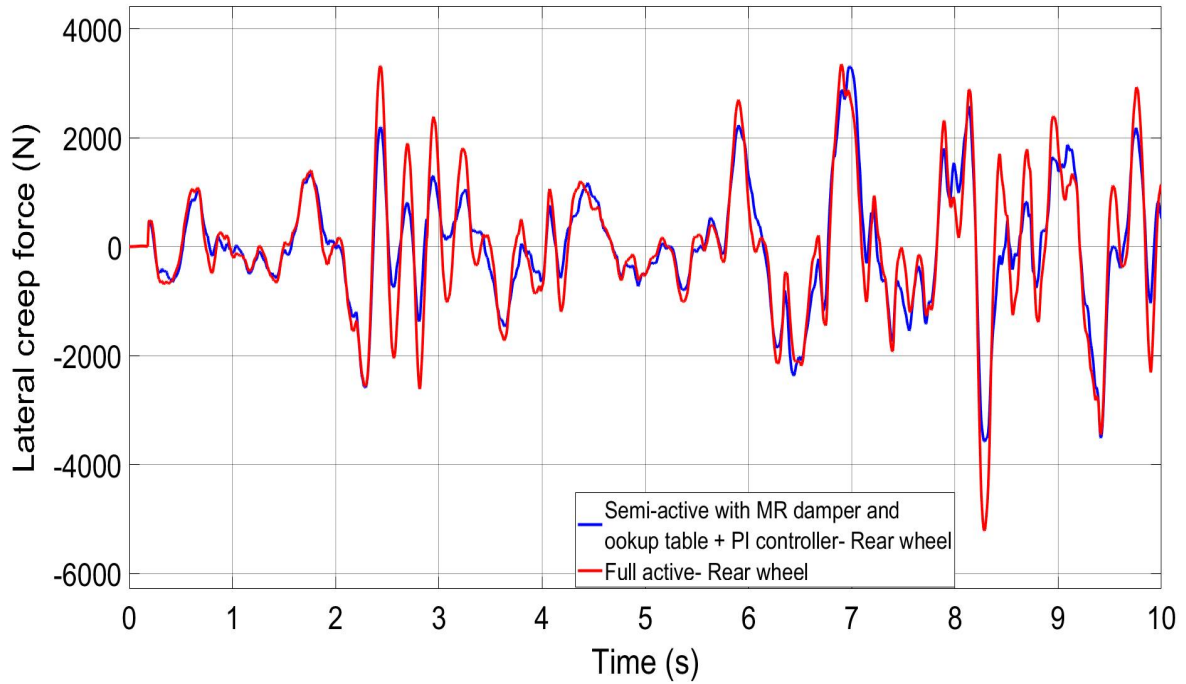


Figure 6-50- Two axle vehicle lateral creep force on measured track, 50 m/s- Rear wheelset

Figures 6-50 and 6-51 show the longitudinal creep forces of the wheelsets on measured track. It is noticeable that the valuation of the creep forces is important while the control torque has been affected by both lateral and longitudinal creep.

There is a large spike at the beginning in the longitudinal forces for both front and rear wheelsets. This is caused by the measured track irregularities do not start from zero – in this case the initial lateral displacement of the track is 0.6458mm – a small value by large enough to result in the initial high contact force as the creep coefficient is typical very large. The longitudinal creep force equation is:

$$-\frac{Lgf_{11}}{v_s} \dot{\psi}_{w1} + \frac{\lambda f_{11}}{r_0} (y_{t1} - y_{w1}) + \frac{Lgf_{11}}{R_1} - \frac{r_0 f_{11}}{v_s} \dot{\phi}_{w1}$$

therefore y_{t1} value after multiple in $\frac{\lambda f_{11}}{r_0}$ at time zero is 2927N.

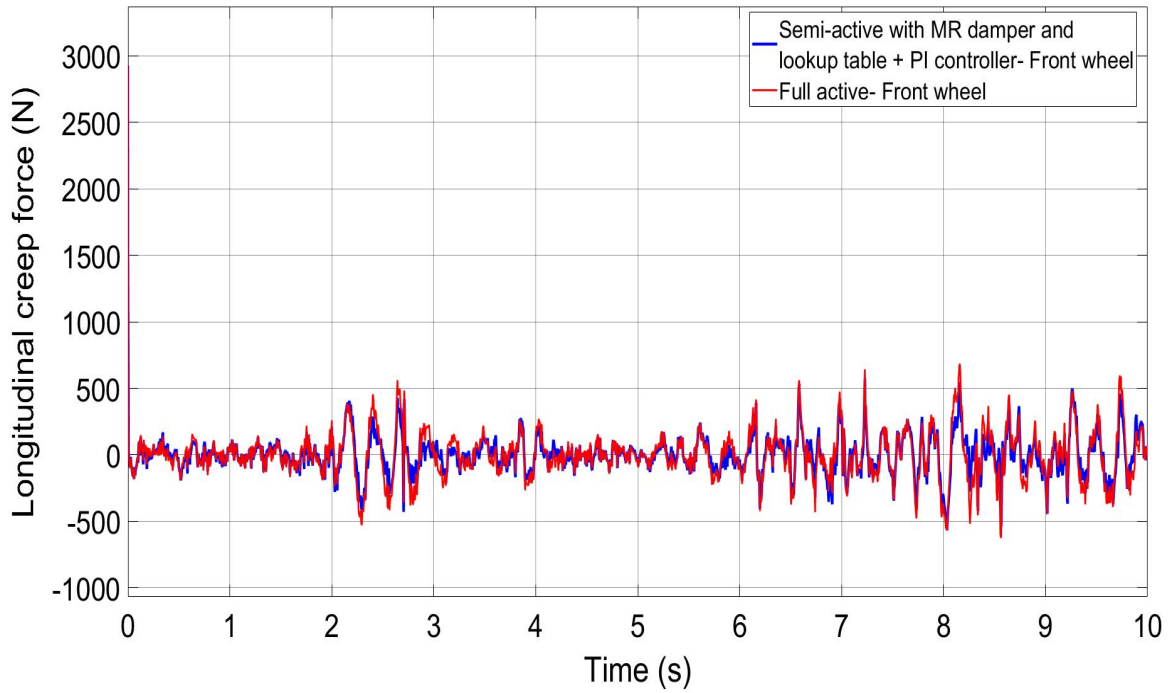


Figure 6-51- Two axle vehicle longitudinal creep force on measured track, 50 m/s- Front wheelset

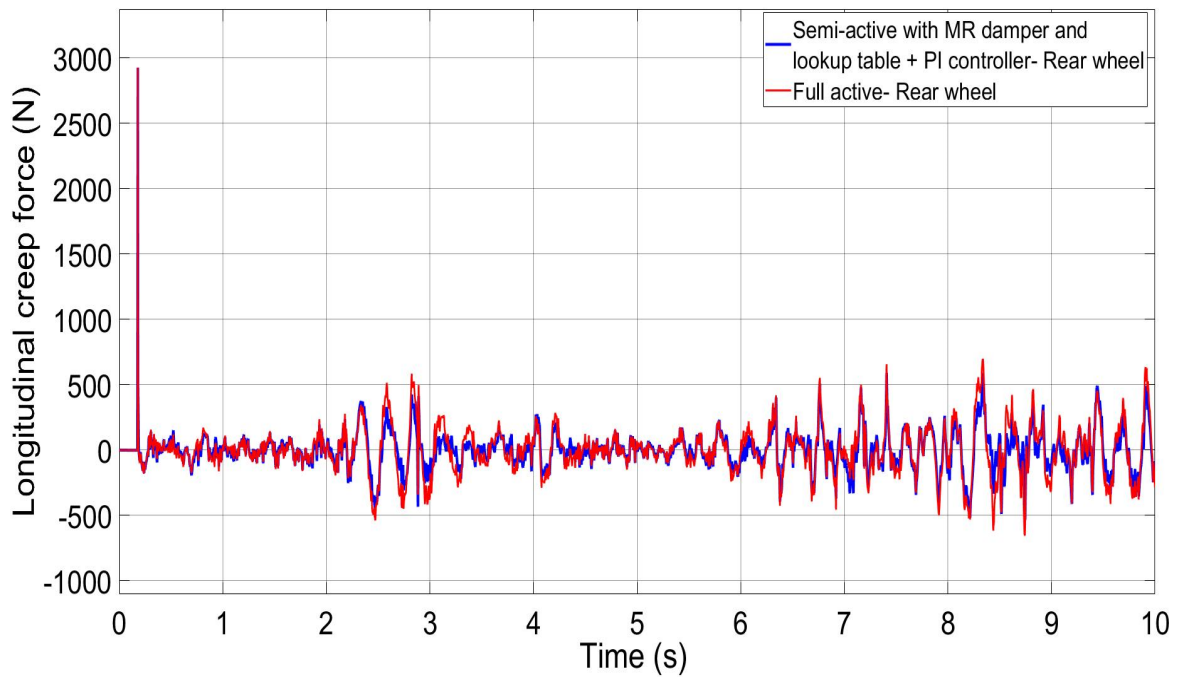


Figure 6-52- Two axle vehicle longitudinal creep force on measured track, 50 m/s- Rear wheelset

Figures 6-53 and 6-54 illustrate the longitudinal creep forces of the wheelsets on the measured track. As it shows in figures, the semi-active control is able to produce the control forces similar to that in the active controller.

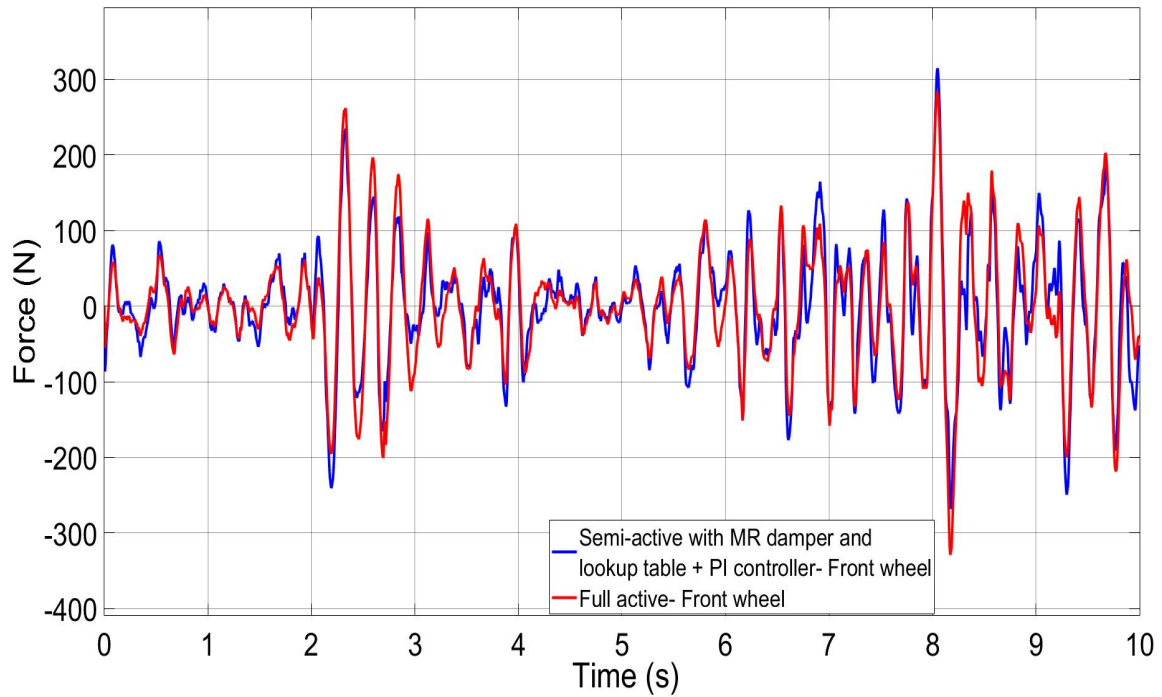


Figure 6-53- Two axle vehicle control force on measured track, 50 m/s- Front wheelset

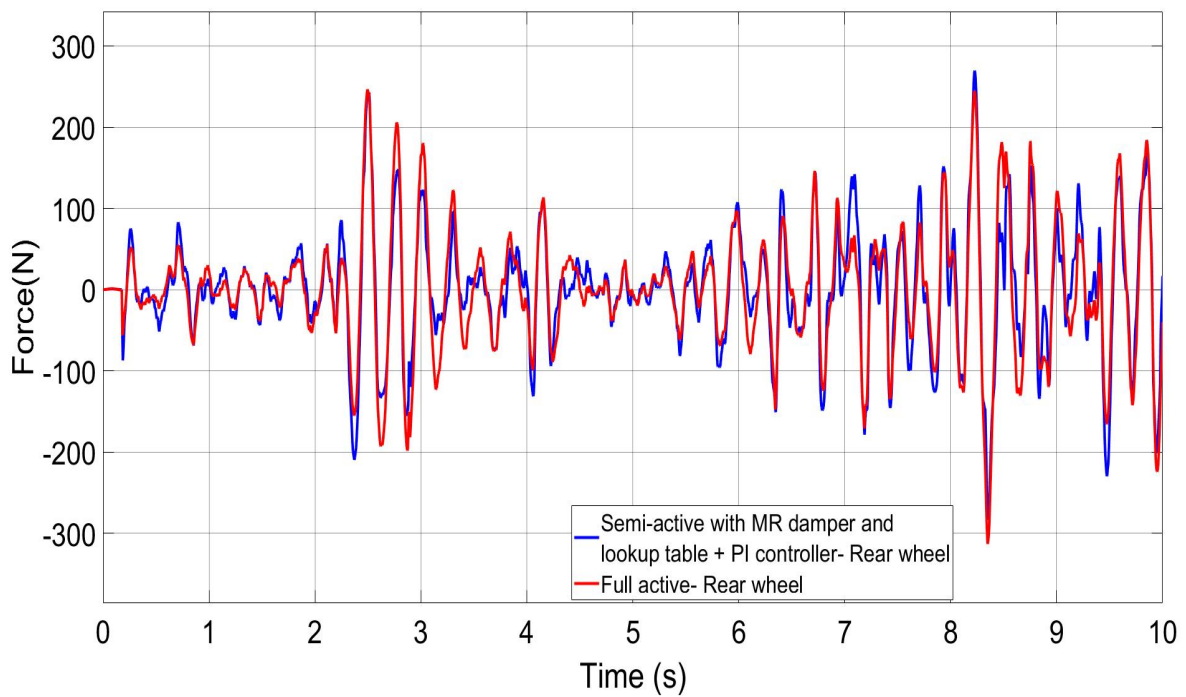


Figure 6-54- Two axle vehicle control force on measured track, 50 m/s- Rear wheelset

Figures 6-55 and 6-56 show the control power of the wheelsets on the measured track. It is clear that, similar to the previous cases, both controllers dissipate the energy only on the real track as well.

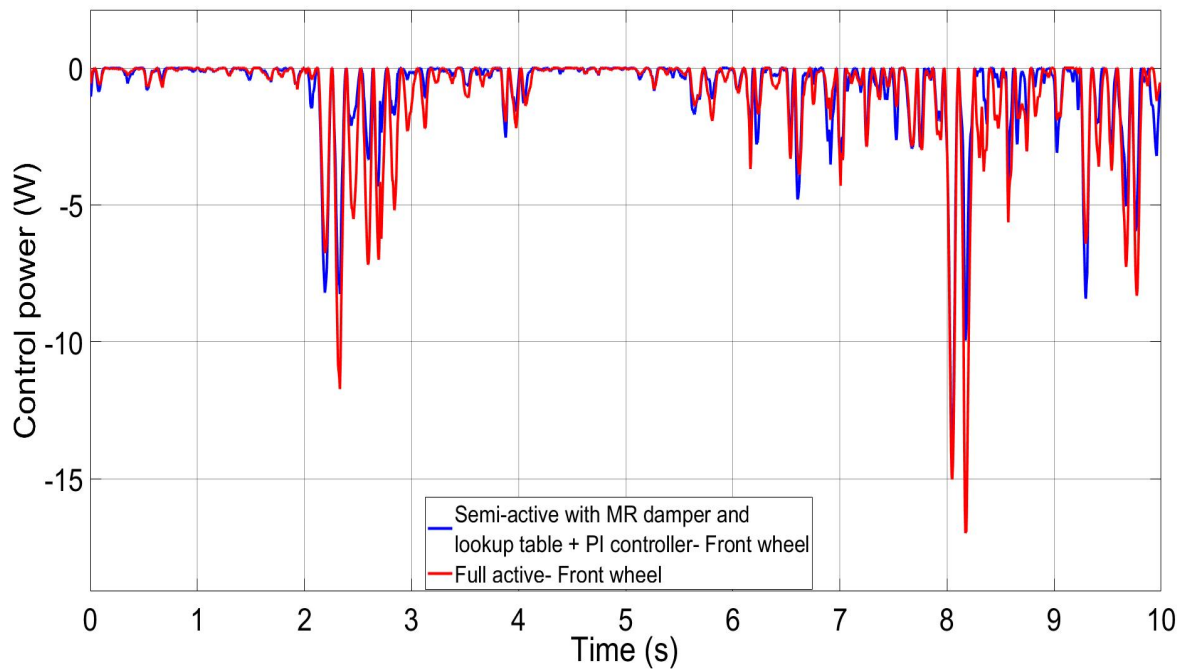


Figure 6-55- Two axle vehicle control power on measured track, 50 m/s- Front wheelset

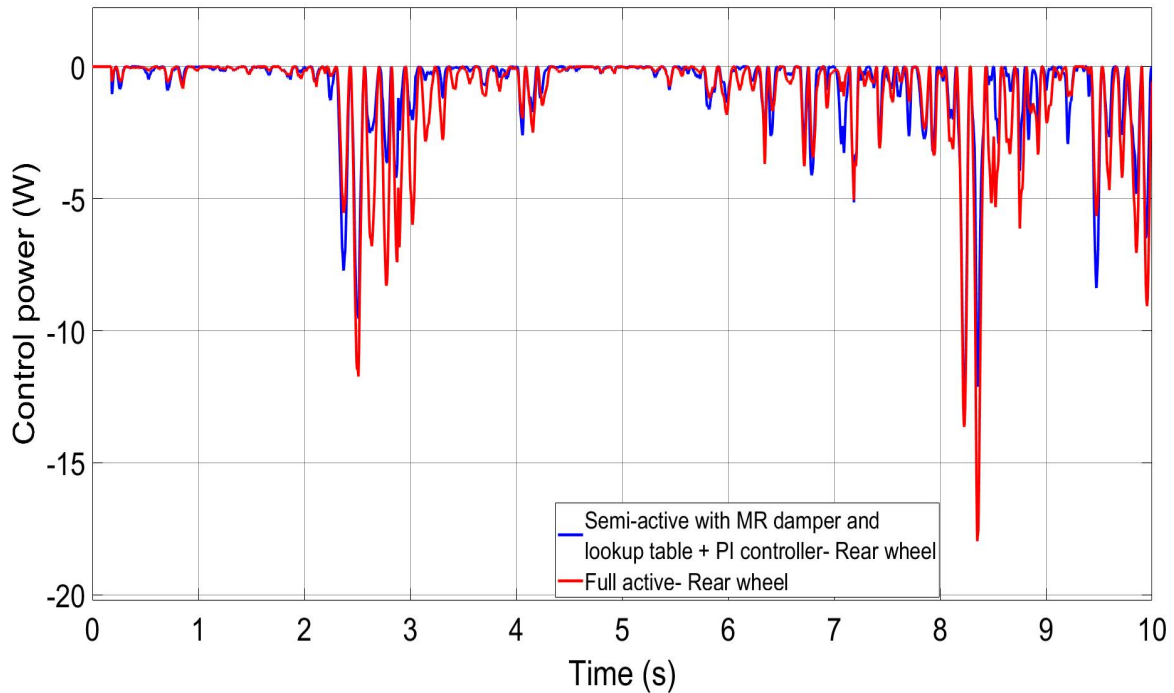


Figure 6-56- Two axle vehicle control power on measured track, 50 m/s- Rear wheelset

6.4 Bogie vehicle

6.4.1 Curve track

This section presents the simulation results from the bogie vehicle at the vehicle speeds of 83 and 20 m/s on curve tracks, including the angle of attack, lateral deflection, lateral creep force, longitudinal creep force, control force and control power for the front and rear bogie.

Figure 6-57 to 6-60 compare the angle of attack (yaw motion) for full active controller and semi-active controller for the front and rear bogies.

As shown in the figures, the semi active controller at the speed of 83m/s performs in the same way as the full active. There is an equal angle of attack between the four wheelsets (two bogies) on the steady curve, to deliver the suitable lateral creep forces for the cant deficiency. Also, at the speed of 20m/s, the angles of attack for semi active controller for the front bogie match well with angle of attack of active controller. However, there is some minor difference in the angle of attack for the rear bogie when compared to that the full active controller. It is noticeable that angle of attacked reduce in both speeds compare to two axle vehicles due bogie vehicle required less lateral creep forces to counter the centrifugal forces.

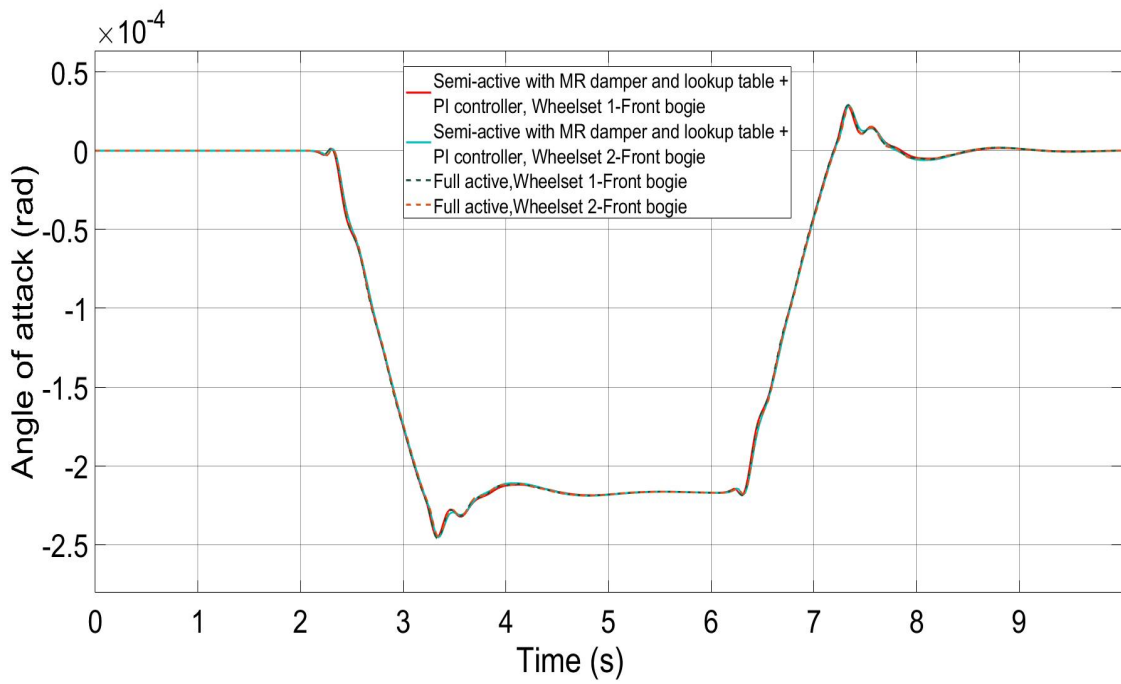


Figure 6-57- Bogie vehicles angle of attack on curve, 83 m/s- Front bogie

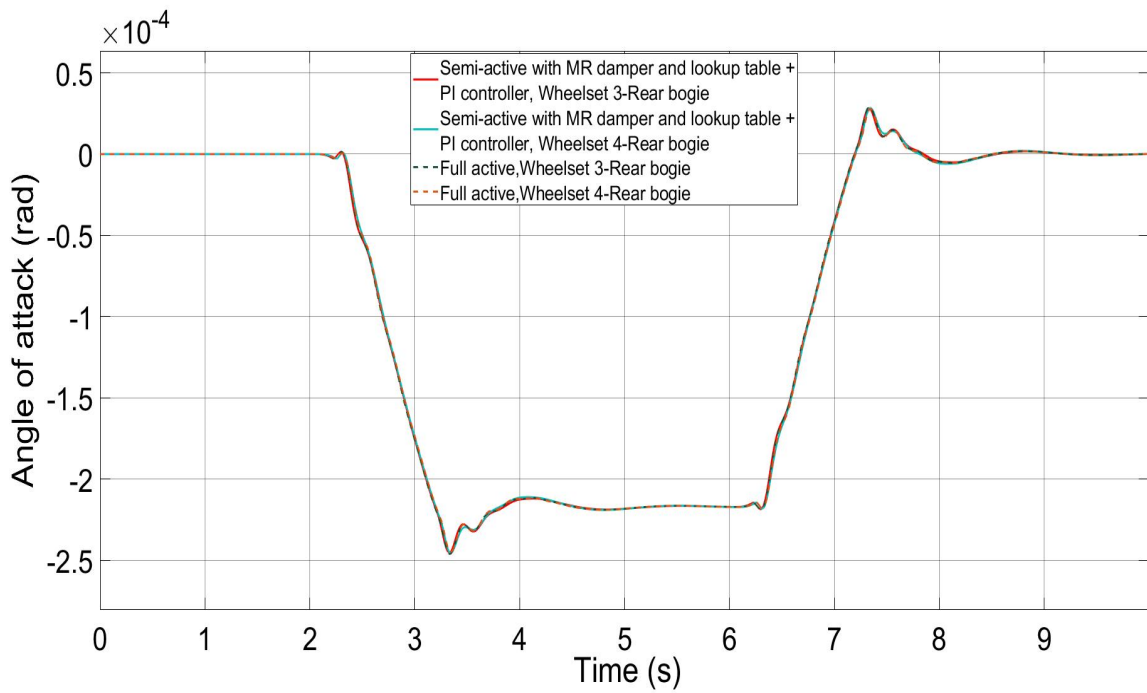


Figure 6-58- Bogie vehicles angle of attack on curve, 83 m/s- Rear bogie

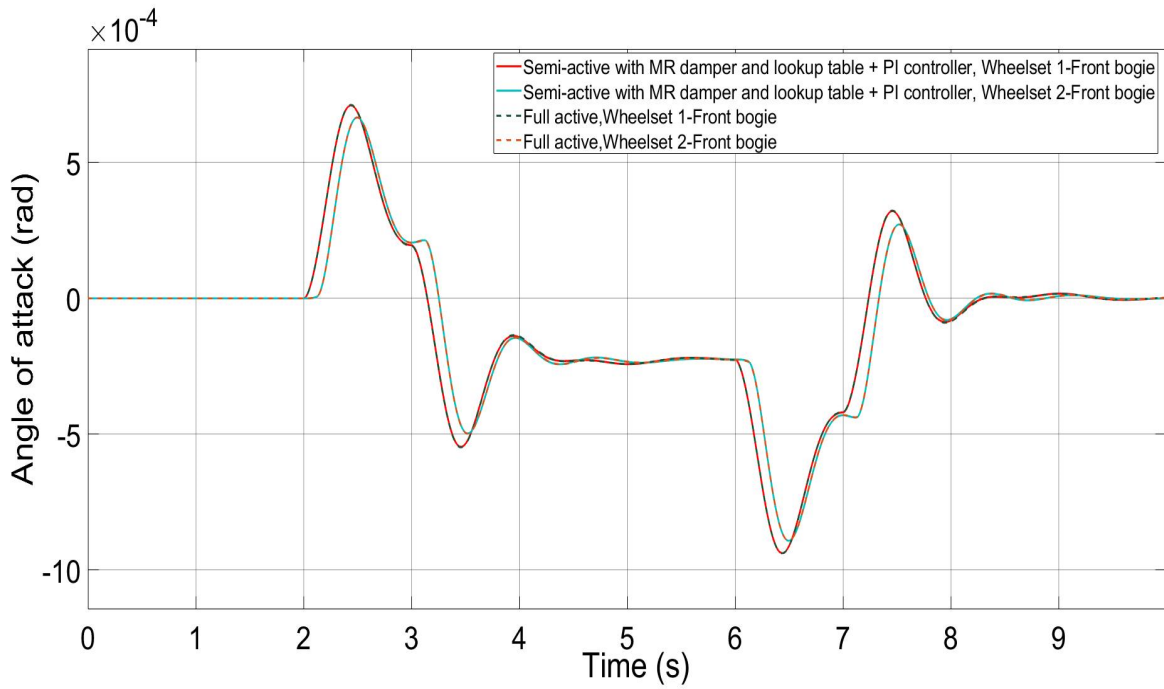


Figure 6-59- Bogie vehicles angle of attack on curve, 20m/s- Front bogie

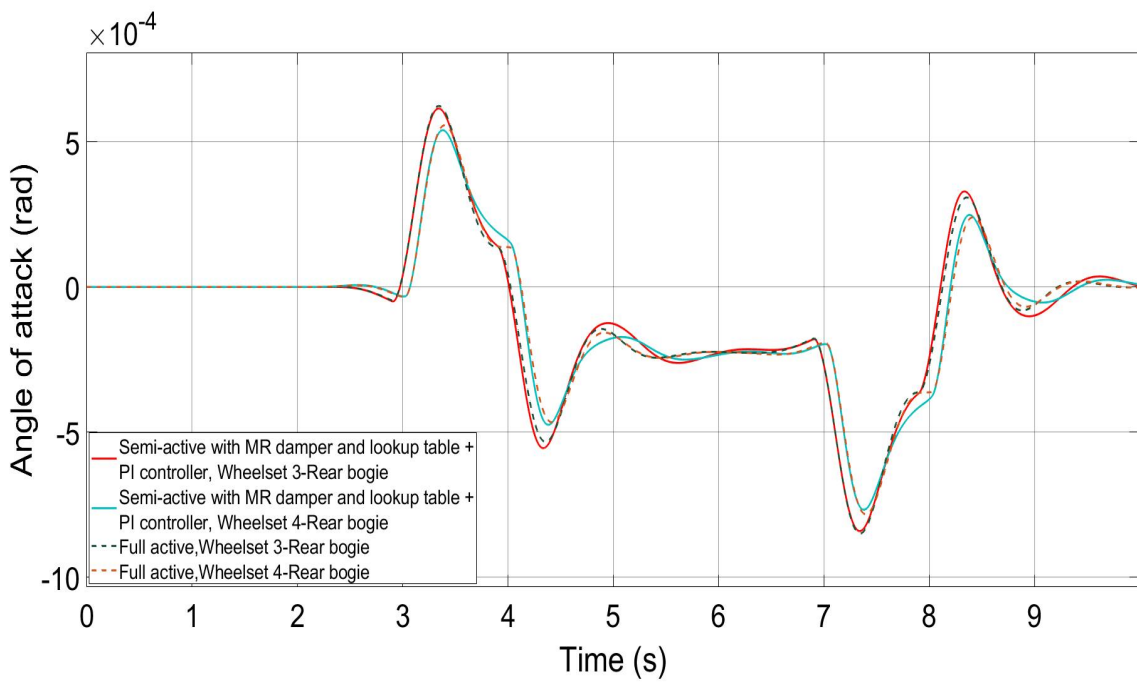


Figure 6-60- Bogie vehicles angle of attack on curve, 20m/s- Rear bogie

Figures 6-61 to 6-64 show the lateral displacements between wheelset and track for the full active controller and semi-active controller in the front and rear bogies.

The lateral displacements at speed of 83 m/s in front and rear bogie is 0.49 mm and 8.7 mm in the front and rear bogie at speed of 20 m/s, which are all within the wheel flange contact limits.

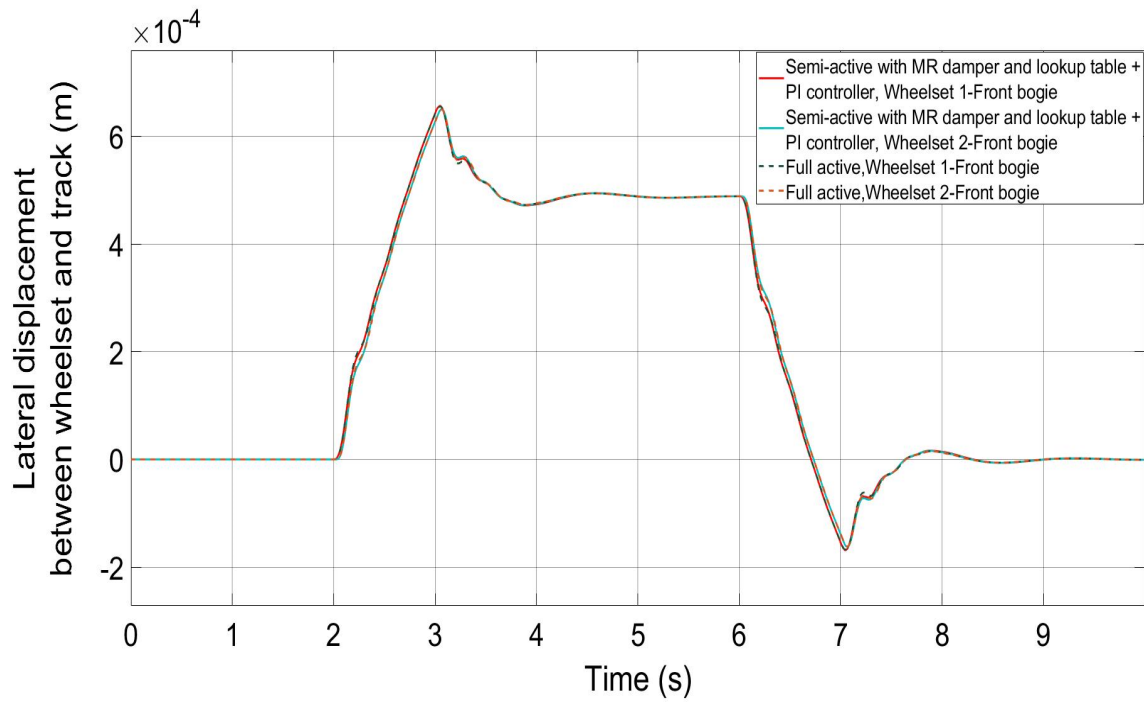


Figure 6-61- Bogie vehicles lateral displacement between wheelset and track on curve, 83 m/s- Front bogie

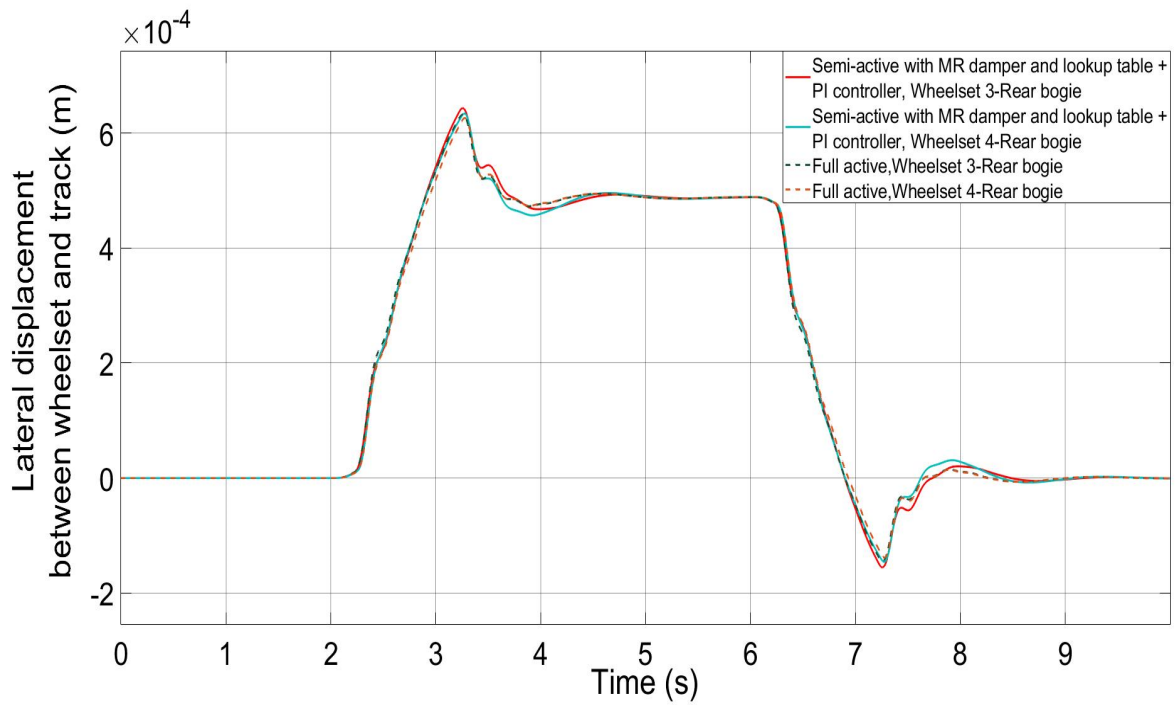


Figure 6-62- Bogie vehicles lateral displacement between wheelset and track on curve, 83 m/s- Rear bogie

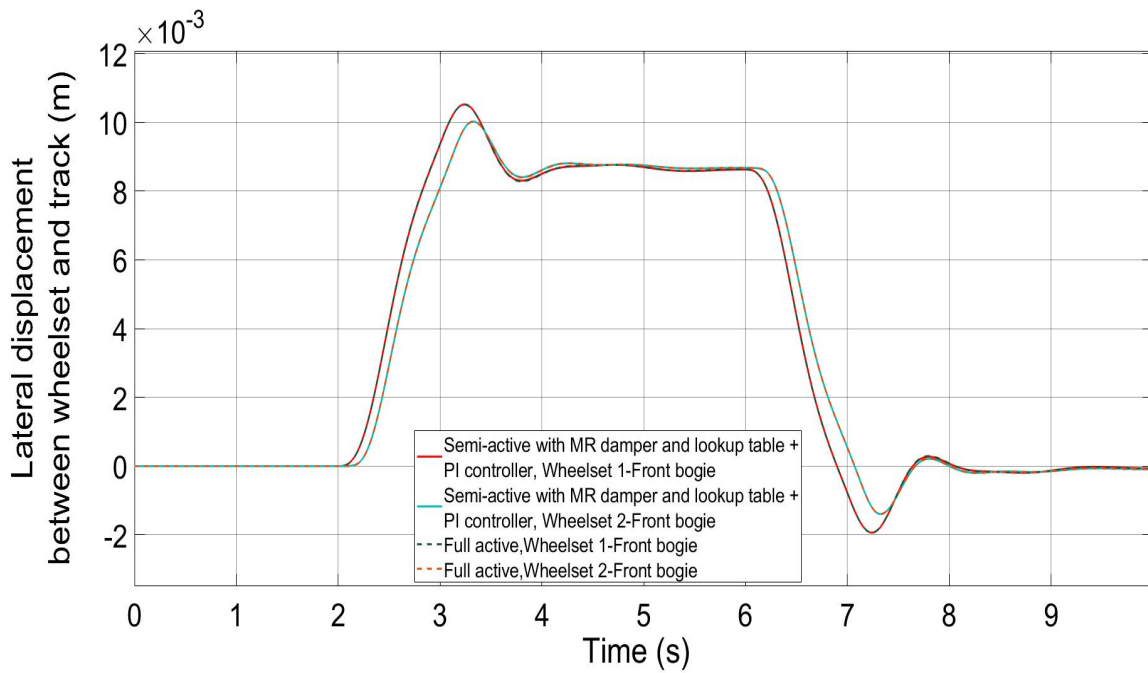


Figure 6-63- Bogie vehicles lateral displacement between wheelset and track on curve, 20 m/s- Front bogie

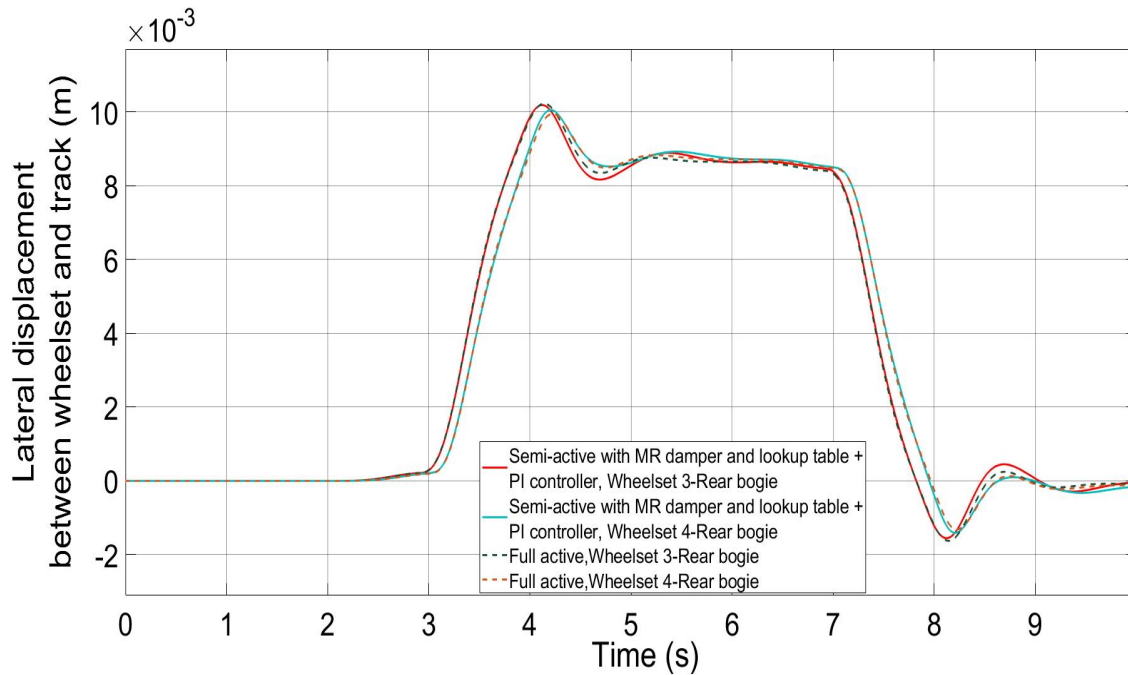


Figure 6-64- Bogie vehicles lateral displacement between wheelset and track on curve, 20 m/s- Rear bogie

Figures 6-65 to 6-68 show the lateral creep forces for the full active controller and semi-active controller in the front and rear bogies.

Again, there is a good match in the lateral creep force between the full active controller and semi-active controller. The lateral creep force in the front and rear bogie is -4369N for 83m/s and -4300N for the front and -4800N for rear bogie at speed of 20 m/s which is lower than that of the two-axle vehicle. As explained above these lateral creep forces occur as a reaction force to the centrifugal force of the curved track.

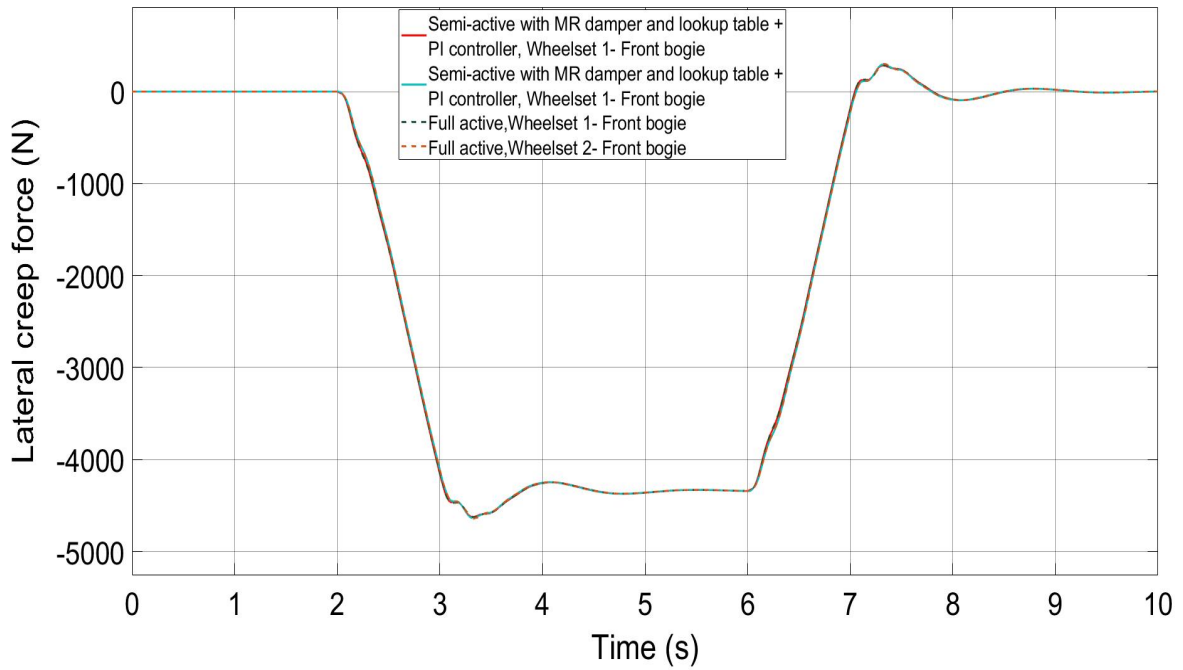


Figure 6-65- Bogie vehicle lateral creep force on curve track, 83 m/s- Front bogie

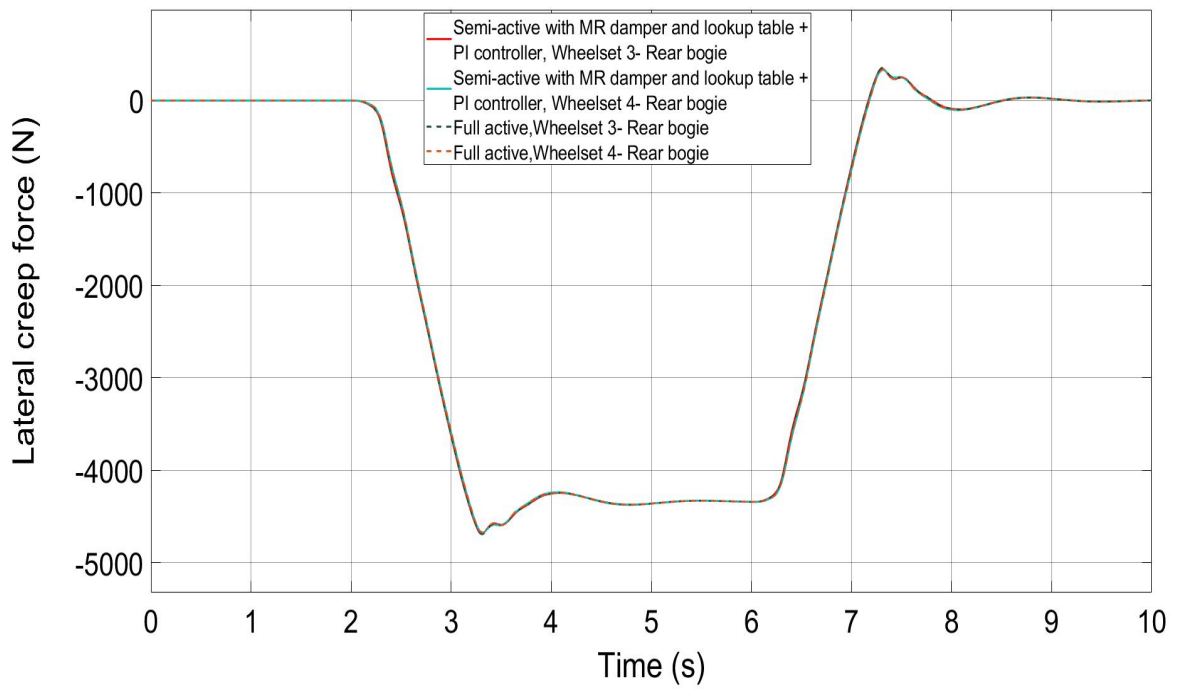


Figure 6-66- Bogie vehicle lateral creep force on curve track, 83 m/s- Rear bogie

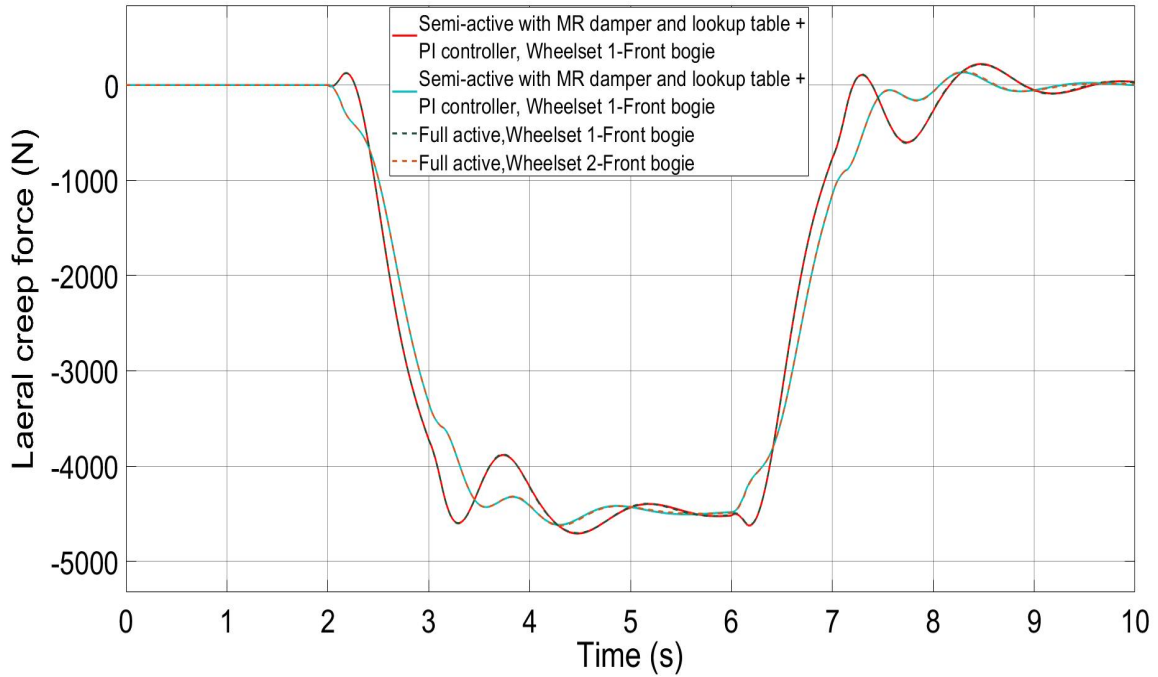


Figure 6-67- Bogie vehicle lateral creep force on curve track, 20 m/s- Front bogie

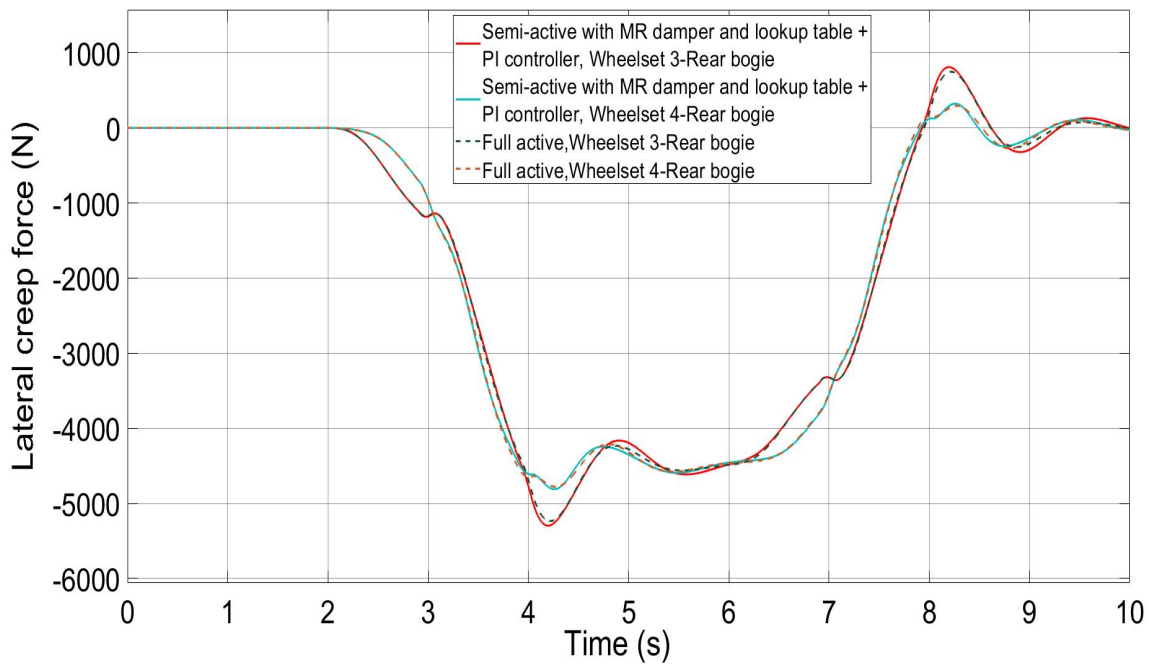


Figure 6-68- Bogie vehicle lateral creep force on curve track, 20 m/s- Rear bogie

Figures 6-69 to 6-72 show the longitudinal creep forces for full active controller and semi-active controller in the front and rear bogies.

The longitudinal creep force in the semi-active controller for the full bogie vehicle performs better than that of the two-axle vehicle. As it shows in figures below, the longitudinal creep force for semi active controller at both speed of 83 m/s and 20m/s are very much similar to active controller longitudinal creep force.

The maximum and minimum longitudinal creeps force in the front bogie for full active controller are ± 14.82 N at wheelset 1, ± 14.36 N at wheelset 2 and for semi-active controller ± 15.47 N at wheelset 1 and ± 14.80 N at wheelset 2. In the rear bogie is ± 15.08 N at wheelset 3 for the full active controller and ± 16.32 N at wheelset 4 and for the semi-active controller ± 15.98 N at wheelset 3 and ± 15.61 N at wheelset 4 at speed of 83 m/s.

Also, the maximum and minimum longitudinal creep forces at the speed of 20 m/s in the front bogie for full active and semi- active controller is ± 26.8 N at wheelset 1, ± 22.7 N at wheelset 2 and in the rear bogie ± 26.4 N at wheelset 3 and ± 22.3 N at wheelset 4.

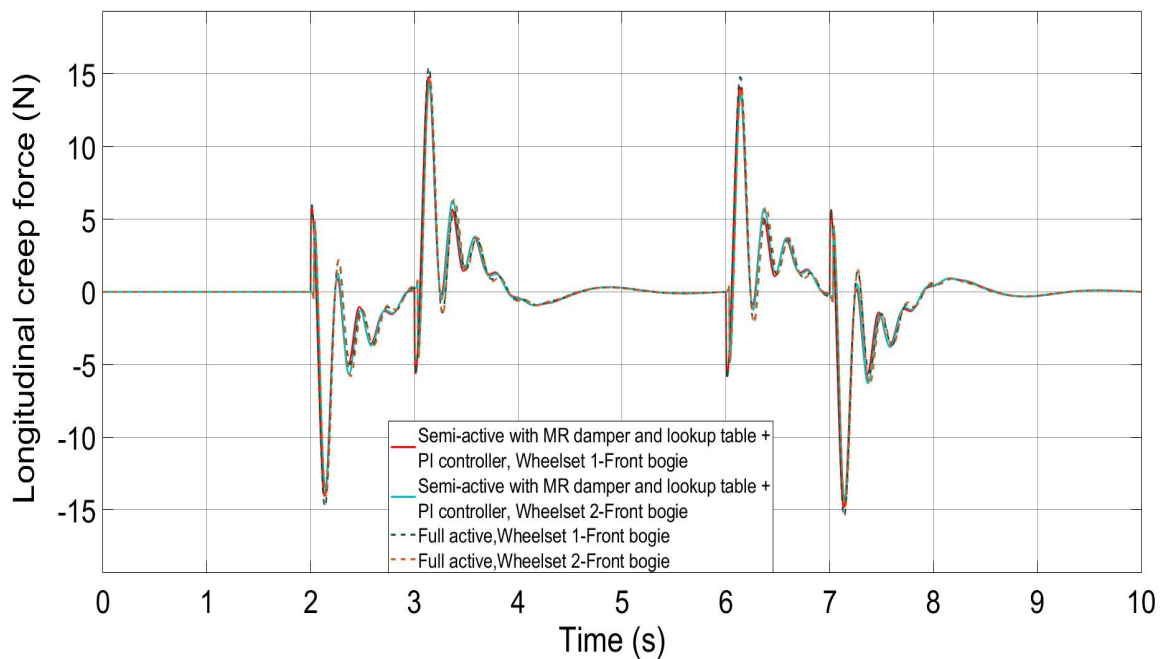


Figure 6-69- Bogie vehicle longitudinal creep force on curve track, 83 m/s- Front bogie

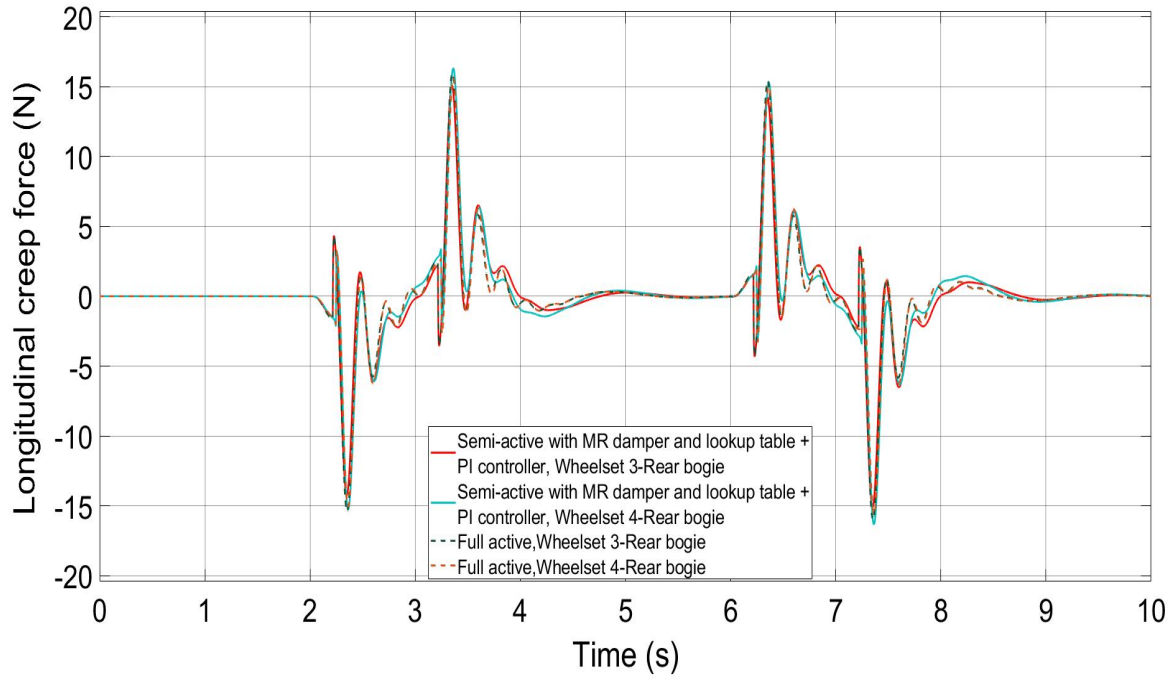


Figure 6-70- Bogie vehicle longitudinal creep force on curve track, 83 m/s- Rear bogie

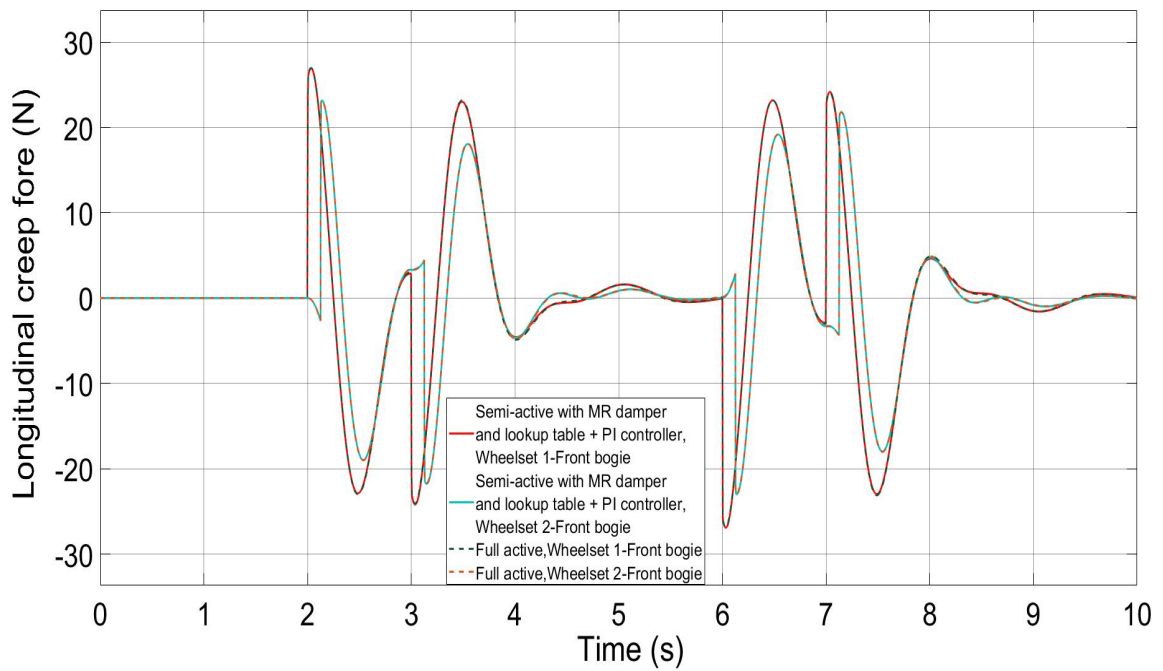


Figure 6-71- Bogie vehicle longitudinal creep force on curve track, 20 m/s- Front bogie

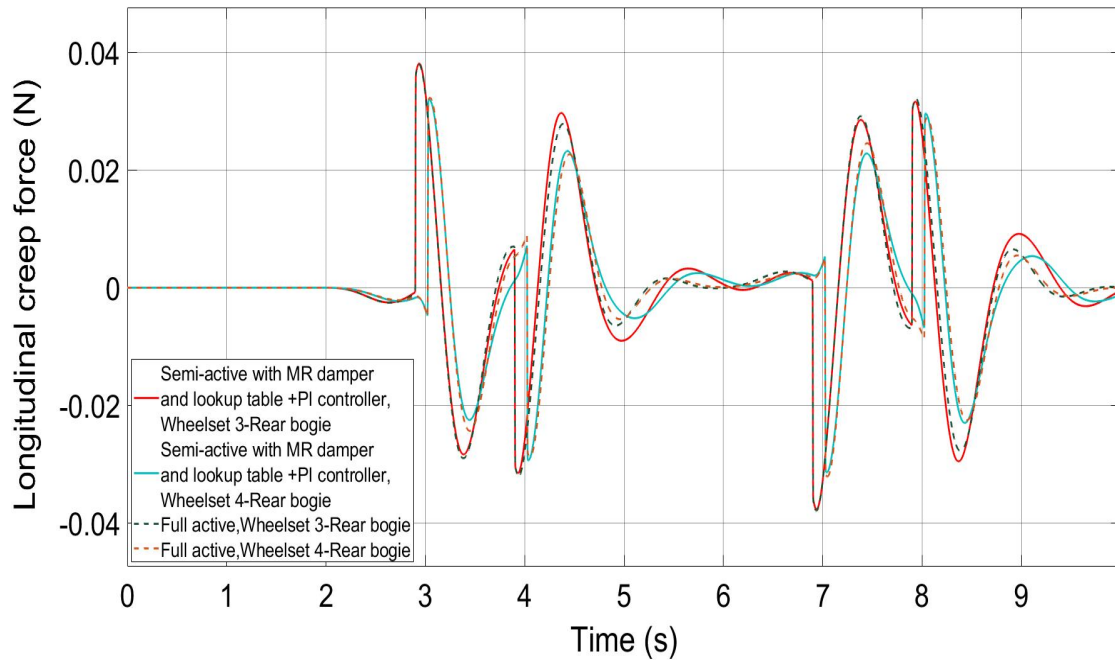


Figure 6-72- Bogie vehicle longitudinal creep force on curve track, 20 m/s- Rear bogie

Figures 6-73 to 6-76 show the control effort generated by the full active controller and semi-active controller in the front and rear bogie.

It is necessary for the control effort to balance the longitudinal creep force, as illustrated in figures 6-73 to 6-76. Furthermore, it is clear that controller force generated by the semi active controller follows the same pattern as that generated by the full active controller.

The maximum and minimum control force generated in the front bogie for the full active controller is ± 11.87 N at wheelset 1, ± 11.48 N at wheelset 2 and for the semi-active controller ± 11.997 N at wheelset 1 and ± 11.46 N at wheelset 2 and in the rear bogie for full active controller is ± 11.75 N at wheelset 3, ± 13.35 N at wheelset 4 and for semi-active controller ± 12.31 N at wheelset 3 and ± 12.101 N at wheelset 4 at speed of 83 m/s.

The maximum and minimum control force generated in the front bogie for full active and semi-active controller is ± 15.28 N at wheelset 1, ± 12.33 N at wheelset 2 subsequently in the rear bogie ± 12.3 N at wheelset 3, ± 1.1 N at wheelset 4 for full active controller and ± 13.4 N at wheelset 3 and ± 12.5 N at wheelset 4 for semi-active controller at speed of 20 m/s.

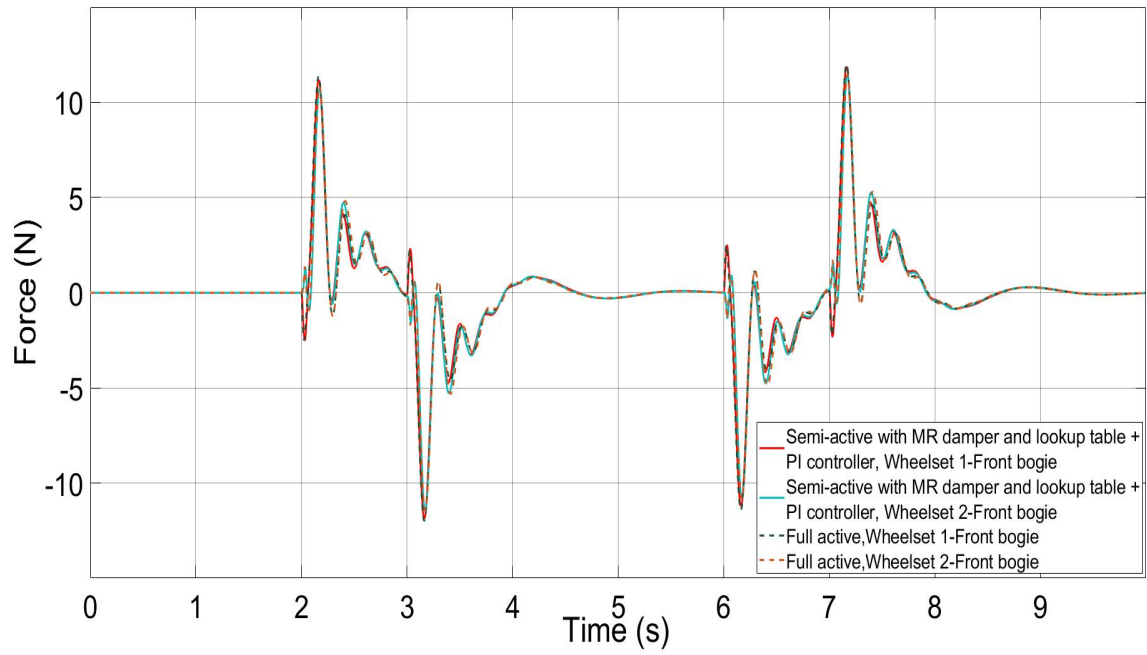


Figure 6-73- Bogie vehicle control force on curved track, speed 83.3 m/s- Front bogie

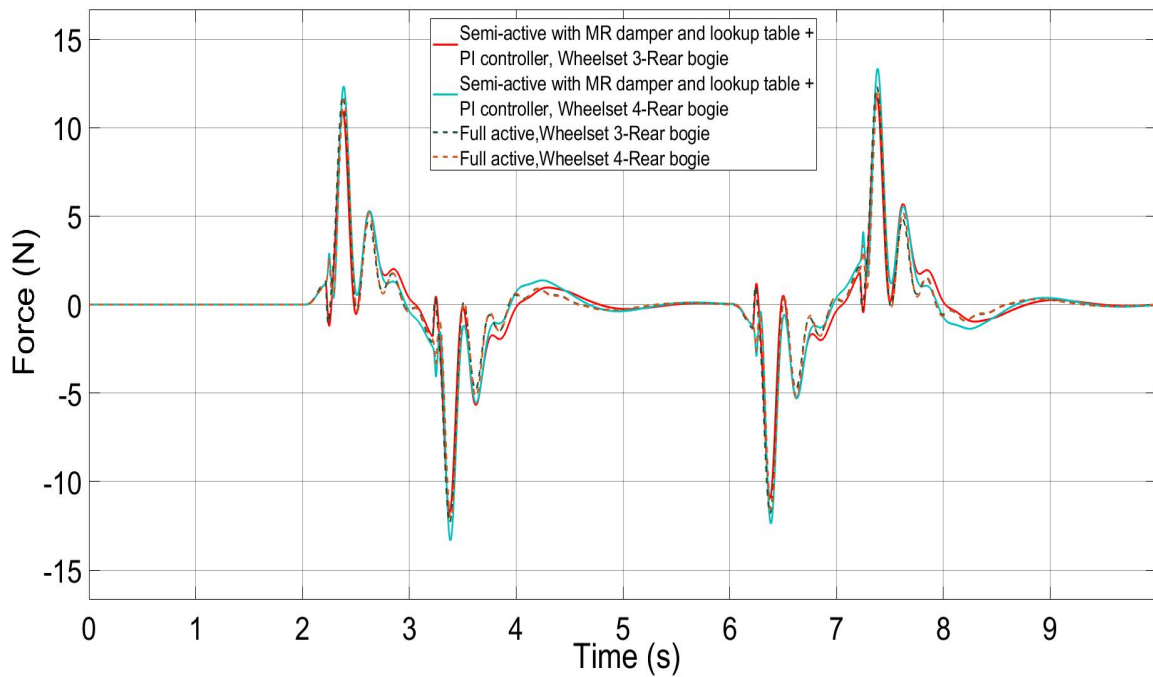


Figure 6-74- Bogie vehicle control force on curved track, speed 83.3 m/s- Rear bogie

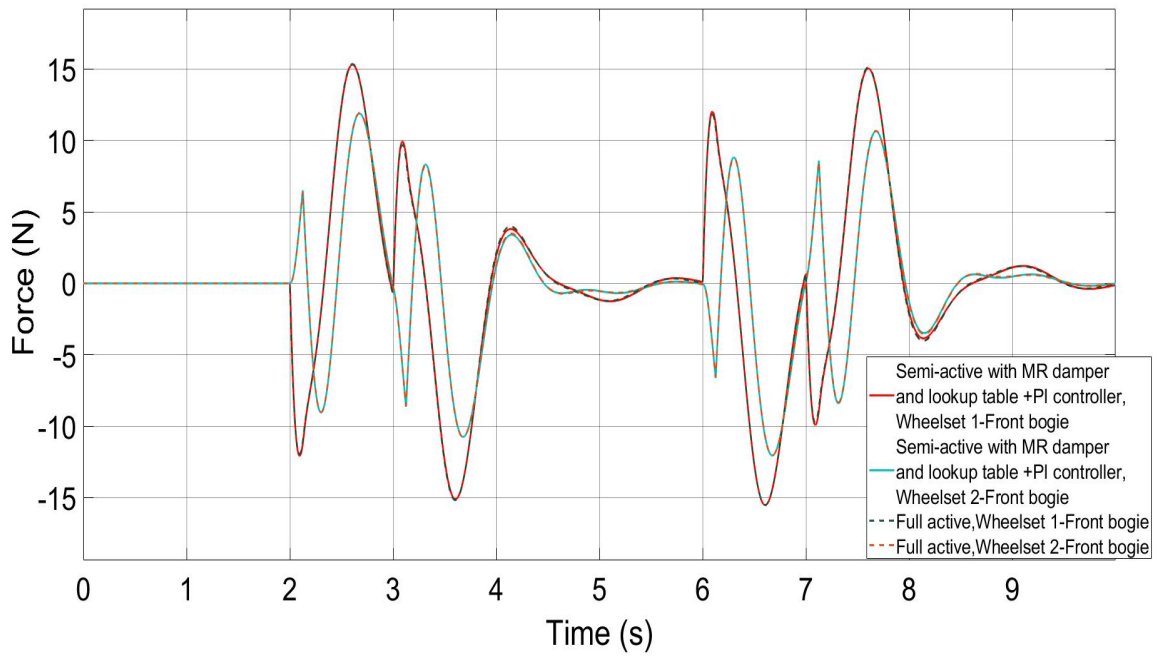


Figure 6-75- Bogie vehicle control force on curved track, speed 20 m/s- Front bogie

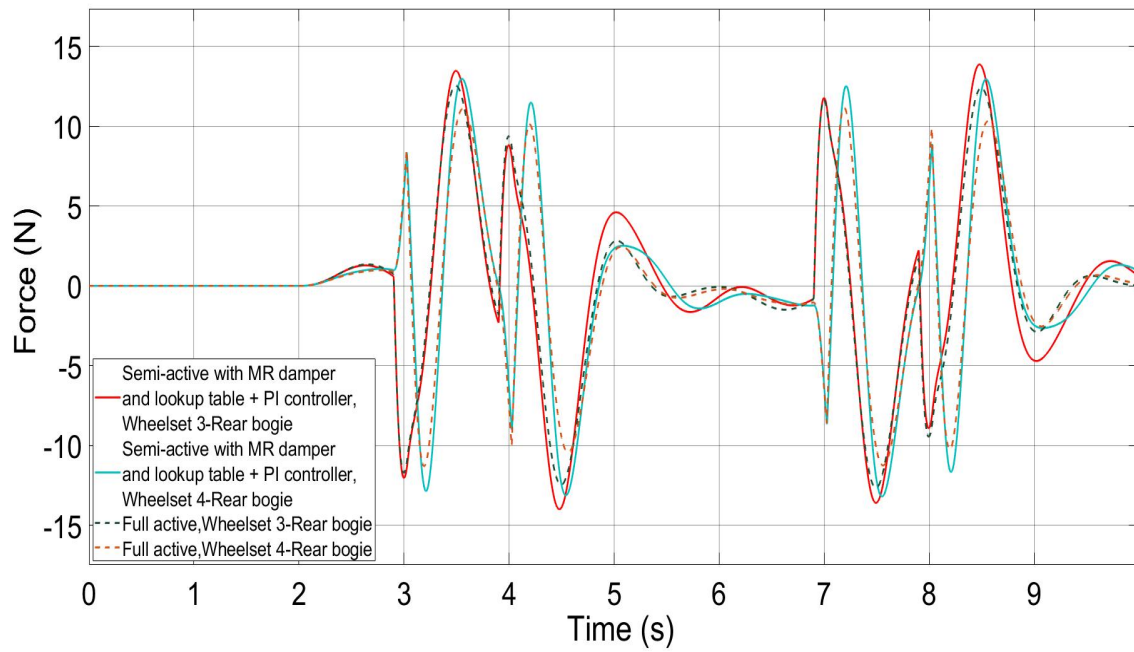


Figure 6-76- Bogie vehicle control force on curved track, speed 20 m/s- Rear bogie

Figures 6-77 to 6-80 illustrate the control power generated by the full active controller and semi-active controller in the front and rear bogie.

As shown in the figures, the control power is nearly zero when the vehicle is travelling on the steady curved of the track. From the figures, it is clear that the both controllers only dissipate the energy from the wheelset and therefore there is no need of provide any extra energy.

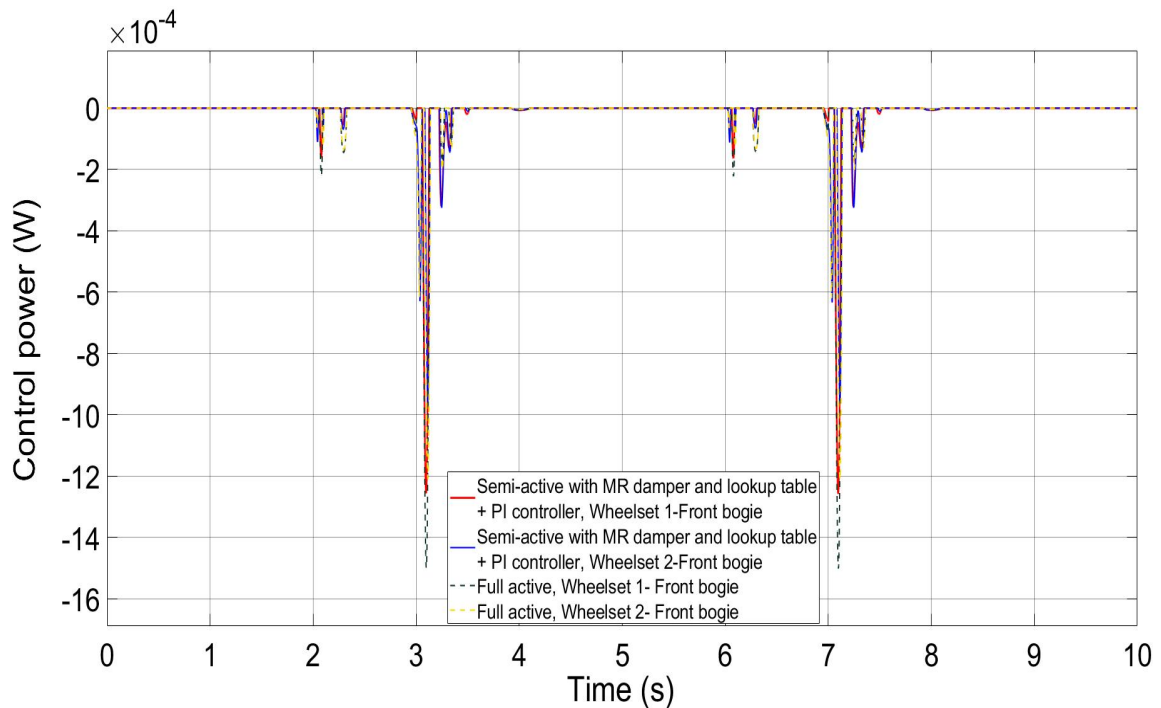


Figure 6-77- Bogie vehicle control power on curved track, speed 83.3 m/s- Front bogie

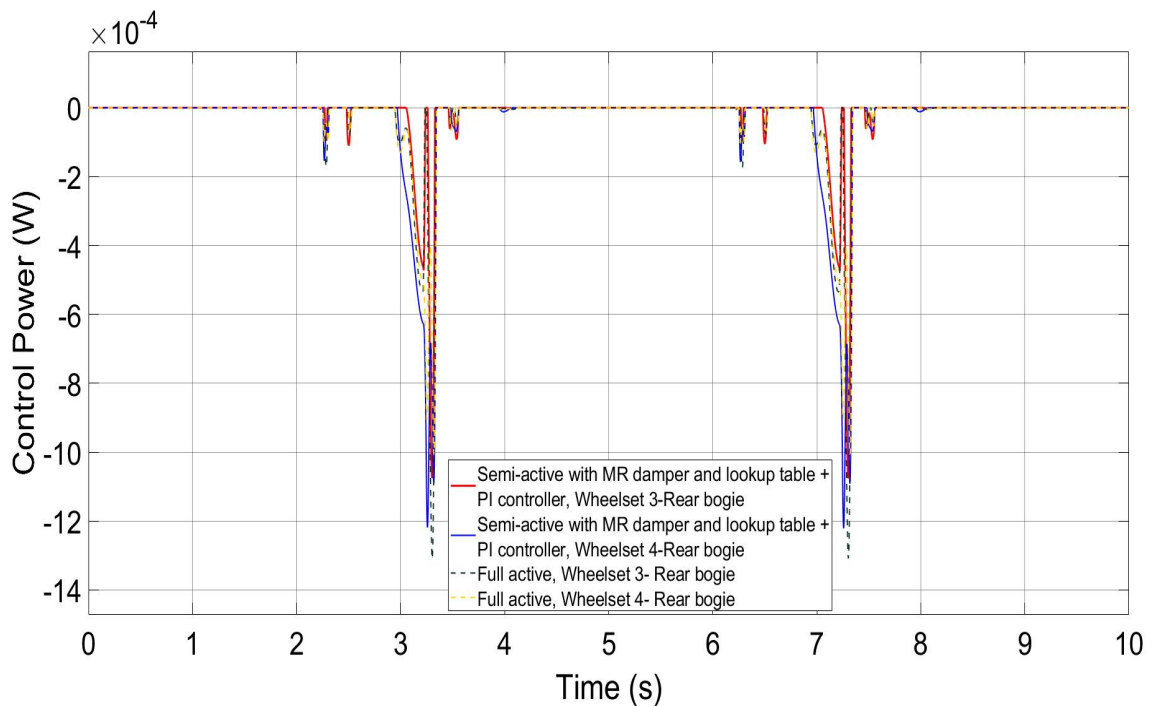


Figure 6-78- Bogie vehicle control power on curved track, speed 83.3 m/s- Rear bogie

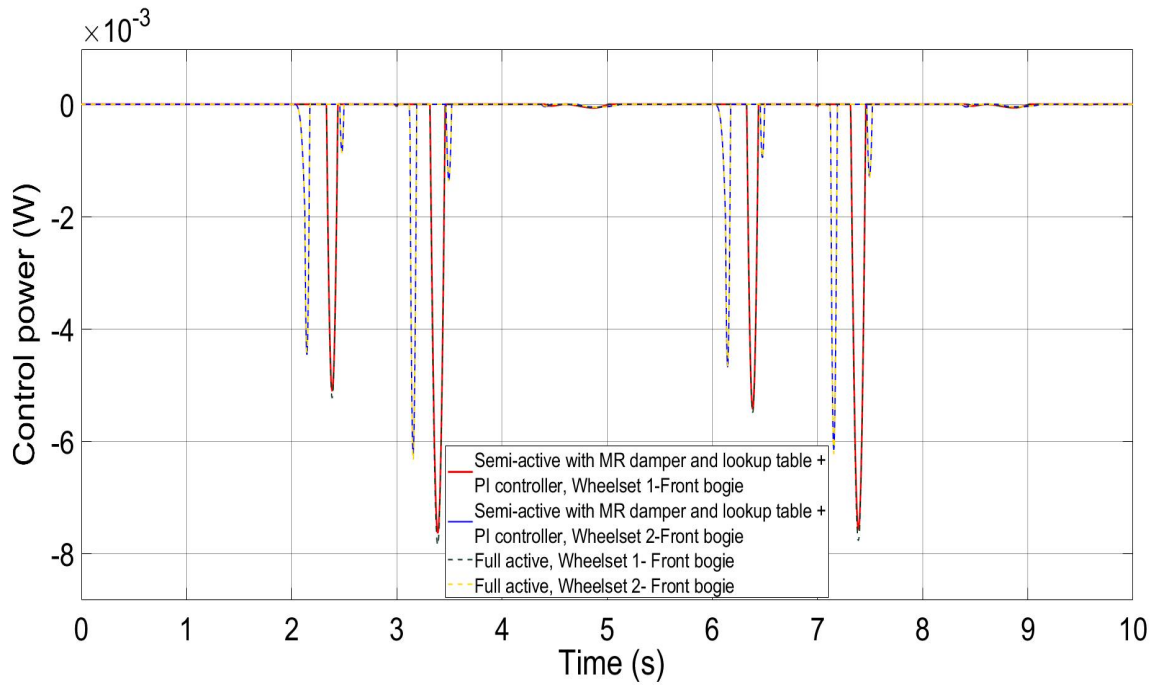


Figure 6-79- Bogie vehicle control power on curved track, speed 20 m/s- Front bogie

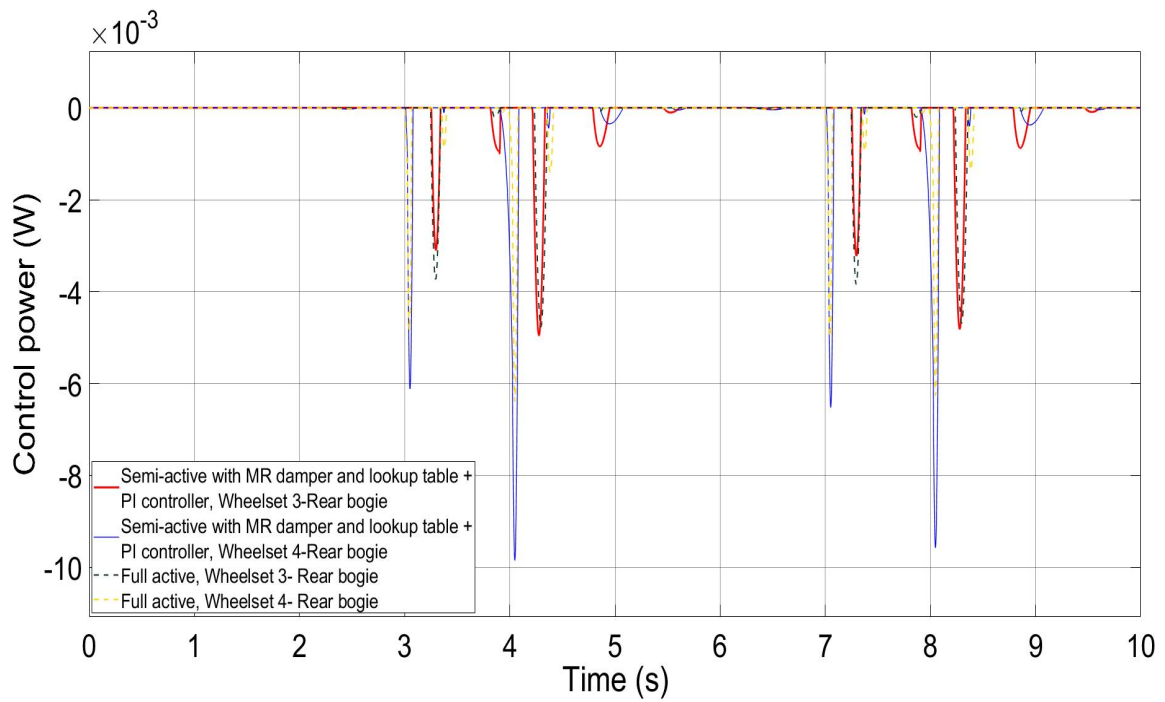


Figure 6-80- Bogie vehicle control power on curved track, speed 20 m/s- Rear bogie

6.4.2 Straight Track with Track Irregularities (Generic Track Data Irregularity)

This section presents the simulation results of the bogie vehicle at 83 m/s using generic random track input. Similar to the previous sections, the angle of attack, lateral deflection, lateral creep force, longitudinal creep force, control force, control power and torque for the front and rear wheelsets are presented.

Figures 6-81 and 6-82 show the angle of attack for active controller and semi-active controller in the front and rear bogie. As shown in the figures, the angle of attack for semi-active controller is very similar to the result of full active controller with the time delay between wheelsets/bogies.

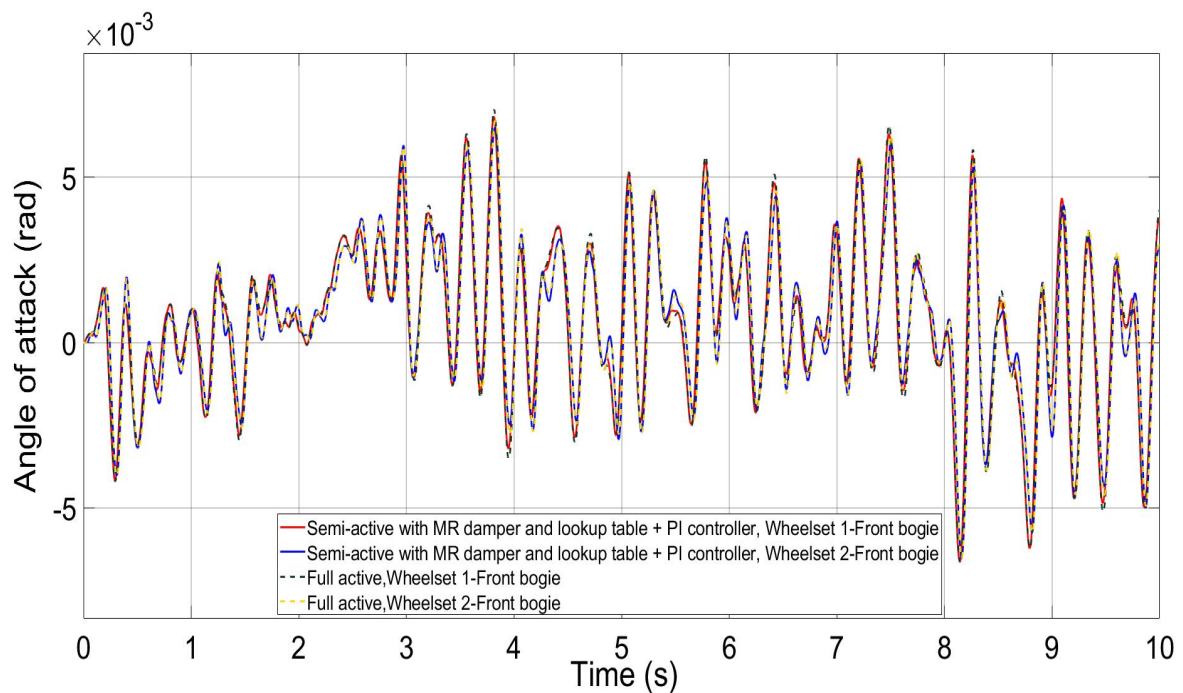


Figure 6-81- Bogie vehicles angle of attack on computer generic track, 83 m/s- Front bogie

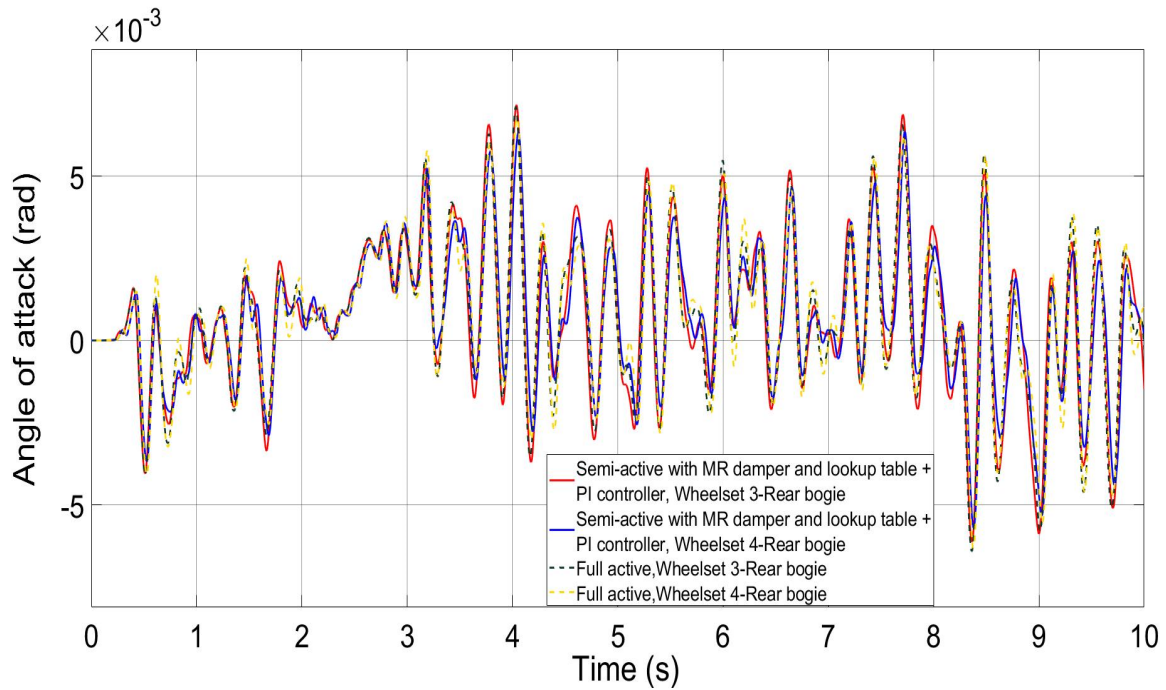


Figure 6-82- Bogie vehicles angle of attack on computer generic track, 83 m/s- Rear bogie

Figures 6-83 and 6-84 display the lateral deflections for active controller and semi-active controller in the front and rear bogie. The results show that the semi active controller lateral displacement is very close to the result of full active controller with delay between the wheelsets with the peak less than 10mm, i.e., within the flange contact limits.

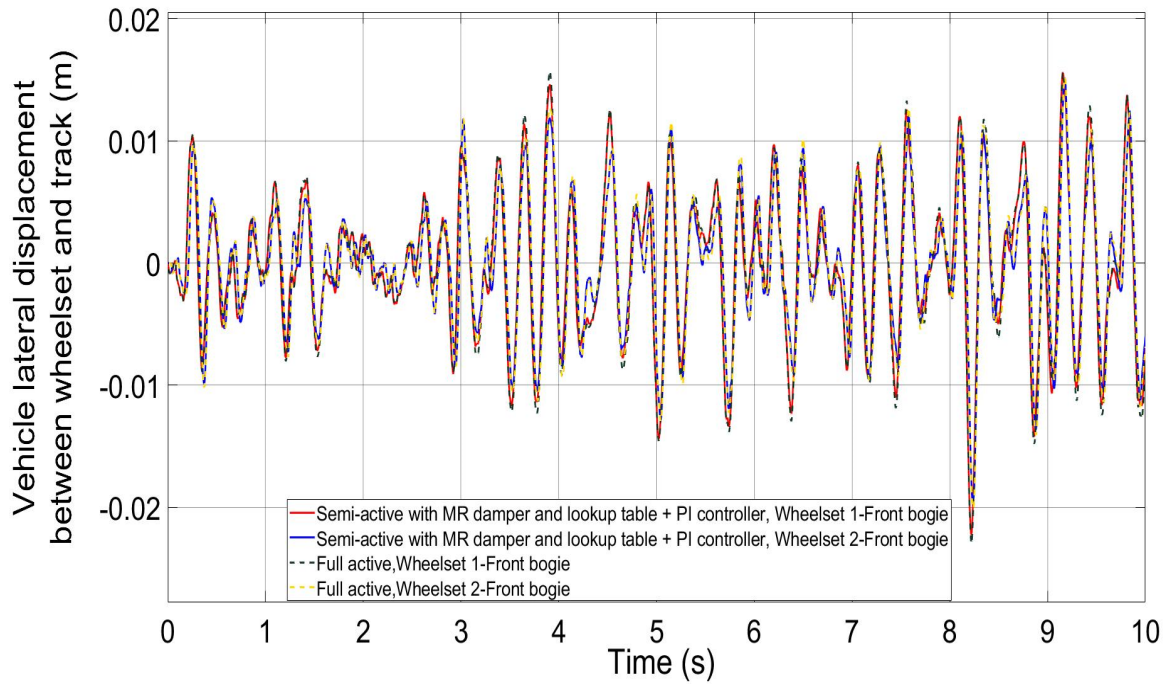


Figure 6-83- Bogie vehicles lateral displacement between wheelset and track on computer generic track, 83 m/s- Front bogie

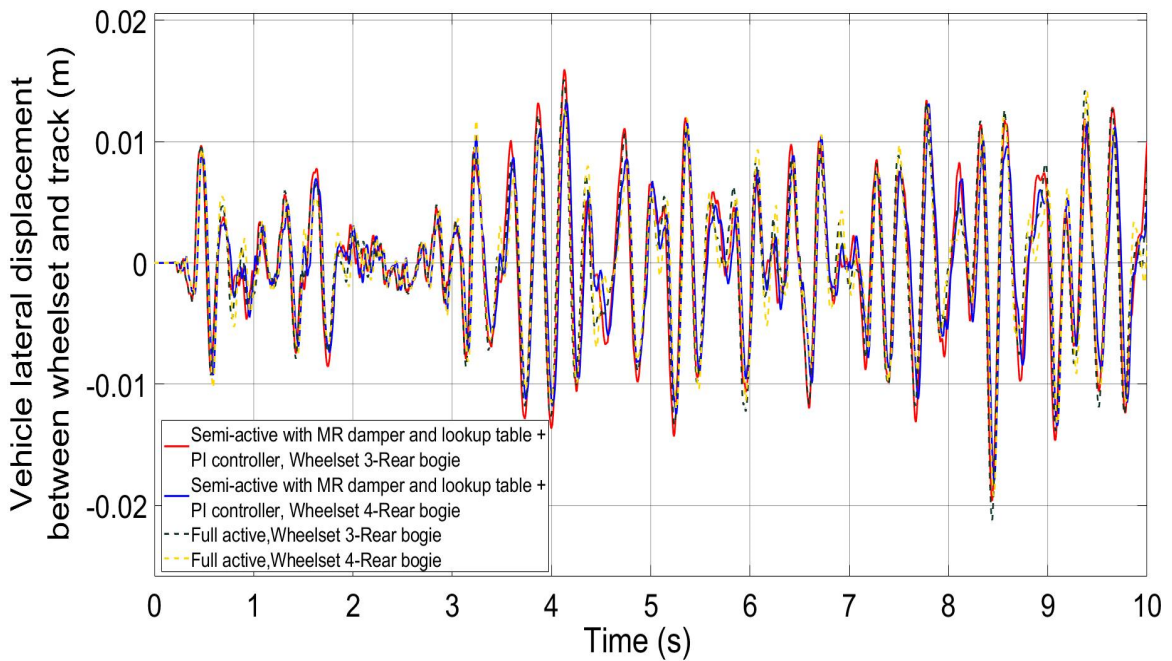


Figure 6-84- Bogie vehicles lateral displacement between wheelset and track on computer generic track, 83 m/s- Rear bogie

Figures 6-85 and 6-86 illustrate the lateral creep forces for the active controller and semi-active controller in the front and rear bogie. The angle of attack and the lateral velocity of the wheelset are the reason of lateral creep forces, but the lateral creep force is more effected by the angle of attack rather than the lateral velocity.

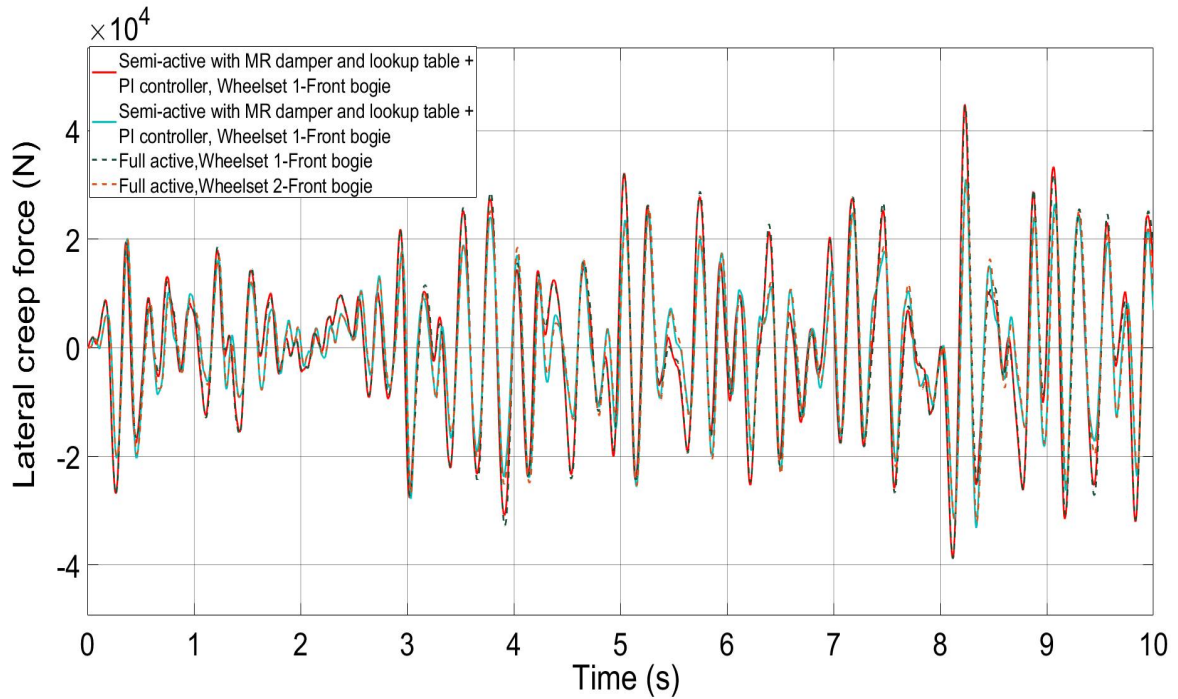


Figure 6-85- Bogie vehicles lateral creep force on computer generic track, 83 m/s- Front bogie

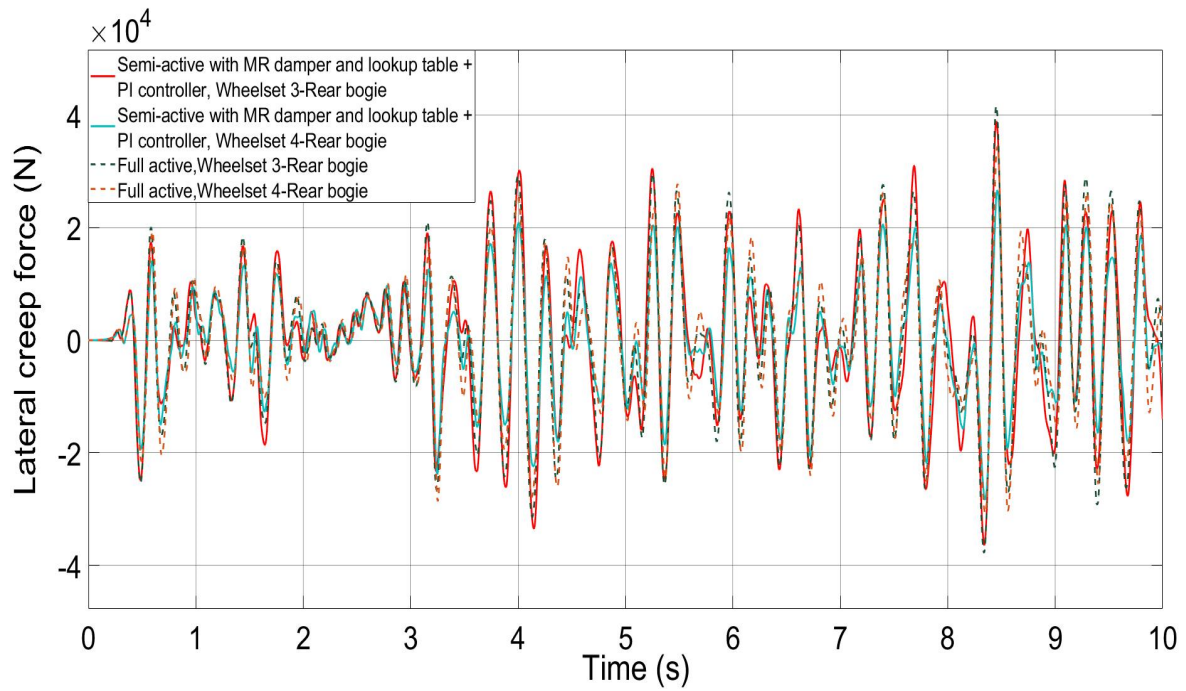


Figure 6-86- Bogie vehicles lateral creep force on computer generic track, 83 m/s- Rear bogie

Figures 6-87 and 6-88 demonstrate the longitudinal creep forces for the active controller and semi-active controller in the front and rear bogies. The longitudinal creep force for the front and rear bogie has a similar pattern. The longitudinal creep force is mainly caused by the lateral displacement between wheelset and the yaw velocity of the wheelset.

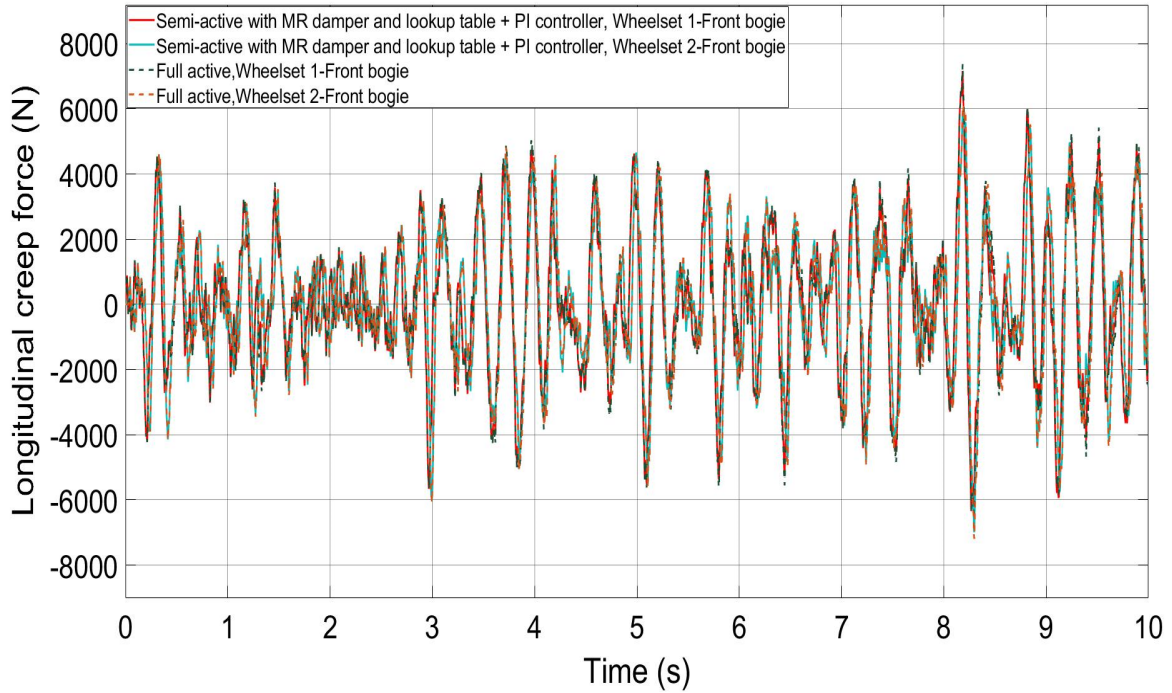


Figure 6-87- Bogie vehicles longitudinal creep force on computer generic track, 83 m/s-
Front bogie

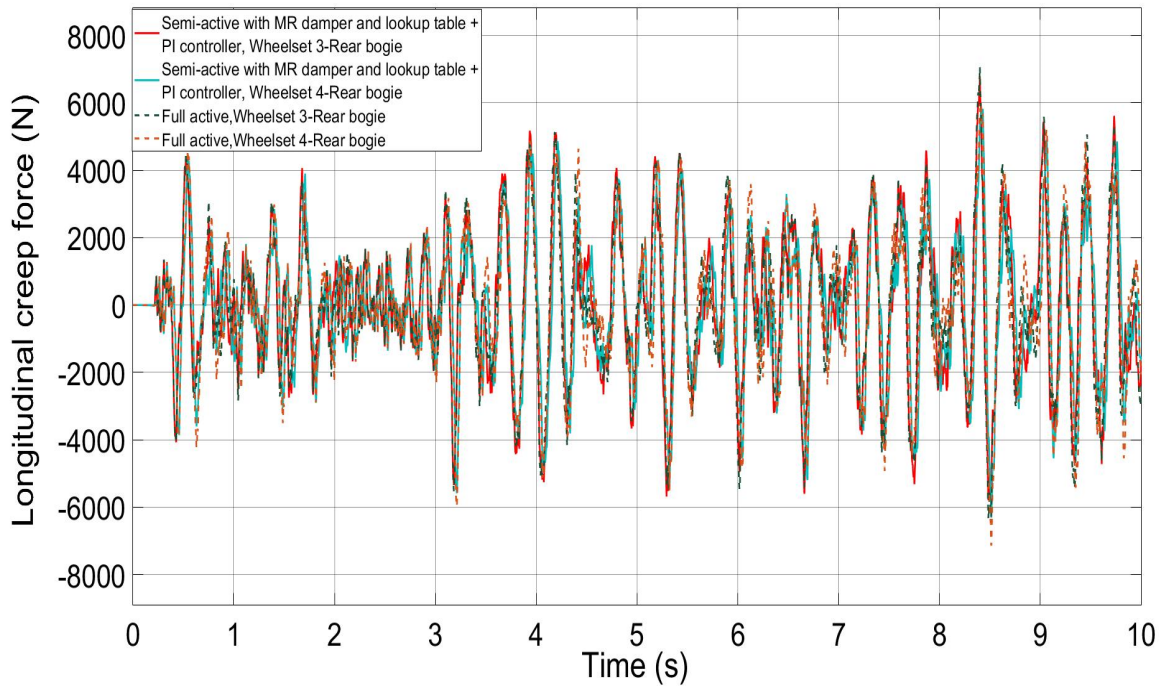


Figure 6-88- Bogie vehicles longitudinal creep force on computer generic track, 83 m/s-
Rear bogie

Figures 6-89 and 6-90 show the control forces generated by the active controller and semi-active controller in the front and rear bogie.

The results show that the force generated by the semi active controller matches well with that generated by the full active controller.

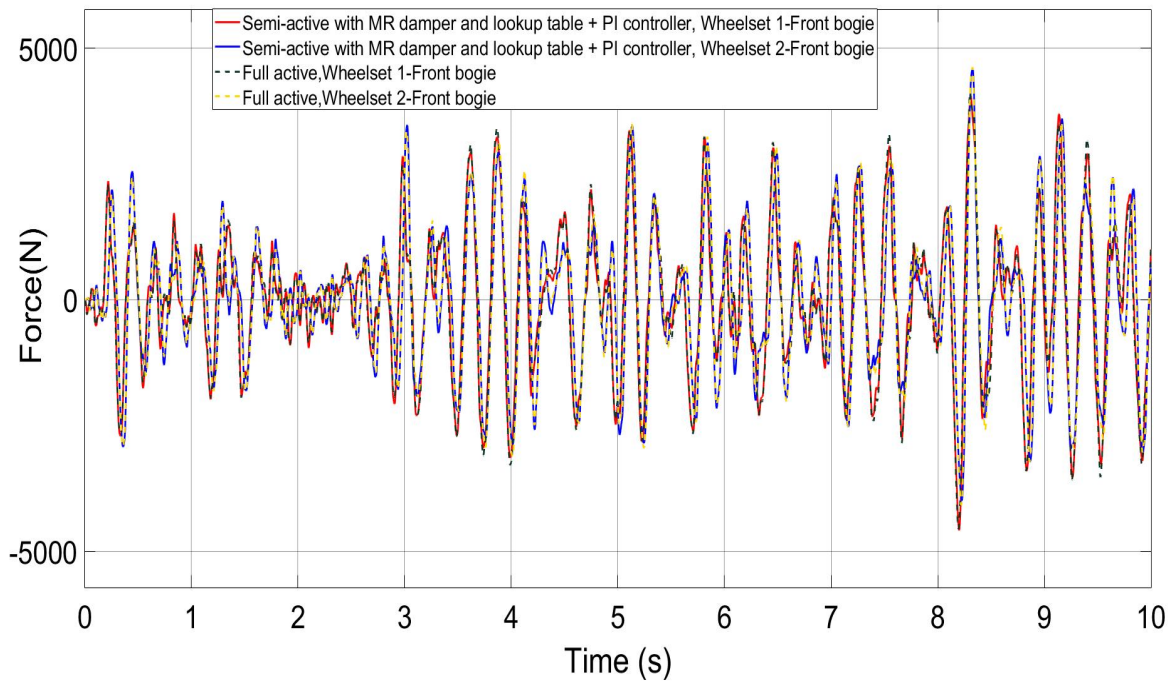


Figure 6-89- Bogie vehicles control force on computer generic track, 83 m/s- Front bogie

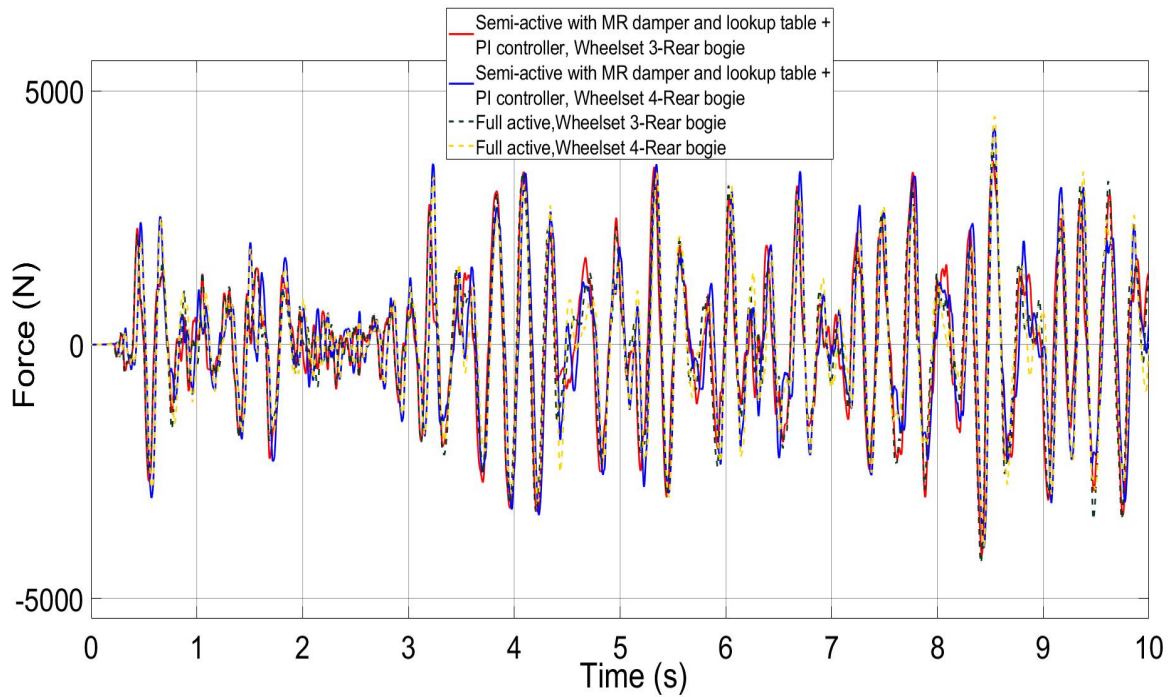


Figure 6-90- Bogie vehicles control force on computer generic track, 83 m/s- Rear bogie

Figures 6-91 and 6-92 illustrate the control powers for the full active controller and semi-active controller in front and rear bogie. It shows that the power generated by the semi active controller is almost slightly less than full active control power however sometime can be larger than active control power. Though, the most important point is both controllers only dissipate the energy from the wheelset and there is no requirement to provide any additional energy.

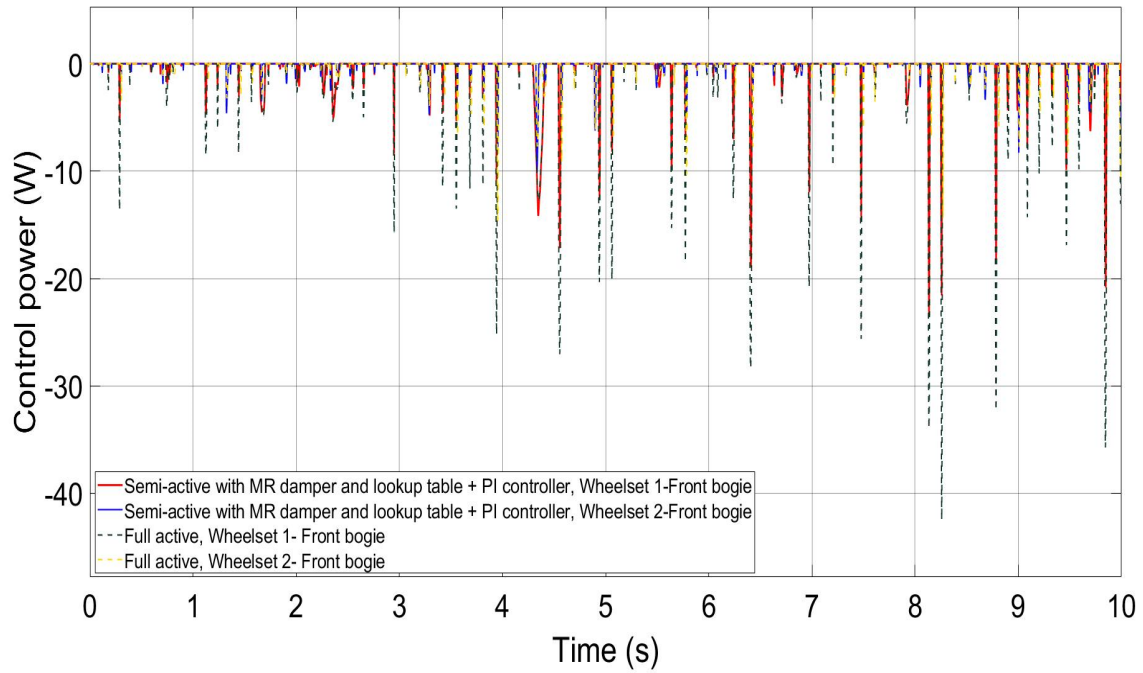


Figure 6-91- Bogie vehicles control power on computer generic track, 83 m/s- Front bogie

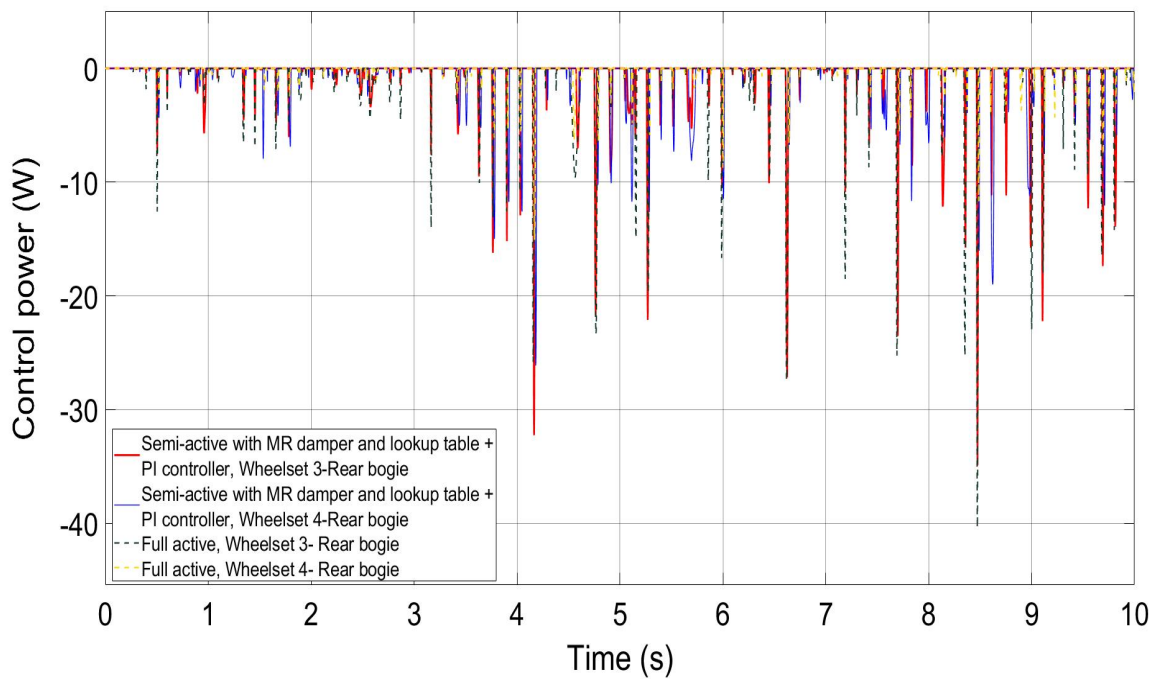


Figure 6-92- Bogie vehicles control power on computer generic track, 83 m/s- Rear bogie

6.4.3 Straight Track with Irregularity (Measured Track Data)

This section presents the simulation results of the bogie vehicle at 50 m/s using the Measured Track Data.

Figures 6-93 and 6-94 show the angles of attack for active controller and semi-active controller in the front and rear bogies. The angle of attack in the full active controller is marginally higher than angle of attack in semi-active controller.

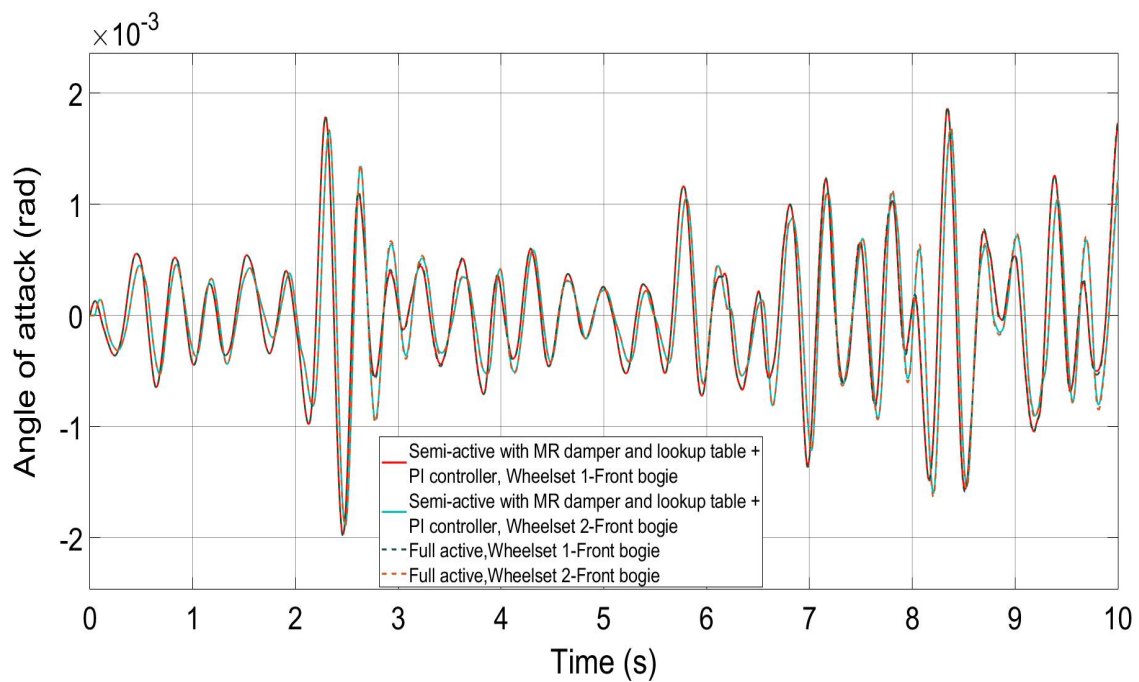


Figure 6-93- Bogie vehicles angle of attack on measured track, 50 m/s- Front bogie

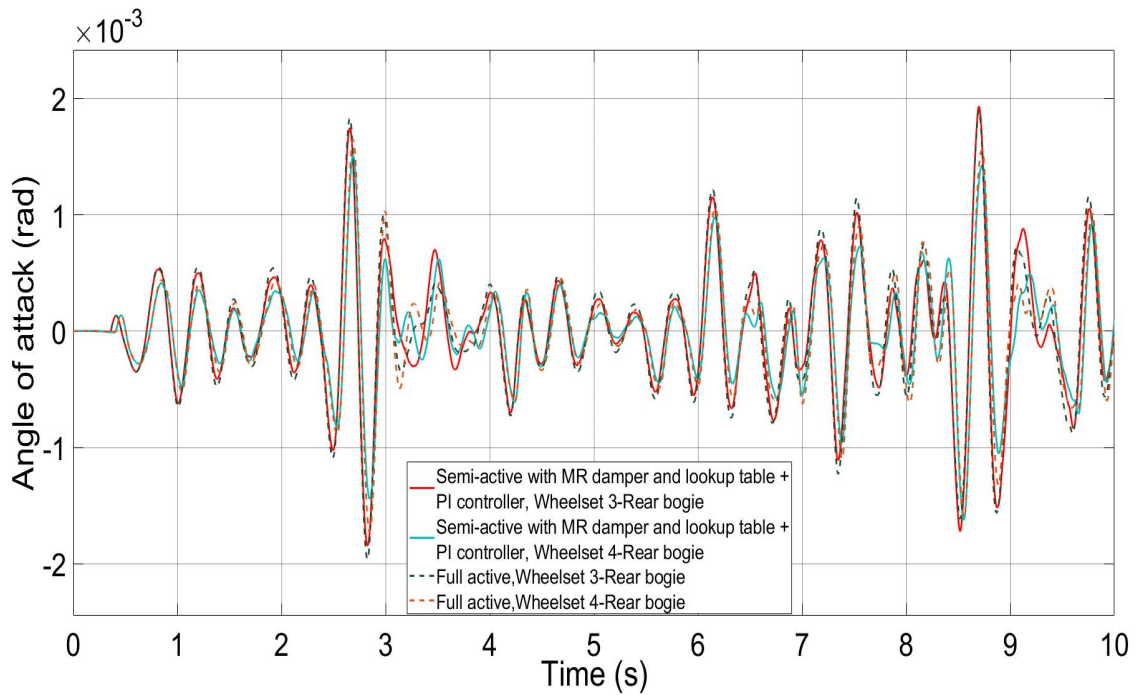


Figure 6-94- Bogie vehicles angle of attack on measured track, 50 m/s- Rear bogie

Figures 6-95 and 6-96 show the lateral displacements between the wheelset and track for the active controller and semi-active controller in the front and rear bogies. The semi-active controller appears to present better track following ability than the full active controller, though in both cases, the lateral displacements are well within the flange clearance.

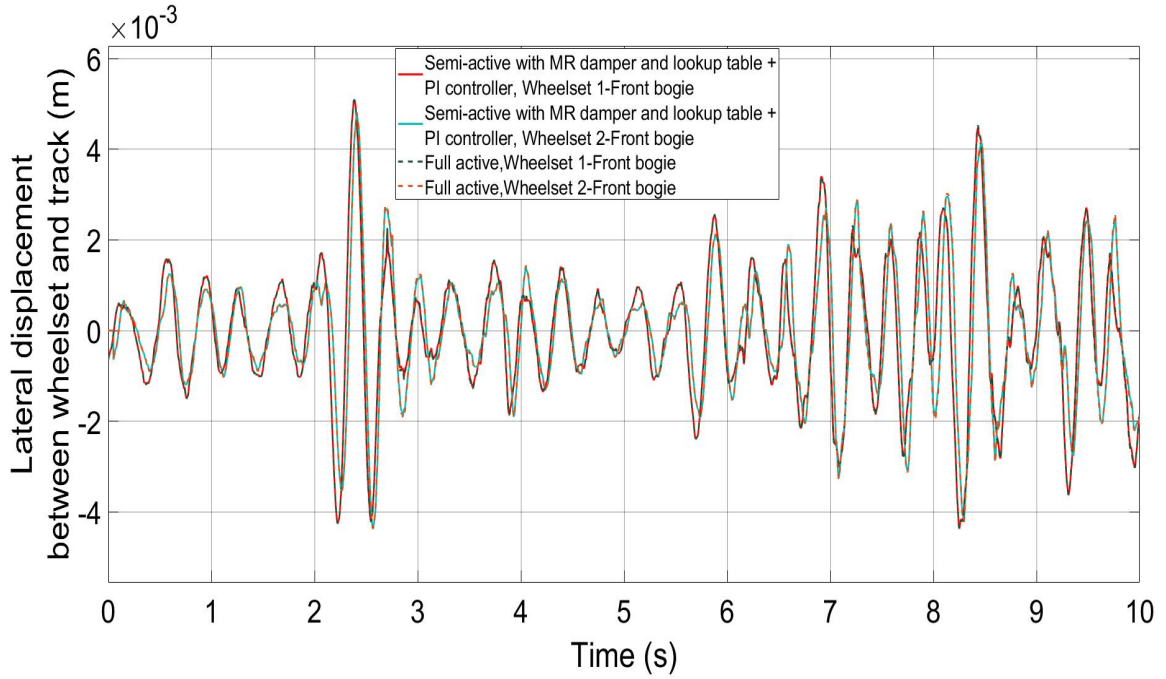


Figure 6-95- Bogie vehicles lateral displacement between wheelset and track on measured track, 50 m/s- Front bogie

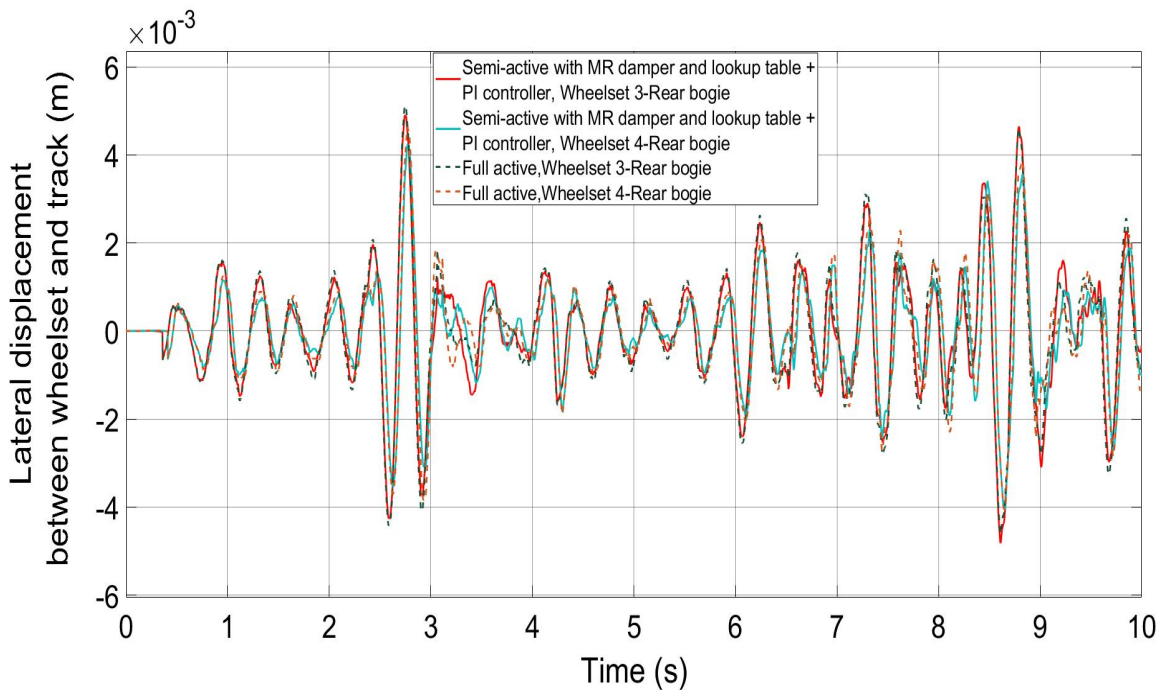


Figure 6-96- Bogie vehicles lateral displacement between wheelset and track on measured track, 50 m/s- Rear bogie

Figures 6-97 and 6-98 show the lateral creep forces for the active controller and semi-active controller in the front and rear bogies. The values of the lateral creep force for front and rear bogies have a very similar pattern, as the wheelsets lateral displacement and angle of attack behaviour are very similar in response to track irregularities.

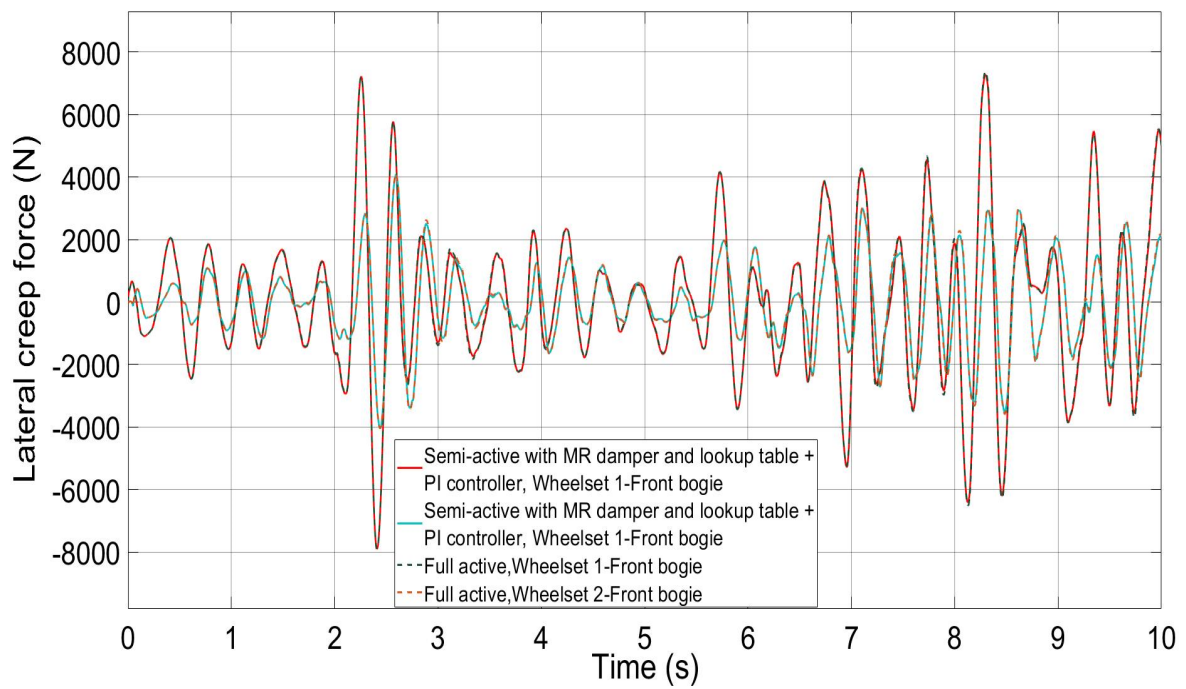


Figure 6-97- Bogie vehicles lateral creep force on measured track, 50 m/s- Front bogie

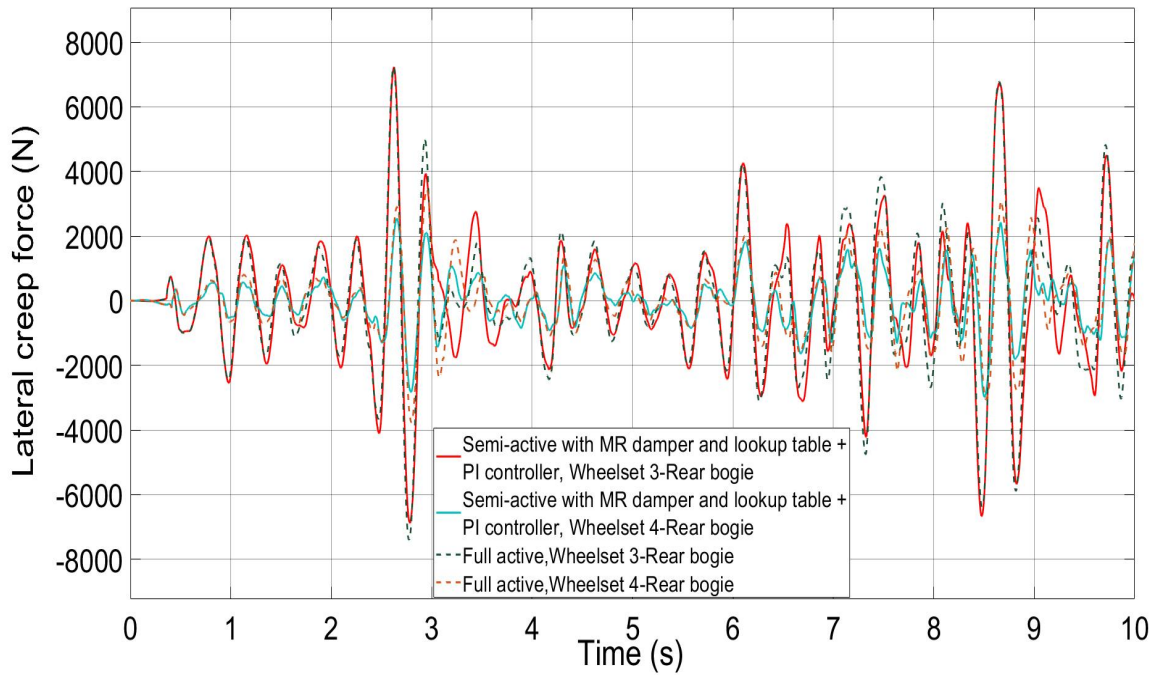


Figure 6-98- Bogie vehicles lateral creep force on measured track, 50 m/s- Rear bogie

Figures 6-99 and 6-100 show the longitudinal creep forces for the active controller and semi-active controller in the front and rear bogies. As shown in figures, the longitudinal creep forces for the front and rear bogies have comparable patterns. The longitudinal creep force is mostly caused by the lateral displacement between wheelset and the yaw velocity of the wheelset. The assessment of the creep forces is important because both lateral and longitudinal creep forces have effect on the control torque. Also, as it mentioned in section 6.3.3, the spike in the start is due to the track lateral displacement in the measured track data has a non-zero initial value.

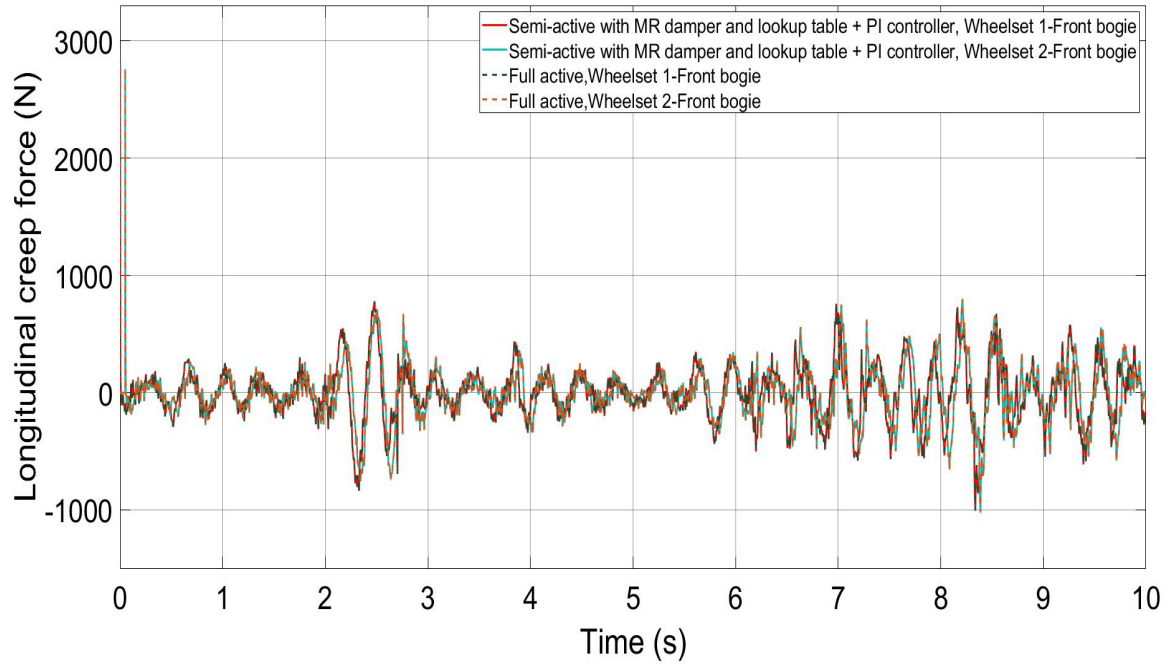


Figure 6-99- Bogie vehicles longitudinal creep force on measured track, 50 m/s- Front bogie

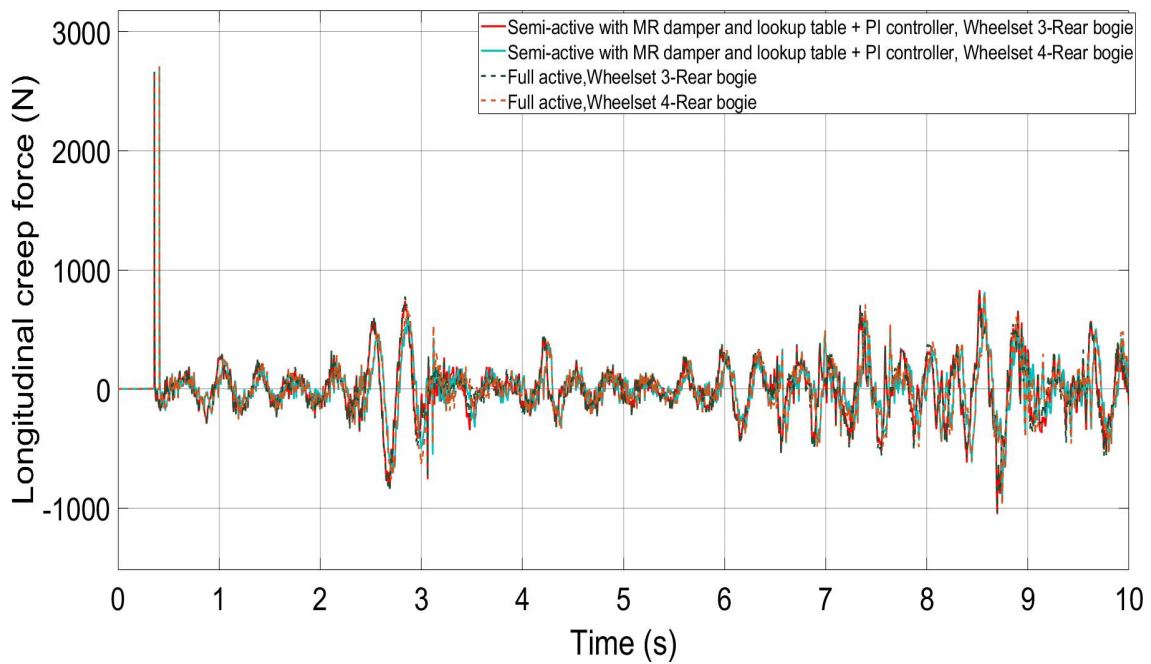


Figure 6-100- Bogie vehicles longitudinal creep force on measured track, 50 m/s- Rear bogie

Figures 6-101 and 6-102 show the control forces generated by the active controller and semi-active controller in the front and rear bogies. As it shows in the figures, the semi-active control is able to produce the control forces very similar to that in the active controller.

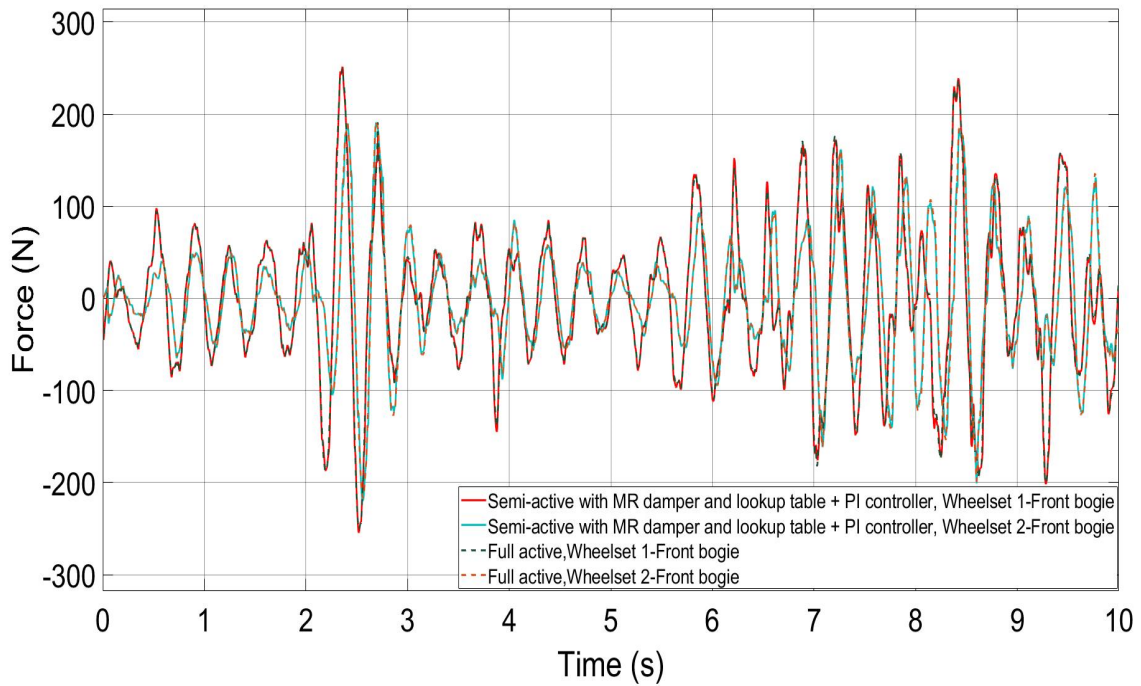


Figure 6-101- Bogie vehicles control force on measured track, 50 m/s- Front bogie

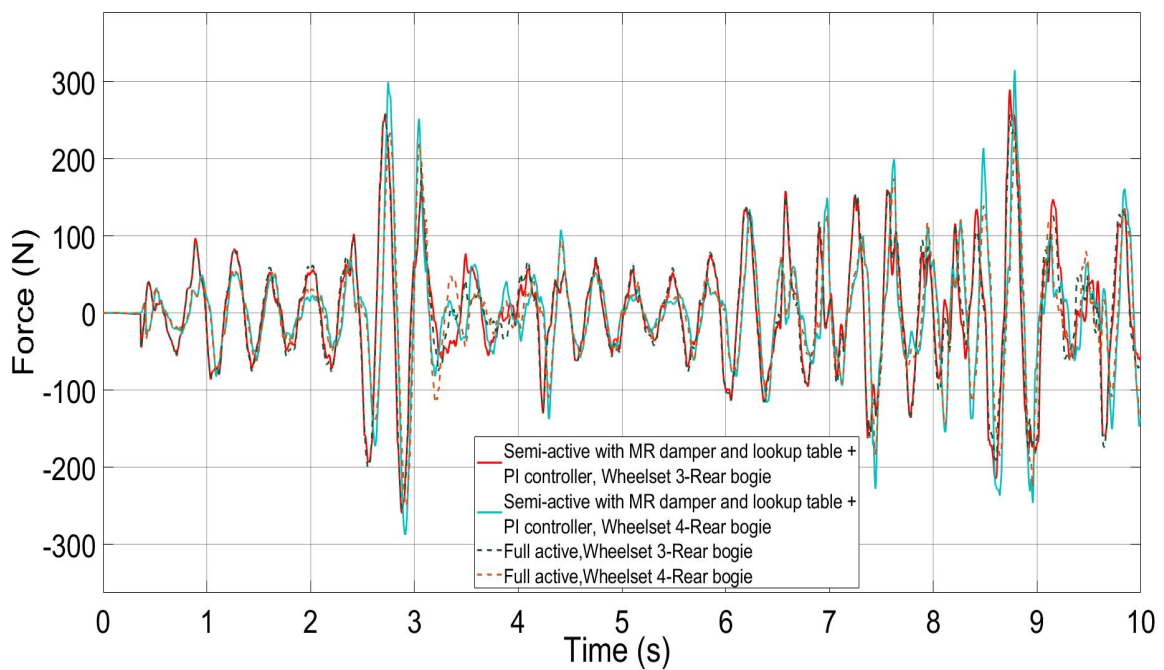


Figure 6-102- Bogie vehicles control force on measured track, 50 m/s- Rear bogie

Figures 6-103 and 6-104 show the control powers for the active controller and semi-active controller in the front and rear bogies. It is clear that like the earlier cases, both controllers dissipate the energy only on the real track.

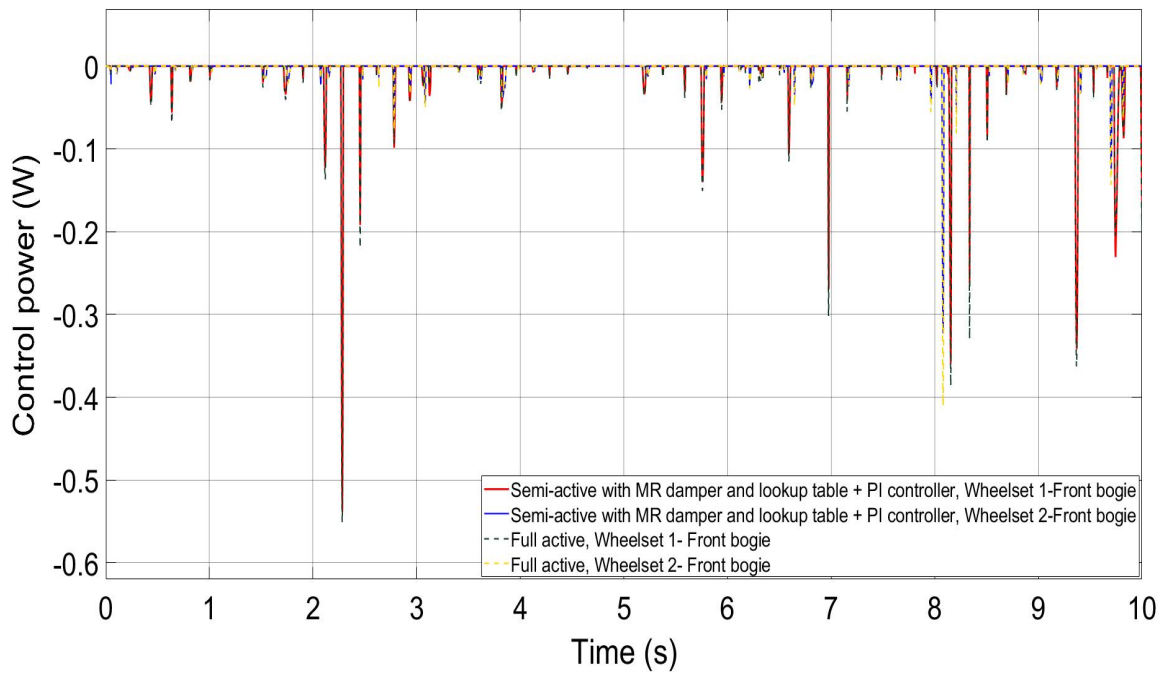


Figure 6-103- Bogie vehicles control power on measured track, 50 m/s- Front bogie

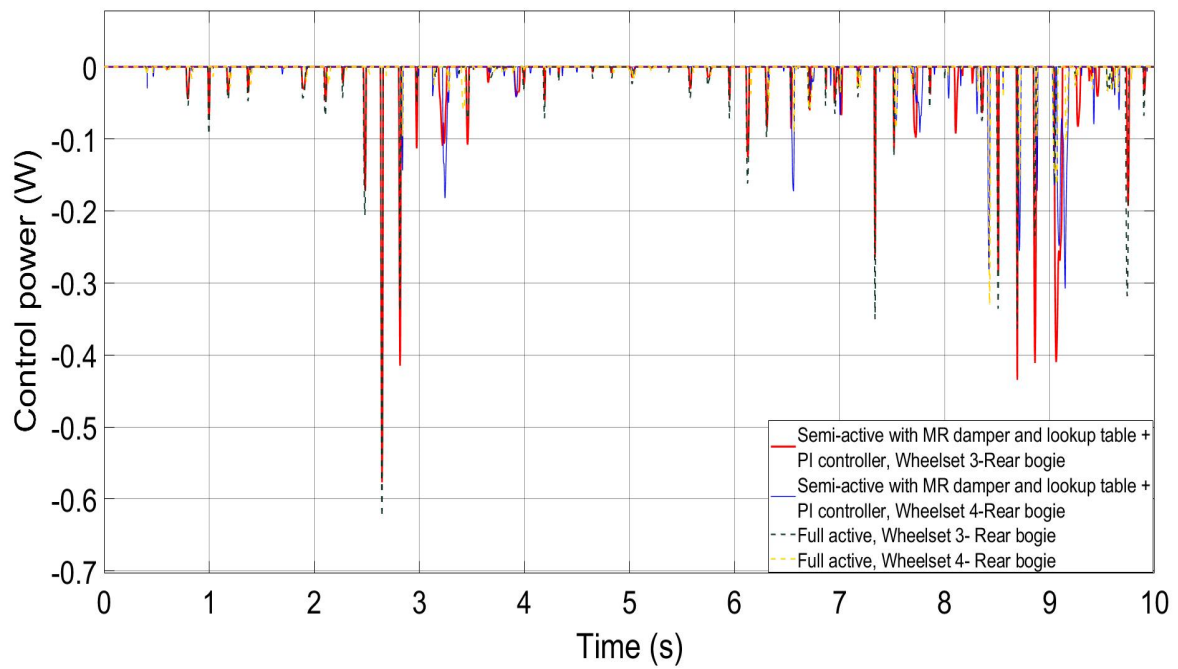


Figure 6-104- Bogie vehicles control power on measured track, 50 m/s- Rear bogie

Tables 6-1 and 6-2 Provide a quantitative performance evaluation of semi-active controller with use of MR damper and look up table for different scenarios simulated in this study.

Table 6-1- Quantitative performance evaluations for Two axle vehicles

Two-axle Vehicles	Curve Track 83 m/s	Curve Track 20 m/s	Straight track with Track Irregularities 83 m/s	Straight track with Irregularities 50 m/s
Angle of attack, front wheel	-7.7×10^{-4} (rad)	-7.6×10^{-4} (rad)	5.9×10^{-3} (rad)	0.86×10^{-3} (rad)
Lateral displacement between wheelset and track, front wheel	4.2×10^{-4} (m)	8.8×10^{-3} (m)	0.0086 (m)	3×10^{-3} (m)
Lateral creep force, front wheel	-15420 (N)	-15940 (N)	1.82×10^4 (N)	2900 (N)
Longitudinal creep force, front wheel	14.52 (N) Max -11.4 (N) Min	41.68 (N) Max -40.74 (N) Min	4640 (N)	500 (N)
Active Control force, front wheel	9.526 (N) Max -12 (N) Min	31.47 (N) Max -32.32 (N) Min	3000 (N)	315 (N)
Active control power, front wheel	-12.6×10^{-3} (W)	-0.143 (W)	-610 (W)	-10 (W)

Table 6-2- Quantitative performance evaluations for Bogie vehicles

Bogie Vehicles	Curve Track 83 m/s	Curve Track 20 m/s	Straight track with Track Irregularities 83	Straight track with Irregularities 50 m/s
Angle of attack, front wheel	-2.18×10^{-4} (rad)	-2.3×10^{-4} (rad)	5.9×10^{-3} (rad)	1.71×10^{-3} (rad)
Lateral displacement between wheelset and track, front wheel	0.49×10^{-3} (m)	8.7×10^{-3} (m)	0.014 (m)	4.8×10^{-3} (m)
Lateral creep force, front wheel	-4369N (N)	-4300 (N)	4.3×10^4 (N)	7050 (N)
Longitudinal creep force, front wheel	15.47 (N) Max -15.47 (N) Min	26.8 (N) Max -26.8 (N) Min	6890 (N)	869 (N)
Active Control force, front wheel	11.99 (N) Max -11.99 (N) Min	15.28 (N) Max -15.28 (N) Min	4120 (N)	253 (N)
Active control power, front wheel	-12.4×10^{-4} (W)	-7.8×10^{-3} (W)	-24 (W)	-0.55 (W)

6.5 Summery

This chapter has carried out a comprehensive evaluation on the proposed semi-active scheme for the stability and guidance control of railway wheelsets and compared with the full active control using computer simulations.

Two different vehicle configurations (a two-axle vehicle, and a conventional bogie vehicle) and different track conditions (curve track at speed of 83m/s and 20 m/s, straight track with irregularity at speed of 83m/s and measured track at speed of 50 m/s) are included. The control scheme used in the simulation include the semi-active control laws, the MR damper and also, the local control of the MR damper. The results show that the semi-active controller can perform as well as the active controller.

Chapter 7: Conclusions and future work

7.1 Conclusions

This research has focussed on the development of a semi active control strategy for the primary suspensions for independently rotating wheelset, with the main objective to improve guidance and ride stability.

A literature review was first carried out to study the previous work and to establish a fundamental understanding of railway wheelset dynamics, railway vehicle suspensions, the concepts of active control and semi active control studies. Active technology in rail vehicles is categorised into two main classes: the first is the primary active suspension, which improves running stability and/or wheelset guidance; and the second is the active secondary suspension, which helps to improve passenger ride comfort.

From the literature review, with the application of a full-active control suspension system, levels of dynamic performance can be obtained that are not possible with a passive suspension system.

Practical issues have to be considered in the development of active suspension. For instance, the controller developed must be robust against parameter variations, some feedback signals are costly and problematic to measure and thus it ultimately becomes essential to use alternative and cheaper methods.

In dynamic models of railway vehicles, the order is high, and the system is very interactive between different motions. Hence, some form of dynamic simplification needs to be employed in the development of active control systems. The trade-off between curving and stability is a particularly critical issue, where the main benefits are expected to result through the use of semi-active solutions. The performance of the lateral secondary suspension in a high-speed railway vehicle is more important than in conventional railway vehicles in terms of both comfort and stability.

Most semi-active control strategies are fixed structure controls and are based on matching the force demanded to the extent this is feasible within the limits imposed by the minimum and

maximum damper settings. These limitations restrict the performance of semi-active suspension systems. Therefore, the literature review led to the identification of knowledge gaps and potential research topics for this study.

This was followed by the development of the mathematical models representing the single independently rotating wheelsets, the Two-Axle Vehicle with Independently Rotating Wheelsets and conventional bogie railway vehicle and the implementation of the models in the MATLAB Simulink platform. Also, a mathematical model of the modified Bouc-Wen model (prototype of magnetorheological dampers) was developed to represent the dynamic behaviour of a magnetorheological dampers.

The models were then used to design and fine-tune the active controllers. An analysis of the power requirements of such active control approaches was also completed leading to the development of the semi-active control strategy for independently rotating wheelsets in the next step. MR dampers are used as the control device for the proposed semi-active control. However, a controller is essential to control current in order for MR dampers to generate the desired force. Due to complexity of mathematical models and highly nonlinear magnetorheological damper inverse model method has been used as a local magnetorheological damper controller. The technique used in this study for inverse model is Lookup table. The lookup table has been used to attain controlled current regarding to demanded damping force, the controlled current is fed to the magnetorheological damper.

This study followed up by model the full active steering control systems for independently rotating wheelset in MATLAB Simulink platform, based on measured relative rotation speed of the two wheels on the same axle, and the relative yaw velocity between the wheelset and vehicle body as the required feedback.

Next step shows the design details of a novel semi-active scheme for the control of independently rotating wheelsets (IRW) in railway vehicles, using magnetorheological (MR) dampers to provide the necessary stabilization and guidance control. Magnetorheological (MR) dampers are used to replace the actuators in the full active control, leading to a solution that would be cheaper in costs and smaller in size than the full active control systems. Because the semi-active control devices such as MR dampers can only dissipate energy, one of the keys focuses of the study is to develop and verify the control strategy that does not require the injection of power into the system in the provision of the stability control and

guidance/steering. To ensure that the MR dampers will produce the control force as demanded by the wheelset control, a lookup table for the inverse MR damper model is used in this study to obtain the control current according to the desired damping force, whereas a local PI control is also used to improve the robustness of the MR damper control. Computer simulations are used to demonstrate that the MR dampers with the combination of the local feedforward and feedback controls can produce the output forces in semi-active control conditions.

Finally, a comprehensive evaluation of the proposed semi-active controller was carried out by comparing the results of the semi active controller with the full active controller for both the two-axle vehicle and the conventional bogie vehicle. The performance of the semi-active control was assessed using a number of different track conditions including the irregularities and curved tracks at different operating speeds.

The key finding of the study is that the control of independently rotating wheelset for guidance and stability can be achieved without the need of power injection and the semi-active control scheme with the use of MR dampers proposed in this study has shown to perform as well as the full active control. For the two-axle vehicle and the conventional bogie vehicle used in the study, it has been demonstrated that the proposed control scheme is able to steer the wheelsets to follow the different curved and straight tracks and to avoid the undesirable flange contact that is often the case with the use of passive suspensions.

7.2 Further Work

Further research can focus on the use of different types of variable damper, comparisons could be drawn against the performance of the MR damper.

Hydraulic servo system, variable stiffness system or Electrorheological (ER) dampers are examples of variable dampers which could be implemented in the system and compared with MR damper.

Furthermore, future study can focus on use of a more comprehensive vehicle model (to include all other motions and non-linear properties of wheel-rail contact) for the performance evaluation in order to make the system more realistic – as these models are only for the plan-view motions. The plan-view models are sufficient for control design, but do not represent the full vehicle dynamics.

In addition to absolute stiffness control strategy, other full active classical control strategies such as active yaw/lateral damping as well as model-based active control schemes such as H_∞ control and H_2 optimal control (which are explained in the Chapter 2) can be evaluated while actuator dynamics are taken in to consideration such that practical implementations of these wheelset control strategies can be explored.

Reference

1. Givoni, M., *Development and Impact of the Modern High-speed Train: A Review*. Transport reviews, 2006. 26(5): p. 593-611.
2. Hanson, C.E., J.C. Ross, and D.A. Towers, *High-speed ground transportation noise and vibration impact assessment*. 2012.
3. Raghunathan, R.S., H.-D. Kim, and T. Setoguchi, *Aerodynamics of high-speed railway train*. Progress in Aerospace sciences, 2002. 38(6): p. 469-514.
4. Zolotas, A.C. and R.M. Goodall, *Modelling and control of railway vehicle suspensions*, in *Mathematical Methods for Robust and Nonlinear Control*. 2007, Springer. p. 373-411.
5. Li, H., *Measuring systems for active steering of railway vehicles*. 2001, © Hong Li.
6. Mei, T. and R. Goodall. *Wheelset control strategies for a two-axle railway vehicle*. in *The Dynamics Of Vehicles On Roads And On Tracks-Supplement To Vehicle System Dynamics, Volume 33. Proceedings Of The 16th Iavsd Symposium Held In Pretoria, South Africa, August 30-September 3, 1999*. 2000.
7. Goodall, R., *Practical strategies for controlling railway wheelsets independently rotating wheels*. 2003.
8. Gretschel, M. and L. Bose. *A mechatronic approach for active influence on railway vehicle running behaviour*. in *The Dynamics Of Vehicles On Roads And On Tracks-Supplement To Vehicle System Dynamics, Volume 33. Proceedings Of The 16th Iavsd Symposium Held In Pretoria, South Africa, August 30-September 3, 1999*. 2000.
9. Powell, A., et al. *Comparison of the mechanical steering system used on the MF88 trains of the Paris Metro with an active guidance system*. in *International Congress Railtech'98 "Technology for Business Needs*. 1998.
10. Satou, E. and M. Miyamoto, *Dynamics of a bogie with independently rotating wheels*. Vehicle System Dynamics, 1992. 20(sup1): p. 519-534.
11. Eickhoff, B., *The application of independently rotating wheels to railway vehicles*. Proceedings of the Institution of Mechanical Engineers, Part F: Journal of Rail and Rapid Transit, 1991. 205(1): p. 43-54.
12. Goodall, R. and H. Li, *Solid axle and independently-rotating railway wheelsets-a control engineering assessment of stability*. Vehicle System Dynamics, 2000. 33(1): p. 57-67.
13. Metered, H.A. and P. Bonello, *Modelling and control of magnetorheological dampers for vehicle suspension systems*. 2010: University of Manchester.
14. Wang, D. and W. Liao, *Semi-active suspension systems for railway vehicles using magnetorheological dampers. Part I: system integration and modelling*. Vehicle System Dynamics, 2009. 47(11): p. 1305-1325.

15. Geldhof, G., *Semi-active vibration dynamics control of multi-cart systems using a magnetorheological damper*. 2013, M. Sc. Thesis, Chalmers University of Technology, Goteborg, Sweden.
16. Hasan, A.Z.S.C., *Modelling and Simulation of Modified Skyhook Control for Semi-active Suspension*. 2011, UMP.
17. Kotb Ata, W.G.M., *Intelligent Control of Tracked Vehicle Suspension*. 2014.
18. Firth, G.R., *The performance of vehicle suspensions fitted with controllable dampers*. 1991, University of Leeds.
19. Eroglu, M.A., *Observer based control of an magnetorheological damper*. 2013, University of Sheffield.
20. Orvnäs, A., *Active secondary suspension in trains: a literature survey of concepts and previous work*. 2008: KTH.
21. Mehmood, A., A.A. Khan, and A.A. Khan, *Vibration Analysis Of Damping Suspension Using Car Models*". International Journal of Innovation and Scientific Research, 2014. 9(2): p. 202-211.
22. Weerasooriya, L., *Analysis on actuator dynamics in active wheelset control*. 2019, University of Salford.
23. Baillie, A.S., *Development of a fuzzy logic controller for an active suspension of an off-road vehicle fitted with terrain preview*. 1999: Royal Military College of Canada Kingston, Ontario.
24. Biglarbegian, M., W. Melek, and F. Golnaraghi. *Intelligent control of vehicle semi-active suspension systems for improved ride comfort and road handling*. in *Fuzzy Information Processing Society, 2006. NAFIPS 2006. Annual meeting of the North American*. 2006. IEEE.
25. Goodall, R., *Active railway suspensions: Implementation status and technological trends*. *Vehicle System Dynamics*, 1997. 28(2-3): p. 87-117.
26. Fagerlund, J., *Towards Active Car Body Suspension in Railway Vehicles*. 2009.
27. Iwnicki, S., *Handbook of railway vehicle dynamics*. 2006: CRC press.
28. Bruni, S., et al., *Control and monitoring for railway vehicle dynamics*. *Vehicle System Dynamics*, 2007. 45(7-8): p. 743-779.
29. Goodall, R., S. Bruni, and T. Mei, *Concepts and prospects for actively controlled railway running gear*. *Vehicle System Dynamics*, 2006. 44(sup1): p. 60-70.
30. Mei, T.X. and R.M. Goodall, *Use of multiobjective genetic algorithms to optimize inter-vehicle active suspensions*. *Proceedings of the Institution of Mechanical Engineers, Part F: Journal of Rail and Rapid Transit*, 2002. 216(1): p. 53-63.
31. Karnopp, D., *Active damping in road vehicle suspension systems*. *Vehicle System Dynamics*, 1983. 12(6): p. 291-311.
32. Park, J.H. and O.O. Park, *Electrorheology and magnetorheology*. *Korea-Australia Rheology Journal*, 2001. 13(1): p. 13-17.
33. Hammood, H.F., *Improvement of semi-active control suspensions based on gain-scheduling control*. 2018, University of Salford.

34. Butz, T. and O. Von Stryk, *Modelling and Simulation of Electro-and Magnetorheological Fluid Dampers*. ZAMM-Journal of Applied Mathematics and Mechanics/Zeitschrift für Angewandte Mathematik und Mechanik, 2002. 82(1): p. 3-20.
35. Savaresi, S.M., et al., *Semi-Active Suspension Technologies and Models-CHAPTER 2*.
36. Wang, D. and W. Liao, *Semi-active suspension systems for railway vehicles using magnetorheological dampers. Part II: simulation and analysis*. Vehicle System Dynamics, 2009. 47(12): p. 1439-1471.
37. Tseng, H.E. and D. Hrovat, *State of the art survey: active and semi-active suspension control*. Vehicle system dynamics, 2015. 53(7): p. 1034-1062.
38. Mei, T. and R. Goodall, *Recent development in active steering of railway vehicles*. Vehicle System Dynamics, 2003. 39(6): p. 415-436.
39. Anneli, O., *Methods for reducing vertical carbody Vibrations of a rail vehicle*. KTH Engineering Sciences, Sweden, 2010.
40. Sugahara, Y., et al., *Suppression of vertical bending and rigid-body-mode vibration in railway vehicle car body by primary and secondary suspension control: results of simulations and running tests using Shinkansen vehicle*. Proceedings of the Institution of Mechanical Engineers, Part F: Journal of Rail and Rapid Transit, 2009. 223(6): p. 517-531.
41. Li, H. and R.M. Goodall, *Linear and non-linear skyhook damping control laws for active railway suspensions*. Control Engineering Practice, 1999. 7(7): p. 843-850.
42. Zhou, R., A. Zolotas, and R. Goodall. *H ∞ -based control system and its digital implementation for the integrated tilt with active lateral secondary suspensions in high speed trains*. in *Proceedings of the 32nd Chinese Control Conference*. 2013. IEEE.
43. Selamat, H. and S.D.A. Bilong. *Optimal controller design for a railway vehicle suspension system using Particle Swarm Optimization*. in *2013 9th Asian Control Conference (ASCC)*. 2013. IEEE.
44. STRIBERSKY, A., et al., *Design and evaluation of a semi-active damping system for rail vehicles*. Vehicle System Dynamics, 1998. 29(S1): p. 669-681.
45. Liao, W. and D. Wang, *Semiactive vibration control of train suspension systems via magnetorheological dampers*. Journal of intelligent material systems and structures, 2003. 14(3): p. 161-172.
46. Goodall, R., G. Freudenthaler, and R. Dixon, *Hydraulic actuation technology for full-and semi-active railway suspensions*. Vehicle System Dynamics, 2014. 52(12): p. 1642-1657.
47. Aggarwal, M., *Comparative analysis of passenger ride comfort using various semi-active suspension alternatives*. 2014.
48. Félix-Herrán, L.C., et al. *Modeling and control for a semi-active suspension with a magnetorheological damper including the actuator dynamics*. in *2008 Electronics, Robotics and Automotive Mechanics Conference (CERMA'08)*. 2008. IEEE.
49. K-Karamodin, A. and H. H-Kazemi, *Semi-active control of structures using neuro-predictive algorithm for MR dampers*. Structural Control and Health Monitoring: The

- Official Journal of the International Association for Structural Control and Monitoring and of the European Association for the Control of Structures, 2010. 17(3): p. 237-253.
50. Ok, S.-Y., et al., *Semi-active fuzzy control of cable-stayed bridges using magneto-rheological dampers*. Engineering structures, 2007. 29(5): p. 776-788.
 51. Tudon-Martinez, J.C. and R. Morales-Menendez, *Adaptive vibration control system for MR damper faults*. Shock and Vibration, 2015. 2015.
 52. Karnopp, D., M.J. Crosby, and R. Harwood, *Vibration control using semi-active force generators*. 1974.
 53. Codeca, F., et al. *Semiactive control of a secondary train suspension*. in *Advanced intelligent mechatronics, 2007 IEEE/ASME international conference on*. 2007. IEEE.
 54. Spelta, C., et al., *Smart-Bogie: Semi-Active Lateral Control of Railway Vehicles*. Asian Journal of Control, 2012. 14(4): p. 875-890.
 55. Yang, Z., et al., *Semi-active control of high-speed trains based on fuzzy PID control*. Procedia Engineering, 2011. 15: p. 521-525.
 56. Liang, T.-y., et al. *Study on semi-active secondary suspension of railway vehicle*. in *Transportation, Mechanical, and Electrical Engineering (TMEE), 2011 International Conference on*. 2011. IEEE.
 57. Sugahara, Y., T. Takigami, and M. Sampei, *Suppressing vertical vibration in railway vehicles through primary suspension damping force control*. Journal of system design and dynamics, 2007. 1(2): p. 224-235.
 58. Mei, T., H. Li, and R. Goodall, *Kalman filters applied to actively controlled railway vehicle suspensions*. Transactions of the Institute of Measurement and Control, 2001. 23(3): p. 163-181.
 59. Shen, G. and R. Goodall, *Active yaw relaxation for improved bogie performance*. Vehicle System Dynamics, 1997. 28(4-5): p. 273-289.
 60. Mei, T. and R.M. Goodall, *Robust control for independently rotating wheelsets on a railway vehicle using practical sensors*. IEEE Transactions on Control Systems Technology, 2001. 9(4): p. 599-607.
 61. Gretzschel, M. and L. Bose, *A new concept for integrated guidance and drive of railway running gears*. Control Engineering Practice, 2002. 10(9): p. 1013-1021.
 62. Perez, J., et al., *Combined active steering and traction for mechatronic bogie vehicles with independently rotating wheels*. Annual Reviews in Control, 2004. 28(2): p. 207-217.
 63. Cheli, F., et al. *Motion control of a bogie with independently motorised wheels*. in *IEEE 10th International Power Electronics and Motion Control Conference (EPE-PEMC 2002)*. 2002. IEEE.
 64. Michitsuji, Y. and Y. Suda, *Running performance of power-steering railway bogie with independently rotating wheels*. Vehicle System Dynamics, 2006. 44(sup1): p. 71-82.
 65. Mohan, A. and M. Ahmadian. *Nonlinear investigation of the effect of primary suspension on the hunting stability of a rail wheelset*. in *Rail Conference, 2004. Proceedings of the 2004 ASME/IEEE Joint*. 2004. IEEE.

66. Wickens, A., *Dynamic stability of articulated and steered railway vehicles guided by lateral displacement feedback*. *Vehicle System Dynamics*, 1994. 23(S1): p. 541-553.
67. Goodall, R. and T. Mei. *Mechatronic strategies for controlling railway wheelsets with independently rotating wheels*. in *2001 IEEE/ASME International Conference on Advanced Intelligent Mechatronics. Proceedings (Cat. No. 01TH8556)*. 2001. IEEE.
68. Perez, J., L. Mauer, and J.M. Busturia, *Design of active steering systems for bogie-based railway vehicles with independently rotating wheels*. *Vehicle System Dynamics*, 2002. 37(sup1): p. 209-220.
69. Gonzalez, F., et al., *Use of active steering in railway bogies to reduce rail corrugation on curves*. *Proceedings of the Institution of Mechanical Engineers, Part F: Journal of Rail and Rapid Transit*, 2007. 221(4): p. 509-519.
70. Perez, J., J. Busturia, and R. Goodall, *Control strategies for active steering of bogie-based railway vehicles*. *Control Engineering Practice*, 2002. 10(9): p. 1005-1012.
71. Mirzapour, M., *Fault tolerant strategy for actively controlled railway wheelset*. 2015, Salford University.
72. Pacchioni, A., R.M. Goodall, and S. Bruni, *Active suspension for a two-axle railway vehicle*. *Vehicle System Dynamics*, 2010. 48(S1): p. 105-120.
73. Abood, K.H.A. and R.A. Khan, *Investigation to improve hunting stability of railway carriage using semi-active longitudinal primary stiffness suspension*. *Journal of Mechanical Engineering Research*, 2010. 2(5): p. 97-105.
74. Gajdar, T. and I. Rudas. *Active and Semi-active control of uncertain railway wheelset*. in *Proceedings of IECON'95-21st Annual Conference on IEEE Industrial Electronics*. 1995. IEEE.
75. Baiasu, D., G. Ghita, and I. Sebesan. *Control system with magnetorheological fluid device for mitigation of the railway vehicle hunting oscillations*. in *Journal of Physics: Conference Series*. 2013. IOP Publishing.
76. Foo, E. and R. Goodall, *Active suspension control of flexible-bodied railway vehicles using electro-hydraulic and electro-magnetic actuators*. *Control Engineering Practice*, 2000. 8(5): p. 507-518.
77. Gysen, B.L., et al., *Active electromagnetic suspension system for improved vehicle dynamics*. *IEEE Transactions on Vehicular Technology*, 2009. 59(3): p. 1156-1163.
78. Pollard, M., *Active suspensions enhance ride quality*. *Railway Gazette International*, 1983. 139(11): p. 850-853.
79. Sasaki, K., S. Kamoshita, and M. Enomoto. *A design and bench test of multi-modal active suspension of railway vehicle*. in *Proceedings of IECON'94-20th Annual Conference of IEEE Industrial Electronics*. 1994. IEEE.
80. Hirata, T., S. Koizumi, and R. Takahashi, *H_{∞} control of railroad vehicle active suspension*. *Automatica*, 1995. 31(1): p. 13-24.
81. Hedrick, J.K. and D. Wormley, *Active suspensions for ground transport vehicles-a state of the art review*. 1975.

82. Niksefat, N. and N. Sepehri, *Designing robust force control of hydraulic actuators despite system and environmental uncertainties*. IEEE Control Systems Magazine, 2001. 21(2): p. 66-77.
83. Mei, T. and R. Goodall, *Stability control of railway bogies using absolute stiffness: sky-hook spring approach*. Vehicle System Dynamics, 2006. 44(sup1): p. 83-92.
84. Weerasooriya, L. and T. Mei, *Active wheelset control—actuator dynamics and power requirements*, in *Dynamics of Vehicles on Roads and Tracks Vol 2*. 2017, CRC Press. p. 735-740.
85. Park, J., et al., *A practical approach to active lateral suspension for railway vehicles*. Measurement and Control, 2019. 52(9-10): p. 1195-1209.
86. Brabie, D., *SIMULATION OF ACTIVE LATERAL SUSPENSION IN RAILWAY VEHICLES: PARAMETRIC STUDIES FOR AN ELECTRO MECHANICAL ACTUATOR*. TRITA-FKT, 2002(2002: 09).
87. Grimm, J.J., *Electromagnetic linear actuator—design, manufacture and control*. 2009.
88. Goodall, R., *Actuator technologies for secondary active suspensions on railway vehicles*. STECH'93, 1993: p. 377-382.
89. Pollard, M. and N. Simons, *Passenger comfort—the role of active suspensions*. Proceedings of the Institution of Mechanical Engineers, Part D: Transport Engineering, 1984. 198(3): p. 161-175.
90. Norinao, H., *Active and semi-active suspensions smooth 300 km/h ride*. Railway Gazette International, 1997: p. 241-242.
91. Ji, Y., L. Ren, and J. Zhou, *Boundary conditions of active steering control of independent rotating wheelset based on hub motor and wheel rotating speed difference feedback*. Vehicle System Dynamics, 2018. 56(12): p. 1883-1898.
92. Shin, Y.-J., et al., *Improvement of ride quality of railway vehicle by semiactive secondary suspension system on roller rig using magnetorheological damper*. Advances in Mechanical Engineering, 2014. 6: p. 298382.
93. Ward, C.P., et al., *Adhesion estimation at the wheel–rail interface using advanced model-based filtering*. Vehicle System Dynamics, 2012. 50(12): p. 1797-1816.
94. Ren, H., et al., *State observer-based sliding mode control for semi-active hydro-pneumatic suspension*. Vehicle System Dynamics, 2016. 54(2): p. 168-190.
95. Lu, Z.-G., X.-J. Sun, and J.-Q. Yang, *Integrated active control of independently rotating wheels on rail vehicles via observers*. Proceedings of the Institution of Mechanical Engineers, Part F: Journal of Rail and Rapid Transit, 2017. 231(3): p. 295-305.
96. Tang, J., *Passive and semi-active airspring suspensions for rail passenger vehicles—theory and practice*. Proceedings of the Institution of Mechanical Engineers, Part F: Journal of Rail and Rapid Transit, 1996. 210(2): p. 103-117.
97. Jezequel, L., et al., *Improvement of very high speed trains comfort with preview semi-active suspensions*. Vehicle System Dynamics, 1992. 20(sup1): p. 299-313.

98. O'Neill, H. and G. Wale, *Semi-active suspension improves rail vehicle ride*. Computing & Control Engineering Journal, 1994. 5(4): p. 183-188.
99. Carlson, J.D., D. Catanzarite, and K. St. Clair, *Commercial magneto-rheological fluid devices*. International Journal of Modern Physics B, 1996. 10(23n24): p. 2857-2865.
100. Gao, G. and S. Yang. *Semi-active control performance of railway vehicle suspension featuring magnetorheological dampers*. in *Industrial Electronics and Applications, 2006 1ST IEEE Conference on*. 2006. IEEE.
101. Shen, Y., et al., *Semi-active control of hunting motion of locomotive based on magnetorheological damper*. International Journal of Innovative Computing, Information and Control, 2006. 2(2): p. 323-329.
102. Sun, S., et al., *Improving the critical speeds of high-speed trains using magnetorheological technology*. Smart Materials and Structures, 2013. 22(11): p. 115012.
103. Oh, J.-S., et al., *Vibration control of a semi-active railway vehicle suspension with magneto-rheological dampers*. Advances in Mechanical Engineering, 2016. 8(4): p. 1687814016643638.
104. Lau, Y. and W. Liao, *Design and analysis of magnetorheological dampers for train suspension*. Proceedings of the Institution of Mechanical Engineers, Part F: Journal of Rail and Rapid Transit, 2005. 219(4): p. 261-276.
105. Allotta, B., et al., *Design and optimization of a semi-active suspension system for railway applications*. Journal of Modern Transportation, 2011. 19(4): p. 223-232.
106. Maganti, G.B., S.N. Singh, and W. Yim. *On absolute stability and semi-active control of a magnetorheological fluid vibration suppression system*. in *Systems Engineering, 2005. ICSEng 2005. 18th International Conference on*. 2005. IEEE.
107. Ata, W. and A. Salem, *Semi-active control of tracked vehicle suspension incorporating magnetorheological dampers*. Vehicle System Dynamics, 2017. 55(5): p. 626-647.
108. Kim, H.-C., et al., *CONTROL PERFORMANCE OF SEMI-ACTIVE RAILWAY VEHICLE SUSPENSION USING MR DAMPER*.
109. Allotta, B., et al. *Comparison of different control approaches aiming at enhancing the comfort of a railway vehicle*. in *Advanced Intelligent Mechatronics (AIM), 2010 IEEE/ASME International Conference on*. 2010. IEEE.
110. Hu, G., et al., *Vibration control of semi-active suspension system with magnetorheological damper based on hyperbolic tangent model*. Advances in Mechanical Engineering, 2017. 9(5): p. 1687814017694581.
111. Sleiman, H., et al. *Modelling and inversion-based control of a magnetorheological vehicle suspension*. in *Vehicle Power and Propulsion Conference (VPPC), 2010 IEEE*. 2010. IEEE.
112. Prabakar, R., C. Sujatha, and S. Narayanan, *Response of a quarter car model with optimal magnetorheological damper parameters*. Journal of Sound and Vibration, 2013. 332(9): p. 2191-2206.
113. Yu, M., et al., *Study on MR semi-active suspension system and its road testing*. Journal of intelligent material systems and structures, 2006. 17(8-9): p. 801-806.

114. Du, H., K.Y. Sze, and J. Lam, *Semi-active H_∞ control of vehicle suspension with magneto-rheological dampers*. Journal of Sound and Vibration, 2005. 283(3): p. 981-996.
115. Choi, S.-B., S.-K. Lee, and Y.-P. Park, *A hysteresis model for the field-dependent damping force of a magnetorheological damper*. Journal of sound and vibration, 2001. 245(2): p. 375-383.
116. Choi, S.-B., H.-S. Lee, and Y.-P. Park, *H8 Control Performance of a Full-Vehicle Suspension Featuring Magnetorheological Dampers*. Vehicle System Dynamics, 2002. 38(5): p. 341-360.
117. Shin, Y.-J., et al., *Semi-active control to reduce carbody vibration of railway vehicle by using scaled roller rig*. Journal of mechanical science and technology, 2012. 26(11): p. 3423-3431.
118. Fleps-Dezaße, M. and J. Pitzer. *Modelling and parameter identification of a semi-active vehicle damper*. in *Proceedings of the 10 th International Modelica Conference; March 10-12; 2014; Lund; Sweden*. 2014. Linköping University Electronic Press.
119. Li, W., et al., *Testing and steady state modeling of a linear MR damper under sinusoidal loading*. Smart Materials and Structures, 2000. 9(1): p. 95.
120. Spencer Jr, B., et al., *Phenomenological model for magnetorheological dampers*. Journal of engineering mechanics, 1997. 123(3): p. 230-238.
121. Kamath, G.M. and N.M. Wereley, *Nonlinear viscoelastic-plastic mechanisms-based model of an electrorheological damper*. Journal of Guidance, Control, and Dynamics, 1997. 20(6): p. 1125-1132.
122. Seong, M.-S., S.-B. Choi, and Y.-M. Han, *Damping force control of a vehicle MR damper using a Preisach hysteretic compensator*. Smart materials and structures, 2009. 18(7): p. 074008.
123. Zong, L.-H., et al., *Semi-active H_∞ control of high-speed railway vehicle suspension with magnetorheological dampers*. Vehicle System Dynamics, 2013. 51(5): p. 600-626.
124. Yao, G., et al., *MR damper and its application for semi-active control of vehicle suspension system*. Mechatronics, 2002. 12(7): p. 963-973.
125. Guo, D. and H. Hu, *Nonlinear stiffness of a magneto-rheological damper*. Nonlinear Dynamics, 2005. 40(3): p. 241-249.
126. Ashour, O., C.A. Rogers, and W. Kordonsky, *Magnetorheological fluids: materials, characterization, and devices*. Journal of intelligent material systems and structures, 1996. 7(2): p. 123-130.
127. Maneetham, D. and N. Afzulpurkar, *Modeling, simulation and control of high speed nonlinear hydraulic servo system*. Journal of Automation Mobile Robotics and Intelligent Systems, 2010. 4: p. 94-103.
128. Oh, S.K., Y.H. Yoon, and A.B. Krishna, *A study on the performance characteristics of variable valve for reverse continuous damper*. World Academy of Science, Engineering and Technology, 2007. 32: p. 123-128.

129. Jugulkar, L.M., S. Singh, and S.M. Sawant, *Analysis of suspension with variable stiffness and variable damping force for automotive applications*. Advances in Mechanical Engineering, 2016. 8(5): p. 1687814016648638.
130. Peel, D., R. Stanway, and W. Bullough, *Dynamic modelling of an ER vibration damper for vehicle suspension applications*. Smart Materials and Structures, 1996. 5(5): p. 591.
131. Sims, N., et al., *Controllable viscous damping: an experimental study of an electrorheological long-stroke damper under proportional feedback control*. Smart materials and structures, 1999. 8(5): p. 601.
132. Yerrawar, R., et al., *Performance Comparison of Semi-Active Suspension and Active Suspension System Using MATLAB/Simulink*. International Journal of Innovative Research in Science, Engineering and Technology, 2014. 3(12): p. 18293-18299.
133. Derbyshire, D., *Development of an intelligent sensing technique for active control of railway vehicles with independently rotating wheels*. 2015, Manchester Metropolitan University.
134. Mei, T. and R. Goodall, *Modal controllers for active steering of railway vehicles with solid axle wheelsets*. Vehicle System Dynamics, 2000. 34(1): p. 25-41.
135. Weiss, K.D., J.D. Carlson, and D.A. Nixon, *Viscoelastic properties of magneto-and electro-rheological fluids*. Journal of Intelligent Material Systems and Structures, 1994. 5(6): p. 772-775.
136. Goncalves, F.D., J.-H. Koo, and M. Ahmadian, *A review of the state of the art in magnetorheological fluid technologies-Part I: MR fluid and MR fluid models*. The Shock and Vibration Digest, 2006. 38(3): p. 203-219.
137. Smyth, A.W., et al., *Development of adaptive modeling techniques for non-linear hysteretic systems*. International journal of non-linear mechanics, 2002. 37(8): p. 1435-1451.
138. Stanway, R., J. Sproston, and N. Stevens, *Non-linear modelling of an electro-rheological vibration damper*. Journal of Electrostatics, 1987. 20(2): p. 167-184.
139. Unsal, M., *Semi-active vibration control of a parallel platform mechanism using magnetorheological damping*. 2006, PhD Thesis, University of Florida, Gainesville, FL.
140. Mei, T., R. Goodall, and H. Li. *Kalman filter for the state estimation of a 2-axle railway vehicle*. in *Control Conference (ECC), 1999 European*. 1999. IEEE.
141. Wang, P., T. Mei, and J. Zhang. *Towards self-powered lateral active suspension for railway vehicles*. in *Control (CONTROL), 2014 UKACC International Conference on*. 2014. IEEE.
142. Mei, T. and R. Goodall, *Optimal control strategies for active steering of railway vehicles*. IFAC Proceedings Volumes, 1999. 32(2): p. 2915-2920.
143. Mei, T. and R. Goodall, *Control for Railway Vehicles*. CONTROL SYSTEMS, ROBOTICS AND AUTOMATION–Volume XX: Industrial Applications of Control Systems-I, 2009: p. 108.
144. Jiang, J.Z., et al., *Passive suspensions incorporating inerters for railway vehicles*. Vehicle System Dynamics, 2012. 50(sup1): p. 263-276.

Appendix A: Parameter values

<i>Symbols</i>	<i>Parameters Value for two-axle railway vehicle</i>	<i>Parameters Value for conventional bogie railway vehicle</i>
C_{py}	37kNs/m	37kNs/m
C_{px}	-	0Ns/m
C_{sy}	-	52kNs/m
r_0	0.45m	0.45m
g	9.8m/s ²	9.8m/s ²
m_v	30,000kg	32,000 kg
m_w	1,250kg	1,1400750kg
m_b	-	3296 kg
L_v	4.5m	9 m
L_g	0.7m	1.25 m
J_w	700 kg m ²	1400 kg m ²

J_v	558,800 kg m ²	2,240,000 kg m ²
J_ϕ	100 kg m ²	100 kg m ²
f_{11}, f_{22}	10MN	10MN
R_1, R_2	3500 for 83.3 m/s 1250 for 50 m/s 200 for 20 m/s	3500 for 83.3 m/s 1250 for 50 m/s 200 for 20 m/s
θ_{c1}, θ_{c2}	6°	6°
K_{py}	511kN/m	15,000kN/m
K_{sy}	-	350kN/m
K_{sx}	-	340kN/m
V_s	83.3, 20, 50 m/s	83.3, 20, 50 m/s
λ	0.2	0.2